Polymerizable Peptide Monomers for the Targeted and Intracellular Delivery of Cancer Therapeutics

Hanna Kern

A dissertation submitted
in partial fulfillment of the requirements of
the degree of

Doctor of Philosophy

University of Washington
2016

Reading Committee:

Patrick Stayton, Chair
Anthony Convertine
Oliver Press

Program Authorized to Offer Degree:
Bioengineering

University of Washington

Abstract

Polymerizable Peptide Monomers for the Targeted and Intracellular Delivery of Cancer Therapeutics

Hanna Kern

Chair of the Supervisory Committee:
Professor Patrick Stayton
Department of Bioengineering

For the treatment of cancer, peptides hold great potential as both targeting and therapeutic agents. One particularly promising anti-cancer strategy is peptides derived from the third Bcl-2 homology domain (BH3), which antagonize pro-survival Bcl-2 proteins and induce apoptosis. Unfortunately, before the clinical potential of peptides can be realized, a number of drug delivery barriers must be overcome. Namely, peptides have short circulation half-lives, are susceptible to degradation by extracellular proteases, and are unable to cross cell membranes and access intracellular targets.

An antibody-targeted, pH-responsive polymeric system was recently developed and implemented for the intracellular delivery of the pro-apoptotic BH3 peptide BIM[1]. Unfortunately, the delivery properties of this system were limited by the poor stability of the disulfide-linkage used for conjugating BIM to the polymeric carrier. It was the objective of this thesis to develop highly stable polymer-peptide conjugates for the targeted and intracellular delivery cancer drugs.

Initially, steric hindrance was investigated for enhancing the stability and delivery properties of disulfide-linked polymer-BIM conjugates. Two methyl groups were introduced onto the peptide's disulfide-adjacent carbon by substituting BIM's C-terminal cysteine with

pencillamine and conjugating the peptide to the polymeric carrier via disulfide exchange. In a murine xenograft model of B-cell lymphoma, steric hindrance significantly enhanced conjugate stability, peptide half-life and peptide deposition into tumors. However, benefits were relatively minor with much left to be desired.

Next an enzyme-labile peptide linker was developed that is highly stable in human serum and efficiently cleaved in cancer cells to release active BIM peptide. A methacrylamido-peptide macromonomer containing BIM capped with a four amino acid (FKFL) cathepsin B substrate was synthesized and directly integrated into the polymeric delivery vehicle via RAFT polymerization. The resulting cathepsin-B cleavable BIM prodrug system demonstrated potent apoptotic activity in ovarian cell cultures and is currently being investigated for apoptotic activity and therapeutic efficacy in intraperitoneal ovarian cancer xenograft model.

Lastly, peptide monomer technology was alternatively implemented for tumor-specific targeting. A peptide monomer containing the EGFR-targeting sequence GE11[2] was polymerized into a hydrophilic polymeric drug delivery system in combination with an ester-linked camptothecin prodrug monomer. GE11 was shown to enhance targeting and activity of the polymeric prodrug in ovarian cancer cell cultures.

[1] *Berguig GY, Convertine AJ, Frayo S, Kern HB, Procko E, Roy D, Srinivasan S, Margineantu DH, Booth G, Palanca-Wessels MC, Baker D, Hockenbery D, Press OW, Stayton PS. Intracellular delivery system for antibody-Peptide drug conjugates. Mol Ther. 2015 May;23(5):907-17.*

[2] *Li Z, Zhao R, Wu X, Sun Y, Yao M, Li J, Xu Y, Gu J. Identification and characterization of a novel peptide ligand of epidermal growth factor receptor for targeted delivery of therapeutics. FASEB J. 2005 Dec;19(14):1978-85.*

TABLE OF CONTENTS

CHAPTER 1. Introduction and Background

1.1 Clinical Significance

Cancer is a leading cause of death worldwide. In 2012, there were 14 million new cases and 8.2 million cancer-related deaths (14.6% of all human deaths)[1]. In the coming decades, the number of new cases is expected to rise to as high as 22 million[1]. In the United States, an astounding 39.5 percent of men and women will be diagnosed with cancer during their lifetimes[2].

Cancer is a heterogenous group of diseases characterized by uncontrolled cell growth. In 2000, Hanahan and Weinberg defined six "hallmark" capabilities of cancer cells: (1) self-sufficiency in growth signaling, (2) insensitivity to anti-growth signals, (3) evasion of apoptosis, (4) limitless replicative potential, (5) induction and sustainment of angiogenesis, and (6) metastasis and tissue invasion[3]. In 2011, two additional "hallmarks" were proposed: (1) abnormal metabolic pathways and (2) evading the immune system[4]. At a fundamental level, cancer is a disease of genetics, caused by damage to growth-promoting oncogenes and/or growth-inhibiting tumor suppressor genes. The large majority of cancers (90-95%) can be attributed to environmental factors including tobacco, diet and obesity, infections, radiation, stress and pollutants[5]. The remaining 5-10% are believed to be due to inherited genetics[5].

Traditional methods of cancer treatment include surgical excision, chemotherapy and radiation. Unfortunately, these techniques are severely limited by dose-limiting toxicities, resistant cancer phenotypes, and incomplete elimination of the tumor. Chemotherapy and radiation function by targeting rapidly dividing cells and consequently cause significant toxicity to healthy tissues such as the bone marrow and gastrointestinal tract. Severe side effects include

immunosuppression, anemia, thrombocytopenia, hair loss, diarrhea, and nausea and vomiting. Consequently, a pressing need exists for new treatments with higher specificity and efficacy.

1.2. The Promise of Peptide Therapeutics

Anticancer peptides present a promising alternative for the treatment of cancer. Peptide therapeutics generally function by mimicking and/or inhibiting specific protein-protein interactions. Based on accrued knowledge of protein sequence, structure, and interactions, peptides can be "rationally" designed to target almost any protein of interest. This includes a number of protein targets that have been deemed "undruggable" by small molecule technologies[6]. In addition, peptides bind their targets with high specificity, reducing the potential for off-target sides effects. The ease of peptide design and manufacturing promises an arsenal of peptides capable of inhibiting all variety of oncogenic mechanisms[7]. This makes peptides particularly relevant to the emerging paradigm of personalized medicine[7]. Diagnostic advances are rapidly permitting the determination of patient-specific oncogenic aberrations. Based on this information, efficacious peptide cocktails could be tailored for each patient. To date, the clinical success of therapeutic peptides has been limited by a number of delivery hurdles. However, if these barriers can be overcome, the potential of anticancer peptides is limitless.

Of particular promise are peptides that target the pro-survival proteins responsible for evading apoptosis.

1.3. Regulation of Apoptosis by B-cell Lymphoma 2 (Bcl-2) Proteins

Apoptosis is the highly regulated process of programmed cell death. At the cellular level, it is characterized by morphological changes including blebbing, cell shrinkage, nuclear

fragmentation, chromatin condensation, and engulfment by phagocytes[8]. Apoptosis is important for eliminating damaged and infected cells and maintaining tissue health. Activation of apoptosis occurs through both extrinsic and intrinsic signaling mechanisms. The extrinsic or death receptor pathway is triggered by extracellular factors (tumor necrosis factor, Fas ligand) binding to transmembrane receptors[9]. The intrinsic pathway is triggered at the mitochondria by a variety of stress signals including hypoxia, reactive oxygen species, growth factor withdrawal, DNA damage, radiation and chemotherapy[10]. Mitochondrial apoptosis is closely regulated by the B-cell lymphoma 2 (Bcl-2) protein family[11] **(Figure 1.1)**.

The Bcl-2 protein family consists of three related subfamilies sharing between one and four Bcl-2 homology (BH) domains. Each subfamily is composed of either pro-apoptotic or anti-apoptotic regulators. The first subfamily is pro-apoptotic and consists of Bcl-2 associated X protein (Bax) and Bcl-2 antagonist/killer protein (Bak). Bax and Bak directly trigger apoptosis through oligomerization, mitochondrial pore formation, cytochrome c release and caspase activation[11]. The second pro-survival Bcl-2 subfamily consists of Bcl-2 and Bcl-2-like proteins (Bcl-xl, Mcl-1, Bcl-w, Bfl1, A1) containing BH1-4 domains[11]. Bcl-2-like proteins inhibit apoptosis by binding to and sequestering Bak and Bax. Bak and Bax are bound in a highly conserved hydrophobic pocket formed by the BH1-3 domains[11]. The pro-survival Bcl-2 proteins are balanced by a third pro-apoptotic subfamily, the BH3-only proteins. The BH3-only proteins (Bim, Bid, Bad, Noxa, Puma) are potent inducers of apoptosis[11]. They function indirectly by binding competitively to the hydrophobic BH1-3 pocket and freeing Bax and Bak[11]. In addition, it is believed that certain BH3-only proteins (Bim and Bid) directly induce apoptosis through activating interactions with Bax and Bak[11].

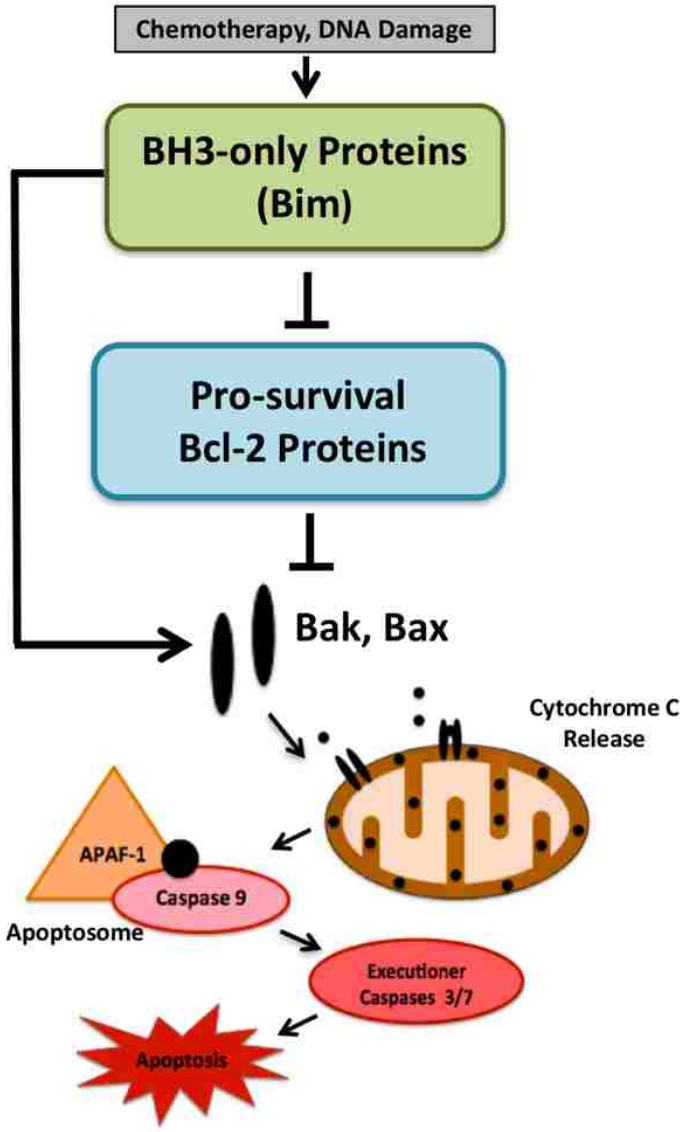

Figure 1.1. The mitochondrial pathway of apoptosis.

The relative balance between pro-apoptotic and pro-survival Bcl-2 proteins constitutes a "switch" that determines apoptotic activation in any given cell. Under normal circumstances, the pro-survival Bcl-2 proteins constrain Bak/Bax under conditions of health, and the BH3-only proteins activate Bak/Bax under conditions of stress. In cancer, overexpression of pro-survival Bcl-2 proteins often disrupts this balance and impairs apoptosis[12-13]. Consequently, pro-survival

Bcl-2 proteins present a logical and promising therapeutic target. Adding further to this promise is the discovery that Bcl-2 overexpressing cells are frequently "primed for death," with only minor alterations in the pro-survival/pro-apoptotic balance required for restoring apoptosis[14].

1.4. Therapeutic Inhibition of Pro-survival Bcl-2 Proteins

1.4.1 Small molecules

Structural information on the BH3 binding domain and advances in drug design have permitted the development of a number of small molecule Bcl-2 inhibitors. These compounds, known as "BH3 mimetics," have demonstrated varying levels success in preclinical and clinical studies. Obatoclax (GX15-070), a synthetic derivative of prodiginine, is a pan-Bcl-2 inhibitor that binds to all pro-survival Bcl-2 proteins with low micromolar affinity[15]. Unfortunately, in phase I/II trials, Obatoclax demonstrated low activity likely related to sub-optimal binding[16-17]. The plant-derived product gossypol and its synthetic derivatives (ABT-101, TW37, ApoG2, BI-97CI) bind to Bcl-2, Bcl-xL, and Mcl-1 with moderate affinities[18]. As a single agent, gossypol and its enantiomer AT-101 have exhibited only limited anticancer activity[17]. However, in combination with rituximab, some benefits were found in patients with follicular lymphoma[17]. Of much greater promise is ABT-737, which was developed in the mid-2000s using Structure Activity Relationships-by-nuclear magnetic resonance (SAR-by-NMR). ABT-737 binds to Bcl-2, Bcl-xl, and Bcl-w with very high sub-nanomolar affinities[19]. ABT-737's orally bioavailable analogue ABT-263 (Navitoclax) began clinical testing in 2006. Modest activity was observed in phase I/II trials of relapsed-refractory chronic lymphocytic

leukemia (CLL)[20-21]. However, Navitoclax's efficacy was compromised by dose-limiting thrombocytopenia resulting from inhibition of Bcl-xl in platelets[21]. ABT-199 is a redesign of Navitoclax that binds to Bcl-2 with much higher affinity (Ki < 1 nM) than Bcl-xl (Ki > 50 nM) and Bcl-w (Ki > 200 nM) and, consequently, spares platelets[22]. In Phase I trials, very good responses to ABT-199 were observed in patients with relapsed-refractory CLL and non-Hodgkin's lymphoma (NHL)[17,23]. In comparison to Navitoclax, dose-dependent thrombocytopenia was significantly reduced and much higher drug doses could be administered. The most significant toxicity observed with ABT-199 was tumor lysis syndrome (TLS) resulting from rapid induction of apoptosis[17]. In May of 2015, the FDA granted ABT-199 breakthrough therapy designation in 17p deletion relapsed-refractory CLL. It is currently undergoing phase I/II trials in patients with CLL, small lymphocytic leukemia (SLL), acute myeloid leukemia (AML), NHL and multiple myeloma.

1.4.2 BH3 Peptides

ABT-199's recent success in clinical trials is an exciting development. However, small molecule inhibitors continue to be plagued by binding limitations (ABT-199 only binds Bcl-2) and/or off-target toxicity. An alternative class of antagonists are peptides derived from the BH3 binding domains of pro-apoptotic Bcl-2 proteins. Short (~20 amino acids) BH3-derived peptides have shown potent apoptotic activity similar to that of their native proteins[10,24-25]. Pro-apoptotic BH3 peptides can be synthesized from both BH3-only proteins (Bim, Bad, Noxa, Puma) and apoptotic effectors (Bak and Bax)[10]. Peptide target specificities vary with those of the template protein. Some BH3 domains (Bim, Puma) bind to all pro-survival proteins, while others bind selectively. For instance, the Noxa BH3

domain binds preferentially to Mcl-1 and Bfl-1[26]. Consequently, peptides can be rationally designed to either broadly or narrowly target pro-survival Bcl-2 proteins. In addition, specificity differences may permit the tailoring of peptide cocktails for cancer-specific and/or patient-specific activity.

1.4.2.1 The BIM Peptide

Of particular therapeutic interest are peptides derived from the BH3 domain of Bim. Bim possesses one of the most potent BH3 domains due to dual pro-apoptotic activities: (1) Bim broadly binds with high affinity to all pro-survival proteins, and (2) Bim directly activates apoptosis by binding to Bax[27-28]. In addition, Bim is believed to be a key mediator of apoptotic-induction by radiation and chemotherapeutic agents[29]. All signs indicate that the BIM peptide is poised to make a broad clinical impact, if it can be effectively targeted and delivered into tumors.

1.5. Peptide Drug Delivery Barriers (Figure 1.2)

Before the clinical potential of therapeutic peptides can be realized, a unique and challenging set of drug delivery barriers must be addressed:

- Poor stability.
- Protease degradation.
- Kidney filtration.
- Opsoninization and clearance by macrophages of the reticuloendothelial system (RES).
- An inability, due to large size and hydrophilicity, to diffuse across cell membranes.
- An inability to escape endosomes following uptake by receptor-mediated endocytosis.

- Non-specific delivery and toxicity.

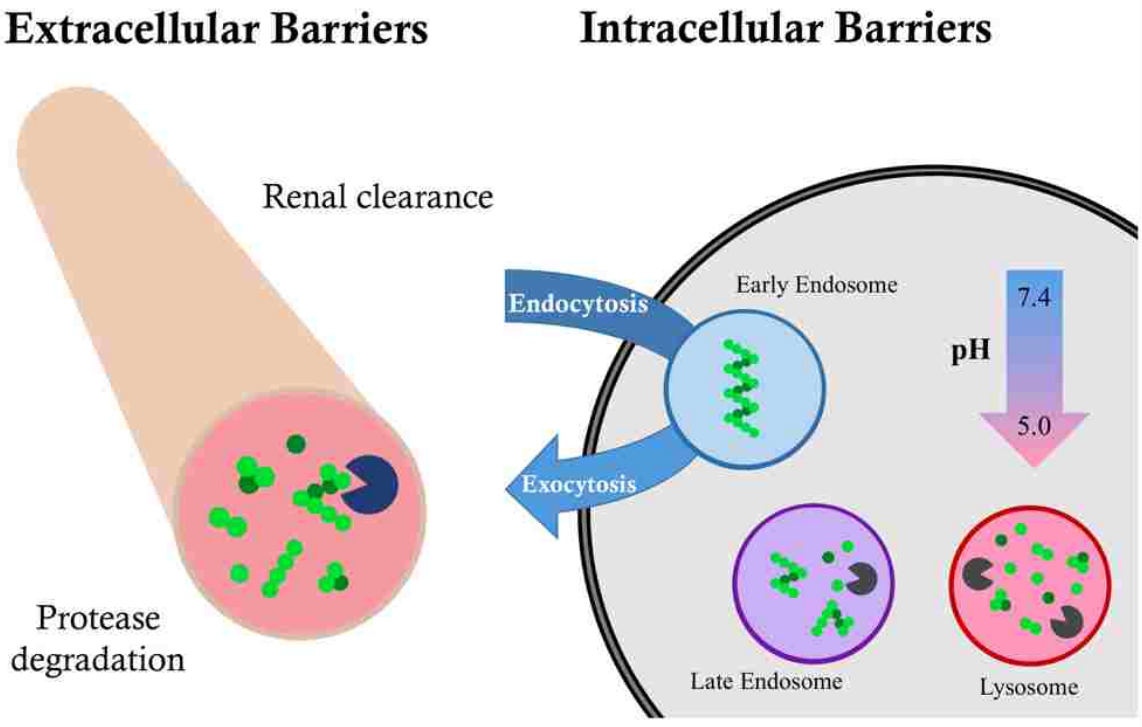

Figure 1.2. Peptide delivery barriers.

1.6. Strategies for the Delivery of Therapeutic Peptides

Numerous strategies exist for overcoming the above delivery barriers. These include but are not limited to internalizing cell penetrating peptides, peptide stabilization through stapling, formulation into nanoparticles, modification with polyethylene glycol (PEG), tumor-specific targeting, and pH-responsive polymers for endosomal escape.

1.6.1 Cell Penetrating Peptides

To enhance cellular uptake, biomacromolecules or nanocarriers can be modified with cell penetrating peptides (CPPs)[30]. CPPs mimic viruses in their ability to translocate across cell

membranes, and are capable of delivering cargoes with high molecular weights. Common examples include the transactivation transcription factor (TAT) derived from HIV-1 and attenapendia (penetratin) derived from Drosophila[31-32]. CPP transport properties are a result of short sequences that are rich in basic amino acid residues[30]. The mechanisms of CPP-mediated entry vary, but include electrostatic interactions, hydrogen bonding, macropinocytosis and endocytosis[30]. Limitations of CPPs include protease degradation, non-specific cell uptake, and an inability to escape the endo/lysosomal pathway. Consequently, they are frequently combined with other drug delivery approaches.

Fusion of the TAT CPP to the pro-apoptotic peptide BIM successfully enhanced intracellular peptide delivery and pro-apoptotic activity[33]. TAT-BIM was shown to rapidly internalize and induce apoptosis in T-cell lymphoma (EL4), pancreatic cancer (Panc-02) and melanoma (B16) cell cultures. In corresponding xenograft models of melanoma and pancreatic cancer, intratumoral injections on TAT-BIM significantly inhibited tumor growth.

1.6.2 Peptide Stapling

Alpha-helices are common secondary structures in protein-protein interactions and constitute the binding domains of BH3-only proteins. Unfortunately, alpha-helical peptides exhibit high conformational entropy and poor helicity in solution[34]. This reduces peptide binding affinity, decreases cell permeability (by increasing the energy of backbone desolvation), and exposes peptide bonds to preoteolytc degradation[34]. Consequently, conformational stabilization can significantly improve the inherent activity of alpha-helical peptides. Initial efforts at stablization involved lactam or disulfide cross-links between the side chains of successive alpha-helical turns[10]. More recently, hydrocarbon staples have been

introduced using non-natural olefin-conjugated amino acids and a ring-closing metathesis reaction[34].

Hydrocarbon stapling has effectively increased the structural stability, cell permeability, and potency of a variety of BH3 peptides[29,35-36]. These peptides are known as stabilized alpha helix of Bcl-2 domains (SAHB). Notably, a SAHB designed from the BIM BH3 domain bound with high affinity to both anti-apoptotic (Bcl-xl, Bcl-w, Mcl-1 and A1) and pro-apoptotic (Bax and Bak) targets, and restored BH3-dependent cell death in ABT-737-resistant hematologic cancer cell lines[29]. BIM SAHB also inhibited tumor growth in an AML xenograft model both as a single agent and in combination with ABT-263[29].

1.6.3 Nanoparticle Carriers

In anticancer nanoparticles, therapeutic molecules (peptides, siRNA, small molecule drugs) are assembled with other materials such as lipids and polymers[37]. Nanoparticle formulations offer numerous drug delivery advantages. They increase drug half-lives, shield drugs from degradation, carry large drug loads, and can enhance tumor localization and cellular uptake[37]. In addition, nanoparticles are easily modified with other functionalities including PEG, CPPs, and targeting ligands[10].

The pharmaceutical properties of nanoparticles are highly dependent on both particle size and surface properties. For tumor delivery, particles should be 10-100 nanometers in diameter[37]. The lower threshold is to prevent elimination by the kidneys, and the upper limit permits particles to pass out of blood vessels and diffuse through tumor tissues. Modulation of surface properties is key for preventing nanoparticle aggregation, interactions with extracelluar proteins, and clearance by the RES. Generally, to minimize non-specific

interactions, nanoparticles should be sterically stabilized and exhibit a neutral or slightly negative charge[37].

1.6.4 Modification with Polyethylene Glycol (PEG)

Modification of protein drugs and nanocarriers with polyethylene glycol (PEG) confers numerous pharmaceutical advantages. PEG is a flexible, water-soluble and highly hydrated polymer that creates a hydrophilic protective layer[38]. As a consequence of these properties, "PEGylation" effectively increases solubility and stability, decreases immunogenicity and toxicity, prevents opsoninization and RES clearance, and dramatically prolongs circulation half-lives[38]. However, it can also negatively impact cellular uptake, escape from endosomes, and drug activity[10]. For example, PEGylation of cationic liposomes reduced toxicity at the expense of transfection efficiency[39]. These limitations may be addressed, in part, by incorporating "sheddable" PEG layers[40].

1.6.5 Targeting

Tumor-specific targeting can enhance drug delivery, activity, and specificity. Tumor targeting strategies rely on physiological distinctions between normal and cancerous tissues. Both passive and active targeting modalities are useful in cancer nanomedicine.

Passive targeting of nanoparticles into tumors occurs via the enhanced permeation and retention (EPR) effect first described by Matsumura and Maeda in the 1980s[41]. Tumor tissues are characterized by extensive angiogenesis and vascular abnormalities that enhance their permeability to particulates. These abnormalities include highly proliferating endothelial cells, decreased pericytes and smooth muscle, and defective basement membranes. In addition,

inefficient lymphatic drainage and venous return lead to high retention in the interstitial space. As a result, long-circulating nanoparticles selectively accumulate in tumors via both diffusion and convection mechanisms. Passive targeting effects can be harnessed in the great majority of cancers. Exceptions include hypovascular malignancies such as those of the prostate and pancreas[42].

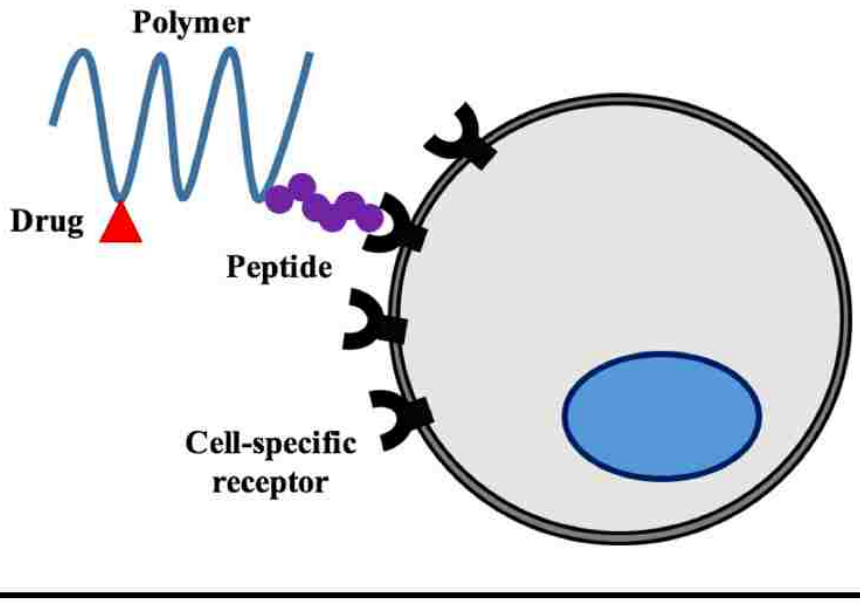

Figure 1.3. Peptides binding to cell-specific receptors may be employed for active drug targeting.

Active targeting is achieved through ligands that bind to receptors disproportionately expressed at the tumor site. Targeting ligands may be monoclonal antibodies (mAbs), antibody fragments, peptides (**Figure 1.3)**, lectins or metabolites. A large number of receptors overexpressed by tumors or tumor vasculature present promising targeting candidates. Internalizing receptors are particular attractive for enhancing the uptake and intracellular delivery of biologics. Transferrin receptor, folate receptor, and epidermal growth factor receptor (EGFR) are examples of internalizing receptors that have been widely investigated in drug delivery[42].

Streptavidin (SA)-conjugated monoclonal antibodies have been developed by Dr. Oliver Press' lab for active targeting of biotin-conjugated drugs and delivery platforms. Both αCD22-SA and Herceptin-SA are relevant to this work.

1.6.5.1 αCD22

αCD22-SA conjugated to a biotinylated diblock copolymer significantly enhanced siRNA uptake and gene knockdown in DoHH2 lymphoma and CD22-transduced Hela-R cells[43]. CD22 is a B-cell specific transmembrane protein expressed in 60-80% of B-cell cancers[44]. CD22 constitutively internalizes and so presents an attractive pathway for intracellular drug delivery[44]. In addition, CD22 has been widely investigated for the targeted delivery of radioisotopes, toxins, chemotherapeutics, and doxorubicin liposomes[44].

1.6.5.2 Herceptin

Herceptin-SA conjugates may be employed for targeting and uptake into breast or ovarian cancers[45]. Herceptin (Trastuzumab, Genentech) is a humanized antibody FDA-approved for the treatment of breast cancers positive for Human Epidermal Growth Factor Receptor 2 (HER2/neu). Approximately 20% of breast cancers and 8-32% of ovarian cancers overexpress HER2/new. Herceptin and its fragments have been employed previously for the active targeting of PEG-modified adenovirus[46], immunoliposomes[47], a pH-responsive triblock (PLGLA-b-histidine-b-PEG) nanocarrier,[48] and a pH-responsive diblock polymer designed for intracellular siRNA delivery[49](**Figure 1.4)**.

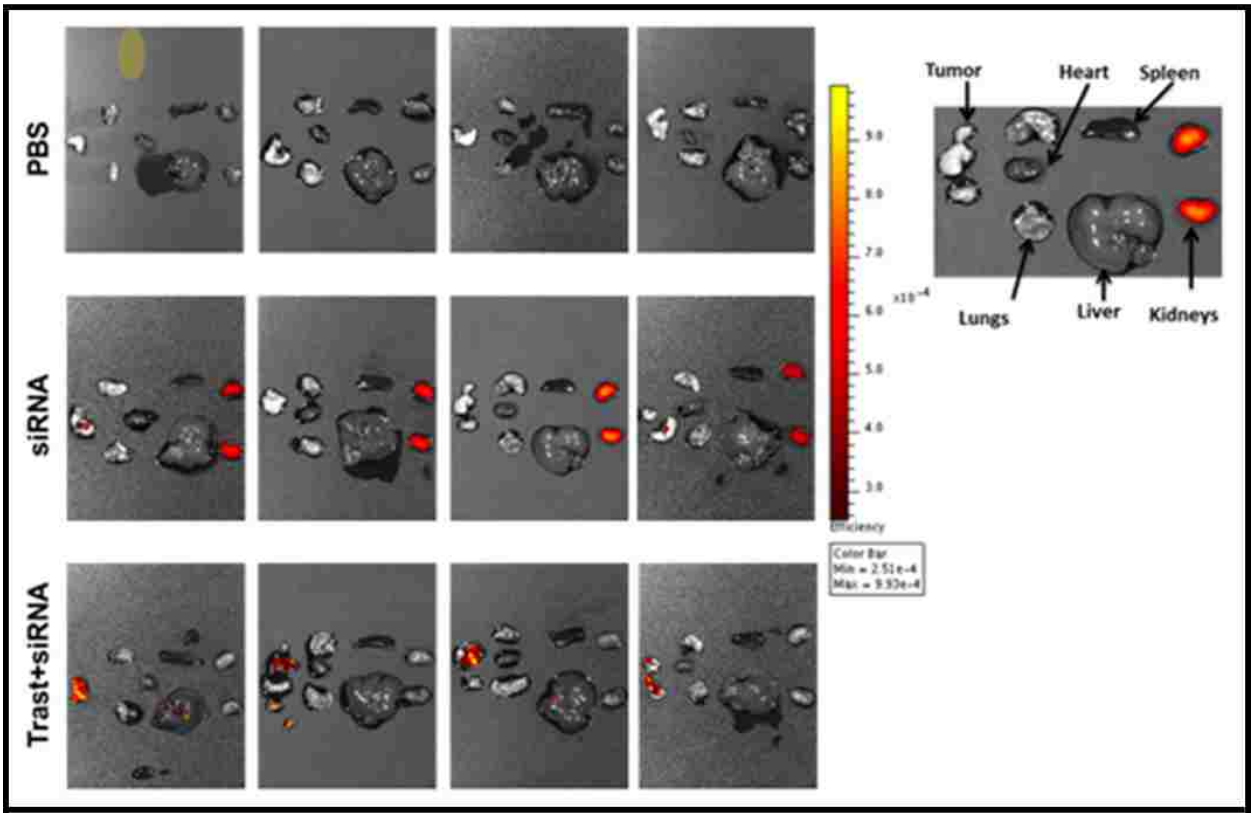

Figure 1.4. A Trastuzumab-targeted nanoparticle delivery system enhances the delivery of siRNA to intraperitoneal ovarian tumors. Mice bearing SKOV3 EA8 luciferase-expressing xenografts were injected with PBS or Cy 5.5-labeled siRNA alone or complexed with a Transuzumab targeted polymeric delivery vehicle. After 24 hours, mice were euthanized and organs were harvested and imaged *ex vivo* to visualize biodistribution of the fluorescently labeled siRNA. [Palanca-Wessels et al., *Oncotarget*, 2016].

1.6.6 pH-responsive Polymers for Endosomal Escape

A critical delivery hurdle for intracellular peptide delivery is escape from the harsh endo/lysosomal environment into the cell cytosol. To aid in this escape, a number of pH--responsive polymeric carriers have been developed that disrupt membranes at the acidic pHs found in endo/lysosomal compartments. Ionizable groups such as carboxylic acids, phosphoric acids, and amines confer the pH-dependent activity of these polymers[50].

A number of cationic materials (poly(lysine), poly(ethylenimine), etc.) harness what is known as the "proton sponge effect[51]." These polymers absorb protons and buffer against acidification, which in turn leads to increased proton and counterion influx, osmotic swelling, and permeation of endo/lysosomal vesicles. While cationic materials have proven effective for endosomal escape, they are limited by high cytotoxicity, poor stability, and non-specific uptake.

Alternatively, polymers can be synthesized containing pH-sensitive "switch" residues that trigger disruptive hydrophobic interactions with membranes. *Convertine et al*. described a diblock polymer siRNA-carrier composed of a positively charged 2-(dimethylamino)ethyl methacrylate (DMAEMA) block for siRNA binding, and a second pH-responsive block consisting of positively charged DMAEMA, negatively charged propyl acrylic acid (PAA), and hydrophobic butyl methacrylate (BMA)[52]. At acidic pHs, protonation of PAA's carboxyl groups resulted in a hydrophobic block (with a net positive charge) that exhibited endolytic activity. Subsequently, *Manganiello et al*. developed a similar micelle carrier for DNA delivery[53]. The pH-responsive block of this carrier consisted of a mixture of N,N-diethylaminoethyl methacrylate (DEAEMA) and BMA. At endo/lysosomal pHs, protonation of DEAEMA's tertiary amines increases the block's positive charge, destabilizes polymer micelles, and exposes hydrophobic membrane-interactive BMA residues.

1.7. An Intracellular Delivery System for Pro-apoptotic Peptides

Recently, a pH-responsive diblock copolymer was developed for the intracellular delivery of pro-apoptotic peptides such as BIM (**Figure 1.5**)[54]. Synthesized via RAFT polymerization, the first biocompatible "stealth" block was composed of the hydrophilic monomer polyethylene glycol

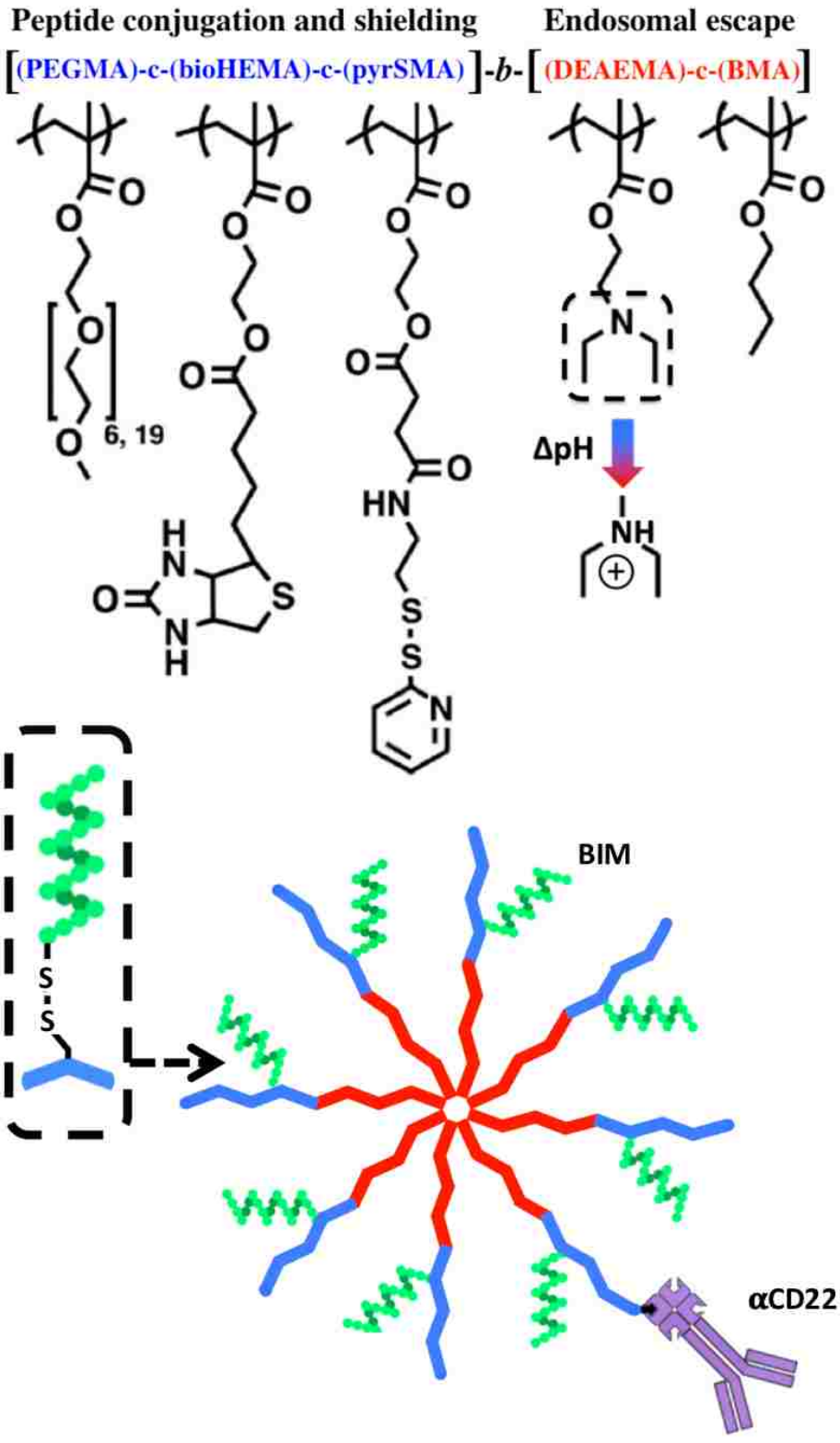

Figure 1.5. Antibody-targeted, pH-responsive polymeric micelles for intracellular BIM delivery [Berguig et al., *Mol Ther*, 2015].

methacrylate ($PEGMA_{950}$, MW=950 Da), the thiol-reactive monomer pyrSMA for conjugation to cysteine-modified peptides, and biotin-conjugated hydroxyethyl methacrylate (bioHEMA) for binding to cancer-specific antibody-streptavidin conjugates. The second pH-responsive endosomolytic block was composed of 60% DEAEMA and 40% BMA.

The described polymer (Pol950) was employed with anti-CD22 targeting for the enhanced delivery and therapeutic efficacy of BIM in a murine B-cell lymphoma cancer model. To assess the activity of αCD22-polymer-BIM conjugates, mice bearing xenografts of a Burkitt's lymphoma cell line (Ramos) were administered four doses of subtherapeutic chemotherapy (cyclophosphamide and bortezomib) in combination with αCD22-polymer-BIM L62E (negative control peptide) or αCD22-polymer-BIM. Treatment with αCD22-polymer-BIM conjugates was found to suppress tumor growth and extended overall survival in comparison to αCD22-polymer-BIM L62E (**Figure 1.6**).

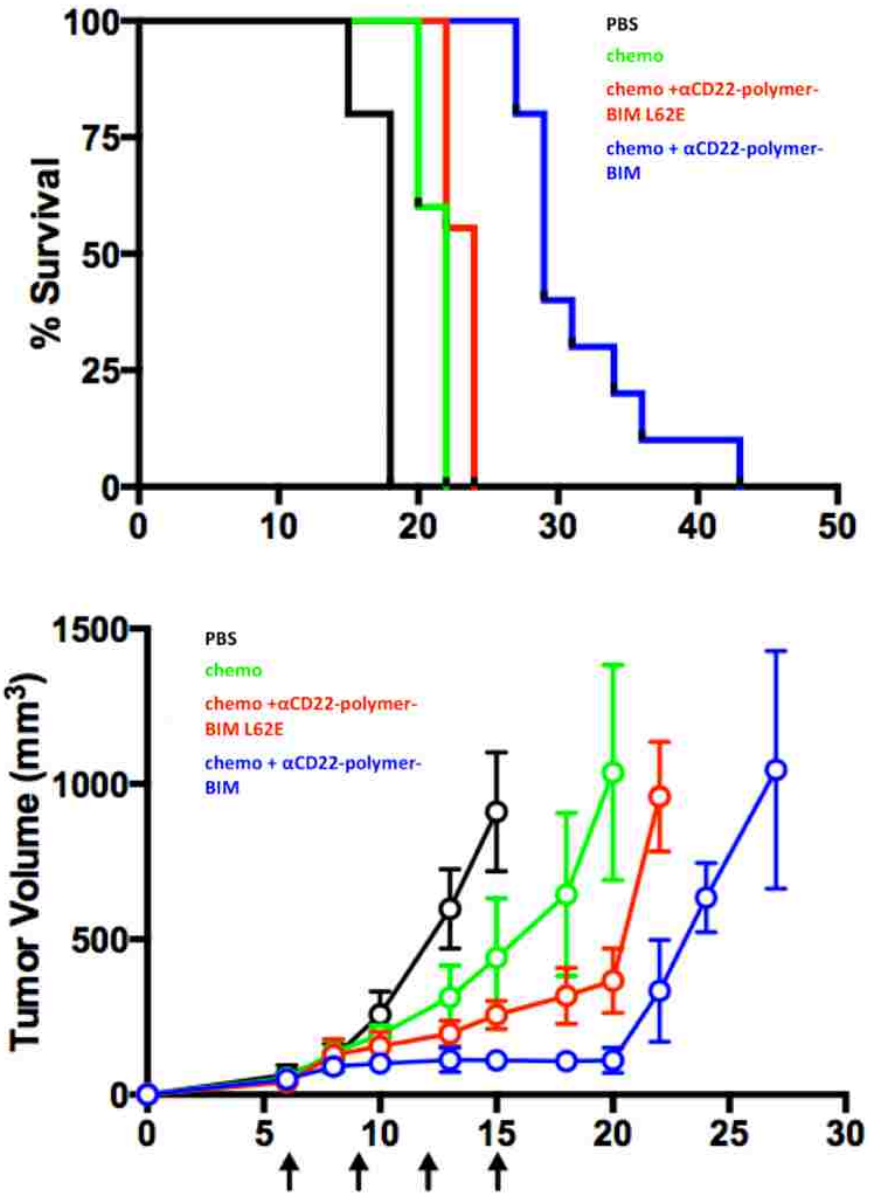

Figure 1.6. Antibody-polymer-peptide conjugates in combination with low dose chemotherapy suppress tumor growth and prolong survival. On days 0, 3, 6 and 9, mice bearing Ramos xenografts (n=10) were injected IP with chemotherapy [**chemo**] 30 minutes prior to IV injection with **αCD22-polymer-BIM L62E** or **αCD22-polymer-BIM**.

Despite this promising therapeutic activity, the polymer-peptide disulfide linkage was found to be unstable in a pharmacokinetic study in mice using dual radiolabled [^{3}H]αCD22-polymer-

[^{14}C]BIM conjugates (**Figure 1.4)**. Linker stability was measured as the ratio of BIM to αCD22 in the blood over time. At 24 hours post-injection, the BIM:αCD22 ratio had decreased from 90:1 to 39:1. These findings are consistent with previous reports using disulfide linkages in antibody-drug conjugates, which estimate a linkage half-life on the order of 24-48 hours[56-56]. An improved linker design promises to further enhance BIM's deposition into tumors, internalization into cancer cells, and therapeutic efficacy in vivo.

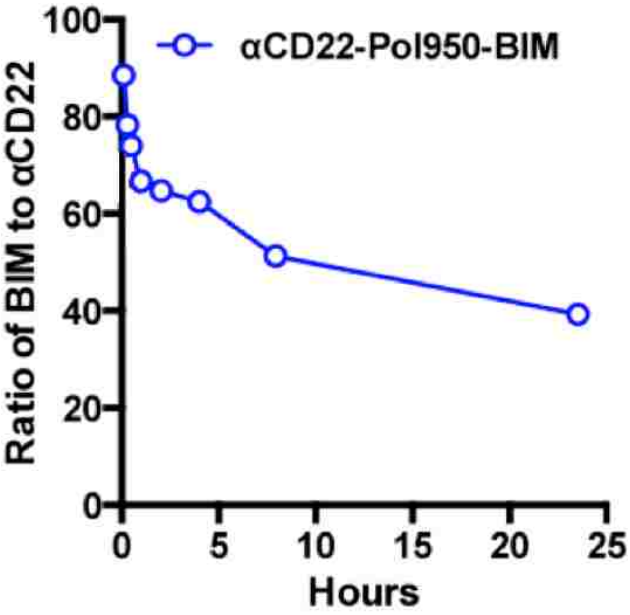

Figure 1.7. Disulfide-linked polymer-BIM conjugates exhibit poor circulation stability. The pharmacokinetics of dual-radiolabeled αCD22-Pol950-BIM conjugates in tumor bearing mice were measured for ^{3}H-labeled αCD22 and ^{14}C-labeled BIM (n=3). The stability of Pol-BIM conjugates was evaluated by following the BIM/αCD22 ratio in the blood over time, with an initial injected ratio of 90:1.

REFERENCES

[3] World Cancer Report 2014. *World Health Organization*. 2014.

[4] *National Cancer Institute*. Cancer Statistics. Retrieved November 6, 2015 from http://www.cancer.gov/about-cancer/what-is-cancer/statistics.

[5] Hanahan D, Weinberg RA. The hallmarks of cancer. *Cell*. 2000 Jan 7;100(1):57-70.

[6] Hanahan D, Weinberg RA. Hallmarks of cancer: the next generation. *Cell*. 2011 Mar 4;144(5):646-74.

[7] Anand P, Kunnumakkara AB, Sundaram C, Harikumar KB, Tharakan ST, Lai OS, Sung B, Aggarwal BB. Cancer is a preventable disease that requires major lifestyle changes. *Pharm Res*. 2008 Sep;25(9):2097-116.

[8] Tsomaia N. Peptide therapeutics: targeting the undruggable space. *Eur J Med Chem*. 2015 Apr 13;94:459-70.

[9] Bidwell GL 3rd, Raucher D. Therapeutic peptides for cancer therapy. Part I - peptide inhibitors of signal transduction cascades. *Expert Opin Drug Deliv*. 2009 Oct;6(10):1033-47.

[10] Taylor RC, Cullen SP, Martin SJ. Apoptosis: controlled demolition at the cellular level. Nat Rev Mol Cell Biol. 2008 Mar;9(3):231-41.

[11] Wajant H. The Fas signaling pathway: more than a paradigm. Science. 2002 May 31;296(5573):1635-6.

[12] Li H, Nelson CE, Evans BC, Duvall CL. Delivery of intracellular-acting biologics in pro-apoptotic therapies. Curr Pharm Des. 2011;17(3):293-319.

[13] Czabotar PE, Lessene G, Strasser A, Adams JM. Control of apoptosis by the BCL-2 protein family: implications for physiology and therapy. Nat Rev Mol Cell Biol. 2014 Jan;15(1):49-63.

[14] Vaux DL, Cory S, Adams JM. Bcl-2 gene promotes haemopoietic cell survival and cooperates with c-myc to immortalize pre-B cells. Nature. 1988 Sep 29;335(6189):440-2.

[15] Yip KW, Reed JC. Bcl-2 family proteins and cancer. Oncogene. 2008 Oct 27;27(50):6398-406.

[16] Certo M, Del Gaizo Moore V, Nishino M, Wei G, Korsmeyer S, Armstrong SA, Letai A. Mitochondria primed by death signals determine cellular addiction to antiapoptotic BCL-2 family members. Cancer Cell. 2006 May;9(5):351-65.

[17] Nguyen M, Marcellus RC, Roulston A, Watson M, Serfass L, Murthy Madiraju SR, Goulet D, Viallet J, Bélec L, Billot X, Acoca S, Purisima E, Wiegmans A, Cluse L, Johnstone RW, Beauparlant P, Shore GC. Small molecule obatoclax (GX15-070) antagonizes MCL-1 and overcomes MCL-1-mediated resistance to apoptosis. Proc Natl Acad Sci U S A. 2007 Dec 4;104(49):19512-7.

[18] Hwang JJ, Kuruvilla J, Mendelson D, Pishvaian MJ, Deeken JF, Siu LL, Berger MS, Viallet J, Marshall JL. Phase I dose finding studies of obatoclax (GX15-070), a small molecule pan-BCL-2 family antagonist, in patients with advanced solid tumors or lymphoma. Clin Cancer Res. 2010 Aug 1;16(15):4038-45.

[19] Anderson MA, Huang D, Roberts A. Targeting BCL2 for the treatment of lymphoid malignancies. Semin Hematol. 2014 Jul;51(3):219-27.

[20] Paoluzzi L, Gonen M, Gardner JR, Mastrella J, Yang D, Holmlund J, Sorensen M, Leopold L, Manova K, Marcucci G, Heaney ML, O'Connor OA. Targeting Bcl-2 family members with the BH3 mimetic AT-101 markedly enhances the therapeutic effects of chemotherapeutic agents in in vitro and in vivo models of B-cell lymphoma. Blood. 2008 Jun 1;111(11):5350-8.

[21] Oltersdorf T, Elmore SW, Shoemaker AR, Armstrong RC, Augeri DJ, Belli BA, Bruncko M, Deckwerth TL, Dinges J, Hajduk PJ, Joseph MK, Kitada S, Korsmeyer SJ, Kunzer AR, Letai A, Li C, Mitten MJ, Nettesheim DG, Ng S, Nimmer PM, O'Connor JM, Oleksijew A, Petros AM, Reed JC, Shen W, Tahir SK, Thompson CB, Tomaselli KJ, Wang B, Wendt MD, Zhang H, Fesik SW, Rosenberg SH. An inhibitor of Bcl-2 family proteins induces regression of solid tumours. Nature. 2005 Jun 2;435(7042):677-81.

[22] Roberts AW, Seymour JF, Brown JR, Wierda WG, Kipps TJ, Khaw SL, Carney DA, He SZ, Huang DC, Xiong H, Cui Y, Busman TA, McKeegan EM, Krivoshik AP, Enschede SH, Humerickhouse R. Substantial susceptibility of chronic lymphocytic leukemia to BCL2 inhibition: results of a phase I study of navitoclax in patients with relapsed or refractory disease. J Clin Oncol. 2012 Feb 10;30(5):488-96.

[23] Wilson WH, O'Connor OA, Czuczman MS, LaCasce AS, Gerecitano JF, Leonard JP, Tulpule A, Dunleavy K, Xiong H, Chiu YL, Cui Y, Busman T, Elmore SW, Rosenberg SH, Krivoshik AP, Enschede SH, Humerickhouse RA. Navitoclax, a targeted high-affinity inhibitor of BCL-2, in lymphoid malignancies: a phase 1 dose-escalation study of safety, pharmacokinetics, pharmacodynamics, and antitumour activity. Lancet Oncol. 2010 Dec;11(12):1149-59.

[24] Souers AJ, Leverson JD, Boghaert ER, Ackler SL, Catron ND, Chen J, Dayton BD, Ding H, Enschede SH, Fairbrother WJ, Huang DC, Hymowitz SG, Jin S, Khaw SL, Kovar PJ, Lam LT, Lee J, Maecker HL, Marsh KC, Mason KD, Mitten MJ, Nimmer PM, Oleksijew A, Park CH, Park CM, Phillips DC, Roberts AW, Sampath D, Seymour JF, Smith ML, Sullivan GM, Tahir SK, Tse C, Wendt MD, Xiao Y, Xue JC, Zhang H, Humerickhouse RA, Rosenberg SH, Elmore SW. ABT-199, a potent and selective BCL-2 inhibitor, achieves antitumor activity while sparing platelets. Nat Med. 2013 Feb;19(2):202-8.

[25] ABT-199 shows effectiveness in CLL. Cancer Discov. 2014 Sep;4(9):OF7.

[26] Cosulich SC, Worrall V, Hedge PJ, Green S, Clarke PR. Regulation of apoptosis by BH3 domains in a cell-free system. Curr Biol. 1997 Dec 1;7(12):913-20.

[27] Boohaker RJ, Lee MW, Vishnubhotla P, Perez JM, Khaled AR. The use of therapeutic peptides to target and to kill cancer cells. Curr Med Chem.2012;19(22):3794-804.

[28] Ploner C, Kofler R, Villunger A. Noxa: at the tip of the balance between life and death. Oncogene. 2008 Dec;27 Suppl 1:S84-92.

[29] Mérino D, Giam M, Hughes PD, Siggs OM, Heger K, O'Reilly LA, Adams JM, Strasser A, Lee EF, Fairlie WD, Bouillet P. The role of BH3-only protein Bim extends beyond inhibiting Bcl-2-like prosurvival proteins.

[30] Delgado-Soler L, Pinto M, Tanaka-Gil K, Rubio-Martinez J. Molecular determinants of Bim(BH3) peptide binding to prosurvival proteins. J Chem Inf Model. 2012 Aug 27;52(8):2107-18.

[31] LaBelle JL, Katz SG, Bird GH, Gavathiotis E, Stewart ML, Lawrence C, Fisher JK, Godes M, Pitter K, Kung AL, Walensky LD. A stapled BIM peptide overcomes apoptotic resistance in hematologic cancers. J Clin Invest. 2012 Jun;122(6):2018-31.

[32] Torchilin V. Intracellular delivery of protein and peptide therapeutics. Drug Discov Today Technol. 2008 Autumn;5(2-3):e95-e103.

[33] Frankel AD, Pabo CO. Cellular uptake of the tat protein from human immunodeficiency virus. Cell. 1988 Dec 23;55(6):1189-93.

[34] Derossi D, Joliot AH, Chassaing G, Prochiantz A. The third helix of the Antennapedia homeodomain translocates through biological membranes. J Biol Chem. 1994 Apr 8;269(14):10444-50.

[35] Kashiwagi H, McDunn JE, Goedegebuure PS, Gaffney MC, Chang K, Trinkaus K, Piwnica-Worms D, Hotchkiss RS, Hawkins WG. TAT-Bim induces extensive apoptosis in cancer cells. Ann Surg Oncol. 2007 May;14(5):1763-71.

[36] Verdine GL and Hilinski GJ. Stapled Peptides for Intracellular Drug Targets. Methods in Enzymology. 2012.

[37] Walensky LD, Kung AL, Escher I, Malia TJ, Barbuto S, Wright RD, Wagner G, Verdine GL, Korsmeyer SJ. Activation of apoptosis in vivo by a hydrocarbon-stapled BH3 helix. Science. 2004 Sep 3;305(5689):1466-70.

[38] Cohen NA, Stewart ML, Gavathiotis E, Tepper JL, Bruekner SR, Koss B, Opferman JT, Walensky LD. A competitive stapled peptide screen identifies a selective small molecule that overcomes MCL-1-dependent leukemia cell survival. Chem Biol. 2012 Sep 21;19(9):1175-86.

[39] Davis ME, Chen ZG, Shin DM. Nanoparticle therapeutics: an emerging treatment modality for cancer. Nat Rev Drug Discov. 2008 Sep;7(9):771-82.

[40] Duncan R. Polymer therapeutics as nanomedicines: new perspectives. Curr Opin Biotechnol. 2011 Aug;22(4):492-501.

[41] Wang XL, Xu R, Lu ZR. A peptide-targeted delivery system with pH-sensitive amphiphilic cell membrane disruption for efficient receptor-mediated siRNA delivery. J Control Release. 2009 Mar 19;134(3):207-13.

[42] Li SD, Huang L. Stealth nanoparticles: high density but sheddable PEG is a key for tumor targeting. J Control Release. 2010 Aug 3;145(3):178-81.

[43] Matsumura Y, Oda T, Maeda H. [General mechanism of intratumor accumulation of macromolecules: advantage of macromolecular therapeutics]. Gan To Kagaku Ryoho. 1987 Mar;14(3 Pt 2):821-9.

[44] Danhier F, Feron O, Préat V. To exploit the tumor microenvironment: Passive and active tumor targeting of nanocarriers for anti-cancer drug delivery. J Control Release. 2010 Dec 1;148(2):135-46.

[45] Palanca-Wessels MC, Convertine AJ, Cutler-Strom R, Booth GC, Lee F, Berguig GY, Stayton PS, Press OW. Anti-CD22 antibody targeting of pH-responsive micelles enhances small interfering RNA delivery and gene silencing in lymphoma cells. Mol Ther. 2011 Aug;19(8):1529-37.

[46] Sullivan-Chang L, O'Donnell RT, Tuscano JM. Targeting CD22 in B-cell malignancies: current status and clinical outlook. BioDrugs. 2013 Aug;27(4):293-304.

[47] Hudis CA. Trastuzumab--mechanism of action and use in clinical practice. N Engl J Med. 2007 Jul 5;357(1):39-51.

[48] Kim PH, Sohn JH, Choi JW, Jung Y, Kim SW, Haam S, Yun CO. Active targeting and safety profile of PEG-modified adenovirus conjugated with herceptin. Biomaterials. 2011 Mar;32(9):2314-26.

[49] Kirpotin DB, Drummond DC, Shao Y, Shalaby MR, Hong K, Nielsen UB, Marks JD, Benz CC, Park JW. Antibody targeting of long-circulating lipidic nanoparticles does not increase tumor localization but does increase internalization in animal models. Cancer Res. 2006 Jul 1;66(13):6732-40.

[50] Zhou Z, Badkas A, Stevenson M, Lee JY, Leung YK. Herceptin conjugated PLGA-PHis-PEG pH sensitive nanoparticles for targeted and controlled drug delivery. Int J Pharm. 2015 Jun 20;487(1-2):81-90.

[51] Palanca-Wessels MC, Booth GC, Convertine AJ, Lundy BB, Berguig GY, Press MF, Stayton PS, Press OW. Antibody targeting facilitates effective intratumoral siRNA nanoparticle delivery to HER2-overexpressing cancer cells. Oncotarget. 2016 Feb 23;7(8):9561-75.

[52] Schmaljohann D. Thermo- and pH-responsive polymers in drug delivery. Adv Drug Deliv Rev. 2006 Dec 30;58(15):1655-70.

[53] Ma D. Enhancing endosomal escape for nanoparticle mediated siRNA delivery.Nanoscale. 2014 Jun 21;6(12):6415-25.

[54] Convertine AJ, Diab C, Prieve M, Paschal A, Hoffman AS, Johnson PH, Stayton PS. pH-responsive polymeric micelle carriers for siRNA drugs. Biomacromolecules. 2010 Nov 8;11(11):2904-11.

[55] Manganiello MJ, Cheng C, Convertine AJ, Bryers JD, Stayton PS. Diblock copolymers with tunable pH transitions for gene delivery. Biomaterials. 2012 Mar;33(7):2301-9.

[56] Berguig GY, Convertine AJ, Frayo S, Kern HB, Procko E, Roy D, Srinivasan S, Margineantu DH, Booth G, Palanca-Wessels MC, Baker D, Hockenbery D, Press OW, Stayton PS. Intracellular delivery system for antibody-Peptide drug conjugates. Mol Ther. 2015 May;23(5):907-17.

[57] Ducry L, Stump B. Antibody-drug conjugates: linking cytotoxic payloads to monoclonal antibodies. Bioconjug Chem. 2010 Jan;21(1):5-13.

[58] Sanderson RJ, Hering MA, James SF, Sun MM, Doronina SO, Siadak AW, Senter PD, Wahl AF. In vivo drug-linker stability of an anti-CD30 dipeptide-linked auristatin immunoconjugate. Clin Cancer Res. 2005 Jan 15;11(2 Pt 1):843-52.

CHAPTER 2. Objectives

For the treatment of cancer, peptides hold enormous potential as both targeting and therapeutic agents. Of particular therapeutic promise is the peptide BIM, which broadly and potently inhibits pro-survival Bcl-2 proteins and induces apoptosis. Unfortunately, a number of drug delivery barriers have limited the clinical application of peptides. Namely, peptides have short circulation half-lives, are susceptible to degradation by extracellular proteases, and are unable to cross cell membranes and access intracellular targets. Previously, a polymeric, antibody-targeted, intracellular delivery system was developed for peptides with cytosolic targets and successfully employed for BIM delivery in a mouse xenograft model. However, a number of design limitations need to be addressed before the full potential of this carrier can be realized. The disulfide linkage used to conjugate the BIM peptide exhibited poor stability in the blood, reducing peptide half-life. In addition, due to antibody dosing limits, only low antibody-to-polymer ratios can be achieved, which may lead to suboptimal tumor targeting. To improve upon these aspects, this thesis defined the following specific objectives:

1. Employ steric hindrance to enhance the stability and delivery properties of disulfide-linked polymer-BIM conjugates in a murine xenograft model of B-cell lymphoma.

2. Develop a polymerizable cathepsin B-cleavable BIM peptide macromonomer that is highly stable in human serum and efficiently cleaved inside cancer cells to release active BIM peptide. Integrate the peptide macromonomer into a diblock polymeric intracellular delivery system.

3. Evaluate the therapeutic efficacy of the cathepsin B-cleavable BIM polymer in a clinically relevant intraperitoneal mouse model of ovarian cancer.

4. Develop a polymerizable peptide monomer that targets the epidermal growth factor receptor (EGFR) overexpressed in a wide array of epithelial cancers. Demonstrate the utility of the EGFR-targeting peptide monomer for enhancing the delivery of a polymeric prodrug to ovarian cancer cells.

In meeting these objectives, this thesis develops a new class of polymerizable peptide monomers with both tumor-targeting and therapeutic functions. These highly stable peptide monomers can be directly and stoichiometrically integrated into biocompatible copolymers in a single polymerizable step without the need for additional post-synthetic conjugation and purification steps. Furthermore, this versatile technology can be easily adapted for a broad range of diseases and drug targets.

CHAPTER 3. Steric Hindrance Enhances the Stability and Delivery Properties of Disulfide-linked Polymer-BIM Conjugates

Abstract

A diblock polymeric micelle carrier was recently described for the tumor-targeted intracellular delivery of BIM. The first polymer block consisted of hydrophilic polyethylene glycol units, a pyridyl disulfide (PDS) monomer for conjugation to thiol-modified drugs, and a biotin functionality for binding to cancer-specific antibody-streptavidin (SA) conjugates. The second hydrophobic block was composed of a pH-responsive formulation that facilitates endosomal escape. The corresponding polymer-BIM conjugates demonstrated promising anti-tumor activity in a murine xenograft model of B-cell lymphoma. However, the disulfide linkage used to conjugate BIM exhibited poor blood stability that compromised the full potential of the carrier system. In this chapter steric hindrance was employed to enhance the stability and delivery properties of the disulfide-linked polymer-BIM conjugates. Two methyl groups were introduced onto the BIM peptide'sdisulfide-adjacent carbon by substituting its C-terminal cysteine residue with pencillamine. A new pyridyl disulfide monomer was also synthesized with two PDS-adjacent methyl groups and equivalent diblock copolymers were synthesized with and without hindered PDS moieties. Quantification of pyridine-2-thione release showed that hindered BIM (hBIM) conjugated to unhindered polymer with higher efficiency than the original BIM peptide. However, the hindered peptide failed to conjugate to the hindered PDS groups, likely due to the high steric interference of four methyls. Unhindered BIM conjugated to the hindered polymer, but with much lower efficieny. Consequently, polymer-peptide conjugates hindered by two peptide-side methyl groups were selected for further evaluation. In comparisons to polymer-BIM, hindered polymer-hBIM conjugates demonstrated approximately a 5-fold increase in resistance to DTT-reduction, as

measured by RP-HPLC. MALDI-TOF MS analysis showed a correlating increase in conjugate stability in human serum. In SKOV3 ovarian cancer cell cultures, the hindered polymer-hBIM conjugates demonstrated more potent cell-killing activity than unhindered polymer-BIM conjugates. To evaluate the effects of steric hindrance on conjugate stability *in vivo*, a pharmacokinetic and biodistribution study was conducted in granta-519 tumor-bearing mice using dual-radiolabled [^{3}H]polymer-[^{14}C]peptide conjugates. Steric hindrance significantly enhanced conjugate stability, peptide half-life, and peptide deposition into tumors.

3.1 Introduction

Previously, RAFT polymerization was employed to synthesize a series of pH-responsive diblock copolymers that improve the pharmacokinetic properties of biologic drugs (peptides, protein, siRNA, etc.) and facilitate endosomal escape to the cell cytosol[1-3]. Pyridyl disulfide groups were incorporated into the polymers for reversible conjugation to thiol-modified drugs, and one such carrier was conjugated to the pro-apoptotic BIM peptide modified on its C-terminus with cysteine[1]. The carrier successfully enhanced intracellular peptide delivery and apoptotic activity in a murine xenograft model of B-cell lymphoma[1].

While these initial findings demonstrate the therapeutic promise of polymer-BIM conjugates, the reducible disulfide linkage offered poor control over peptide release *in vivo*. Disulfide linkages aim to exploit the highly reducing cytosolic environment for intracellular drug release, but have consistently demonstrated poor stability in systemic circulation[4]. In the case of polymer-BIM conjugates, a pharmacokinetic study in mice found the plasma half-life of BIM to be significantly shorter than that of the carrier, likely due to reductive cleavage[1]. Consequently,

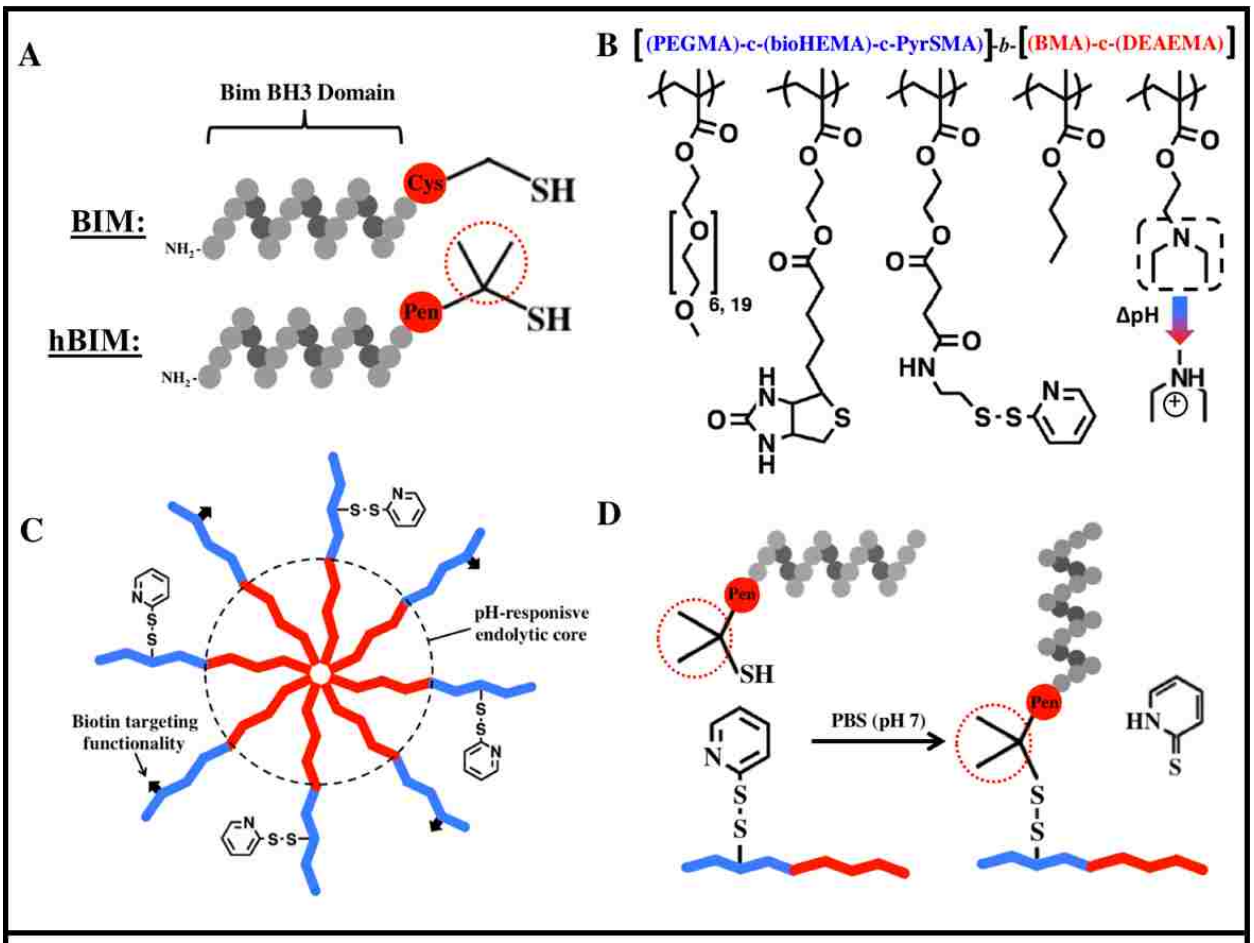

Figure 3.1. Sterically hindered disulfide-linked polymer-BIM conjugates. (A) To create a sterically hindered BIM peptide (hBIM), two methyl groups were introduced by substituting the C-terminal cysteine (Cys) residue with pencillamine (Pen). **(B)** A diblock copolymer was synthesized for intracellular peptide delivery. The first block contains biocompatible PEG units for stability and shielding, biotin for binding to antibody-streptavidin conjugates, and pyridyl disulfide (PDS) groups for conjugation to peptide. The second block consists of diethylaminoethyl methacrylate (DEAEMA) and butyl methacrylate (BMA), a pH-responsive endosomolytic formulation. **(C)** The diblock copolymers assemble into micelles in aqueous solution at pH 7.0-7.4. **(D)** Hindered BIM (hBIM) is conjugated to the polymer via disulfide exchange.

improving the circulation stability of the polymer-peptide conjugates will be critical for increasing peptide delivery into tumors and realizing the full potential of BIM and other therapeutic peptides.

One strategy for enhancing disulfide bond stability is steric hindrance. In antibody-drug conjugates, adding methyl groups onto the carbon atoms adjacent to a disulfide linkage decreased

bond sensitivity to reduction[5-7]. Furthermore, the degree of chemical stability varied directly with the number of methyl substituents (1-4) or the degree of steric interference[8].

The objective of this work was to employ steric hindrance to enhance the stability of polymer-BIM conjugates. Two methyl groups were introduced onto the carbon adjacent to the peptide's sulfhydryl group by substituting the C-terminal cysteine residue for the derivative penicillamine (**Figure 3.1A**). The resulting sterically hindered BIM peptide (hBIM) was conjugated by disulfide exchange to a diblock copolymer designed for intracellular peptide delivery (**Figure 3.1B-D**). The first polymer blocked contained the thiol-reactive monomer pyridyl disulfide methacrylate (pyrSMA), a biotin-containing monomer for binding to cancer-specific antibody-streptavidin conjugates, and polyethylene glycol units for biocompatibility and stability. The second polymer block was composed of a pH-responsive formulation that drives micelle formation at physiological pH and destabilizes membranes at the acidic pH values found within endosomes. A polymer containing pyridyl disulfide units hindered by two additional methyl groups was also investigated. However, hindered polymer could not practically be conjugated to the hindered peptide due to a high degree of steric hindrance. Consequently, polymer-hBIM conjugates hindered by two peptide-side methyl groups were selected for further investigation both *in vitro* and in a mouse xenograft model of B-cell lymphoma.

3.2 Materials and Methods

3.2.1 Peptide Synthesis

FMOC protected (L) amino acids (EMD Millipore) and FMOC protected pencillamine (Fmoc-Pen(Trt)-OH, AnaSpec) were used to synthesize BIM, hindered BIM (hBIM), and BIM L62E peptides with the following sequences: MRPEIWIAQELRRIGDEFNAC (BIM), MRPEIWIAQELRRIGDEFNAPen (hBIM), and MRPEIWIAQEERRIGDEFNAC (BIM L62E). Peptides were synthesized on a solid support (rink amide MBHA resin (100-200 mesh), EMD Millipore) using standard FMOC chemistry and an automated PS3 peptide synthesizer (Protein Technologies). Following synthesis, peptides were deprotected and cleaved from the resin by treatment with trifluoroacetic acid/triisopropylsilane/H_2O/1,2-ethanedithiol (95:2:2:1, v/v/v/v) for 4 hours and precipitated in cold ether/hexane (6:4, v/v). Crude peptide precipitates were purified by reverse phase high performance liquid chromatography (RP-HPLC) on a Jupiter 5 μm C18 300Å column (Phenomenx) with an Agilent 1260 HPLC. Ion trap mass spectrometry with electrospray (Bruker Esquire) was used to confirm the molecular weights of the purified peptides.

3.2.2 Synthesis of Pyridyl Disulfide Monomers.

3.2.2.1 Synthesis of pyrSMA.

N-hydroxysuccinimide (NHS, 4.89 g, 0.0425 mol) was added to mono-2 (methacryloyloxy)ethyl succinate) (SMA, 8.9 g, 0.0387 mol) dissolved in chloroform (300 mL) and stirred under N_2 for 30 minutes at room temperature followed by 30 minutes at 0 ^{o}C. Next, N,N'-dicyclohexyl carbodimide (DCC, 9.57 g, 0.0464 mol) and 4-

(dimethylamino)pyridine (66 mg) were added to the solution and allowed to react for 1 h at 0 ^{o}C followed by 22 h at room temperature under nitrogen atmosphere. Following the reaction, dicyclhexylurea precipitate was filtered twice. A solution of of 2-pyridyldithiolethylamine hydrochloride (1.0 g, 0.0045 mol) and Et3N (1.13 g, 0.0112 mol) was prepared by stirring for 30 min at 0 ^{o}C, after which the NHS-activated SMA (2.2 g, 0.0067 mol) in chloroform (65 mL) was added drop wise over the course of an hour and allowed to react overnight at room temperature. The reaction solution was washed with 150 mL of H_20 3X in a separating funnel. Organic extracts were washed with brine, dried over Na_2SO_4, filtered, and concentrated under vacuum. Column chromatography was employed to purify the crude mixture, yielding 1.62 g of pure product (yield = 60.5%).

3.2.2.2 Synthesis of sterically hindered pyrSMA.

First, 2-(Pyridyldithio)-2-methyl-propylamine Hydrochloride was synthesized. 2,2-dipyridyl disulfide (5.0 g, 22.69 mmol) was dissolved in 40 mL methanol and 1.8 mL glacial acetic acid. The solution was added to a solution of 1-amino-2-methyl-2-propanethiol hydrochloride (1.6 g, 11.30 mmol) in 20 mL methanol over 30 minutes. The reaction was stirred under N_2 for 40 h at room temperature and then concentrated under reduced pressure to give approximately 10 mL volume. The oily yellow product was precipitated by the addition of 100 mL cold ether and the precipitate was again purified by redissolving in 20 mL methanol and precipitating with 100 mL cold ether (4 times). Yield = 2.07 g (72.9 %). Next, to synthesize hindered pyrSMA monomer, mono-2-(methacryloyloxy)ethyl succinate (SMA) 1.84 g (8 mmol) in 50 mL CH_2Cl_2 was first

cooled in an ice bath. To this solution, N-hydroxysuccinimide 943 mg (8.2 mmol) and N-N'- dicyclohexylcarbodimide 1.73 g (8.4 mmol) were added. After 10 min, the ice bath was removed and the reaction mixture was stirred at room temperature for 16 h. The byproduct dicyclohexylurea was filtered off, and the filtrate containing activated SMA-NHS ester was directly added to a stirred solution of 2-(pyridyldithio)-2-methyl-propylamine hydrochloride 1.88 g (7.5 mmol) and N,N- diisopropylethylamine 5.25 mL (30 mmol) in 80 mL CH_2Cl_2 at 0 0C. After 10 min, the reaction mixture was warmed to room temperature and stirred for 5h. Solvent was evaporated under reduced pressure and the residue obtained was diluted with 200 mL ethyl acetate. The organic phase was washed with water (2 X 100 mL), dried over anhydrous sodium sulfate and concentrated under reduced pressure. The crude product was purified by silica gel column chromatography using 75 % ethyl acetate in hexane. Overall yield for two steps: 2.85 g (89.2 %).

3.2.3 RAFT Synthesis of Diblock Copolymers

First a macroCTA consisting of N,N-diethylaminoethyl methacrylate (DEAEMA) and butyl methacrylate (BMA) was polymerized under nitrogen atmosphere in dioxane (50 wt% monomer) at 70 °C for 6 hours using 4-cyanopentanoic acid dithiobenzoate (CTP) as the chain transfer agent (CTA) and azobis(4-cyanopentanoic acid) (ABCVA) as the radical initiator. The molar composition of the reaction feed was 60% DEAEMA and 40% BMA, and the initial monomer ($[M]_o$) to CTA ($[CTA]_o$) to initiator ($[I]_o$) ratio was 200:1:0.1. The resulting macroCTA, poly[(DEAEMA)-co-(BMA)], was purified by dialysis in acetone for 48 hours, followed by dialysis in water for 24 hours, and dried by lyophilization. The macroCTA was then employed for

block copolymerization of 300 Da poly(ethylene glycol) methyl ether methacrylate ($PEGMA_{300}$) and pyridyl disulfide methacrylate (pyrSMA). Two different polymers were synthesized using pyrSMA synthesized with or without two methyl groups hindering the pyridyl disulfide. These polymers were abbreviated hindered Pol300 (hPol300) or Pol300, respectively. The block copolymerizations were conducted for 24 hours at 70 °C under nitrogen atmosphere in an equal by volume mixture of dimethyl sulfoxide (DMSO) and dioxane (20 wt% monomer and macroCTA). The molar composition of the monomer feed was 90% $PEGMA_{300}$ and 10% pyrSMA, and the $[M]_o$:$[mCTA]_o$:$[I]_o$ ratio was 50:1:0.1. The resulting diblock copolymers were precipitated in petroleum ether, redissolved in acetone, and reprecipitated 4X. The polymers were then dialyzed in acetone for 48 hours, precipitated once more in petroleum ether, vacuum dried and lyophilized.

For in vivo experiments, an equivalent polymer was synthesized containing PEGMA monomers of molecular weight 950 Da (Pol950) as previously reported[1]. For macroCTA synthesis, PEGMA (80 mol%), pyrSMA (10 mol%), and biotin hydroxyl ethyl methacrylate (bioHEMA) (10 mol%) were copolymerized under nitrogen atmosphere in DMSO (20 wt% monomer) at 70 °C for 18 hours using 4-cyanopentanoic acid dithiobenzoate (CTP) as the chain transfer agent (CTA) and azobis(4-cyanopentanoic acid) (ABCVA) as the radical initiator. The initial monomer ($[M]_o$) to CTA ($[CTA]_o$) to initiator ($[I]_o$) ratio was 25:1:0.1. Following synthesis, the polymer was precipitated in diethyl ether, dissolved in acetone and reprecipitated 6 times before being dried by lyophilization. The macroCTA was then employed for block copolymerization of N,N-diethylaminoethyl methacrylate (DEAEMA) and butyl methacrylate (BMA) at a molar feed ratio of 60:40. Block copolymerization was conducted for 8 hours at 70 °C under nitrogen atmosphere in 1,4-dioxane (50 wt% monomer). The $[M]_o$:$[mCTA]_o$:$[I]_o$ ratio was 200:1:0.1. The resulting diblock copolymer was precipitated 4 times in petroleum ether and lyophilized.

3.2.4 Polymer Characterization by Gel Permeation Chromatography (GPC), 1H-NMR and RP-HPLC

To measure the number average molecular weights (M_n) and polydispersities (PDIs) of the polymers, GPC was conducted using Tosoh SEC TSK GEL α-3000 and α-4000 columns (Tosoh Bioscience), a 1200 Series liquid chromatography system (Agilent), and a miniDAWN TREOS three-angle light scattering instrument with an Optilab TrEX refractive index detector (Wyatt Technology). The mobile phase was 0.1 wt% lithium bromide in HPLC-grade N,N-dimethylformamide at 60 °C and a flow rate of 1 mL/min. The compositions of the macroCTA and diblock copolymers were confirmed by ^{1}H-NMR spectroscopy (Bruker avance DRX 499) in $CDCL_3$.

3.2.5 Formulation of Polymer Micelles

Aqueous polymer solutions were prepared by first dissolving the polymer in ethanol at 100 mg/mL followed by rapid dilution into phosphate buffer saline (PBS) to a concentration of 10 mg/mL. Absorbance at 290 nm was measured to determine polymer extinction coefficients. Ethanol was removed by centrifugal dialysis (Amicon Ultra, 5 mL, 3K MWCO, Millipore) in phosphate buffer saline (PBS), and final polymer concentrations were determined spectrophotometrically.

3.2.6 Formulation of Polymer-peptide Conjugates

BIM, hBIM or BIM L62E peptides were conjugated to the PDS functionalities of the polymer micelles. Concentrated (0.01 M) peptide stocks in DMSO were added to polymer

solutions (500 μM) in PBS and incubated at room temperature overnight. Peptide to polymer rations of 2:1, 1:1, and 1:2 were investigated. Conjugation was quantified by spectrophotometric detection of 2-pyridinethione (343 nm, $\varepsilon = 8{,}080\ M^{-1}cm^{-1}$) released from the polymer via disulfide exchange. Reversible conjugation was further confirmed by SDS-PAGE analysis of conjugates (8-16% Tris-Glycine Mini Protein Gels (Bio-Rad), 5 μg peptide per well) in the presence and absence of 10-fold excess TCEP. Conjugation of hBIM to the hindered version of the polymer was also attempted in methanol at similar peptide and polymer concentrations.

3.2.7 Reduction of Polymer-peptide Conjugates by Dithiotheitol (DTT)

Polymer-peptide conjugates were formulated in a pH 5.8 phosphate buffer (100 mM phosphate, 150 mM NaCl) at a concentration of 50 μM. Reduction reactions were initiated by addition of 10 mM DTT. At various time points, aliquots were removed from the reaction solutions and immediately analyzed by RP-HPLC. Percent conjugate reduction (i.e. peptide release) was reported relative to a free peptide standard. Pseudo first-order rate constants were calculated by nonlinear regression fitting of percent peptide release (Y) versus time (x) to an exponential one-phase association equation:

$$Y = Y_0 + Y_{plateau}*(1-\exp(-K*x))$$

Analysis was conducted on GraphPad Prism software using the following constraints: $Y_o = 0$ and $Y_{plateau} = 100$.

3.2.8 Stability of Polymer-peptide Conjugates in Human Serum

Polymer-peptide conjugates (4 mM, PBS) were added to human serum for a final concentration of 400 μM and incubated at 37 °C. At various time points, 40 μL aliquots of the

mixture were withdrawn and 40 μL of acetonitrile was added to precipitate serum proteins and extract peptide products. Precipitated solutions were centrifuged at 13,000 rpm for 10 min and supernatants were analyzed by MALDI-TOF MS using a Bruker Autoflex II.

3.2.9 Sizing of Micelles by Dynamic Light Scattering

The hydrodynamic diameters of the polymer-peptide conjugates were determined by dynamic light scattering (DLS) using a Nanoseries Zetasizer (Malvern). Measurements were taken of 0.25 mg/mL polymer solutions in phosphate buffers (100 mM phosphate, 150 mM NaCl) of varying pH (5.8-7.4). Mean particle diameter was reported as the number average $\pm$ the half width of three independently prepared formulations.

3.2.10 pH-responsive Hemolysis Assay

The ability of the polymers to induce pH-dependent membrane destabilization was assessed via a red blood cell hemolysis. Briefly, polymer-peptide conjugates (20 μg polymer/mL) were incubated with human red blood cells in a phosphate buffers (100 mM phosphate, 150 mM NaCl) of varying pH (5.8-7.4) for 1 hour at 37 °C. Percent red blood cell lysis (hemolysis) was then quantified by measuring hemoglobin release (abs 541 nm) relative to a 100% lysis control (0.1% Triton X-100).

3.2.11 Cell Viability Assay

The cell killing activity of the conjugates was evaluated using the CellTiter 96 Aqueous One Solution Cell Proliferation Assay (MTS) (Promega). SKOV3 cells were plated in a 96-well plate at a density of 7,000 cells per well and allowed to adhere for 24 hours. Cells were then

incubated with 100 μL of polymer solution at concentrations ranging from 0-10 μM for 48 hours. At 48 hours, cell viability was quantified by adding 20 μL of [3-(4,5-dimethylthiazol-2-yl)-5-(3-carboxymethoxyphenyl)-2-(4-sulfophenyl)-2H-tetrazolium (MTS) reagent to each well, incubating for 30 minutes, and measuring the absorbance at 490 nm on a plate reader.

3.2.12 Formation of Tumor Xenografts

Animal experiments were conducted according to the Guide for the Care and Use of Laboratory Animals of the National Institutes of Health and protocols approved by the Fred Hutchinson Cancer Research Center Institutional Animal Care and Use Committee (FHCRC IACUC). Every attempt was made to minimize animal suffering. Female BALC/c nu/nu mice (Harlan Sprague Dawley) aged 6-8 weeks were injected subcutaneously in the right flank with $1x10^7$ granta-519 cells to form solid human xenografts. Mice were fed a biotin-free diet (Harlan Taklad) for 5-7 days prior to injection with antibody-streptavidin (Ab-SA) conjugates. Mice were euthanized by carbon dioxide overexposure in accordance with the American Veterinary Medical Association (AVMA) guidelines.

3.2.13 Radiolabeling of Polymer-peptide Conjugates

For investigating pharmacokinetics and biodistribution, Pol950 was labeled with ^{3}H and the BIM and hBIM peptides were labeled with ^{14}C. For polymer labeling, the R group of the polymer chain transfer agent was reacted in DMF with a 10 molar excess of NHS and DCC (2 hours, 25 °C), after which NHS-functionalized polymer was isolated by precipitation in petroleum ether and lyophilized. The ^{3}H label, propylamine n-[2,3-3H] hydrochloride (30-60 Ci/mmol, American Radiolabeled Chemicals), was dissolved in anhydrous DMF, treated with a 500-fold

excess of DIEA (2 hour, 25 °C), and then reacted for two hours with 50-fold excess NHS-Pol950 dissolved in DCM. Unreacted propylamine was removed by a 2 hour purge with air, and labeled polymer was precipitated in petroleum ether and vacuum dried for 48 hours. For peptide labeling, BIM and hBIM were reacted with a 3-fold excess of acetic anhydride [1-14C] (50-60 mCi/mmol, American Radiolabeled Chemicals) in anhydrous DMF for 2 hours at room temperature. Labeled peptides were precipitated in ether/hexane (60/40, v/v) and vacuum dried for 48 hours.

3.2.14 Pharmacokinetics and Biodistribution of Polymer-peptide Conjugates

Radiolabled polymer and peptides were conjugated as described previously. To incorporate antibody targeting, αCD22-streptavidin (SA) was mixed with conjugate solutions and incubated for 2 hours to permit biotin-streptavidin binding. Groups of 5 mice were injected via tail vein with either [^{3}H]Pol950-[^{14}C]BIM, αCD22-[^{3}H]Pol950-[^{14}C]BIM, or αCD22-[^{3}H]Pol950-[^{14}C]hBIM conjugates. Per mouse doses of polymer, peptide, and antibody were 90 nmoles, 65 nmoles, and 1.4 nmoles, respectively. Blood was drawn via retro-orbital bleed (10 uL, n=3) at 5m, 15m, 30m, 1h, 2h, 4h, 8h, and 24h, and immediately solubilized in Solvable (Perkin Elmer). At 24 hours, mice were sacrificed and tissues (tumors, lung, liver, spleen, stomach, kidney, small intestine, large intestines and muscle) were harvested, weighed, and homogenized in solvable as per the manufacturer's instructions (Perkin Elmer). Homogenized and decolored samples were diluted in ULTIMA GOLD (Perkin Elmer), vortexed, equilibrated overnight at room temperature, and read in a scintillation counter. Biodistribution measurements were reported as % injected dose per gram of tissue (%ID/g). Pharmacokinetic data were fit to a 2-compartmental nonlinear decay model using GraphPad Prism software.

3.3. Results

3.3.1 Synthesis of Sterically Hindered Disulfide-linked Polymer-BIM Conjugates

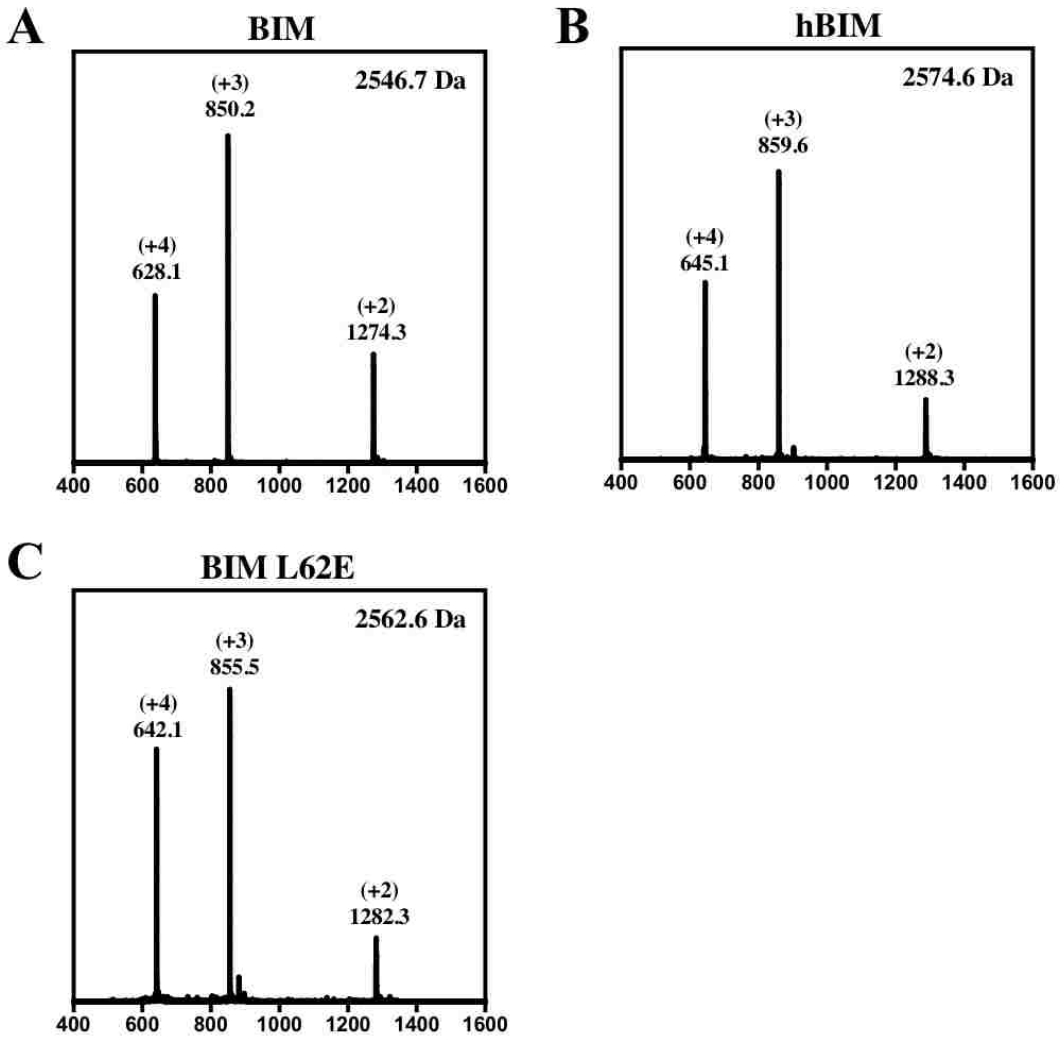

Figure 3.2. Mass spectra of (A) BIM, (B) hBIM, and (C) BIM L62E. Peptides were synthesized by FMOC solid phase synthesis and purified by RP-HPLC.

3.3.1.1 Peptide and Polymer Synthesis and Characterization

It was the objective of this chapter to sterically block disulfide bond reduction by incorporating methyl groups onto the carbon atoms adjacent to the disulfide bond. Two

such methyl groups were added to the BIM peptide by substituting BIM's C-terminal cysteine residue with pencillamine during peptide synthesis. Mass spectrometry (**Figure 3.2**) of BIM and the hindered BIM (hBIM) peptide demonstrated a 28 Da difference in mass corresponding to two hydrogen to methyl substitutions. As a negative control, a nonactive peptide (BIM L62E) was synthesized by a single amino acid substitution within the BIM motif.

Two methyl groups were also incorporated into the polymeric micelle system previously developed for intracellular BIM delivery. The described diblock copolymer consists of a pH-responsive hydrophobic block of DEAEMA and BMA, and a hydrophilic block containing $PEGMA_{300}$, bioHEMA, and pyrdiyl disulfide methacrylate (pyrSMA) (**Figure 3.3 A**) for conjugation to peptide via disulfide exchange. In this work a new pyrSMA monomer was synthesized containing two methyl groups on the carbon atom adjacent to the pyridyl disulfide. The ^{1}H-NMR spectrum of the hindered pyrSMA monomer is shown in **Figure 3.3B**. Two equivalent polymers were then synthesized with either the original pyrSMA or hindered pyrSMA monomer. These polymers were termed Pol300 or hindered Pol300 (hPol300), respectively. Targeted and experimentally determined characteristics of Pol300 and hPol300 are summarized in **Table 3.1**, and GPC and 1H-NMR polymer characterization data are included in **Figure 3.4.** The molecular weights and PDIs of Pol300 and hPol300 were determined to be 31,900 Da and 32,500 Da, and 1.09 and 1.11, respectively. The pyridyl disulfide content of the polymers was determined by measuring pyridine-2-thione absorbance (343 nm, $\varepsilon = 8080\ M^{-1}cm^{-1}$) following polymer reduction with a 20-fold excess of the reducing agent TCEP. Pol300 and hPol300 were found to contain 2 and 2.1 PDS groups per polymer chain, respectively.

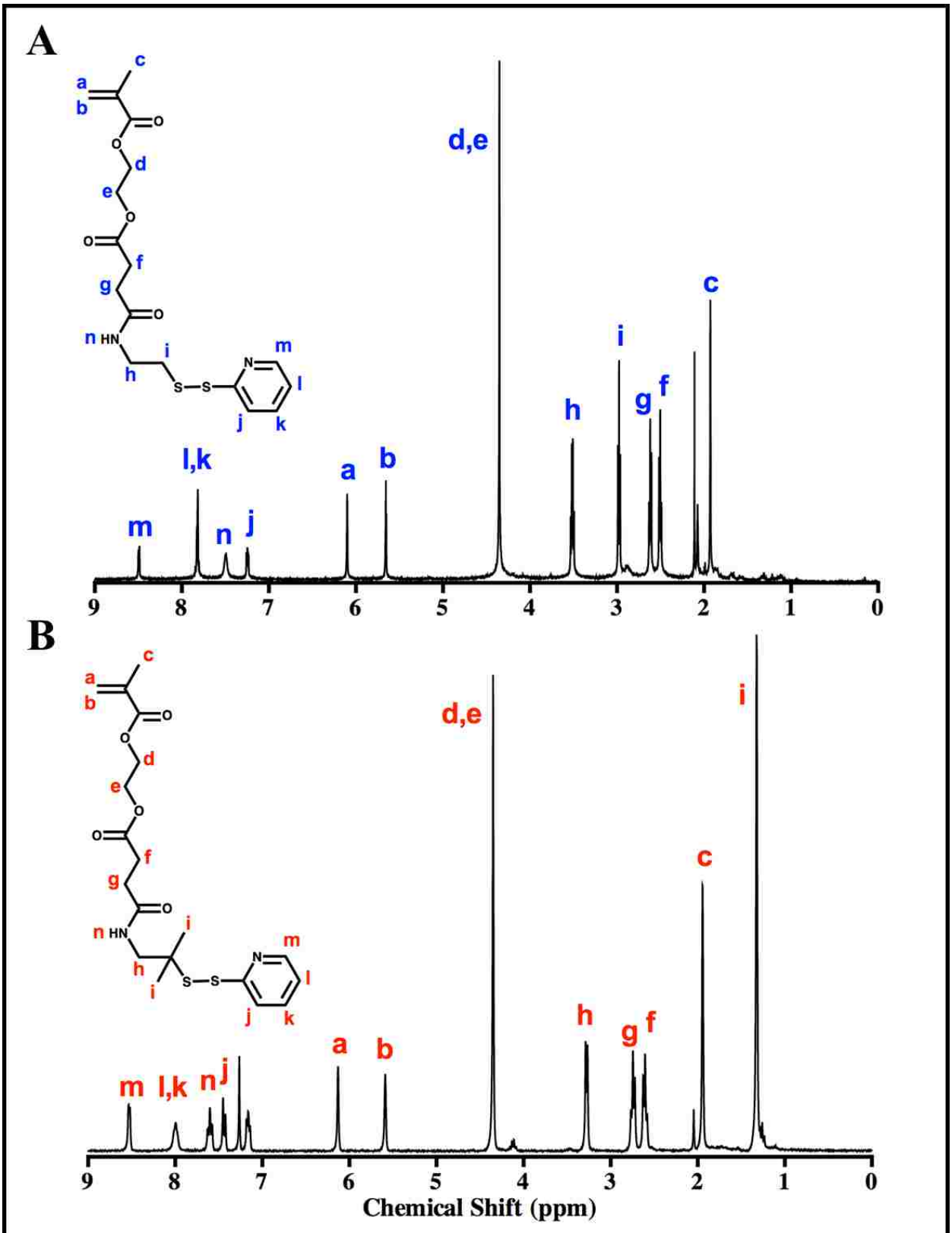

Figure 3.4. ^{1}H-NMR spectra of the (A) pyrSMA and (B) hindered pyrSMA monomers in $CDCl_3$ at 300 MHz.

Polymer	macroCTA					Diblock Copolymer				
	DP	% feed / comp		M_n	PDI	DP	% feed / comp		M_n	PDI
		DEAEMA	BMA				$PEGMA_{300}$	pyrSMA		
Pol300	200	60 / 56	40 / 44	16,800	1.05	50	88/96	10/4	31,900	1.09
hPol300	200	60 / 56	40 / 44	16,800	1.05	50	88/96	10/4	32,500	1.11

Table 3.1. Characterization of diblock copolymers containing unhindered (Pol300) or hindered (hPol300) pyridyl disulfide groups. A pH-responsive poly[(DEAEMA)-co-(BMA)] macroCTA was synthesized with a targeted composition of 60% DEAEMA and 40% BMA. The macroCTA was then employed for block copolymerization of $PEGMA_{300}$, bioHEMA, and pyrSMA monomer. Two diblock copolymers were synthesized using pyrSMA either with or without two methyl groups on the carbon atom adjacent to the disulfide bond. Polymer molecular weights (M_ns) and polydispersities (PDIs) were determined by GPC, molar compositions were determined by ^{1}H-NMR, and PDS content was determined by measuring pyridine-2-thione absorbance (343 nm) following reduction with 100X TCEP.

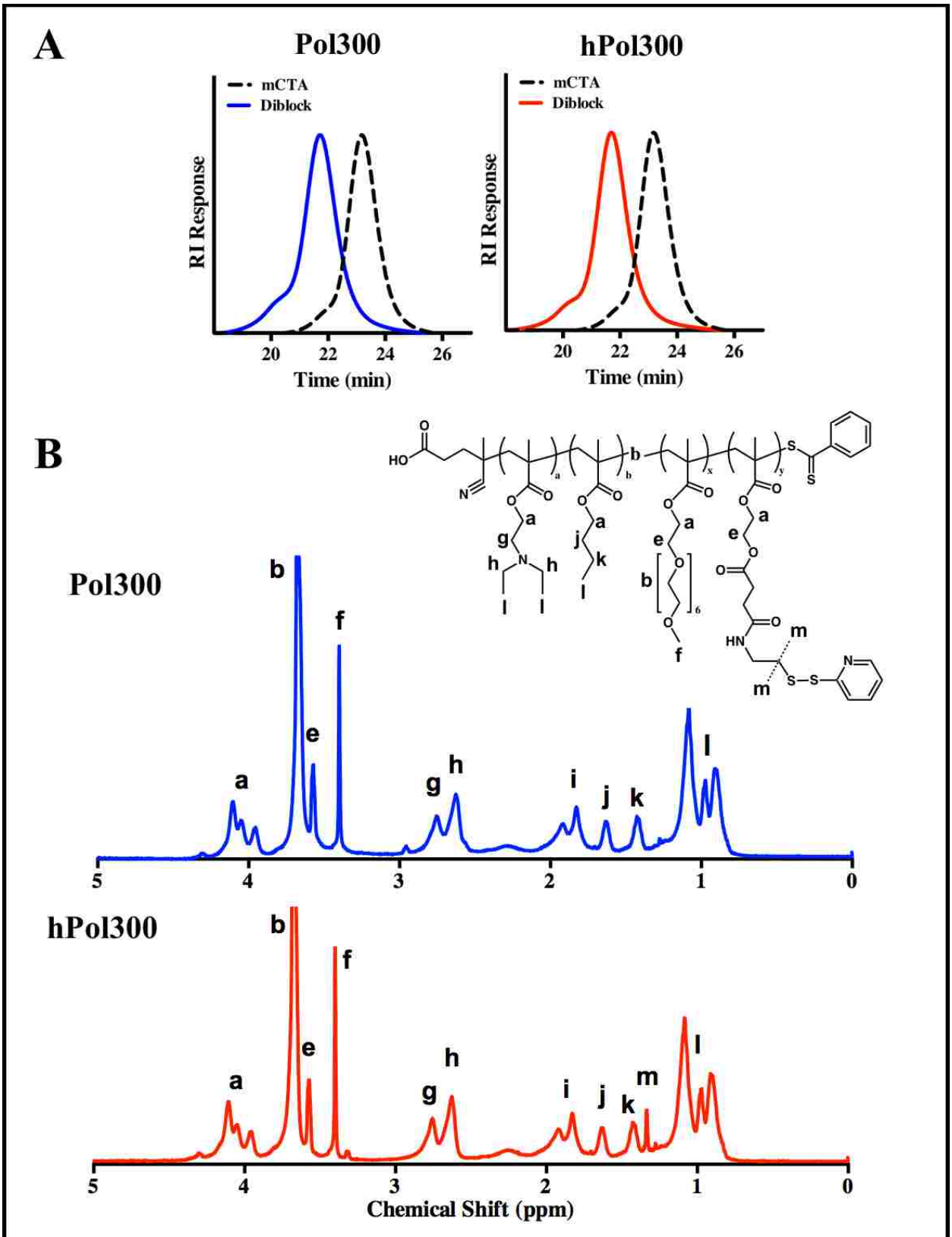

Figure 3.4. (A) GPC traces and (B) ^{1}H-NMR spectra of diblock copolymer synthesized with $PEGMA_{300}$ and unhindered (Pol300) or hindered pyrSMA monomer (hPol300).

3.3.1.2 Polymer-peptide Conjugation

The peptides were conjugated to the polymers via disulfide exchange as illustrated in **Figure 3.1D**. Reactions were conducted in PBS at various peptide:polymer ratios (2:1, 1:1, and 1:2) and conjugation was quantified by spectrophotometric measurement of 2-pyridinethione release (**Figure 3.5A)**. SDS-PAGE analysis of 1:1 peptide:polymer conjugates further confirmed conjugation (**Figure 3.5B**). Both BIM and hBIM conjugated to unhindered Pol300 with high efficiency and, unexpectedly, hBIM was found to conjugate to an even higher degree than unhindered BIM. 77-81% of hBIM reacted with the Pol300's PDS groups in comparison to 54-61% of BIM. This is likely a result of hBIM's decreased propensity for peptide dimer formation. HPLC analysis found that 80% of BIM peptides dimerized following a 24 hour incubation in water, while 100% of hBIM remained unimeric (data not shown). Unfortunately, introducing steric hindrance into the polymer dramatically decreased peptide conjugation. Unhindered BIM conjugated to hPol300 with much lower efficiency (28-35%) than to Pol300, and hBIM did not conjugate to hPol300 at all under aqueous conditions. We also attempted to conjugate hBIM to hPol300 in organic solvent (methanol) without success. It is likely that the high steric interference of four methyl groups prevents conjugation. As a result, Pol300-hBIM conjugates hindered by two peptide-side methyl groups were selected for further evaluation.

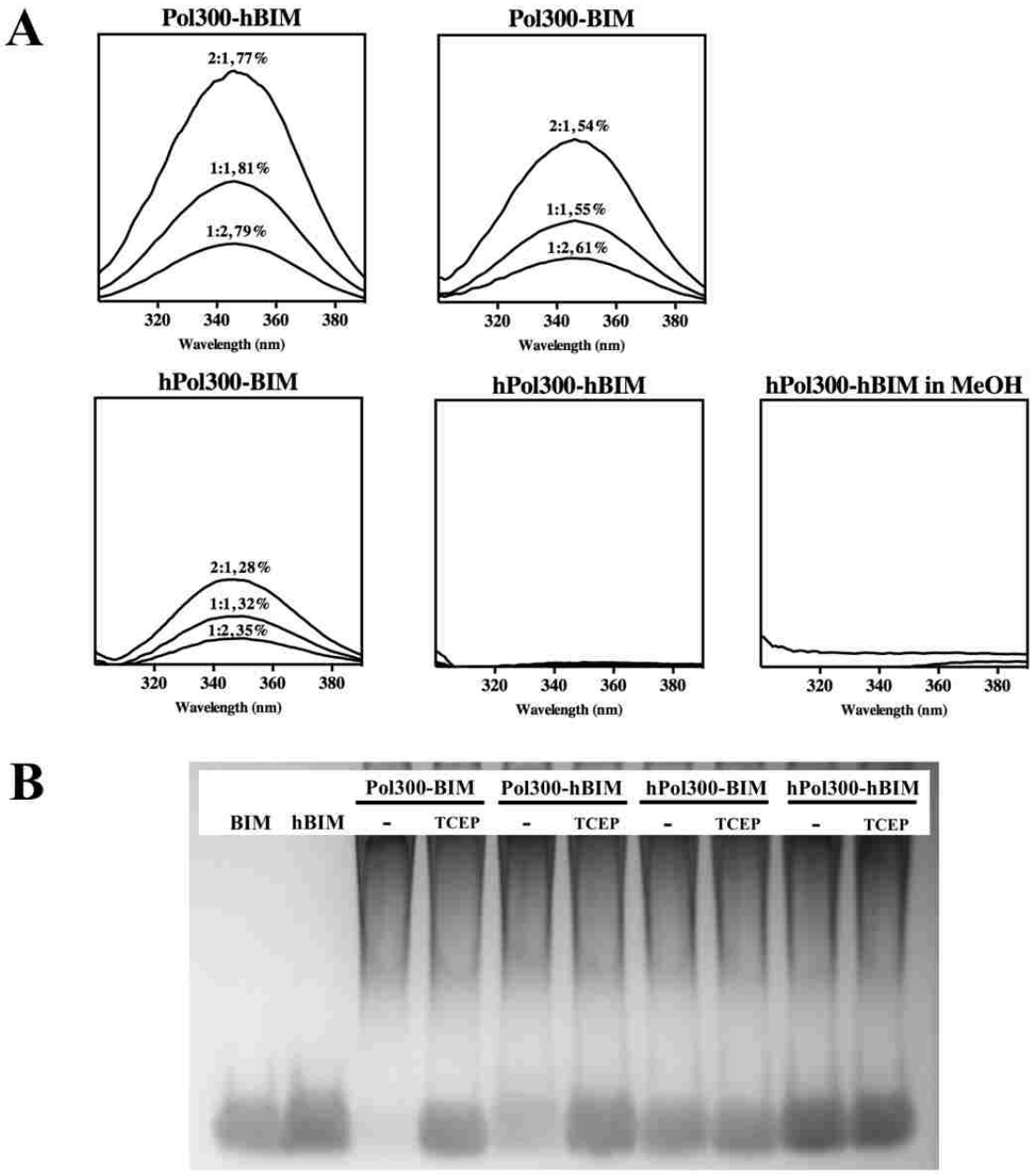

Figure 3.5. Stericially hindered BIM (hBIM) conjugates to unhindered Pol300 with high efficiency, but does not conjugate to hindered polymer (hPol300). (A) BIM and hBIM were allowed to react in PBS with Pol300 and hPol300 at peptide:polymer ratios of 2:1, 1:1, and 1:2. Peptide conjugation was quantified by pyridine-2-thione release (abs 343 nm). At all ratios, hBIM conjugated to Pol300 with higher efficiency than BIM. However, steric hindrance on the polymer side of the disulfide bond dramatically reduced peptide conjugation efficiency, with 0% conjugation observed for hBIM at all peptide:polymer ratios. hPol300-hBIM conjugation was also unsuccessful in methanol (MeOH) **(B)** To confirm reversible disulfide conjugation, 1:1 peptide:polymer conjugates were analyzed by protein gel electrophoresis in the presence and absence of 20X TCEP.

3.3.2 DTT Reduction of Disulfide-linked Polymer-peptide Conjugates

The effect of steric hindrance on disulfide linker stability was initially investigated by incubating Pol300-BIM and Pol300-hBIM conjugates (50 μM) with DTT (10 mM) at pH 5.8. At various time points reaction aliquots were removed and immediately analyzed by RP-HPLC. Hindered Pol300-hBIM conjugates reduced at a significantly slower rate than unhindered Pol300-BIM (**Figure 3.6**). The measured pseudo first-order rate constants for peptide release were 0.018 and 0.86 for Pol300-hBIM and Pol300-BIM, respectively. Steric hindrance through the addition of two methyl groups resulted in a measured 4.89-fold increase in bond stability.

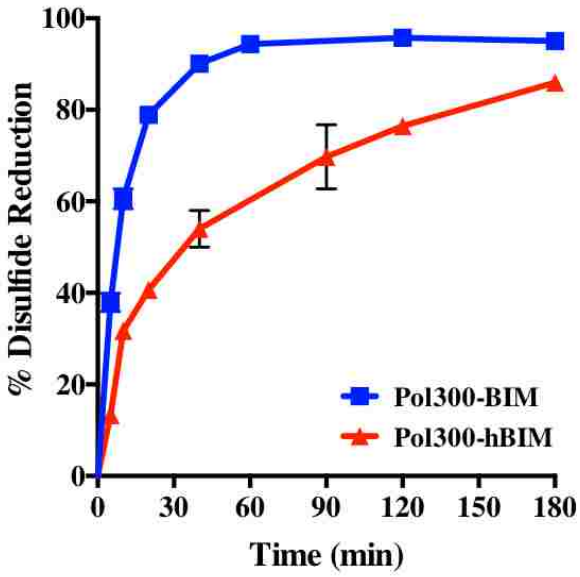

Figure 3.6. Steric hindrance increases disulfide bond stability. Disulfide-linked polymer-peptide conjugates (50 μ M) were incubated with dithiothreitol (10 mM) in phosphate buffer at pH 5.8. RP-HPLC analysis measured percent peptide release overtime relative to a free peptide standard. Pseudo first-order rate constants were determined by nonlinear regression. Conjugates hindered by two peptide-side methyl groups (Pol300-hBIM) exhibited 4.89-fold higher stability relative to unhindered (Pol300-BIM) conjugates.

3.3.3 Stability of Sterically Hindered Polymer-Peptide Conjugates in Human Serum

To investigate the sensitivity of the sterically hindered polymer-peptide linker to reduction in the bloodstream, Pol300-BIM and Pol300-hBIM conjugates were incubated in human serum at 37 °C. At time points ranging from 0 to 6 hours, peptide products were extracted into acetonitrile and analyzed by MALDI-TOF MS. The sterically hindered Pol300-hBIM conjugates demonstrated improved stability over Pol300-BIM conjugates (**Figure 3.7**). hBIM peptide products were not detectable until after 2 hours of incubation, while BIM peptide products were detected as early as 30 minutes. It should be noted, that only modified hBIM and BIM peptides were detected. For BIM (MW = 2547 Da), peaks were detected at 2572 Da (+25 Da) and 2319 (-228 Da). For hBIM (MW = 2575 Da), corresponding peaks were detected at 2600 Da (+25 Da) and 2347 (-228 Da). It cannot be known with certainty what accounts for these peaks. One possibility is that that the larger pair of peaks (2572 Da & 2600 Da) represent BIM and hBIM peptides in which the N-terminal methionine residues have been removed by exopeptidase activity (-131 Da) and the sulfhydryl groups modified with 4-hydroxynonenal (+156 Da). 4-hydroxynonemal is an unsaturated hydroxyalkenal produced by lipid peroxidation that is known to exist extracellularly and react with cysteines[9-11]. In this case, the smaller pair of peaks (2319 Da & 2347 Da) could result from subsequent exopeptidase removal of the next two N-terminal amino acid residues, arginine and proline (-253 Da). Alternatively, the larger pair of peaks might represent complexes with sodium (+23 Da) or sulfhydryl groups modified with cyano (+25 Da). However, in either of these two cases, no explanation could be found for the smaller peaks. It is unlikely that the C-termini of the peptides were removed, as the difference in mass between BIM and hBIM resulting from the two methyls (28 Da) was still manifest. In any case, the sterically hindered disulfide linker was found to offer a significant stability advantage in human serum.

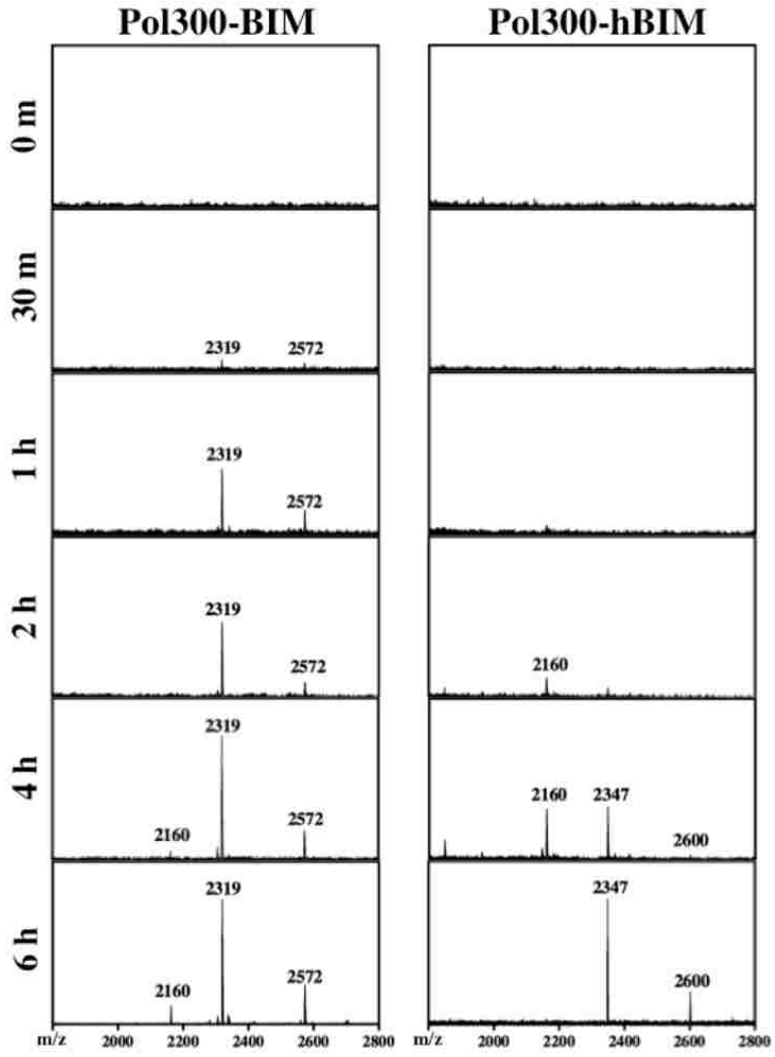

Figure 3.7. Steric hindrance increases conjugate stability in human serum. Polymer-peptide conjugates made with unhindered (Pol300-BIM) and hindered BIM (Pol300-hBIM) were incubated in human serum at 37 °C. At various time points, peptides were extracted into acetonitrile and analyzed by MALDI-TOF MS. BIM peptide products (2319 Da & 2472 Da) were detected at 30 minutes, while the corresponding hBIM peptide peaks (2347 Da & 2600 Da) were only detected at low levels after 2 hours of incubation.

3.3.4 The Activity of Sterically Hindered Polymer-Peptide Conjugates in Ovarian Cancer Cell Cultures

The pH-responsive activity of the polymer-peptide conjugates was confirmed by particle sizing and a red blood cell hemolysis assay. For particle sizing (**Figure 3.8A**), Pol300-BIM, Pol300-hBIM, and Pol300-BIM L62E conjugates were incubated in phosphate buffers of varying pH (7.4-5.8) and hydrodynamic diameters were measured by dynamic light scattering (DLS). At pH 7.4, all conjugates assembled into micelles with diameters of 21-23 nm. As the pH was decreased step-wise to 5.8, the micelles disassembled into unimers with diameters of approximately 6-7 nm.

The corresponding pH-responsive membrane destabilizing activity of the conjugates was demonstrated using a previously developed red cell hemolysis assay (**Figure 3.8B**). Conjugate (polymer conc. = 20 μg/mL) was incubated with red blood cells in buffers of varying pH, and lysis-mediated release of heme (hemolysis) was measured spectrophotometrically (abs 541 nm). All conjugates demonstrated a pH dependent increase in red blood cell lysis, with 0% lysis observed at pH 7.4 and >75% lysis observed at the pHs found in early (6.6) and late endosomes (5.8). These findings confirm the polymer's pH-responsive membrane destabilizing activity and demonstrate that this activity is independent of the nature of the conjugated BIM peptide.

To evaluate the ability of the sterically hindered conjugates to enhance intracellular peptide delivery and activity *in vitro*, SKOV3 cells were treated with Pol300-BIM, Pol300-hBIM, and Pol300-BIM L62E for 48 hours and cell viability was assayed by MTS (**Figure 3.8C**). Both Pol300-BIM and Pol300-hBIM exhibited potent cell-killing activity in comparison to the Pol300-BIM L62E control. Furthermore, the hindered conjugates exhibited slightly better

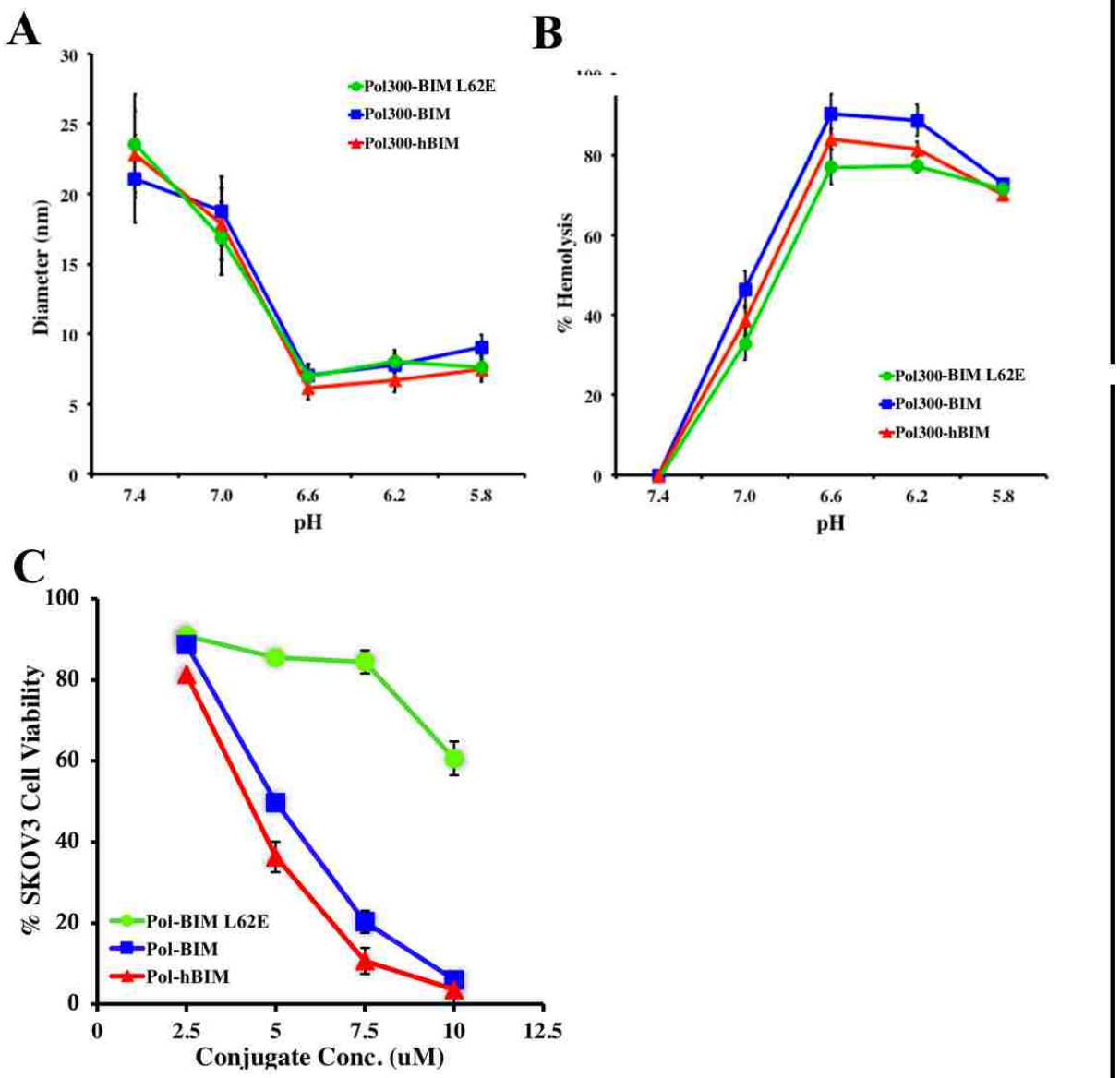

Figure 3.8. Hindered conjugates exhibit greater intracellular peptide delivery and cell-killing activity in ovarian cancer cell cultures. Polymer alone and polymer-peptide conjugates exhibited similar pH-responsive membrane destabilizing activity as demonstrated by **(A)** dynamic light scattering and **(B)** a red blood cell lysis (hemolysis) assay. **(A)** DLS measurements of particle diameters were taken in phosphate buffers of varying pH. At pH 7.4 the conjugates formed micelles of approximately 23 nm diameter, which disassembled into unimers of smaller diameters (6-8 nm) at more acidic pH values. **(B)** Hemolysis demonstrated a corresponding increase in membrane destabilizing activity with decreased pH. Briefly, red blood cells were incubated with conjugates (20 μg/mL polymer) and % heme release was quantified relative to a 0.1% TritonX-100 positive control. **(C)** SKOV3 ovarian cancer cells were treated with 1:1 peptide:polymer conjugates for 48 hours and cell viability was measured by MTS assay. Steric hindrance enhanced BIM-induced cell death.

activity than the unhindered. This is likely due to two advantages offered by steric hindrance: (1) higher polymer-peptide conjugation efficiency, and (2) higher conjugate stability in serum.

3.3.5 Pharmacokinetics and Biodistribution in Mice Bearing B-cell Lymphoma Xenografts

To determine whether increased disulfide stability translates into increased peptide delivery into tumors, a pharmacokinetic and biodistribution study was conducted in mice bearing granta-519 tumors using dual-radiolabeled [^{3}H]polymer-[^{14}C]peptide conjugates. A previously described diblock copolymer synthesized with 950 Da $PEGMA_{950}$ was employed as the delivery vehicle due to its superior circulation properties in comparison to $PEGMA_{300}$. For tumor-specific targeting and uptake, anti-CD22 antibody-streptavidin conjugates were incorporated via biotin-streptavidin binding. Three groups of mice (n=5) were injected intravenously with either [^{3}H]Pol950-[^{14}C]BIM, αCD22-[^{3}H]Pol950-[^{14}C]BIM, or αCD22-[^{3}H]Pol950-[^{14}C]hBIM conjugates. The pharmacokinetics of the polymer and peptides were monitored in the blood over 24 hours. The pharmacokinetic parameters of the polymer (**Figure 3.9A**) were found to be independent of both antibody conjugation and steric hindrance. The Pol950 beta-half lives were 13.21 hr (95% CI: 7.94-39.31), 10.86 hr (95% CI: 7.29-21.24) and 12.00 hr (95% CI: 10.74-27.27) for [^{3}H]Pol950-[^{14}C]BIM, αCD22-[^{3}H]Pol950-[^{14}C]BIM, and αCD22-[^{3}H]Pol950-[^{14}C]hBIM, respectively. In contrast, steric hindrance substantially enhanced the circulation of the peptide (**Figure 3.9B**). The half-lives of BIM with and without antibody targeting were 4.60 hr (95% CI: 4.33-4.91) and 4.39 hr (95% CI: 4.25-4.55). The half-life of sterically hindered hBIM was nearly double at 7.90 hr (95% CI: 7.40-8.48). The blood stability of the disulfide linker was also evaluated by tracking the [^{14}C]peptide:[^{3}H]polymer ratio over time and normalizing to pre-injection (**Figure 3.9C**). It was observed that both ratios dropped over time as the peptide was cleaved off the

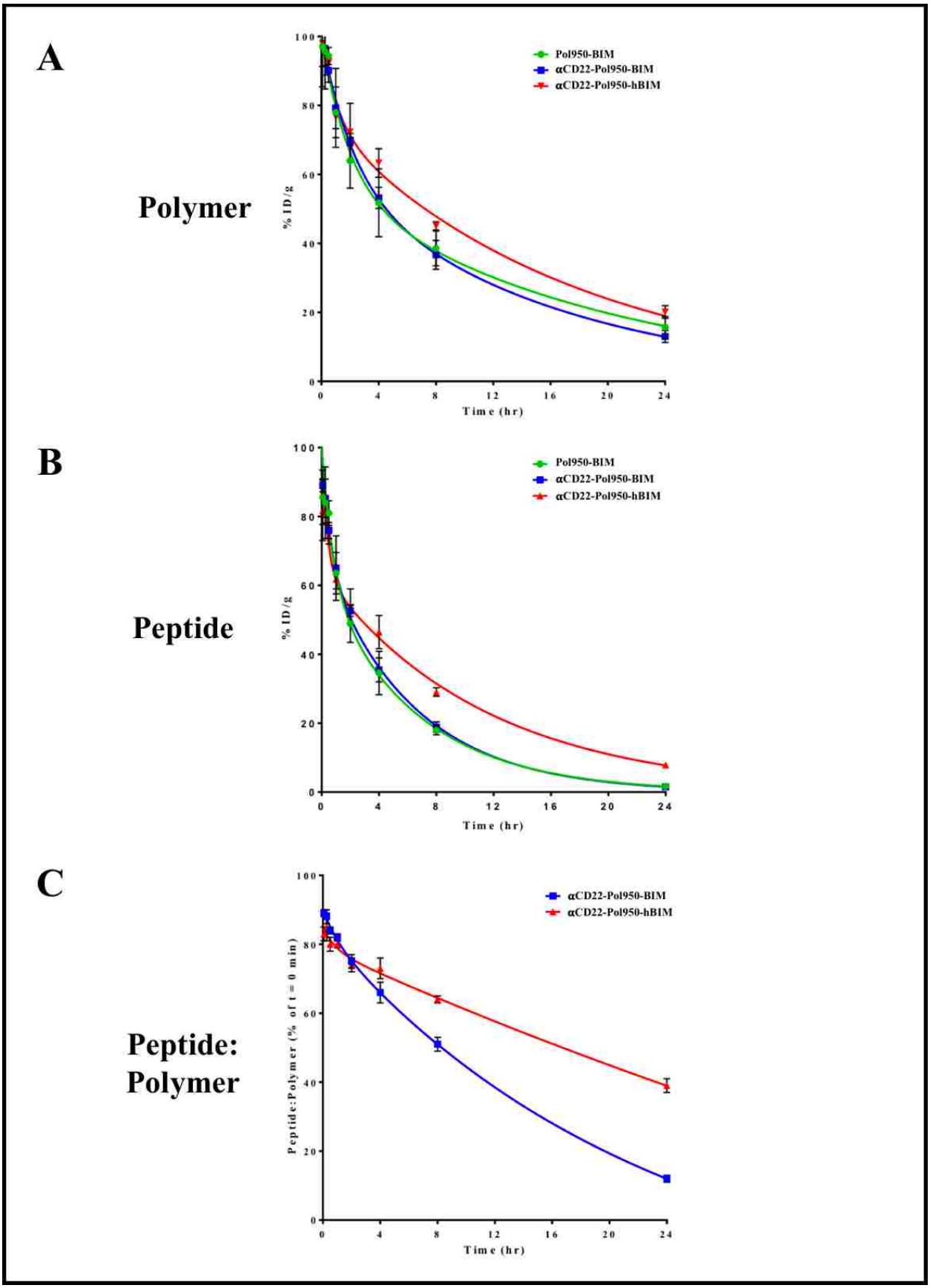
A
Polymer
Pol950-BIM
αCD22-Pol950-BIM
αCD22-Pol950-hBIM
% ID/g
Time (hr)
B
Peptide
Pol950-BIM
αCD22-Pol950-BIM
αCD22-Pol950-hBIM
% ID/g
Time (hr)
C
Peptide:
Polymer
αCD22-Pol950-BIM
αCD22-Pol950-hBIM
Peptide:Polymer (% of t = 0 min)
Time (hr)

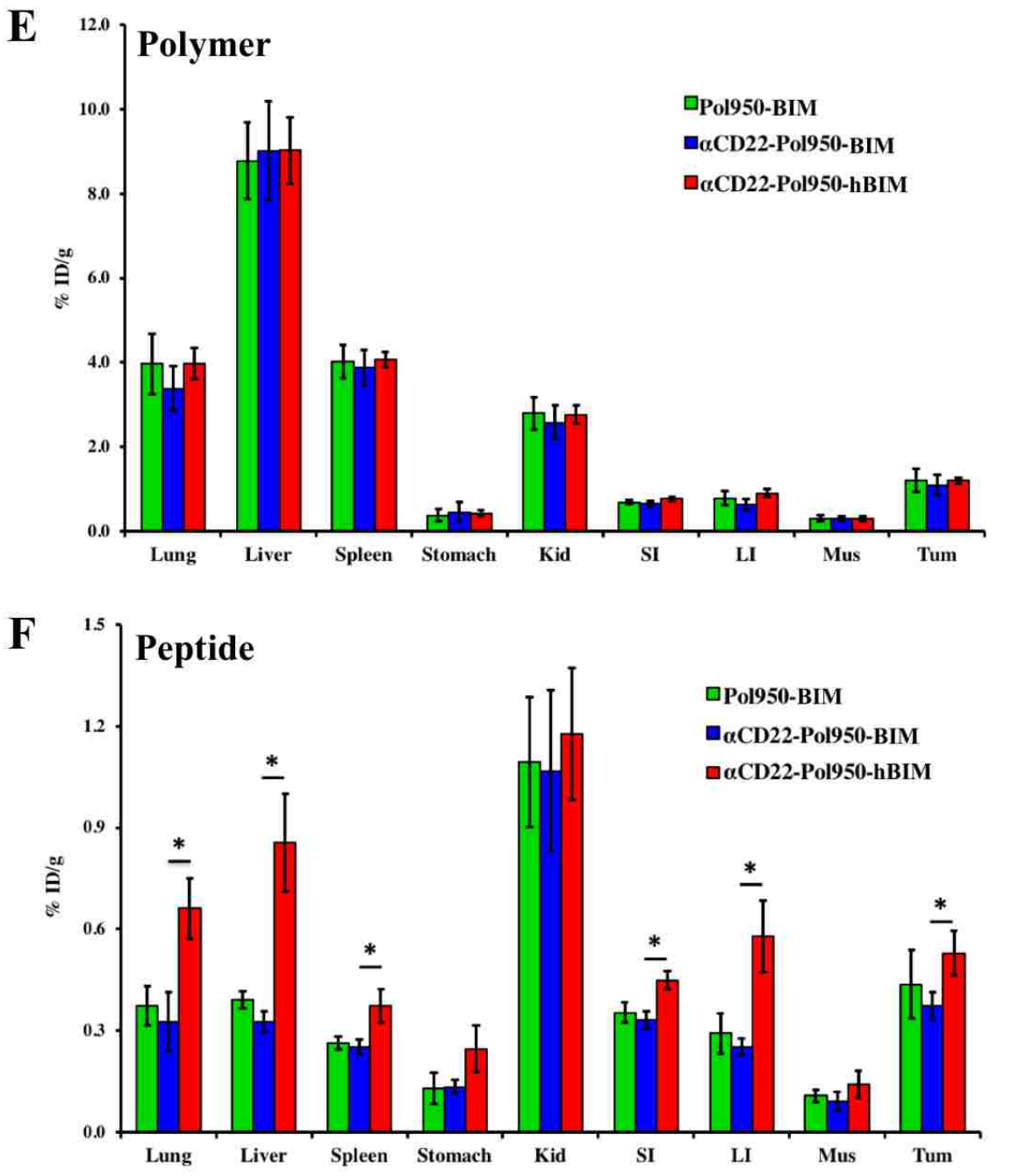

Figure 3.9. Steric hindrance increased peptide half-life and tumor delivery in a B-cell lymphoma xenograft model. Mice (n=5) bearing granta-519 tumors were injected with [^{3}H]Pol950-[^{14}C]BIM, αCD22-[^{3}H]Pol950-[^{14}C]BIM, or αCD22-[^{3}H]Pol950-[^{14}C]hBIM conjugates. The pharmacokinetics of **(A)** ^{3}H-labeled Pol950 and **(B)** ^{14}C-labeled peptide were measured over 24 hours (n=3). Solid lines represent a two compartment open model with $1/y^2$ weighting. **(C)** Disulfide linker stability was measured by tracking the [^{14}C]peptide:[^{3}H]polymer ratio and normalizing to pre-injection. Biodistributions of the **(D)** ^{3}H-labeled Pol950 and **(E)** ^{14}C-labeled peptide were measured at 24 hours.

polymer and cleared from the bloodstream. However, steric hindrance markedly slowed the rate of decrease. After 24 hours, only 12% of BIM was still polymer-conjugated, in comparison to 39% of hBIM.

For biodistribution, 24 hours post-injection the mice were sacrificed and their tissues were harvested, homogenized, and read on a scintillation counter. %ID of polymer/peptide per gram of tissue was calculated for each organ. In all tissues, the amount of polymer did not statistically vary between treatment groups, with approximately 1.09-1.19%/g detected in the tumors (**Figure 3.9D**). Notably, antibody targeting did not increase polymer deposition into tumors. It is likely that passive targeting via enhanced permeability and retention (EPR) is the dominant mechanism of delivery, with αCD22 targeting being important for internalization of the conjugates into tumor cells via receptor-mediated endocytosis.

Steric hindrance resulted in higher levels of peptide detected across all tissues (**Figure 3.9E**). Statistically significant differences between the αCD22-Pol950-BIM and αCD22-Pol950-hBIM conjugates were detected in the lung, liver, spleen, small intestine, large intestine, and tumor. In tumor tissue, the %IDs/g were 0.37 and 0.53 for BIM and hBIM, respectively. These findings are consistent with the enhanced hBIM circulation time reported in the pharmacokinetic data, and are presumably a result of increased tissue exposure.

3.4 Discussion

Before the clinical potential of peptides such as BIM can be realized, unique drug delivery challenges such as poor circulation stability and intracellular delivery must be addressed. Much progress has already been made in developing synthetic carriers to overcome these barriers. Recently, a pH-responsive diblock copolymer conjugated to the BIM through a disulfide linkage demonstrated anti-tumor activity in a B-cell lymphoma xenograft model[1]. To improve on this activity and realize the full potential of this system, it will be important to enhance the stability of the disulfide bond in circulation.

In bioconjugates, the linker is a critical determinant of safety, specificity, and activity. For peptide delivery, the linker must be stable in the blood and cleaved within cancer cells to restore drug activity. Disulfide bonds have proven a popular method of conjugation, as they harness the reductive differential between the intracellular (~10 mM glutathione) and extracellular (~10 uM glutathione) spaces for preferential drug release inside cells[4]. This differential is further augmented in tumor cells, where irregular blood flow and hypoxia stimulate intracellular reductive processes[13]. However, low concentrations of reductive agents (cysteine, glutathione) are also present in the blood, and disulfide cleavage is known to occur in systems with long circulation times[4]. A pharmacokinetic study of disulfide-linked polymer-BIM conjugates showed premature drug release to be a significant problem[1]. The initial peptide to polymer ratio in the blood dropped precipitously over time as peptide was released from the carrier and rapidly cleared from circulation. This must be prevented if the full potential of polymer-BIM conjugates is to be realized.

Introducing groups such as methyls and phenyls onto the carbon atoms adjacent to disulfide bonds decreases accessibility to reducing agents. This technique has been employed previously to

enhance the circulation half-lives and anti-tumor activities of antibody-toxin and antibody-drug conjugates[5-8]. This chapter aimed to increase bond stability through steric hindrance. Two approaches were taken for introducing methyl groups. First, two methyls were incorporated onto the geminal carbon on the peptide side of the disulfide bond by substituting BIM's C-terminal cysteine with the derivative pencillamine. Pencillamine is distinguished by two additional methyl groups on the carbon adjacent to the sulfhydryl. Second, two methyls was introduced on the polymer-side of the disulfide through the synthesis and polymerization of a hindered-PDS monomer (**Figure 3.3).**

Next, an attempt was made to conjugate the unhindered BIM and hindered BIM (hBIM) peptides to diblock copolymers synthesized with unhindered or hindered pyridyl-disulfide monomers. In successful, conjugation reactions would create disulfide bonds protected by zero, two or four methyl groups, depending on the specific peptide-polymer combination. To quantify conjugation, the UV absorbance of pyridine-2-thione (343 nm) release was measured **(Figure 3.5)**. The hindered peptide (hBIM) consistently conjugated to unhindered polymer at higher levels than BIM. It appears the hBIM methyl groups hinder peptide dimer formation to a greater degree and increase the amount of free peptide available to react with polymer. However, steric hindrance on the polymer side of the disulfide bond significantly inhibited conjugation reactions. Unhindered BIM conjugated with very low efficiency, and hBIM did not conjugate at any detectable level. Both aqueous and organic reaction conditions were tested without success. Consequently, polymer-hBIM conjugates hindered by two peptide-side methyl groups were selected as the most promising, and their stability and drug delivery properties were further investigated *in vitro* and *in vivo*.

Steric hindrance was found to significantly enhance the resistance of the polymer-peptide conjugates to reduction. As an initial assessment, Pol300-BIM and Pol300-hbIM conjugates were treated with the reducing agent DTT (pH 5.8) and peptide release was monitored over time. Pol300-hBIM conjugates reduced at a significantly slower rate than Pol300-BIM conjugates. To test linker reduction in the blood, conjugates were incubated in human serum at 37 °C. Over the course of 6 hours, BIM and hBIM peptide products became detectable by MALDI-TOF MS as a result of disulfide bond reduction. Steric hindrance significantly prolonged the appearance of hBIM products. In combination, these findings confirm a steric hindrance stability advantage. However, undesired reduction in serum still occurred at worrying levels. hBIM products were detectable by 2 hours, which is significantly shorter than reported carrier half-lives[1].

The effect of disulfide bond stability on pro-apoptotic activity was investigated in ovarian cancer cell cultures. After 48 hours of treatment, Pol300-hBIM conjugates significantly reduced SKOV3 cell viability in comparison to Pol300-BIM conjugates. The pH-responsive membrane destabilizing activity of the polymer is known to be critical for intracellular peptide delivery and activity. Following receptor-mediated endocytosis, DEAEMA monomers undergo a pH-transition that destabilizes polymeric micelles, exposes the hydrophobic polymer block, permeabilizes endosomal membranes, and permits peptide escape to the cell cytosol[14]. The effects of peptide conjugation on the pH-dependent activity of the polymer were evaluated using dynamic light scattering and a red blood cell lysis assay. The nature of the conjugated peptide (BIM, hBIM, or BIML62E) had no effect on pH-dependent particle sizing or hemolysis results. Consequently, the enhanced activity of Pol300-hBIM does not appear to be the result of altered polymer activity. Instead, it may be due to one or more of three different influences: (i) increased peptide conjugation, (ii) increased linker stability in serum, and (iii) alternated peptide activity due to the

additional methyls. However, since the cysteine residue is not a part of the native BIM structure, the addition of two methyl groups is unlikely to impact intrinsic peptide activity.

In a mouse xenograft model of B-cell lymphoma, steric hindrance significantly enhanced the circulation half-life of BIM and increased delivery into tumors. The peptide half-life nearly doubled from ~4 hours for BIM to ~8 hours for hBIM, presumably due to decreased disulfide reduction in the blood. For antibody-targeted conjugates, the %ID/g of tumor increased from 0.37 for BIM to 0.53 for hBIM.

While steric hindrance did enhance peptide delivery parameters, the hindered conjugates also demonstrated sub-optimal stability. Over 24 hours, the hBIM:polymer ratio in the blood dropped sharply as the peptide was released and cleared from circulation. At 24 hours, only 39% of hBIM was still conjugated. While this was a significant improvement over unhindered BIM (12 % conjugated at 24 hours), much remains to be desired. Increasing the degree of steric hindrance with additional methyl and/or phenyl groups will increase bond stability, but initial results suggest synthesis and conjugation will be complex. Alternatively, an enzyme-labile peptide linker could advantageously combine high chemical stability with rapid and efficient drug release in intracellular compartments[15-16].

REFERENCES

[1] Berguig, G.Y.; Convertine, A.J.; Frayo, S.; Kern, H.B.; Procko, E.; Roy, D.; Srinivasan, S.; Margineantu, D.H.; Booth, G.; Palanca-Wessels, M.C.; Baker, D.; Hockenbery, D.; Press, O.W.; Stayton, P.S. Intracellular delivery system for antibody-peptide drug conjugates. *Mol Ther*. **2015**, 23, 907-17.

[2] Duvall, C.L.; Convertine, A.J.; Benoit, D.S.; Hoffman, A.S.; Stayton, P.S. Intracellular delivery of a proapoptotic peptide via conjugation to a RAFT synthesized endosomolytic polymer. *Mol Pharm*. **2010**, 7, 468-76.

[3] Lundy BB, Convertine A, Miteva M, Stayton PS. Neutral polymeric micelles for RNA delivery. Bioconjug Chem. 2013 Mar 20;24(3):398-407.

[4] Saito G, Swanson JA, Lee KD. Drug delivery strategy utilizing conjugation via reversible disulfide linkages: role and site of cellular reducing activities. Adv Drug Deliv Rev. 2003 Feb 10;55(2):199-215.

[5] Hamann PR, Hinman LM, Beyer CF, Lindh D, Upeslacis J, Flowers DA, Bernstein I. An anti-CD33 antibody calicheamicin conjugate for treatment of acute myeloid leukemia. Choice of linker. Bioconjug Chem. 2002

[6] Xie H, Audette C, Hoffee M, Lambert JM, Blättler WA. Pharmacokinetics and biodistribution of the antitumor immunoconjugate, cantuzumab mertansine(huC242-DM1), and its two components in mice. J Pharmacol Exp Ther. 2004 Mar;308(3):1073-82.

[7] Thorpe PE, Wallace PM, Knowles PP, Relf MG, Brown AN, Watson GJ, Knyba RE, Wawrzynczak EJ, Blakey DC. New coupling agents for the synthesis of immunotoxins containing a hindered disulfide bond with improved stability in vivo. Cancer Res. 1987 Nov 15;47(22):5924-31.

[8] Kellogg BA, Garrett L, Kovtun Y, Lai KC, Leece B, Miller M, Payne G, Steeves R, Whiteman KR, Widdison W, Xie H, Singh R, Chari RV, Lambert JM, Lutz RJ. Disulfide-linked antibody-maytansinoid conjugates: optimization of in vivo activity by varying the steric hindrance at carbon atoms adjacent to the disulfide linkage. Bioconjug Chem. 2011 Apr 20;22(4):717-27.

[9] Kim HJ, Ha S, Lee HY, Lee KJ. ROSics: chemistry and proteomics of cysteine modifications in redox biology. Mass Spectrom Rev. 2015 Mar-Apr;34(2):184-208.

[10] Zhang X, Wang Z, Li J, Gu D, Li S, Shen C, Song Z. Increased 4-hydroxynonenal formation contributes to obesity-related lipolytic activation in adipocytes. PLoS One. 2013 Aug 5;8(8):e70663.

[11] Schwarzer E, Arese P, Skorokhod OA. Role of the lipoperoxidation product 4-hydroxynonenal in the pathogenesis of severe malaria anemia and malaria immunodepression. Oxid Med Cell Longev. 2015.

[12] Delbridge AR, Strasser A. The BCL-2 protein family, BH3-mimetics and cancer therapy.

Cell Death Differ. 2015 Jul;22(7):1071-80.

[13] Balendiran GK, Dabur R, Fraser D. The role of glutathione in cancer. Cell Biochem Funct. 2004 Nov-Dec;22(6):343-52.

[14] Manganiello MJ, Cheng C, Convertine AJ, Bryers JD, Stayton PS. Diblock copolymers with tunable pH transitions for gene delivery. Biomaterials. 2012 Mar;33(7):2301-9.

[15] Doronina SO, Toki BE, Torgov MY, Mendelsohn BA, Cerveny CG, Chace DF, DeBlanc RL, Gearing RP, Bovee TD, Siegall CB, Francisco JA, Wahl AF, Meyer DL, Senter PD. Development of potent monoclonal antibody auristatin conjugates for cancer therapy. Nat Biotechnol. 2003 Jul;21(7):778-84.

[16] Chu DS, Johnson RN, Pun SH. Cathepsin B-sensitive polymers for compartment-specific degradation and nucleic acid release. J Control Release.2012 Feb 10;157(3):445-54.

CHAPTER 4. Cathepsin B-cleavable Polymeric Micelles for the Intracellular Delivery of Pro-apoptotic Peptides.

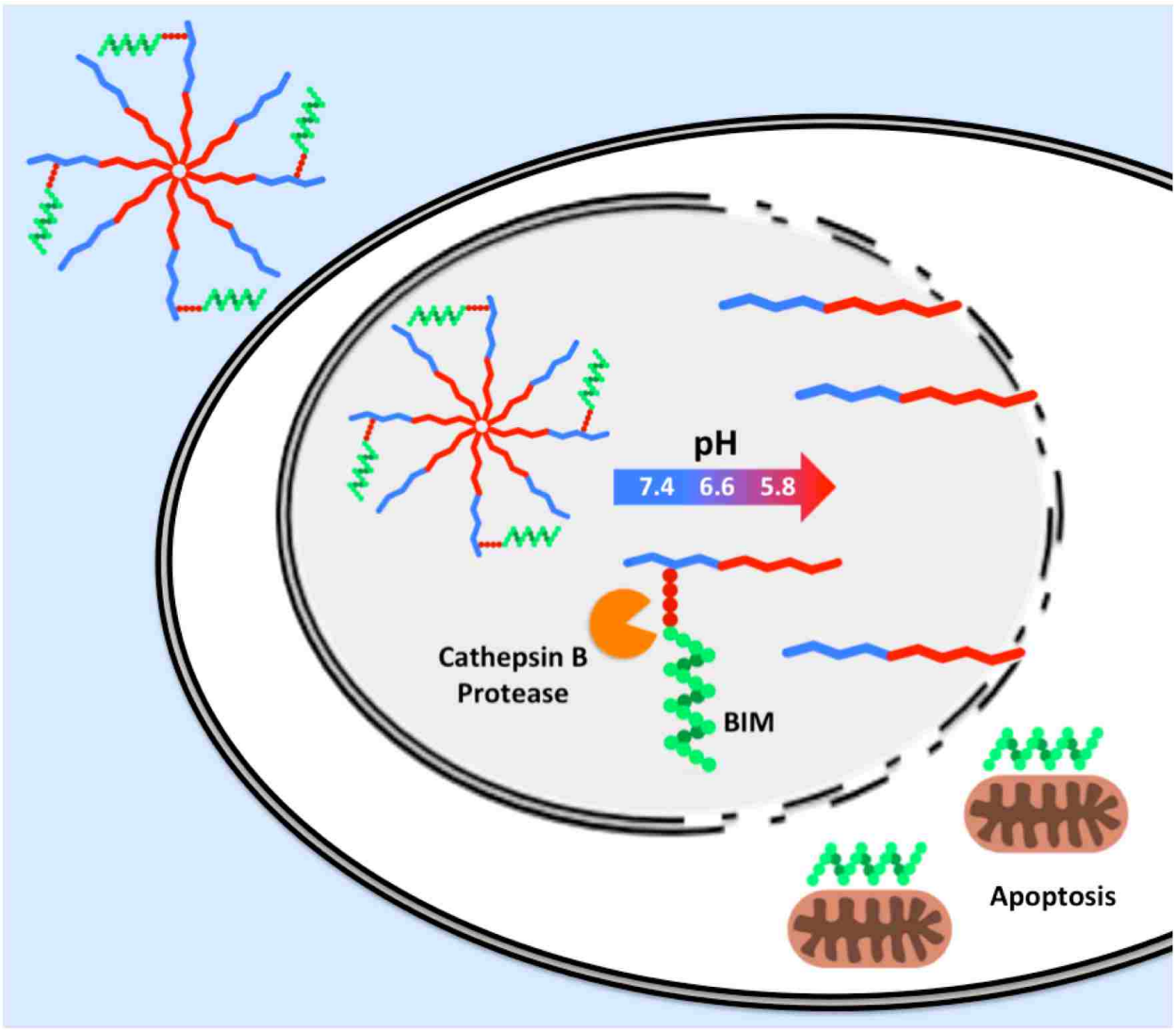

Abstract

This work develops an enzyme-labile peptide linker for polymer-BIM conjugates that is highly stable in human serum and efficiently cleaved inside cancer cells to release active BIM peptide. Described is a peptide macromonomer composed of BIM capped with a four amino acid cathepsin B substrate (FKFL) that possesses high chemical stability but is enzymatically cleaved in endo/lysosomes to release the drug. Employing RAFT polymerization, the peptide

macromonomer was directly integrated into a multifunctional diblock copolymer tailored for peptide delivery. The first polymer block was made as a macro-chain transfer agent (CTA) and composed of a pH-responsive endosomolytic formulation of N,N-diethylaminoethyl methacrylate (DEAEMA) and butyl methacrylate (BMA). The second polymer block was a copolymer polyethylene glycol methacrylate (PEGMA) and the peptide macromonomer. PEGMA monomers of two sizes were investigated (300 Da & 950 Da). Protein gel analysis, high performance liquid chromatography and coupled mass spectrometry (MS) showed that incubation with cathepsin B specifically cleaved the FKFL linker and released active BIM peptide with $PEGMA_{300}$ but not with $PEGMA_{950}$. MALDI-TOF MS showed that incubation of the peptide monomers in human serum resulted in partial cleavage at the FKFL linker after 12 hours. However, formulation of the peptides into polymers protected against serum-mediated peptide degradation. Dynamic light scattering (DLS) demonstrated pH-dependent micelle disassembly (25 nm polymer micelles at pH 7.4 versus 6 nm unimers at pH 6.6), and a red blood cell lysis assay showed a corresponding increase in membrane destabilizing activity (< 1% lysis at pH 7.4 versus 95% lysis at pH 6.6). The full carrier-drug system successfully induced apoptosis in SKOV3 ovarian cancer cells in a dose-dependent manner, in comparison to a control polymer containing a scrambled BIM peptide sequence. Mechanistic analysis verified target-dependent activation of caspase 3/7 activity (8.1-fold increase), and positive annexin V staining (72% increase). The increased blood stability of this enzyme-cleavable peptide polymer design, together with the direct polymerization approach that eliminated post-synthetic conjugation steps, suggests that this new carrier design could provide important benefits for intracellular peptide drug delivery.

4.1 Introduction

A diblock polymeric micelle carrier for the BIM BH3 peptide was recently described that demonstrated anti-tumor activity in a B-cell lymphoma xenograft model[1]. However, the disulfide linkage used to conjugate the BIM peptide was shown to have non-optimal blood stability that compromised the full potential of the carrier system. To address this limitation, Chapter 3 investigated steric hindrance for enhancing disulfide bond stability. Two methyl groups were introduced on the peptide carbon adjacent to the bond and the pharmacokinetics and biodistribution of the peptide and polymer were studied in a mouse xenograft model of B-cell lymphoma. While steric hindrance resulted in a 2-fold increase in peptide half-life, disulfide bond reduction still occurred at a considerable rate.

Design of a polymer-peptide linker that is (a) highly stable in systemic circulation and (b) specifically and efficiently cleaved in intracellular compartments could further enhance the intracellular delivery and therapeutic activity of BIM and other peptide/protein drugs. A peptide linker that is a selective substrate for an intracellular protease is an alternative approach that meets both of the above criteria. Cathespin B is a cysteine protease that functions almost exclusively in

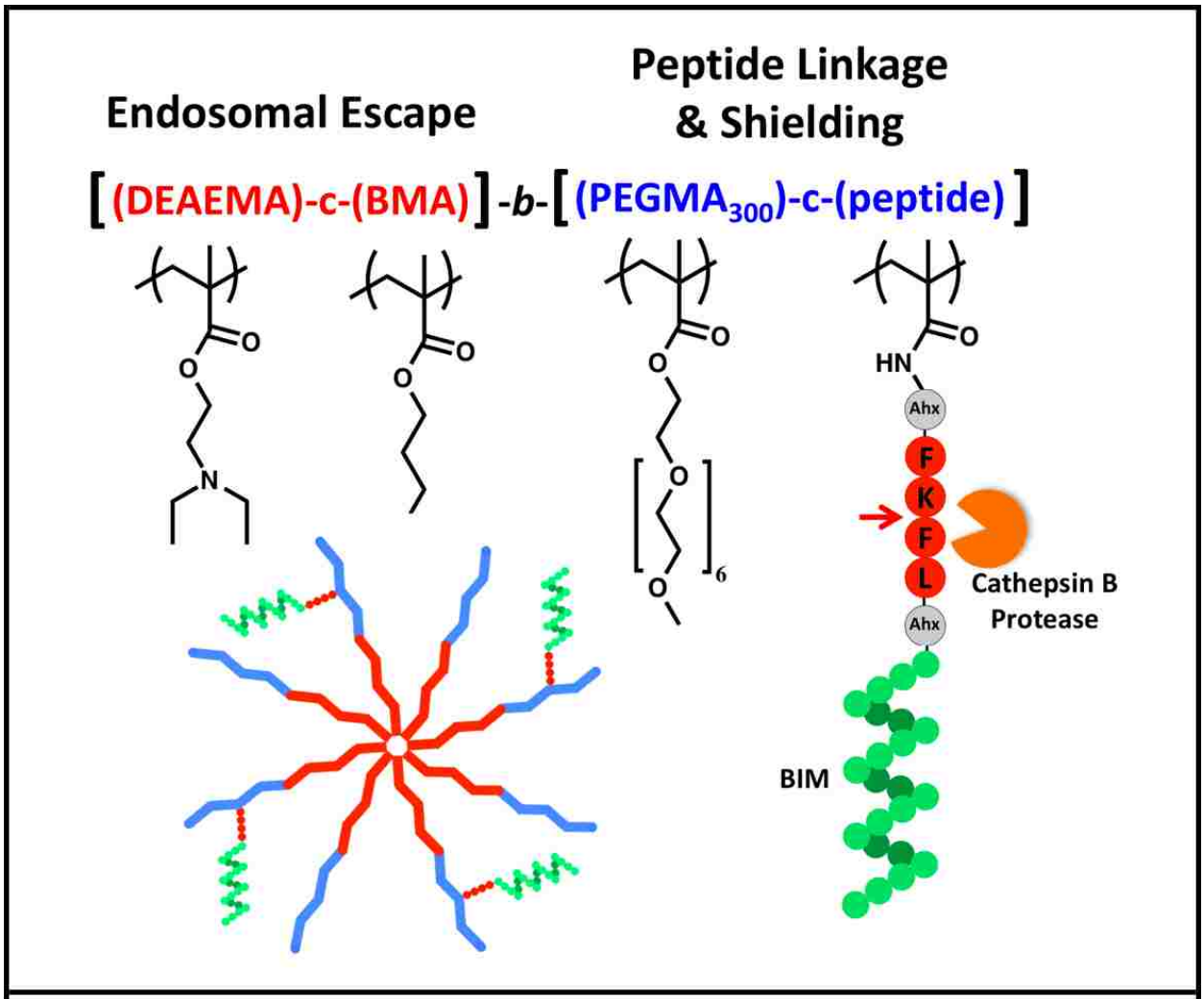

Figure 4.1. Design of a cathepsin-B cleavable diblock copolymer for the intracellular delivery and release of BIM. The first block drives micelle formation at physiological pH (7.4) and destabilizes membranes and facilitates endosomal escape at acidic pH values (5.8-6.6). The second block contains PEG units for biocompatibility and stability and a methacrylamido-peptide macromonomer consisting of BIM capped with a four amino acid (FKFL) cathepsin B substrate flanked on either side by a six carbon spacer (aminohexanoic acid (Ahx)). Cleavage at the FKFL linker by cathepsin B specifically releases BIM inside the endo/lysosomes of target cells.

endosomes and lysosomes[2-5]. Furthermore, cathepsin B-labile linkers have been utilized previously for other drug delivery applications including antibody-drug conjugates (ADCs) and degradable nucleic acid delivery vehicles[6-9].

An additional drawback of disulfide linkages is the added manufacturing complexity associated with post-synthetic peptide conjugation. Conjugation is especially limited in the context of PEG grafts, which provide steric shielding properties, but also block access to pyridyl disulfide moieties during conjugation.

To address both the stability and conjugation limitations of a disulfide linkage, a new carrier system has been designed that utilizes a macromonomer incorporated peptide prodrug (**Figure 4.1**). The peptide macromonomer contains the BIM peptide sequence capped with a well-characterized cathepsin B substrate, phe-lys-phe-leu (FKFL) [10-14]. This sequence is flanked on either side by a six carbon spacer (6-aminohexanoic acid (Ahx)) to facilitate steric access of the enzyme in the context of the PEG grafts. The peptide is functionalized on its N-terminus with methacrylamide and directly and stably integrated into a multifunctional diblock copolymer via RAFT polymerization. The first polymer block is composed of a pH-responsive formulation that drives micelle formation at physiological pH and destabilizes membranes at the acidic pH values found within endosomes[15-16]. The second polymer block contains the peptide macromonomer for BIM delivery and polyethylene glycol units for solubility and stability[1, 17]. Two different PEGMA monomers varying in length (300 Da & 950 Da) were investigated, but only $PEGMA_{300}$ was found to permit adequate cathepsin B access. In ovarian cancer cell cultures, the polymer is shown to facilitate intracellular BIM delivery and induce apoptosis in comparison to a control polymer containing a scrambled BIM sequence.

4.2 Materials and Methods

4.2.1 Synthesis and Characterization of Peptide Macromonomers

Using an automated PS3 peptide synthesizer (Protein Technologies), the following peptides were synthesized on a solid support (rink amide MBHA resin (100-200 mesh), EMD Millipore) from FMOC protected (L) amino acids (EMD Millipore) and an FMOC protected 6-aminohexanoic acid (Ahx) spacer (AnaSpec):

BIM: MRPEIWIAQELRRIGDEFNAC

BIM R64Q: MRPEIWIAQELRQIGDEFNAC

AhxFKBIM: AhxFKMRPEIWIAQELRRIGDEFNAY

AhxFKFLAhxBIM: AhxFKFLAhxMRPEIWIAQELRRIGDEFNAY

FLAhxBIM: FLAhxMRPEIWIAQELRRIGDEFNAY

AhxFKFLAhxScrBIM: AhxFKFLAhxLRMREIIDAYERQFGEPNIWA

For the synthesis of corresponding methacrylamido-peptide monomers, the amino termini of the peptides were deprotected and functionalized with N-succinimidyl methacrylate (TCI America), while still linked to the resin (**Scheme 4.1**). Three peptide monomers were synthesized: MaAhxFKBIM, MaAhxFKFLAhxBIM, and MaAhxFKFLAhxScrBIM. The peptides/monomers were deprotected/cleaved from the resin by treatment with trifluoroacetic acid/triisopropylsilane/H_2O (9.5:2.5:2.5, v/v/v) for 4 hours and precipitated in cold ether. Crude peptides/monomers were purified by reverse phase high performance liquid chromatography (RP-HPLC) on a Jupiter 5 μm C18 300Å column (Phenomenx) with an Agilent 1260 HPLC. Ion trap mass spectrometry with electrospray (Bruker Esquire) was used to confirm the molecular weights of the purified products (**Figure 4.2)**.

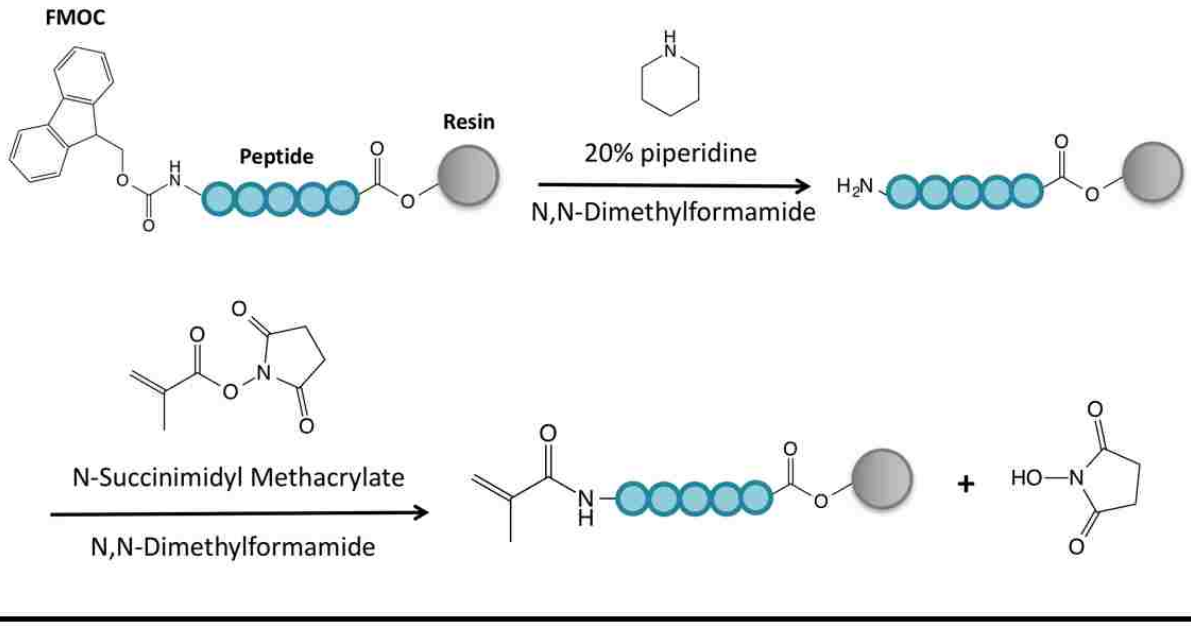

Scheme 4.1. Synthesis of methacrylamido-peptide monomers by coupling of deprotected peptide N-termini with N-hydroxysuccimide-activated methacrylate.

4.2.2 Cytochrome C Release Assay

An initial step in the induction of apoptosis is release of cytochrome C from the mitochondria. To measure intrinsic pro-apoptotic peptide activity, mitochondria were isolated from tumor cells, treated with the appropriate peptide at a relevant dose, and cytochrome c release was assayed. First, 10^9 Granta-519 cells were equilibrated in 5 mL homogenization buffer (0.25 M sucrose, 1 mM EGTA, 10 mM HEPES/NaOH, 0.5% BSA, pH 7.4) containing a Complete EDTA-free Protease Inhibitor Cocktail Tablet (Roche) for 5 min at 4 °C. Cells were then homogenized for 10 min under N_2 pressure (400 psi) in a nitrogen bomb (Parr Instrument Company), after which membrane disruption was confirmed by Trypan Blue Staining. Intact cells were removed by centrifugation (750 g for 10 min) and the supernatant was centrifuged a second time (12,000 g for 12 min) to pellet the mitochondria. The mitochondria pellet was resuspended in 300 µL of wash buffer (0.25 M sucrose, 1 mM EDTA, 10 mM Tris/Hcl, pH 7.4) and quantified by

BCA assay (Sigma). Peptides (0.1-10 μM) were incubated with 25 μg of mitochondria in 50 μl of experimental buffer (125 mM KCl, 10 mM Tris-MOPS, pH 7.4, 5 mM glutamate, 2.5 mM malate, 1 mM KPO_4, 10 μM EGTA-Tris, pH 7.4) for 30 min at 37 °C. Reaction solutions were then centrifuged (18,000 g for 10 min) and cytochrome c release into the supernatant was quantified using a Cytochrome C ELISA kit (Life Technologies). 1% Triton-X100 was employed as a positive control for 100% cytochrome c release.

4.2.3 RAFT Polymer Synthesis

4.2.3.1 Synthesis of Poly(ethylene glycol) Methyl Ether Methacrylate (PEGMA)-peptide Copolymers

The cathepsin B-cleavable BIM peptide macromonomer (MaAhxFKFLAhxBIM) was copolymerized with PEGMA under nitrogen in DMSO (20 wt% monomer) for 24 hours at 70 °C using azobis(4-cyanopentanoic acid) (ABCVA) as the radial initiator and 4-cyanopentanoic acid dithiobenzoate (CTP) as the chain transfer agent (CTA). The molar composition of the reaction feed was 4% peptide monomer and 96% PEGMA. Two different polymers were synthesized using PEGMA monomer of molecular weight 300 Da ($PEGMA_{300}$) or 950 Da ($PEGMA_{950}$). The initial monomer ([M]o) to CTA ([CTA]o) to initiator ([I]o) ratios for poly($PEGMA_{950}$-co-peptide) and poly($PEGMA_{300}$-co-peptide) were 25:1:0.2 and 50:1:0.2, respectively. The resulting polymers were precipitated in diethyl ether and the unreacted peptide monomer was subsequently precipitated in acetone. This two-step precipitation scheme was repeated six times and the isolated polymers were dried by lyophilization.

4.2.3.2 Synthesis of Diblock Copolymers

RAFT copolymerization of a macroCTA consisting of N,N-diethylaminoethyl methacrylate (DEAEMA) and butyl methacrylate (BMA) was conducted under nitrogen atmosphere in dioxane (50 wt% monomer) at 70 °C for 6 hours using 4-cyanopentanoic acid dithiobenzoate (CTP) as the chain transfer agent (CTA) and azobis(4-cyanopentanoic acid) (ABCVA) as the radical initiator. The molar composition of the reaction feed was 60% DEAEMA and 40% BMA, and the initial monomer ($[M]_o$) to CTA ($[CTA]_o$) to initiator ($[I]_o$) ratio was 200:1:0.1. The resulting macroCTA, poly[(DEAEMA)-co-(BMA)], was purified by dialysis in acetone for 48 hours, followed by dialysis in water for 24 hours, and dried by lyophilization. The macroCTA was then employed for block copolymerization of $PEGMA_{300}$ and peptide macromonomer. Two different polymers were synthesized by varying the identity of the peptide monomer: poly[(DEAEMA)-co-(BMA)]-b-[($PEGMA_{300}$)-c-(MaAhxFKFLAhxBIM)] and poly[(DEAEMA)-co-(BMA)]-b-[($PEGMA_{300}$)-c-(MaAhxFKFLAhxScrBIM)]. The polymers are abbreviated as PolCathBIM and PolCathScrBIM, respectively. The block copolymerizations were conducted for 18 hours at 70 °C under nitrogen atmosphere in an equal by volume mixture of dimethyl sulfoxide (DMSO) and dioxane (20 wt% monomer and macroCTA). The molar composition of the monomer feed was 96% $PEGMA_{300}$ and 4% peptide, and the $[M]_o$:$[mCTA]_o$:$[I]_o$ ratio was 45:1:0.1. The resulting diblock copolymers were precipitated 4X in a mixture of petroleum ether and diethyl ether (9:1, v/v) to remove unreacted $PEGMA_{300}$ and solvents. To remove unreacted peptide, the polymers were redissolved in acetone, the peptide monomer was removed by centrifugation, and polymers were re-

precipitated in petroleum ether. This two-step precipitation scheme was repeated 3X and the purified diblock copolymers were lyophilized.

4.2.4 Polymer Characterization by Gel Permeation Chromatography (GPC), ^{1}H-NMR and RP-HPLC

To measure the number average molecular weights (M_n) and polydispersities (PDIs) of the polymers, GPC was conduced using Tosoh SEC TSK GEL α-3000 and α-4000 columns (Tosoh Bioscience), a 1200 Series liquid chromatography system (Agilent), and a miniDAWN TREOS three-angle light scattering instrument with an Optilab TrEX refractive index detector (Wyatt Technology). The mobile phase was 0.1 wt% lithium bromide in HPLC-grade N,N-dimethylformamide at 60 °C and a flow rate of 1 mL/min. The compositions of the polymers were examined by ^{1}H-NMR spectroscopy (Bruker avance DRX 499). For quantification of peptide content, reaction aliquots were collected at T_o and T_x and analyzed by RP-HPLC (abs 280 nm). Percent monomer conversion was calculated by the equation (Peak[T_o]-Peak[T_x])/(Peak[T_o]) and used to estimate mol% peptide per polymer chain.

4.2.5 Formulation of Diblock Copolymers into Micelles

Aqueous polymer solutions were prepared by first dissolving the polymer in DMSO at 100 mg/mL followed by rapid dilution into phosphate buffer saline (PBS) to a concentration of 10 mg/mL. Serial dilutions were made and absorbance at 282 nm was measured to determine extinction coefficients. DMSO was removed by centrifugal dialysis in PBS (Amicon Ultra, 5 mL, 3K MWCO, Millipore), and final polymer concentrations were determined by UV spectrometry.

4.2.6 Cathepsin B Cleavage Assay

Specific cleavage at the FKFL linker by cathepsin B was determined by adapting a method from Dubowchik et al.[6] and Chu et al.[9] Human liver cathepsin B (Enzo Life Sciences) was activated for 15 minutes in a solution of 0.158 mg/mL cathepsin B, 20 mM DTT, and 10 mM EDTA at 37 °C. Peptide or polymer was then solubilized in reaction buffer (10 mM phosphate, 1 mM EDTA, pH 5-7.4, 37 °C) and added to the enzyme solution for a final concentration of 1.28 μg/mL cathepsin B and 65 μM peptide/polymer. At various time points, reaction aliquots were removed, enzymatic activity was halted by addition of a thioprotease inhibitor (E-64 (Thermo Scientific), 26 μg/mL), and RP-HPLC and mass spectrometry were used to quantify cathepsin B cleavage of the FKFL linker. Cleavage of the polymers was also visualized by SDS-PAGE on 8-16% Tris-Glycine Gels (Bio-Rad). For protein gel analyses, reactions were conducted at 3X concentration and 160 μg of polymer was loaded per well.

4.2.7 Serum Stability of Peptide Macromonomers and Diblock Copolymers

The stability of the peptide (FKFL) linker in the presence of serum proteases was evaluated by incubating the peptide monomers and polymers in human serum and analyzing the degradation products over time. Peptide (40 mM, DMSO) or polymer (4 mM, PBS) was added to human serum to a final peptide/polymer concentration of 400 μM and incubated at 37 °C. At various time points, 40 μL aliquots of the mixture were withdraw and 40 μL of acetonitrile was added to precipitate serum proteins and halt protease degradation. Precipitated solutions were centrifuged at 13,000 rpm for 5 min and supernatants were analyzed by MALDI-TOF MS using a Bruker Autoflex II.

4.2.8 Sizing of Micelles by Dynamic Light Scattering

The hydrodynamic diameters of the polymer micelles were determined by dynamic light scattering (DLS) using a Nanoseries Zetasizer (Malvern). Measurements were taken of 0.25 mg/mL polymer solutions in 100 mM phosphate buffer (supplemented with 150 mM NaCl) at pH values ranging from 5.8 to 7.4. Mean particle diameter is reported as the number average $\pm$ the half width of three independently prepared formulations.

4.2.9 pH-responsive Hemolysis Assay

The ability of the polymers to induce pH-dependent membrane destabilization was assessed via a red blood cell hemolysis assay as described previously[18]. Briefly, polymers (60 μg/mL) were incubated for 1 hour at 37 °C with human red blood cells in a 100 mM phosphate buffer (supplemented with 150 mM NaCl) at pH values ranging from 5.8 to 7.4. Percent red blood cell lysis (hemolysis) was quantified by measuring hemoglobin release (abs 541 nm) relative to a 100% lysis control (0.1% Triton X-100).

4.2.10 Cell culture

SKOV3 human ovarian cancer cells (ATCC) were cultured in RPMI 1640 Medium (+L-glutamine, + HEPES) and 3T3 fibroblast cells (ATCC) were cultured in Dulbecco's Modified Eagle's Medium. Mediums were supplemented with 10% FBS (GIBCO) and 1% penicillin/streptomycin (GIBCO), and cells were maintained in log-phase growth at 37 °C and 5% CO_2.

4.2.11 Cell Viability Assay

The cell killing activity of the polymers was initially evaluated using the CellTiter 96 Aqueous One Solution Cell Proliferation Assay (MTS) (Promega). SKOV3/3T3 cells were plated in a 96-well plate at a density of 7,000 cells per well and allowed to adhere for 24 hours. Cells were then incubated with 100 μL of polymer solution at concentrations ranging from 0-10 μM. At 96 hours (SKOV3s) or 120 hours (3T3s), cell viability was quantified by adding 20 μL of [3-(4,5-dimethylthiazol-2-yl)-5-(3-carboxymethoxyphenyl)-2-(4-sulfophenyl)-2H-tetrazolium (MTS) reagent to each well, incubating for 30 minutes, and measuring the absorbance at 490 nm using a plate reader. All experimental groups were run in triplicate and the results from three independent experiments were averaged.

4.2.12 Caspase-3/7 Activity Assay

Induction of apoptotic signaling was measured by assaying for caspase 3/7 activity using a SensoLyte Homogenous AMC Caspase-3/7 Assay Kit (AnaSpec). SKOV3 cells were plated in a black 96-well plate with a clear bottom at a density of 7,000 per well, allowed to adhere for 24 hours, and then treated with polymer at concentrations ranging from 0-10 μM for 72 hours. After 72 hours, assay reagents were mixed with cell culture medium as per the manufacturer's instructions and incubated on a rocker for 24 hours at room temperature. The fluorescence of the AFC fluorophore (excitation/emission = 380nm/500nm) released upon caspase cleavage of the substrate Ac-DEVD-AFC was measured using a plate reader. Percent caspase 3/7 activity was calculated relative to untreated cell cultures.

4.2.13 Annexin V Apoptosis Assay

Induction of apoptosis was measured with a FITC Annexin V/Dead Cell Apoptosis Kit (Invitrogen) as per the manufacturer's instructions. Briefly, SKOV3s cells were plated in 6-well plates at a density of 120,000 cells per well, allowed to adhere for 24 hours, and treated with 10 μM polymer solutions for 72 hours. After 72 hours, cells were trypsinized, rinsed in PBS, centrifuged, resuspended in annexin V binding buffer, and incubated with FITC-annexin V for 15 minutes at room temperature. Cells were then analyzed on a BD LSRII flow cytometer and the percentages of annexin V positive cells were calculated.

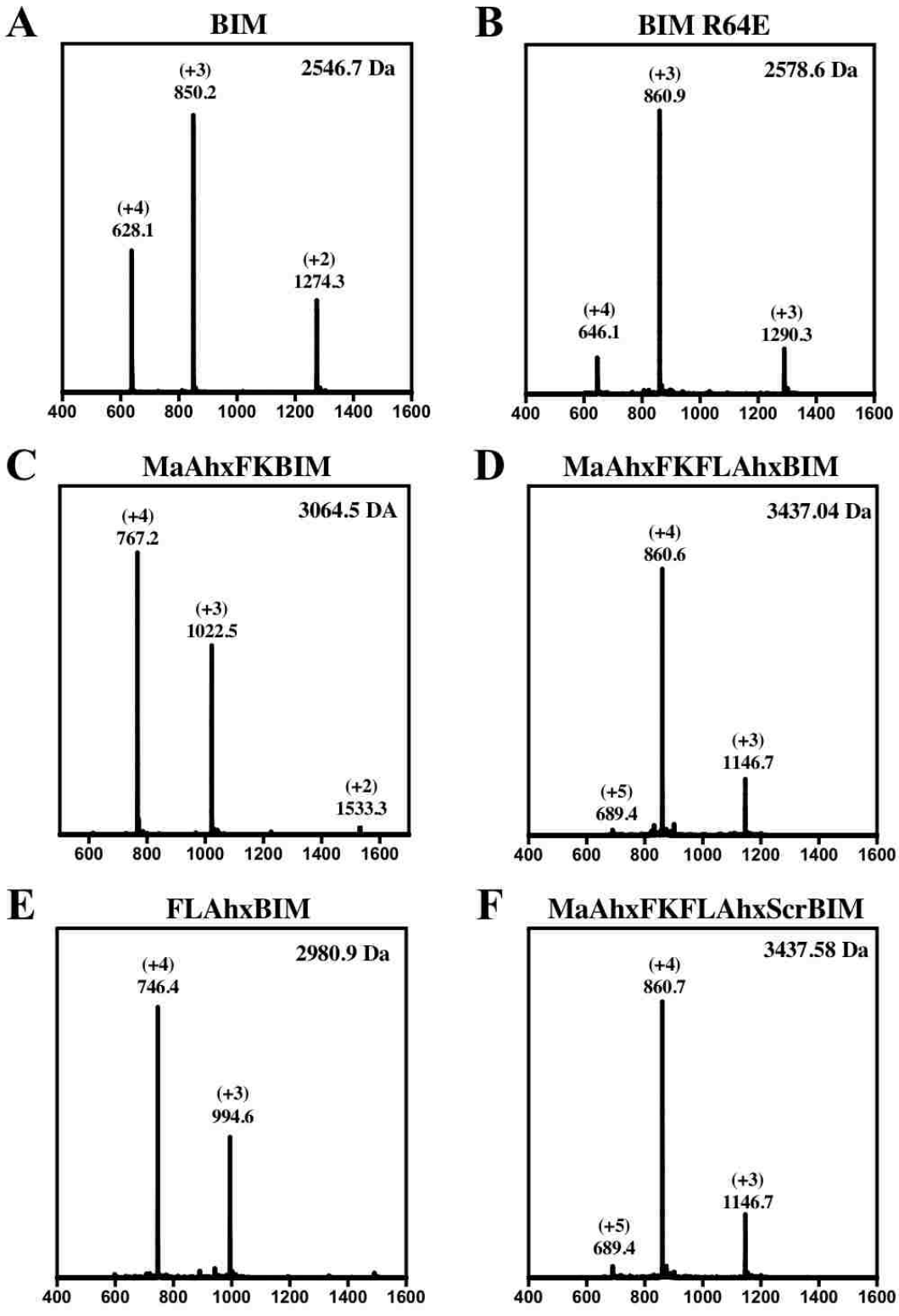

Figure 4.2. The molecular weights of synthesized peptides/monomers were confirmed by mass spectrometry.

4.3 Results

4.3.1 Design of a Cathepsin B-cleavable BIM Peptide Macromonomer

4.3.1.1 Cathepsin B Cleavage of the BIM Peptide

The enzyme cathepsin B was selected for mediating intracellular drug release from the polymer backbone due to its localization in endo-lysomes and its successful implementation for the cleavage of antibody-drug conjugates and of nucleic acid delivery vehicles. To evaluate cathepsin B's potential for release of the BIM peptide, BIM's susceptibility to degradation by cathepsin B was initially investigated. Human cathepsin B was incubated with BIM **(Figure 4.2A)** at a range of endo/lysosomal pH values (5.0-7.4), at various time points the reactions were halted by the addition of a thioprotease inhibitor (E-64), and the degradation products were analyzed by RP-HPLC and MS. At pH 5.0, cathepsin B was found to specifically cleave BIM between arginine (R) 64 and isoleucine (I) 65 (**Figure 4.3**). However, cleavage of BIM occurred at a relatively slow rate, with only 50% of peptide cleaved after 30 minutes and 98% cleaved after 2 hours. In addition, cathepsin B cleavage of BIM did not occur at higher pH values (6.6 & 7.4).

The peptide substrate for cathepsin B is conventionally notated as P2-P1-P1'-P2', with cleavage occurring P1 and P1'. Numerous reports have systematically examined the amino acids at these positions to optimize for cathepsin B cleavage. These studies have shown that arginine is the preferred amino acid for the P1 position and hydrophobic amino acids are preferred at P1' and P2'. It is therefore of no surprise that some degree of cathepsin B cleavage occurs between R64 and I65 within the BIM peptide.

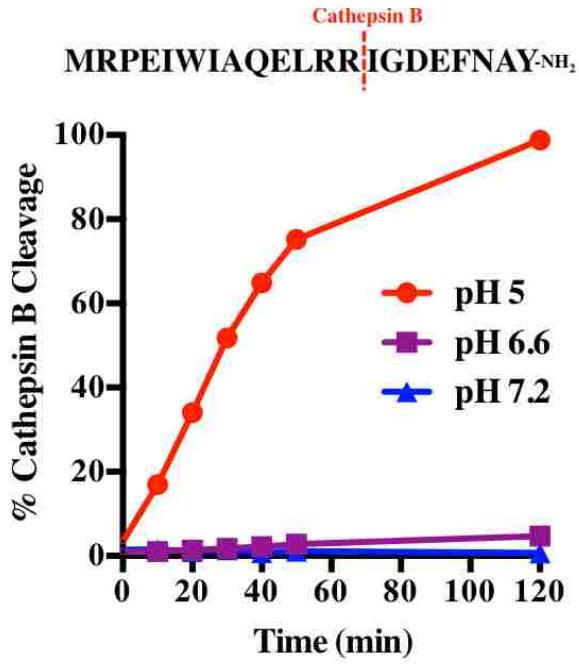

Figure 4.3. Cathepsin B cleaves the BIM peptide. BIM peptide was incubated with human cathepsin B in buffers of varying pH. Over time, enzymatic cleavage was stopped by addition of a thioprotease inhibitor (E-64) and reaction products were analyzed by LC-MS. At pH 5.0, but not at pHs 6.6 and 7.4, cathepsin B cleaved BIM between the R64 and I65 residues.

In an attempt to abrogate cathepsin B cleavage of BIM, a peptide was synthesized substituting the R64 residue with glutamine (BIM R64Q, **Figure 4.2B**). Computational modeling of BIM binding to its target proteins indicates that the R64 residue is of minimal importance in comparison to I65, which is a highly conserved hydrophobic residue. Replacing arginine with glutamine is a conservative substitution that we hoped would prevent cathepsin B cleavage without impacting BIM's pro-apoptotic activity. Cathepsin B cleavage of BIM R64Q was studied in comparison to native BIM, as was BIM R64Q's ability to induce cytochrome c release from the mitochondria of granta-519 tumor cells (**Figure 4.4**). Unfortunately, BIM R64Q was still cleaved by cathepsin B with kinetics only slightly slower than BIM (**Figure 4.4A**). Furthermore, the

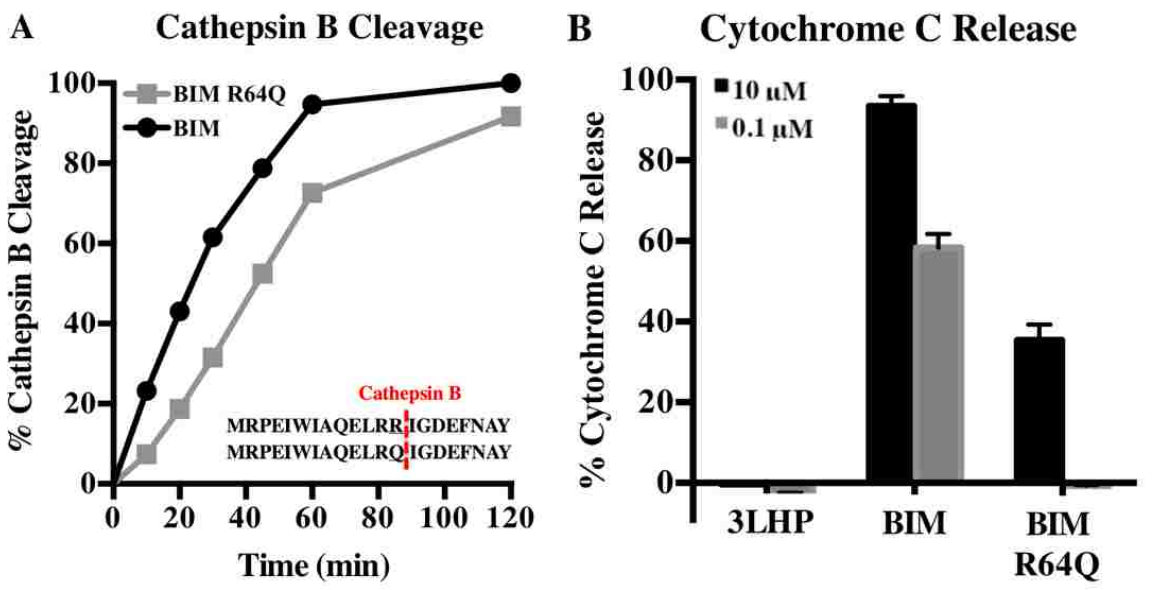

Figure 4.4. The BIM R64Q point mutation fails to abrogate cathepsin B cleavage and negatively impacts pro-apoptotic activity. (A) BIM and BIM R64Q were incubated with human cathepsin B at pH 5.0 and degradation products were analyzed over time by LC-MS. Cleavage represented occurs between amino acids I65 and either R64 (BIM) or Q64 (BIM R64Q). **(B)** Mitochondria were isolated from granta-519 B-cell lymphoma cells and incubated with BIM, BIM R64Q, or a nonactive control protein (3LHP) for 30 minutes. Mitochondria were then pelleted and supernatants were analyzed for cytochrome c by ELISA. Percent cytochrome C release is reported relative to a 1% TritonX-100 positive control.

R64Q mutation significantly reduced the peptides pro-apoptotic activity in granta-519 mitochondria (**Figure 4.4B**). At a concentration of 10 µM, the R64Q mutation reduced cytochrome c releasing activity from 93% to 35%. At a concentration of 0.1 µM, activity was reduced from 91% to 0%. With the exception of lysine, which is an amino acid also highly preferred by cathepsin B, the R64Q substitution was the most conservative that could be made. Consequently, it does not appear to be possible to modify BIM in order to prevent cathepsin B cleavage while also maintaining its biological activity. Instead, a cathepsin B-labile peptide linker should be designed that cleaves with kinetics that far

outpace those of BIM, creating a window of opportunity for BIM to escape from endo/lysomes between release from the polymer backbone and endopeptide degradation.

4.3.1.2 Design of a Cathepsin B-cleavable Linker

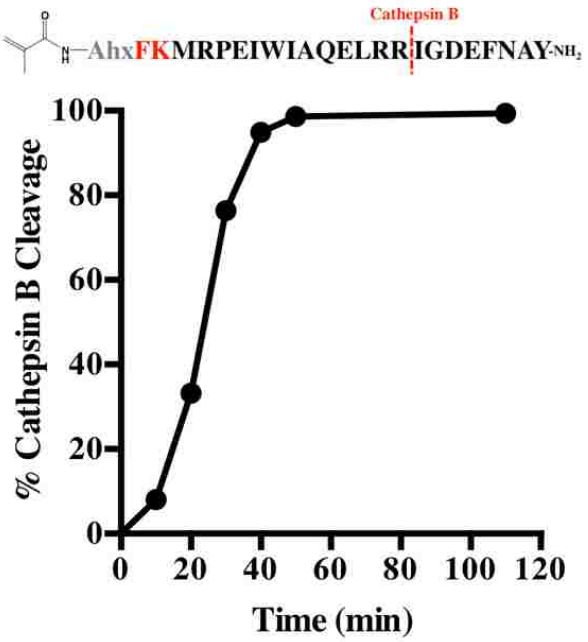

Figure 4.5. Cathepsin B cleavage of MaAhxFKBIM. MaAhxFKBIM was incubated with human cathepsin B at pH 5.0. At various timepoints, enzymatic cleavage was stopped by addition of a thioprotease inhibitor (E-64) and reaction products were analyzed by LC-MS. Cathepsin B did not cleave the FK peptide linker, but did cleave within the BIM peptide motif between the R64 and I65 residues.

The objective was to design a polymerizable, cathepsin B-cleavable BIM peptide macromonomer consisting of the BIM motif capped with a substrate for cathepsin B and functionalized on its N-terminus with methacrylamide (Ma). Initially a peptide monomer termed MaAhxFKBIM (**Figure 4.2C**) was designed in which the most N-terminal residues of BIM, methionine and arginine, filled the P1' and P2' cathepsin B cleavage positions and phenylalanine and lysine residues were placed at P2 and P1, respectively.

The six carbon spacer aminohexanoic acid (Ahx) separated the peptide from an N-terminal methacrylamide monomer. This design was initially chosen because cathepsin B cleavage of MaAhxFKBIM between the intended P1 and P1' positions would release native BIM peptide. Unfortunately, incubation with cathepsin B at pH 5.0 failed to cleave at this site (**Figure 4.5**). The only cleavage that was detectable after two hours was between R64 and I65 within the BIM peptide.

Next an alternative four amino acid, Phe-Lys-Phe-Leu (FKFL), substrate was investigated that was previously optimized for cathepsin B cleavage between the lysine and C-terminal phenylalanine residues. The peptide macromonomer MaAhxFKFLAhxBIM (**Figure 4.2D)** was synthesized with Ahx spacers separating the FKFL substrate on either side from the monomer and BIM peptide drug. Incubation of MaAhxFKFLAhxBIM with human cathepsin B resulted in rapid cleavage at the FKFL linker, with 99% complete by 20 minutes (**Figure 4.6**). Furthermore, cathepsin B cleavage of MaAhxFKFLAhxBIM, in contrast to BIM, was found to be insensitive to changes in pH. Similar cleavage kinetics were observed at pH 5.0, 6.6, and 7.4.

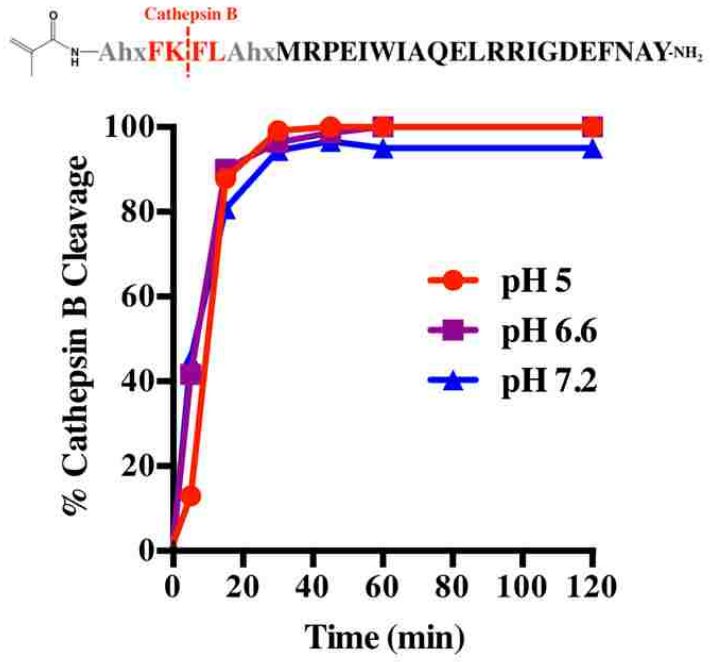

Figure 4.6. Cathepsin B cleavage of MaAhxFKFLAhxBIM. Peptide monomer was incubated with human cathepsin B in buffers of varying pH. Over time, enzymatic cleavage was stopped by addition of a thioprotease inhibitor (E-64) and reaction products were analyzed by LC-MS. Cathepsin B rapidly cleaved the FKFL linker at all tested pH values.

Because cathepsin B cleaves the FKFL substrate between the lysine and C-terminal phenylalanine residues, cleavage of MaAhxFKFLAhxBIM (MW 3437 Da) yields a 2980 Da product consisting of BIM modified on its N-terminus with FLAhx (FLAhxBIM, **Figure 4.2E**). To ensure the FLAhx modification does not impact BIM's pro-apoptotic activity, the ability of FLAhxBIM to induce cytochrome C release from the mitochondria of granta-519 tumor cells was measured and compared to unmodified BIM (**Figure 4.7)**. At a concentration of 10 μM, both FLAhxBIM and BIM induced >90% cytochrome c release in comparison to a positive 1% Triton-X100 control. A negative control protein did not induce any measurable release of cytochrome c. Lower peptide concentrations were not investigated.

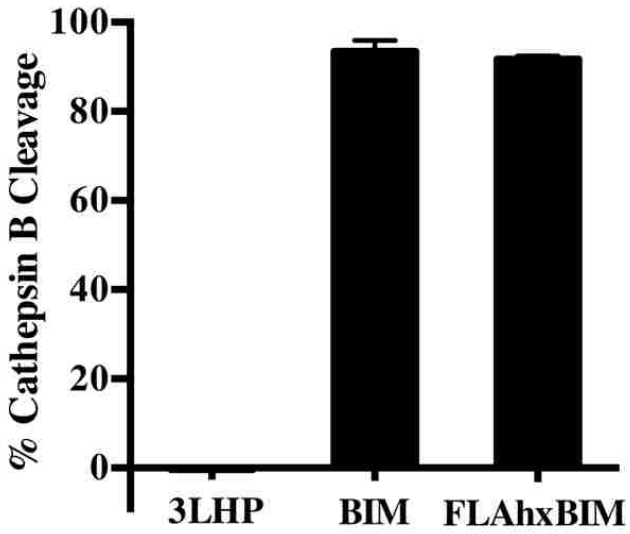

Figure 4.7. Both BIM and FLAhxBIM activate cytochrome c release in granta-519 tumor cells. Mitochondria were isolated from granta-519 B-cell lymphoma cells and incubated with BIM, FLAhxBIM, or a nonactive control protein (3LHP) at a concentration of 10 μM for 30 minutes. Mitochondria were then pelleted and supernatants were analyzed for cytochrome c by ELISA. Percent cytochrome C release is reported relative to a 1% TritonX-100 positive control. N-terminal modification of BIM with FLAhx did not impact its cytochrome c-releasing activity.

These findings recommend MaAhxFKFLAhxBIM as a promising macromonomer design that is cleaved rapidly by cathepsin B to yield a BIM peptide product possessing apoptosis-inducing activity. Consequently, MaAhxFKFLAhxBIM was further investigated for incorporation into polymeric peptide delivery vehicles. As an inactive control, a cathepsin B-cleavable peptide macromonomer containing a scrambled BIM sequence (MaAhxFKFLAhxScrBIM) was also synthesized (**Figure 4.2F)**.

4.3.2 The Effect of PEGMA Chain Length on Cathepsin B Cleavage of Copolymerized Peptide Macromonomer

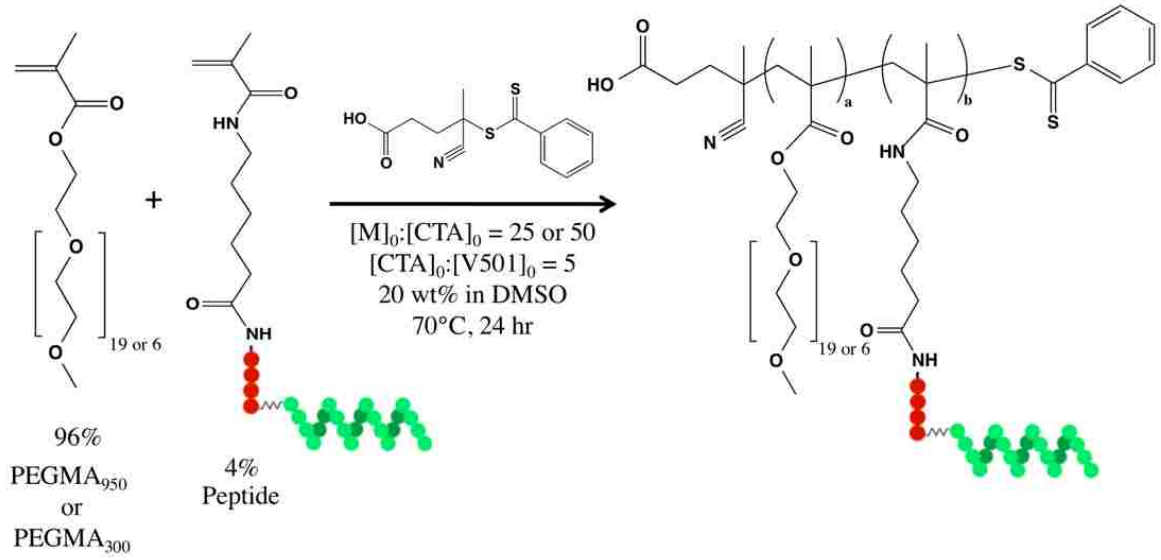

Scheme 4.2. RAFT synthesis of PEGMA-peptide copolymers. The cathepsin B cleavable BIM peptide macromonomer (MaAhxFKFLAhxBIM) was copolymerized with biocompatible long-chain PEGMA of molecular weight 950 Da ($PEGMA_{950}$) or 300 Da ($PEGMA_{300}$), containing 19 or 6 ethylene oxide units, respectively. The molar composition of the feed was 96% PEGMA and 4% peptide monomer. To synthesize polymers of similar size, the selected degrees of polymerization were 25 and 50 for $PEGMA_{950}$ and $PEGMA_{300}$, respectively.

The optimized cathepsin B cleavable BIM peptide macromonomer synthesized in part 4.3.1 (MaAhxFKFLAhxBIM) will be directly polymerized into a pH-responsive diblock copolymer designed to enhance its pharmacokinetic properties and facilitate intracellular drug delivery. Long-chain PEGMA was selected as a comonomer due to its hydrophilicity, biocompatibility, and ability to shield and enhance the circulation half-life of peptide drugs. While the protective properties of PEGMA are advantageous for increasing delivery into tumors, they may hinder cathepsin B-mediated release of BIM from the polymer carrier inside target cells. To ensure enzyme access to the linker/substrate, cathepsin B cleavage of PEGMA-peptide

copolymers was initially investigated. Two polymers were synthesized varying the chain length of the PEGMA monomer. One polymer incorporated a short 300 Da PEGMA monomer containing 6 ethylene oxide units ($PEGMA_{300}$), while the other contained longer 950 Da PEGMA with 19 ethylene oxide units ($PEGMA_{950}$). In a recent pharmacokinetic and biodistribution study of polymer-BIM disulfide-linked conjugates, a polymer containing $PEGMA_{950}$ was found to enhance peptide half-life and tumor delivery in comparison to an equivalent polymer containing $PEGMA_{300}$. However, the impact of chain-length on cathepsin B access to the polymer-peptide linker remains unknown.

Polymer	DP	% feed / comp		M_n	PDI
		PEGMA	Peptide		
Poly(PEGMA950-co-peptide)	25	96 / 95	4 / 5	19,000	1.07
Poly(PEGMA300-co-peptide)	50	96 / 96	4 / 4	18,800	1.08

Table 4.1. Characterization of poly($PEGMA_{950}$-co-peptide) and (B) poly($PEGMA_{300}$-co-peptide. Experimental M_n and PDI values were measured by gel permeation chromatography (GPC). Polymer compositions were determined by monomer depletion using RP-HPLC analysis of reaction aliquots taken at T_o and T_x.

4.3.2.1 Synthesis and Characterization of PEGMA-peptide Copolymers

RAFT synthesis was employed for the copolymerization of peptide monomer (MaAhxFKFLAhxBIM) with either $PEGMA_{950}$ or $PEGMA_{300}$ (**Scheme 4.2**). The molar compositions of the reaction feeds were 4% peptide and 96% PEGMA. In order to produce polymers of roughly equal size, the degrees of polymerization (DP) were 25 and 50 for $PEGMA_{950}$ and $PEGMA_{300}$, respectively.

The characteristics of the synthesized copolymers, termed poly($PEGMA_{950}$-co-peptide) and poly($PEGMA_{300}$-co-peptide), are summarized in **Table 4.1**.

Size-exclusion gel-permeation chromatography (**Figure 4.8**) was employed to measure the experimental molecular weights and polydispersity indexes (PDIs) of the polymers, and monomer conversion was determined by RP-HPLC analysis of reaction aliquots taken at T_o and T_x. Both polymers are approximately 19,000 Da in size and contain 4-5 mol% peptide. This is equivalent to approximately 0.9 and 1.4 peptides per polymer chain for poly(PEGMA$_{950}$-co-peptide) and poly(PEGMA$_{300}$-co-peptide), respectively.

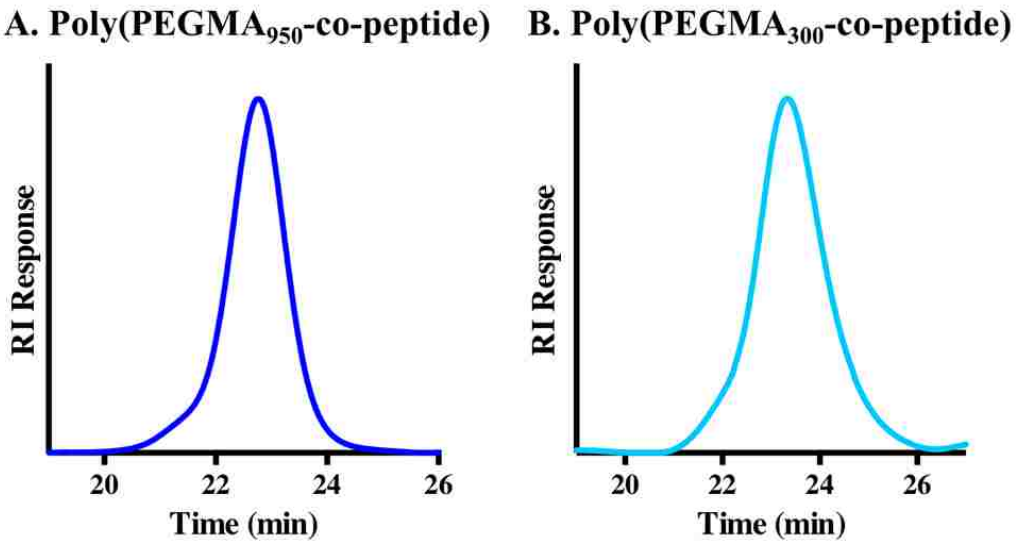

Figure 4.8. GPC-SEC characterization of (A) poly(PEGMA$_{950}$-co-peptide) and (B) poly(PEGMA$_{300}$-co-peptide) by refractive index (RI) detection. Monodisperse PEGMA-peptide copolymers approximately 19,000 Da in size were synthesized.

4.3.2.2 Cathepsin B Cleavage of PEGMA-peptide Copolymers

To evaluate the ability of cathepsin B to access its four amino acid (FKFL) substrate/linker and release BIM peptide, the polymers synthesized in part 4.3.2.1 were incubated with human cathepsin B at pH 6.60 and degradation products were analyzed over time by protein gel electrophoresis (**Figure 4.9**). Cathepsin B failed to cleave poly(PEGMA$_{950}$-co-peptide) at the FKFL linker, as the BIM peptide band was absent at

time points ranging from 0 minutes to 24 hours (**Figure 4.9A**). In contrast, cathepsin B incubation with poly(PEGMA$_{300}$-co-peptide) resulted in the appearance of a peptide band that increased in intensity over the course of two hours (**Figure 4.9B**). It is likely the longer-chain PEGMA$_{950}$ sterically hinders cathepsin B cleavage of copolymerized MaAhxFKFLAhxBIM peptide. Consequently, the PEGMA$_{300}$ monomer was selected for further development.

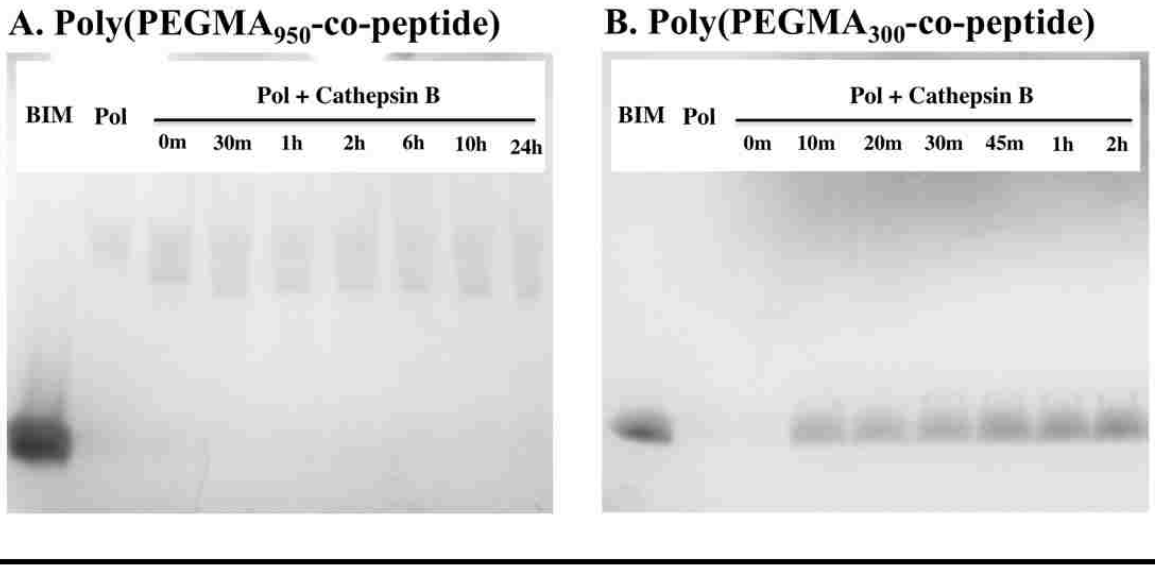

Figure 4.9. Cathepsin B cleavage of the PEGMA-peptide copolymers. In phosphate buffer of pH 6.6, human cathepsin B enzyme was incubated with **(A)** poly(PEGMA$_{950}$-co-peptide) or **(B)** poly(PEGMA$_{300}$-co-peptide). At various timepoints enzymatic cleavage was stopped by addition of a thioprotease inhibitor (E-64) and reaction products were visualized by protein gel electrophoresis. Cathepsin B was found to cleave and release a peptide product of similar size to FLAhxBIM from poly(PEGMA$_{300}$-co-peptide) but not poly(PEGMA$_{950}$-co-peptide).

4.3.3 pH-responsive Cathepsin-B Cleavable Diblock Copolymers

Using RAFT polymerization, the cathepsin B cleavable BIM peptide macromonmer (MaAhxFKFLAhxBIM) and the scrambled BIM control (MaAhxFKFLAhxScrBIM) were directly integrated into pH-responsive diblock copolymers designed for intracellular peptide delivery.

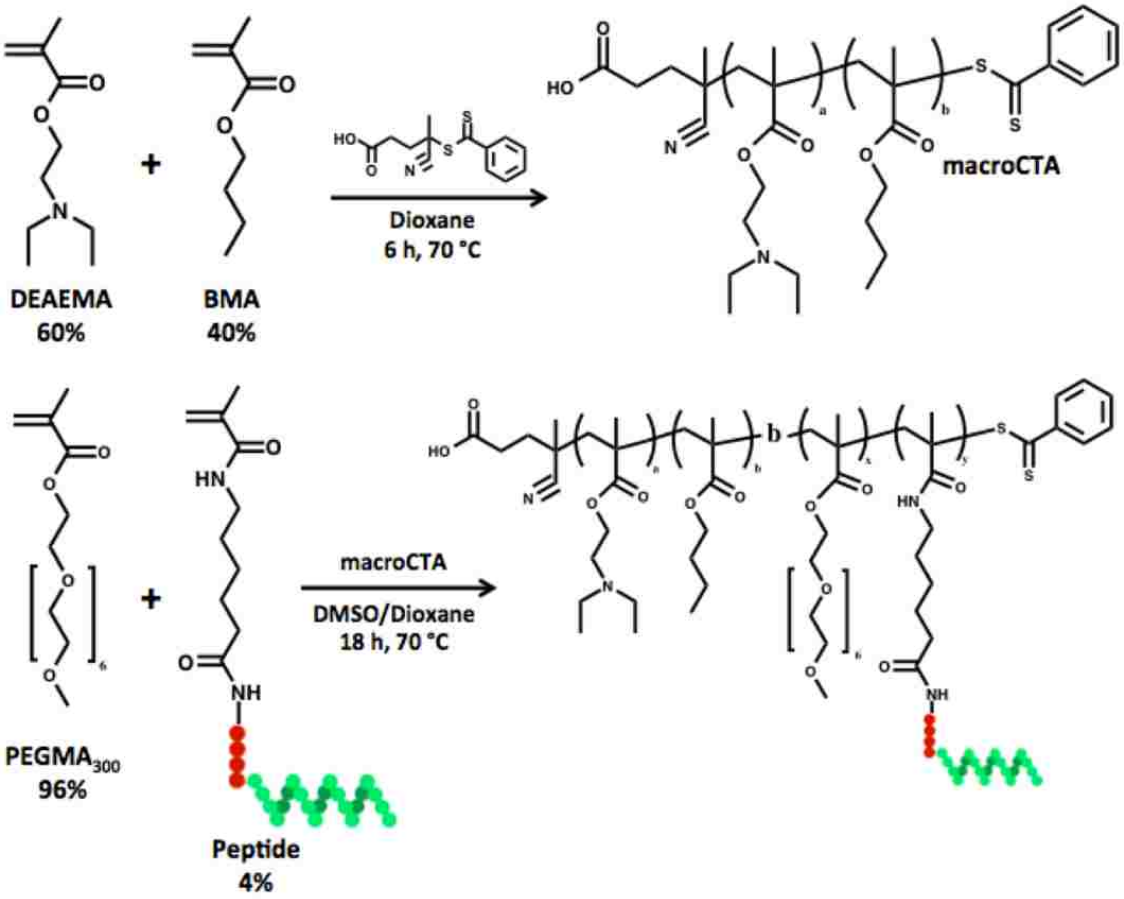

Scheme 4.3. RAFT synthesis of cathepsin B-cleavable diblock copolymers. For the synthesis of diblock copolymers, a pH-responsive poly[(DEAEMA)-co-(BMA)] macroCTA was first synthesized consisting of 60 mol% DEAEMA and 40% BMA. The macroCTA was then employed for the block copolymerization of $PEGMA_{300}$ and peptide monomer at a molar feed ratio of 96:4. Two diblock copolymers were synthesized using either MaAhxFKFLAhxBIM or MaAhxFKFLAhxScrBIM and notated PolCathBIM and PolCathScrBIM, respectively.

4.3.3.1 Synthesis and Characterization of pH-responsive Diblock Copolymers

For the synthesis of diblock copolymers (**Scheme 4.3**), a poly[(DEAEMA)-co(BMA)] macroCTA was first synthesized composed of DEAEMA and BMA at a targeted molar ratio of 60:40. This formulation has been shown previously to possess optimal pH-responsive membrane destabilizing activity and trigger the endosomal release of biologic drugs. The poly[(DEAEMA)-co(BMA)] macroCTA was them employed for

the block copolymerization of $PEGMA_{300}$ (96 mol%) and peptide macromonomer (4 mol %). Two diblock copolymers were synthesized containing either MaAhxFKFLAhxBIM or MaAhxFKFLAhxScrBIM and notated PolCathBIM and PolCathScrBIM, respectively.

Polymer	macroCTA					Diblock Copolymer				
	DP	% feed / comp		M_n	PDI	DP	% feed / comp		M_n	PDI
		DEAEMA	BMA				$PEGMA_{300}$	Peptide		
PolCathBIM	200	60 / 55	40 / 45	16,600	1.07	45	96 / 97	4 / 3	28,700	1.12
PolCathScrBIM	200	60 / 55	40 / 45	16,600	1.07	45	96 / 98	4 / 2	29,200	1.07

Table 4.2. Characterization of the cathepsin B-cleavable diblock copolymers. Polymer molecular weights (M_ns) and polydispersities (PDIs) were determined by GPC. Molar compositions were determined by ^{1}H-NMR and RP-HPLC analysis of reaction aliquots taken at T_o and T_x.

Targeted and experimentally determined characteristics of PolCathBIM and PolCathScrBIM are summarized in **Table 4.2**. GPC and ^{1}H-NMR polymer characterization data for the polymers are shown in **Figure 4.10.** The poly[(DEAEMA)-co(BMA)] macroCTA had a molecular weight of 16,600 g/mol, a narrow PDI (1.07) and a molar composition of 55% DEAEMA and 45%. The molecular weights and PDIs of PolCathBIM and PolCathScrBIM were determined to be 28,700 Da and 29,300 Da, and 1.12 and 1.07, respectively. RP-HPLC analysis of reaction aliquots taken at T_o and T_x were

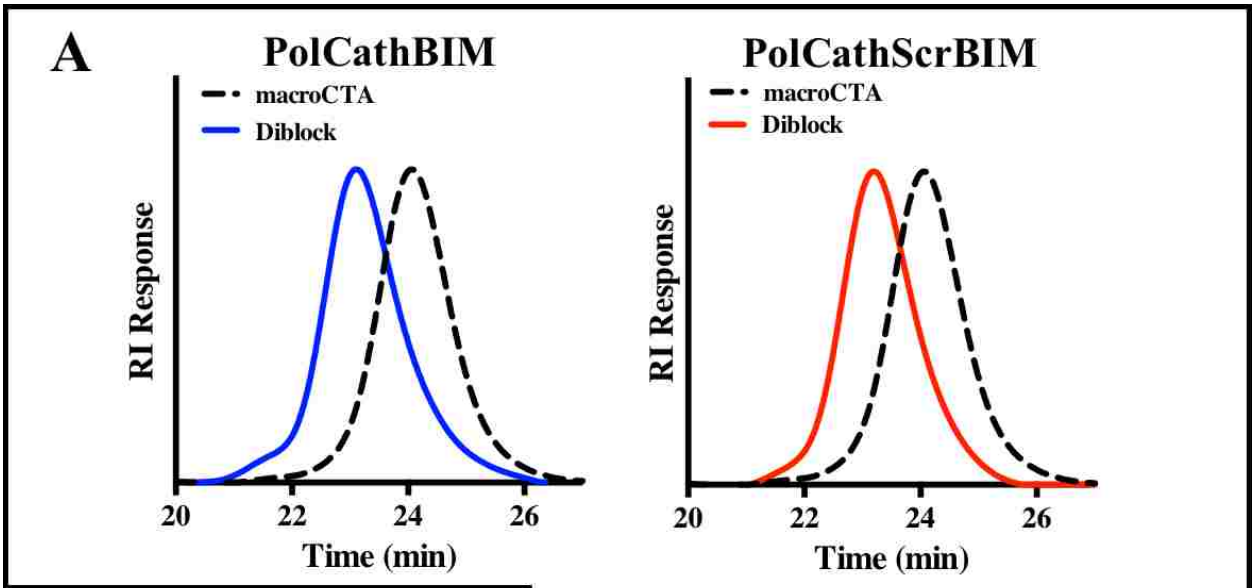

Figure 4.10. Continued on next page.

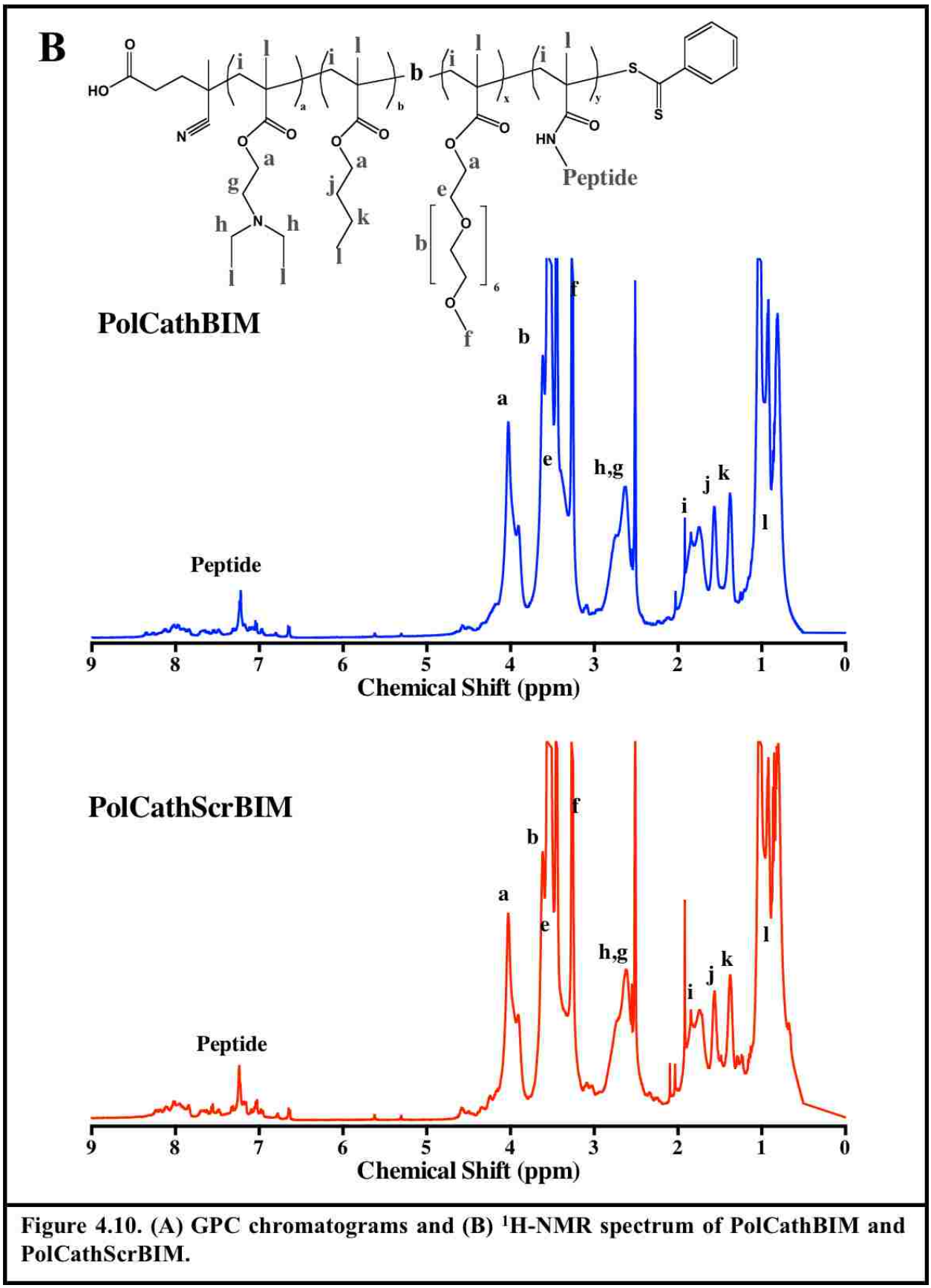

Figure 4.10. (A) GPC chromatograms and (B) ^{1}H-NMR spectrum of PolCathBIM and PolCathScrBIM.

used to determine the peptide content of the polymers. PolCathBIM and PolCathScrBIM contained 0.9 and 0.8 peptide units per polymer chain, respectively.

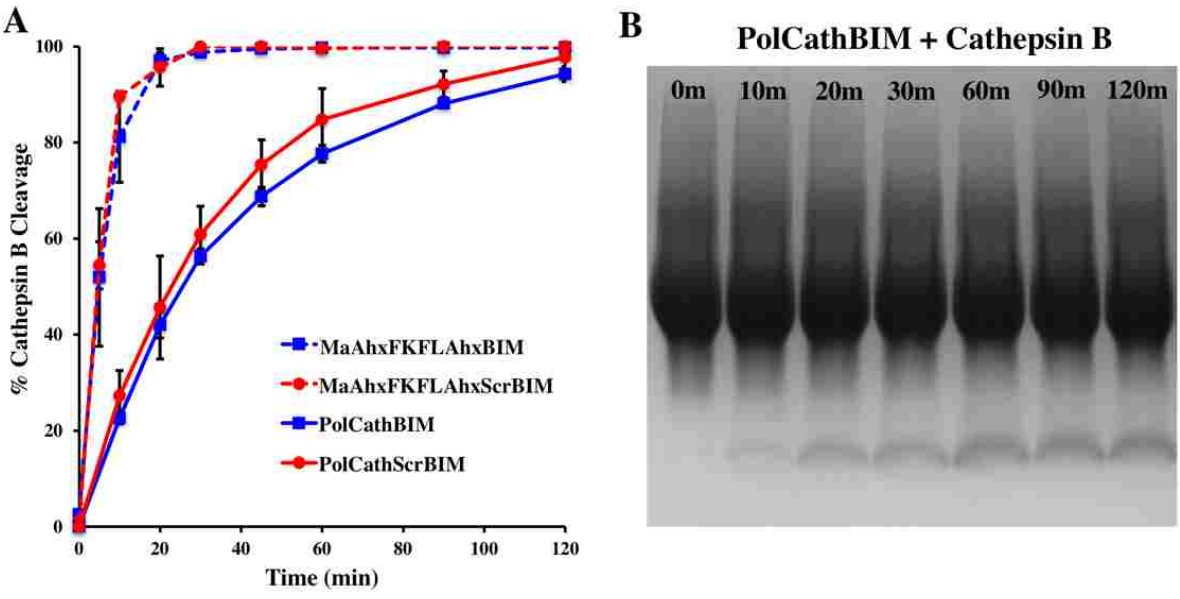

Figure 4.11. Cathepsin B cleavage of the diblock copolymers. (A) Peptide monomers (MaAhxFKFLAhxBIM & MaAhxFKFLAhxScrBIM) and their respective diblock copolymers (PolCathBIM & PolCathScrBIM) were incubated with human liver cathepsin B in phosphate buffer at pH 6.6. At various timepoints the reactions were stopped by addition of E-64 thioprotease inhibitor and reaction products were analyzed by RP-HPLC and MS. Cathepsin B efficiently cleaved the FKFL linker of PolCathBIM and PolCathScrBIM to release FLAhxBIM, although the kinetics were slower than for the peptide monomers alone. **(B)** Peptide release from the backbone of the BIM-containing diblock copolymer was also visualized by protein gel analysis. A BIM peptide band appeared and increased in intensity with incubation time.

4.3.3.2 Cathepsin B Cleavage of pH-responsive Diblock Copolymers

To confirm cathepsin B-mediated cleavage of the FKFL linker, diblock copolymers were incubated with human liver cathepsin B enzyme and degradation products were analyzed overtime by RP-HPLC and MS (**Figure 4.11A)**. Cathepsin B efficiently cleaved PolCathBIM and PolCathScrBIM at the FKFL linker to release the desired (2980 Da) peptide product. However, the kinetics of polymer cleavage were significantly slower than

for the peptide monomers alone, suggesting the PEGMA is still providing some degree of protection. Cathepsin B-mediated release of peptide from PolCathBIM was also visualized by protein gel analysis (**Figure 4.11B**). These findings suggest cathepsin B will release active BIM peptide from its polymeric carrier within the endosomes of cancer cells.

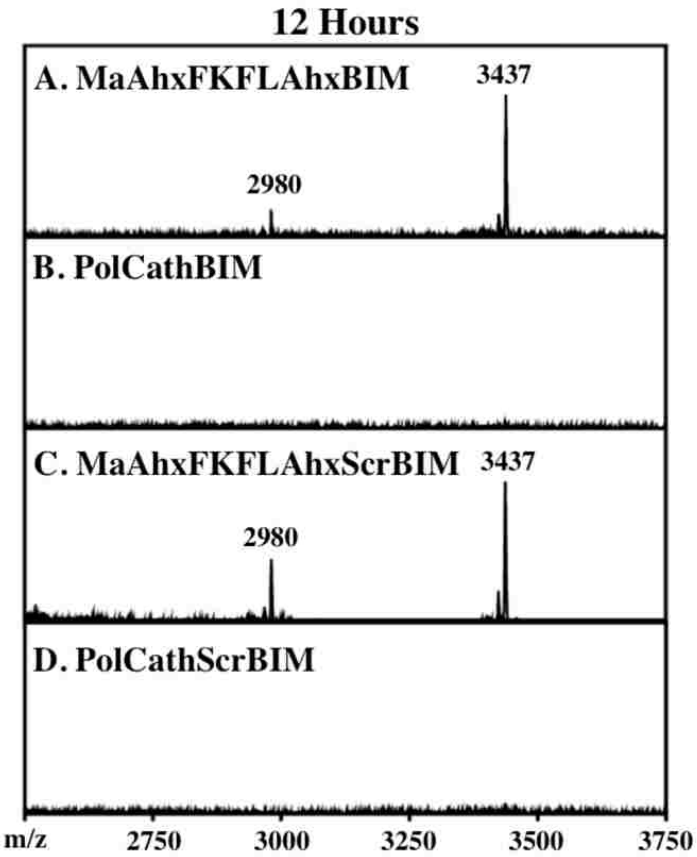

Figure 4.12. Stability of the FKFL linker in human serum. Peptide monomers/polymers (400 μM) were incubated in human serum and peptide products were extracted and analyzed by MALDI-TOF MS. Spectrum at 12 hours are shown. **(A & C)** Peptide monomers (3437 Da) underwent low levels of cleavage at the FKFL linker to release FLAhxBIM (2980 Da). **(B & D)** In contrast, formulation into polymers prevented undesired cleavage of the FKFL linker by serum proteases.

4.3.4 Stability of the FKFL Linker in Human Serum

To investigate the susceptibility of the FKFL peptide linker to extracellular protease degradation, the peptide macromonomers (MaAhxFKFLAhxBIM and MaAhxFKFLAhxScrBIM) and their corresponding diblock copolymers (PolCathBIM and PolCathScrBIM) were incubated in human serum at 37 °C. At timepoints ranging from 0 to 12 hours, peptide products were extracted from the serum into acetonitrile and analyzed by MALDI-TOF MS. For both MaAhxFKFLAhxBIM and MaAhxFKFLAhxscrBIM, intact peptide monomer (3437 Da) was detectable after 12 hours. However, low levels of cleavage at the FKFL linker did occur, with the slow appearance of a 2980 Da peak observed over time. The polymers were found to protect against degradation at the FKFL linker, as the 2980 Da peak was absent at all time points. Representative spectra after 12 hours are shown in **Figure 4.12.**

4.3.5 Micelle Sizing and pH-responsive Membrane Destabilizing Activity

To confirm pH-dependent micelle formation, dynamic light scattering (DLS) was employed to measure particle sizes in phosphate buffers of varying pH (5.8-7.4) (**Figure 4.13A**). At pH 7.4, PolCathBIM and PolCathScrBIM assembled into micelles with hydrodynamic diameters of 25 nm and 26 nm, respectively. As the pH was decreased step-wise to 5.8, the micelles disassembled into unimers with diameters of 6 nm.

The polymers' corresponding pH-responsive membrane destabilizing activity was evaluated using a red blood cell hemolysis assay (**Figure 4.13B**). The polymers (60 μg/mL) were incubated with red blood cells at varying pH values, and the release of heme groups (hemolysis) was measured spectrophotometrically (abs 541 nm). At pH 7.4, no significant red blood cell lysis was observed. However, as the pH was lowered to the values found in early (6.6) and late

endosomes (5.8), a sharp increase in hemolysis occurred, with >95% lysis observed at pH 6.6. These findings demonstrate the potential of these polymers as pH-responsive intracellular delivery vehicles

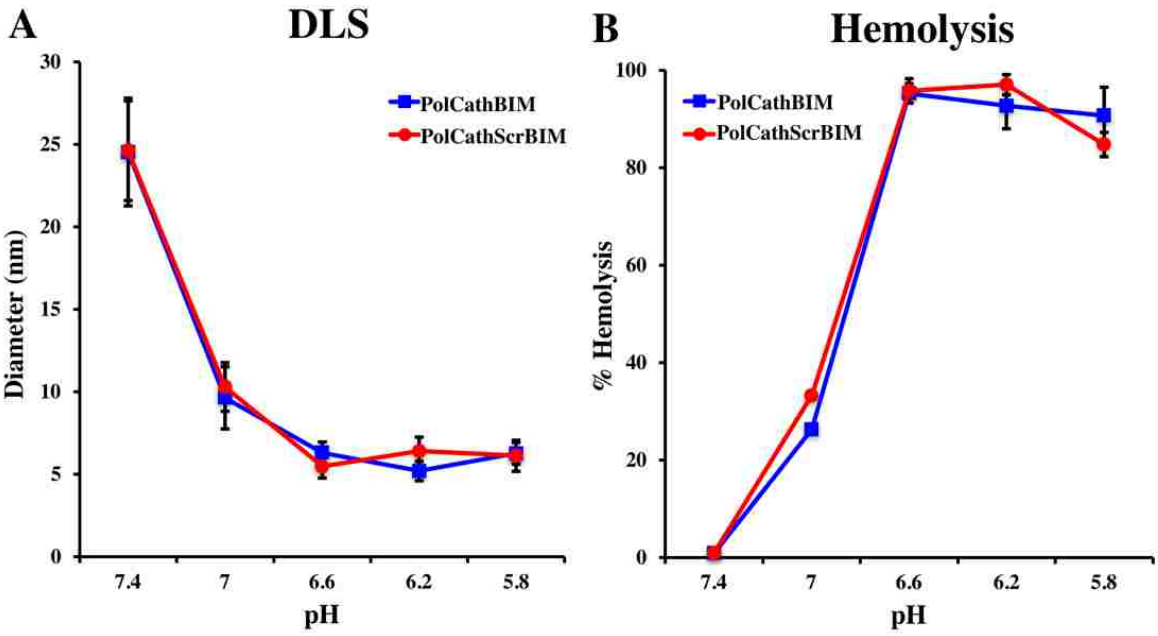

Figure 4.13. The cathepsin B-cleavable diblock copolymers demonstrate pH-responsive membrane destabilizing activity. (A) Dynamic light scattering (DLS) was employed to measure particle diameters in phosphate buffers of varying pH. At pH 7.4 the polymers formed micelles, which disassembled into unimers of smaller diameter at more acidic pH values. **(B)** A red blood cell lysis assay demonstrated a corresponding increase in membrane destabilizing activity with decrease in pH. Red blood cells were incubated with polymers (60 μg/mL) and % heme release was quantified relative to a 0.1% TritonX-100 positive control.

4.3.6 Ovarian Cancer Cell Viability

To assess the anticancer activity of PolCathBIM, a cytotoxicity study was conducted in SKOV3 ovarian cancer cells (**Figure 4.14A)** and 3T3 fibroblasts (**Figure 4.14B)**. PolCathBIM potently induced SKOV3 cell death in a dose dependent fashion. After 96 hours of treatment with 10 μM PolCathBIM, only 25% of SKOV3s remained viable. In contrast, PolCathScrBIM exhibited

minimal toxicity with greater than 90% cell viability observed at all polymer concentrations. In 3T3 fibroblasts, no BIM-mediated cell death was observed. These finding suggest that BIM delivery specifically kills cancer cells with dysregulated Bcl-2 signaling.

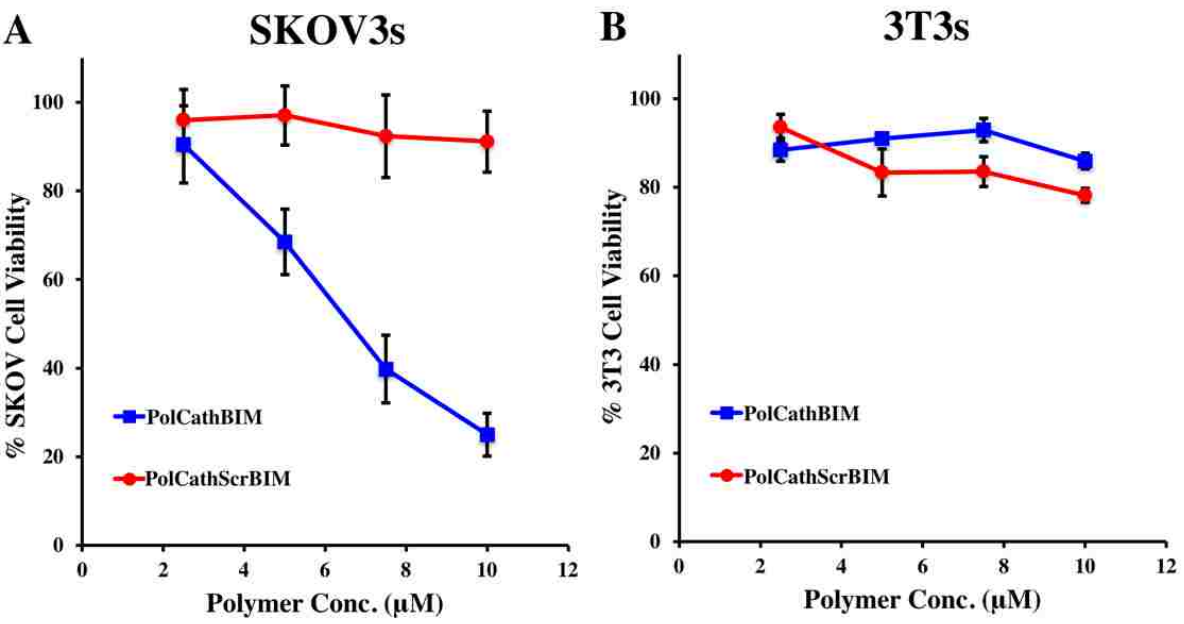

Figure 4.14. The cathepsin B-cleavable BIM polymer induces cell death in ovarian cancer cell cultures. (A) In a dose-responsive manner, PolCathBIM reduced the viability of SKOV3 cells at 96 hours as measured by MTS assay. **(B)** In contrast, no activity was observed in non-cancerous 3T3 cell cultures even after 120 hours of treatment.

4.3.7 Induction of Apoptotic Markers: Caspase 3/7 Activity and Annexin V Staining

Activation of caspase-3 and caspase-7, a critical step in apoptosis, was measured using a profluorescent enzyme substrate. After 72 hours, SKOV3 cells that were treated with polymer containing BIM (PolCathBIM) exhibited a dose-dependent increase in caspase 3/7 activity (**Figure 4.15A**), with 10 μM PolCathBIM resulting in more than 8-fold greater activity. In contrast, cells treated with PolCathScrBIM showed no change relative to untreated cultures.

Early in apoptosis, phosphatidylserine (PS) is translocated from the inner to outer plasma membrane, becoming exposed extracellularly. Consequently, apoptotic cells can be identified by staining with the human anti-coagulant annexin V, which binds to PS with high affinity. Treatment with PolCathBIM (10 μM) significantly increased annexin V staining of SKOV3s, with 87% of cells staining positive after 72 hours (**Figure 4.15B**). In contrast, only 15% of cells treated with PolCathScrBIM stained positive. In combination, these findings indicate that PolCathBIM kills cancer cells by inducing apoptosis.

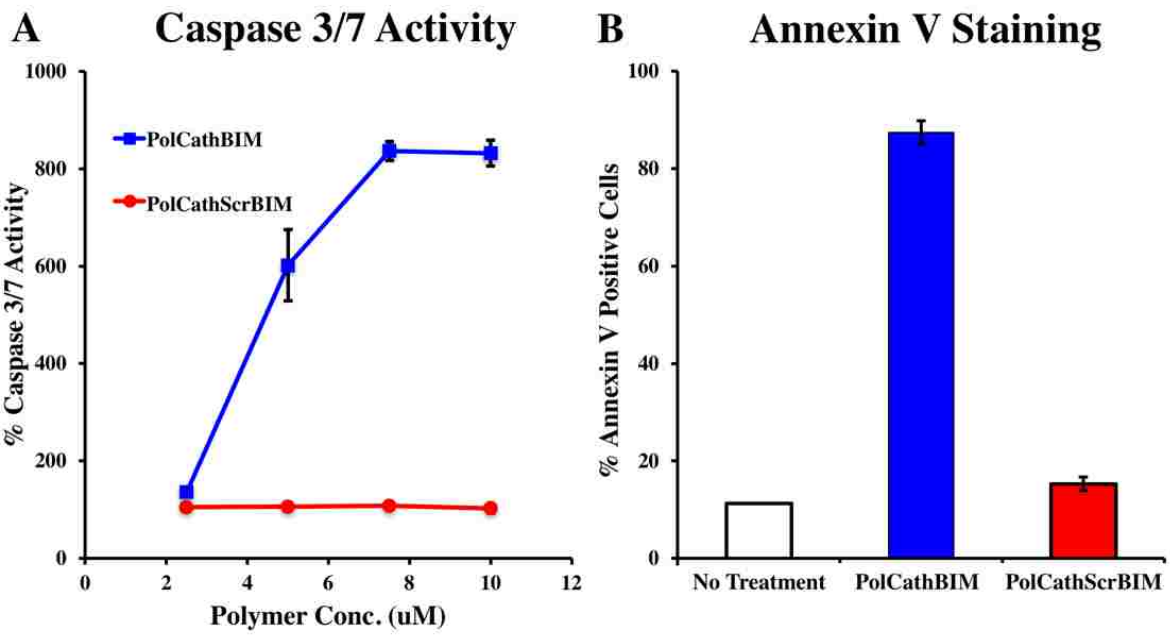

Figure 4.15. The cathepsin B-cleavable BIM polymer induces expression of apoptotic markers in SKOV3 ovarian cancer cells. (A) After 72 hours of polymer treatment, activation of caspase signaling was measured by addition of a pro-fluorescent caspase 3/7 substrate to cell cultures. Percent caspase 3/7 activity is reported relative to untreated cells. **(B)** After 72 hours of treatment with polymer (10 μM), FITC-annexin V dye was added to SKOV3 cultures and flow cytometry was used to measure percent of cells stained positive.

4.4 Discussion

Pro-apoptotic peptides targeting pro-survival Bcl-2 proteins have significant potential for inducing apoptosis and/or restoring chemosensitivity in cancer. However, before this potential can be realized, peptides must overcome a variety of drug delivery barriers. In previous work, RAFT polymerization was employed for the highly controlled synthesis of diblock copolymers tailored for peptide delivery[1,19]. The reported polymers contained a hydrophilic block for biocompatibility and peptide shielding in circulation, a pH-responsive block for escape from endosomes, and PDS groups for reversible disulfide conjugation to cysteine-containing drugs. These polymers successfully enhanced the intracellular delivery and activity of pro-apoptotic peptides in cancer cell cultures and a murine xenograft model of B-cell lymphoma[1,19]. It was the objective of this work to increase the stability of the polymer-peptide linkage by incorporating a chemically stable peptide linker that is specifically cleaved within the endo/lysosomes of cancer cells. This objective was achieved through the synthesis and RAFT polymerization of a peptide macromonomer containing the pro-apoptotic peptide BIM capped with a cathepsin B-labile peptide linker (**Figure 4.1**).

Reducible disulfide linkers have been widely investigated for drug delivery. They aim to harness the high redox potential difference between the oxidizing extracellular environment and reducing intracellular environment for specific release inside cells[20]. Unfortunately, disulfide linkers have proven insufficiently stable in systemic circulation. In a pharmacokinetic study conducted in mice using dual-radiolabeled polymer-BIM conjugates, the peptide to polymer ratio in the blood dropped rapidly over the course of 24 hours[1]. An improved linker designed for high stability in circulation and efficient drug release inside target cells will be critical for enhancing the therapeutic efficacy of peptide drugs such as BIM.

Enzyme labile peptide linkers, specifically those cleaved by endo/lysosomal proteases, offer such an alternative. These linkers are chemically stable in the bloodstream and rapidly and specifically cleaved upon internalization into target cells. Cathepsin B, a ubiquitous cysteine protease in endo/lysosomes, is an ideal candidate for this application. Cathepsin B is only found extracellularly in rare pathological conditions[21-22], its cleavage substrates have been well-characterized[10-14], and cathepsin B-labile linkers have been implemented previously in ADCs[7], doxorubicin prodrugs[8], and degradable nucleic acid delivery vehicles[9].

As a linker, this work employed a four amino acid cathepsin B substrate, FKFL, that is rapidly cleaved between the lysine and C-terminal phenylalanine residues[9]. The substrate was flanked on each side by a six carbon spacer, Ahx, to spatially separate the site of enzymatic cleavage from the peptide drug and polymer backbone. The N-terminus of the BIM peptide was capped with this linker. Consequently, cathepsin B cleavage released a BIM peptide product modified on its N-terminus with FLAhx. Using a cytochrome C release assay, this modification was found to have no impact on BIM's pro-apoptotic activity (**Figure 4.7**). The linker-peptide sequence was functionalized on its N-terminus with methacrylamide and polymerized directly into a pH-responsive diblock copolymer (PolCathBIM) designed to enhance BIM's pharmacokinetic and tumor delivery properties. The pH-responsive hydrophobic block consisted of DEAEMA and BMA, and the hydrophilic block contained peptide and $PEGMA_{300}$. An eqivalent cathepsin-B cleavable control polymer was synthesized containing a scrambled BIM peptide sequence (PolCathScrBIM).

To evaluate the ability of cathepsin B to cleave the FKFL linker, peptide monomers and polymers were incubated with cathepsin B and the degradation products were analyzed over time by RP-HPLC, MS, and protein gel electrophoresis. Cathepsin B cleaved both the peptide

monomers and peptide-containing diblock copolymers (PolCathBIM & PolCathScrBIM) at the FKFL linker (**Figure 4.11A-B**). Polymerization was found to slow the rate of enzymatic cleavage, but greater than 94% of polymer cleavage was still complete by 2 hours.

Previously, diblock copolymers containing $PEGMA_{950}$ demonstrated superior pharmacokinetics and tumor distribution compared to $PEGMA_{300}$ in a B-cell lymphoma xenograft model[1]. To investigate the effect of PEGMA length on cathepsin B cleavage, the BIM peptide macromonomer (MaAhxFKFLAhxBIM) was copolymerized with either $PEGMA_{300}$ or $PEGMA_{950}$. Protein gel analysis showed that $PEGMA_{950}$ effectively blocked cathepsin B access to the FKFL linker, while $PEGMA_{300}$ did not. In the future, placing a longer and/or more hydrophilic spacer between the polymer backbone and enzyme substrate may permit cathepsin B access in the context of $PEGMA_{950}$. Alternatively, block or co-polymerizations of peptide, $PEGMA_{300}$ and $PEGMA_{950}$ might combine the individual strengths of the monomers.

To assess the susceptibility of the FKFL linker to cleavage within the bloodstream, the peptide monomers and diblock copolymers (PolCathBIM & PolCathScrBIM) were incubated in human serum and the degradation products were analyzed over time **(Figure 4.12)**. The peptide monomers were found to cleave at the FKFL linker, but only at very low levels. Completely intact peptide monomer was still detectable at time points as late as 12 hours. Furthermore, extracellular degradation by serum proteases was abrogated by formulation into polymers, with cleavage products undetectable even at later time points. In combination, these findings suggest that the diblock copolymer design strikes an advantageous balance between protecting linker degradation in circulation and permitting cathepsin B access and peptide release upon internalization. However, investigation of alternative cathepsin B substrates may further enhance circulation

stability. In particular, the dipeptide valine-citrulline is known to increase the circulation half-life of ADCs in comparison to phenylalanine-lysine[23].

pH-responsive membrane destabilizing activity is known to be critical for intracellular delivery[15-16,18-19]. After polymer micelles are endocytosed, the acidic environment triggers them to disassemble into unimers, destabilize the endosomal membranes, and release their cargo into the cell cytosol. The pH-dependent activities of PolCathBIM and PolCathSrBIM were assessed by dynamic light scattering and a red blood cell hemolysis assay. At pH 7.4, both polymers formed micelles which then diassembled with decrease in pH to endo/lysosomal values (6.6-5.8) (**Figure 4.13A**). Micelle disassembly correlated strongly with an increase in the polymers' hemolytic activity (**Figure 4.13B),** suggesting that the polymers will be endolytically active.

The peptide BIM is poised to make large impact in the field of cancer therapy if it can be effectively delivered into tumor cells. Consequently, BIM was selected as a model peptide to validate the described polymer delivery vehicle. The cathepsin-B cleavable BIM polymer potently induced cell death in SKOV3 ovarian cancer cells, in comparison to a control polymer containing an inactive peptide sequence **(Figure 4.14A)**. A corresponding increase in caspase 3/7 activity and PS externalization (annexin V staining) was observed, indicating that the mechanism of cell death is BIM-mediated activation of the apoptotic cascade (**Figure 4.15)**. In contrast, the BIM-containing polymer did not exhibit bioactivity in 3T3 fibroblast cultures (**Figure 4.14B)**. This demonstrates the potential of BIM for killing cancer cells while sparing healthy tissues.

Peptide therapeutics possess enormous potential as anti-cancer agents. In this report, an enzyme-cleavable diblock copolymer was validated for the intracellular delivery and activity of the pro-apoptotic peptide BIM in ovarian cancer cell cultures. The described polymer offers two key advantages over previously employed disulfide linkages. First the cathepsin-labile peptide

linker is highly stable in human serum and efficiently cleaved inside target cells. Second, peptide incorporation via RAFT polymerization eliminates post-synthetic conjugation and substantially simplifies material manufacturing. Consequently, this work may represent a small but important step towards realizing the promise of a number of therapeutic peptides with intracellular drug targets.

REFERENCES

[1] Berguig, G.Y.; Convertine, A.J.; Frayo, S.; Kern, H.B.; Procko, E.; Roy, D.; Srinivasan, S.; Margineantu, D.H.; Booth, G.; Palanca-Wessels, M.C.; Baker, D.; Hockenbery, D.; Press, O.W.; Stayton, P.S. Intracellular delivery system for antibody-peptide drug conjugates. *Mol Ther*. **2015**, 23, 907-17.

[2] Roberts, R. Lysosomal cysteine proteases: structure, function and inhibition of cathepsins. *Drug News Perspect*. **2005**, 18, 605-14.

[3] Authier, F.; Métioui, M.; Bell, A.W.; Mort, J.S. Negative regulation of epidermal growth factor signaling by selective proteolytic mechanisms in the endosome mediated by cathepsin B. *J Biol Chem*. 1999, 274, 33723-31.

[4] Blum, J.S.; Fiani, M.L.; Stahl, P.D. Proteolytic cleavage of ricin A chain in endosomal vesicles. Evidence for the action of endosomal proteases at both neutral and acidic pH. *J Biol Chem*. **1991**, 266, 22091-5.

[5] Lautwein, A.; Kraus, M.; Reich, M.; Burster, T.; Brandenburg, J.; Overkleeft, H.S.; Schwarz, G.; Kammer, W.; Weber, E.; Kalbacher, H.; Nordheim, A.; Driessen, C. Human B lymphoblastoid cells contain distinct patterns of cathepsin activity in endocytic compartments and regulate MHC class II transport in a cathepsin S-independent manner. *J Leukoc Biol*. **2004**, 75, 844-55.

[6] Dubowchik, G.M.; Firestone, R.A.; Padilla, L.; Willner, D.; Hofstead, S.J.; Mosure, K.; Knipe, J.O.; Lasch, S.J.; Trail, P.A. Cathepsin B-labile dipeptide linkers for lysosomal release of doxorubicin from internalizing immunoconjugates: model studies of enzymatic drug release and antigen-specific in vitro anticancer activity. *Bioconjug Chem*. **2002**, 13, 855-69.

[7] Doronina, S.O.; Toki, B.E.; Torgov, M.Y.; Mendelsohn, B.A.; Cerveny, C.G.; Chace, D.F.; DeBlanc, R.L.; Gearing, R.P.; Bovee, T.D.; Siegall, C.B.; Francisco, J.A.; Wahl, A.F.; Meyer, D.L.; Senter, P.D. Development of potent monoclonal antibody auristatin conjugates for cancer therapy. *Nat Biotechnol*. **2003**, 21, 778-84.

[8] Shao, L.H.; Liu, S.P.; Hou, J.X.; Zhang, Y.H.; Peng, C.W.; Zhong, Y.J.; Liu, X.; Liu, X.L.; Hong, Y.P.; Firestone, R.A.; Li, Y. Cathepsin B cleavable novel prodrug Ac-Phe-Lys-PABC-ADM enhances efficacy at reduced toxicity in treating gastric cancer peritoneal carcinomatosis: an experimental study. *Cancer*. **2012**, 118, 2986-96.

[9] Chu, D.S.; Johnson, R.N.; Pun, S.H. Cathepsin B-sensitive polymers for compartment-specific degradation and nucleic acid release. *J Control Release*. **2012**, 157, 445-54.

[10] Cezari, M.H.; Puzer, L.; Juliano, M.A.; Carmona, A.K.; Juliano, L. Cathepsin B carboxydipeptidase specificity analysis using internally quenched fluorescent peptides. *Biochem J*. **2002**, 368(Pt 1), 365-9.

[11] Cotrin, S.S.; Puzer, L.; de Souza Judice, W.A.; Juliano, L.; Carmona, A.K.; Juliano, M.A. Positional-scanning combinatorial libraries of fluorescence resonance energy transfer

peptides to define substrate specificity of carboxydipeptidases: assays with human cathepsin B. *Anal Biochem*. **2004**, 335, 244-52.

[12] Hasnain, S.; Hirama, T.; Tam, A.; Mort, J.S. Characterization of recombinant rat cathepsin B and nonglycosylated mutants expressed in yeast. New insights into the pH dependence of cathepsin B-catalyzed hydrolyses. *J Biol Chem*. **1992**, 267, 4713-21.

[13] Dubowchik, G.M.; Firestone, R.A. Cathepsin B-sensitive dipeptide prodrugs. 1. A model study of structural requirements for efficient release of doxorubicin. *Bioorg Med Chem Lett*. **1998**, 8, 3341-6.

[14] Stachowiak, K.; Tokmina, M.; Karpińska, A.; Sosnowska, R.; Wiczk, W. Fluorogenic peptide substrates for carboxydipeptidase activity of cathepsin B. *Acta Biochim Pol*. 2004, 51, 81-92.

[15] Manganiello, M.J.; Cheng, C.; Convertine, A.J.; Bryers, J.D.; Stayton, P.S. Diblock copolymers with tunable pH transitions for gene delivery. *Biomaterials*. **2012**, 33, 2301-9.

[16] Cheng, C.; Convertine, A.J.; Stayton, P.S.; Bryers, J.D. Multifunctional triblock copolymers for intracellular messenger RNA delivery. *Biomaterials*. **2012**, 33, 6868-76.

[17] Lutz, J.F. Polymerization of oligo(ethylene glycol) (meth)acrylates: Toward new generations of smart biocompatible materials. *J Polym Sci A: Polym Chem*. **2008**, 46, 3459–3470.

[18] Convertine, A.J.; Benoit, D.S.; Duvall, C.L.; Hoffman, A.S.; Stayton, P.S. Development of a novel endosomolytic diblock copolymer for siRNA delivery. *J Control Release*. **2009**, 133, 221-9.

[19] Duvall, C.L.; Convertine, A.J.; Benoit, D.S.; Hoffman, A.S.; Stayton, P.S. Intracellular delivery of a proapoptotic peptide via conjugation to a RAFT synthesized endosomolytic polymer. *Mol Pharm*. **2010**, 7, 468-76.

[20] Meister, A.; Anderson, M.E. Glutathione. *Annu Rev Biochem*. **1983**, 52, 711–760.

[21] Hashimoto, Y.; Kakegawa, H.; Narita, Y.; Hachiya, Y.; Hayakawa, T.; Kos, J.; Turk, V.; Katunuma, N. Significance of cathepsin B accumulation in synovial fluid of rheumatoid arthritis. *Biochem Biophys Res Commun*. **2001**, 283, 334-9.

[22] Sinha, A.A.; Jamuar, M.P.; Wilson, M.J.; Rozhin, J.; Sloane, B.F. Plasma membrane association of cathepsin B in human prostate cancer: biochemical and immunogold electron microscopic analysis. *Prostate*. **2001**, 49, 172-84.

[23] Ducry, L.; Stump, B. Antibody-drug conjugates: linking cytotoxic payloads to monoclonal antibodies. *Bioconjug Chem*. **2010**, 21, 5-13

CHAPTER 5. The Apoptotic Activity and Therapeutic Efficacy of the Cathepsin B-cleavable BIM Polymer in an Intraperitoneal Mouse Model of Ovarian Cancer

Abstract

Ovarian cancer is the most common gynecological cancer in the United States and the most deadly cancer among women. Despite treatment with surgery and chemotherapy, more than 75% of women with stage III or IV disease relapse and die. Consequently, the BIM peptide presents a promising alternative therapy as either a single agent or chemosensitizer. It is the objective of Chapter 5 to evaluate the therapeutic efficacy of intracellular BIM delivery in an intraperitoneal (IP) luciferase-expressing xenograft model of ovarian cancer. The cathepsin B-cleavable BIM polymer developed in Chapter 4 was selected for further evaluation due to its dramatically superior stability in comparison to disulfide-linked polymer-peptide conjugates. A biotin functionality was incorporated into the diblock copolymer via RAFT polymerization for binding to cancer-specific Herceptin-streptavidin (SA) conjugates. A toxicity study in healthy mice demonstrated the safety of multiple high (150-250 mg/kg) polymer doses injected IP. Induction of apoptosis is being evaluated by immunohistochemical staining of tumors for cleaved caspase 3 (CC3) and the proliferation marker Ki-67. Lastly, a study evaluating the ability of the BIM delivery system to inhibit tumor growth and prolong animal survival is ongoing. To assess for potential drug synergy, apoptotic activity and tumor growth experiments are conducted in combination with low-dose carboplatin. Impending results will demonstrate the potential of the antibody-targeted peptide prodrug system for cancer therapy and/or suggest avenues for improving the system design.

5.1 Introduction

Ovarian cancer is the most common gynecological cancer in the United States and the most deadly cancer among women. The overall five-year survival is only 45% due to late diagnosis and chemoresistance[1]. At the time of diagnosis, more than 60% of women have stage III or IV disease that has spread within the peritoneal cavity[2]. Standard treatment involves surgical debulking followed by intravenous (IV) platinum (cisplatin or carboplatin) and taxane (paclitaxel or docetaxel) chemotherapy. While this combination is highly efficacious, more than 75% of patients with stage III or stage IV disease will eventually relapse and die[3]. Consequently, the BIM peptide presents a promising alternative therapy as either a single agent or chemosensitizer.

In the majority of cases, ovarian cancer spread is contained in the peritoneal cavity at the time of diagnosis[4]. Intraperitoneal (IP) administration of relevant chemotherapies (cisplatin, carboplatin, paclitaxel, docetaxel) has been shown to permit higher peritoneal drug concentrations and longer peritoneal drug half-lives[5]. Numerous clinical trials have demonstrated improved survival with the incorporation of IP chemotherapy into standard treatment regimens[6-8]. IP administration of nanocarriers has also been investigated for the delivery of chemotherapeutics[9], radioisotopes[10], siRNA[11], and DNA vectors[12] in IP xenograft models. In a peritoneal metastatic gastric cancer model, drug distribution was compared following IP and intravenous (IV) administration of paclitaxel-loaded nanoparticles consisting of 2-methacryloxyethyl phosphorycholine (MPC) and butyl methacrylate (BMA)[13]. IP injection resulted in less drug accumulation in the liver and more rapid and deeper drug penetration into metastatic nodules.

In this work, the apoptotic activity of the cathepsin-B cleavable BIM prodrug system following IP injection is being evaluated in an IP luciferase-expressing SKOV3 xenograft model of ovarian cancer. Luciferase expression advantageously permits serial non-invasive

bioluminescent imaging of tumor burden. Activation of caspase 3/7 enzymes is being evaluated by immunohistochemical staining of tumors for cleaved caspase 3 (CC3) and Ki-67. The degree of nanoparticle/macromolecule penetration usually varies inversely with tumor size. Consequently, both small and large tumors were excised and are being stained for apoptotic markers. A study is also currently underway to evaluate the ability of the BIM delivery system to inhibit tumor growth and prolong animal survival.

For SKOV3 tumor targeting and uptake, Herceptin antibodies are incorporated via streptavidin (SA)-biotin binding. Herceptin is a monoclonal antibody approved for the treatment of HER2/neu+ breast cancers[14]. Steptavidin-conjugated monoclonal antibodies have been extensively developed by Dr. Oliver Press' group for pre-targeted radioimmunotherapies[15]. Previous studies in Dr. Press' lab have demonstrated Herceptin-SA binding and internalization in SKOV3s, and anti-HER2 targeting has been employed successfully in a number of other intracellular drug delivery applications[16-18].

Lastly, the activity of BIM is being investigated in combination with low-dose carboplatin (35 mg/kg). Impaired apoptosis is a hallmark of cancer and a common mechanism of chemoresistance. Consequently, therapeutics such as BIM that reestablish apoptotic signaling may enhance the efficacy of chemotherapy. In SKOV3 cancer cells, Bcl-2 inhibition has been shown to synergize with various chemotherapeutic agents[19-21]. *Chen et al*. tested navitoclax (a small molecule inhibitor of Bcl-2, Bcl-xl and Bcl-2) in combination with 19 chemotherapy drugs across 46 human solid tumor cell lines[21]. One of the most potent combinations was navitoclax and carboplatin in SKOV3s (CI=0.62).

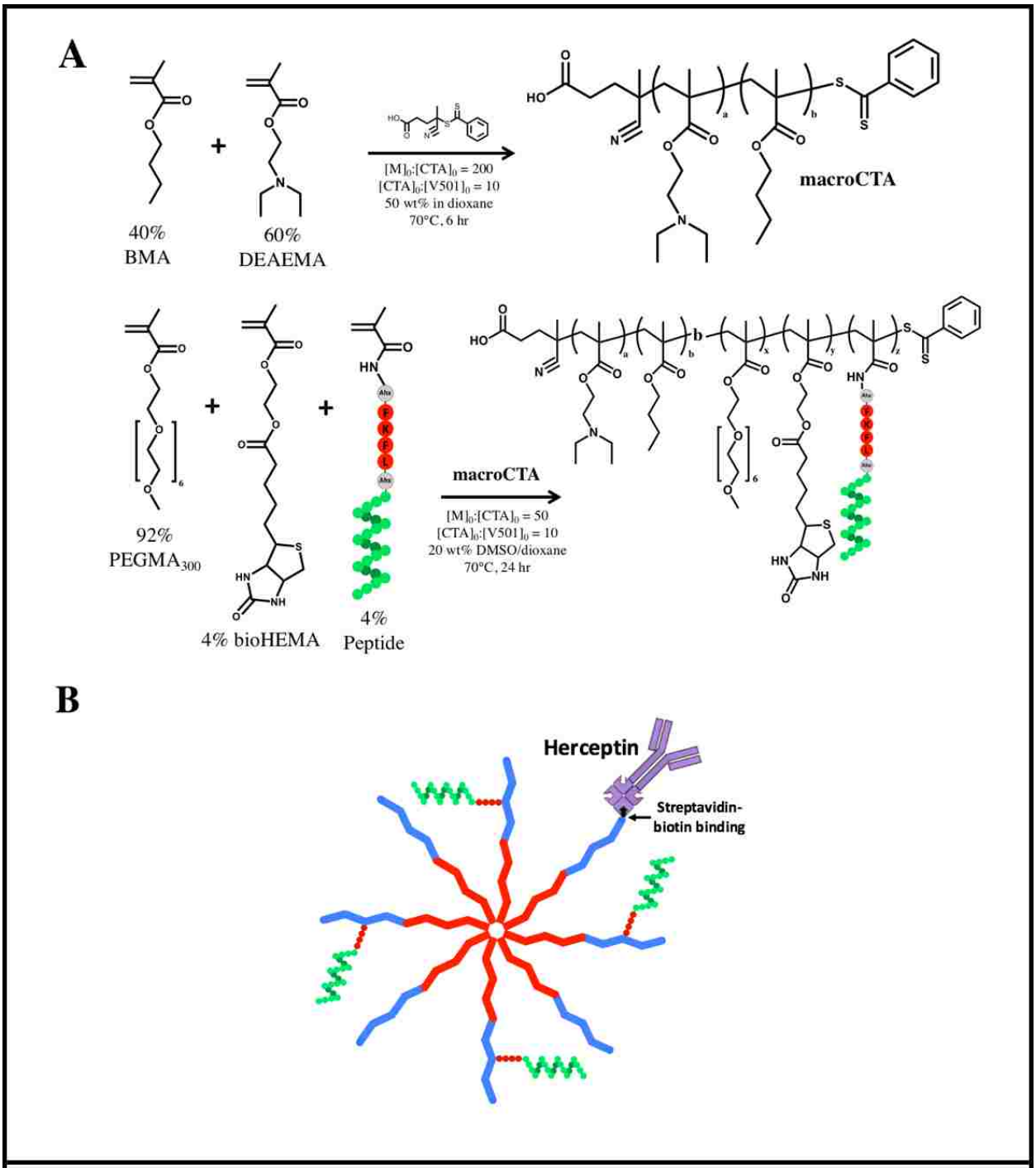

Scheme 5.1. (A) RAFT synthesis of biotin-containing, cathepsin B-cleavable diblock copolymers for the intracellular delivery of BIM. **(B)** The biotin monomer binds to anti-body-streptavidin conjugates for tumor-specific targeting.

To date, the Cathepsin B-cleavable BIM polymer described in Chapter 4 has been resynthesized containing a biotin functionality for binding to Herceptin-SA conjugates (**Scheme 5.1**). A toxicity study in healthy mice demonstrated the safety of multiple high (150-250 mg/kg) polymer doses injected IP. For evaluating markers of apoptosis, excised tumors are currently being stained for CC3 and Ki-67 at Seattle Children's Hospital. For evaluating tumor growth inhibition and animal survival, treatment will be initiated in tumor-bearing mice on May 16, 2016. Pending results will be reported to Supervisory Committee members as they become available.

5.2 Materials and Methods

5.2.1 Synthesis and Characterization of Peptide Macromonomers

Peptides were synthesized from FMOC protected (L) amino acids (EMD Millipore) and an FMOC protected 6-aminohexanoic acid (Ahx) spacer (AnaSpec) on a solid support (rink amide MBHA resin (100-200 mesh), EMD Millipore) using an automated PS3 peptide synthesizer (Protein Technologies). For the synthesis of corresponding methacrylamido-peptide monomers, the amino termini of the peptides were deprotected and functionalized with N-succinimidyl methacrylate (TCI America), while still linked to the resin. Two cathepsin B-cleavable peptide monomers were synthesized containing either BIM or a scrambled BIM (ScrBIM) motif: methacrylamido (Ma)-AhxFKFLAhxMRPEIWIAQELRRIGDEFNAY (MaAhxFKFLAhxBIM) and MaAhxFKFLAhxLRMREIIDAYERQFGEPNIWA (MaAhxFKFLAhxScrBIM). The peptide macromonomers were deprotected/cleaved from the resin by treatment with trifluoroacetic acid/triisopropylsilane/H_2O (9.5:2.5:2.5, v/v/v) for 4 hours and precipitated in cold ether. Crude peptide monomers were purified by reverse phase high performance liquid chromatography (RP-HPLC) on a Jupiter 5 μm C18 300Å column (Phenomenx) with an Agilent 1260 HPLC. Ion trap mass spectrometry with electrospray (Bruker Esquire) was used to confirm the molecular weights of the purified products.

5.2.2 Synthesis of Biotin Monomer

Biotin (2.0 g, 8.19 mmol, 1 eqv.) was dissolved in DMSO (20 mL) in the dark overnight, after which DMAP (4.0 g, 33.7 mmol, 4 eqv.) and HEMA (4.2 g, 33.7 mmol, 4 eqv.) were added to the solution and allowed to dissolve. DIC (5.07 mL, 33.7 mmol, 4 eqv.) was then added and

the reaction was allowed to proceed for 18 hours in the dark. The reaction solution was then filtered, precipitated in cold HEPES buffer (3 ^{o}C, 150 mM, pH 8.4), washed with deionized water and dried under high vacuum. The resulting monomer, biotin-hydroxyethyl methacrylate (bioHEMA), was characterized by 1H-NMR.

5.2.3 RAFT Polymer Synthesis ***(Scheme 5.1)***

The cathepsin-B cleavable BIM polymer described in Chapter 3 was resynthesized to incorporate a biotin monomer, biotin conjugated hydroxyethyl methacrylate (bioHEMA), for binding to antibody-streptavidin (SA) conjugates. First, RAFT copolymerization of a macroCTA consisting of N,N-diethylaminoethyl methacrylate (DEAEMA) and butyl methacrylate (BMA) was conducted under nitrogen atmosphere in dioxane (50 wt% monomer) at 70 °C for 6 hours using 4-cyanopentanoic acid dithiobenzoate (CTP) as the chain transfer agent (CTA) and azobis(4-cyanopentanoic acid) (ABCVA) as the radical initiator. The molar composition of the reaction feed was 60% DEAEMA and 40% BMA, and the initial monomer ($[M]_o$) to CTA ($[CTA]_o$) to initiator ($[I]_o$) ratio was 200:1:0.1. The resulting macroCTA, poly[(DEAEMA)-co-(BMA)], was purified by dialysis in acetone for 48 hours, followed by dialysis in water for 24 hours, and dried by lyophilization. The macroCTA was then employed for block copolymerization of $PEGMA_{300}$, bioHEMA, and peptide monomer. Two different polymers were synthesized by varying the identity of the peptide monomer: poly[(DEAEMA)-co-(BMA)]-b-[($PEGMA_{300}$)-c-(bioHEMA)-c-(MaAhxFKFLAhxBIM)] and poly[(DEAEMA)-co-(BMA)]-b-[($PEGMA_{300}$)-c-(bioHEMA)-c-(MaAhxFKFLAhxScrBIM)]. The polymers are abbreviated as PolCathBIM and PolCathScrBIM, respectively. The block copolymerizations were conducted for 18 hours at 70 °C under nitrogen atmosphere in an equal by volume mixture of dimethyl sulfoxide (DMSO) and dioxane (20 wt%

monomer and macroCTA). The molar composition of the monomer feed was 92% $PEGMA_{300}$, 4% bioHEMA, and 4% peptide, and the $[M]_o$:$[mCTA]_o$:$[I]_o$ ratio was 50:1:0.1. The resulting diblock copolymers were precipitated 4X in a mixture of petroleum ether and diethyl ether (9:1, v/v) to remove unreacted $PEGMA_{300}$ and solvents. To remove unreacted peptide, the polymers were redissolved in acetone, the peptide monomer was removed by centrifugation, and polymers were re-precipitated in petroleum ether. This two-step precipitation scheme was repeated 3X and the purified diblock copolymers were lyophilized.

5.2.4 Polymer Characterization by Gel Permeation Chromatography (GPC), ^{1}H-NMR and RP-HPLC

To measure the number average molecular weights (M_n) and polydispersities (PDIs) of the polymers, GPC was conduced using Tosoh SEC TSK GEL α-3000 and α-4000 columns (Tosoh Bioscience), a 1200 Series liquid chromatography system (Agilent), and a miniDAWN TREOS three-angle light scattering instrument with an Optilab TrEX refractive index detector (Wyatt Technology). The mobile phase was 0.1 wt% lithium bromide in HPLC-grade N,N-dimethylformamide at 60 °C and a flow rate of 1 mL/min. The compositions of the polymers were examined by ^{1}H-NMR spectroscopy (Bruker avance DRX 499). For quantification of peptide content, reaction aliquots were collected at T_o and T_x and analyzed by RP-HPLC (abs 280 nm). Percent monomer conversion was calculated by the equation (Peak[T_o]-Peak[T_x])/(Peak[T_o]) and used to estimate mol% peptide per polymer chain.

5.2.5 HABA

To quantify the bioHEMA available in the polymer for binding to SA or antibody-SA, a 4'-hydroxyazobenzene-2-carboxylic acid (HABA) binding assay was performed as previously described[22-23]. Briefly, SA was incubated with a 40-fold molar excess of HABA in the presence of increasing polymer concentrations. After 1 hour, the displacement of HABA by biotinylated polymer was measured by UV spectroscopy (abs 500 nm) and compared to a biotin standard curve.

5.2.6 Polymer Formulation into Micelles

Aqueous polymer solutions were prepared by first dissolving the polymer in ethanol at 100 mg/mL followed by rapid dilution into phosphate buffer saline (PBS) to a concentration of 10 mg/mL. Serial dilutions were made and absorbance at 282 nm was measured to determine extinction coefficients. Ethanol was removed by centrifugal dialysis in PBS (Amicon Ultra, 5 mL, 3K MWCO, Millipore), and final polymer concentrations were determined by UV spectrometry.

5.2.7 Antibody-polymer Conjugation

Polymer micelles formulated in PBS were incubated with antibody-SA conjugates for 2 hours prior to permit biotin-SA binding. The molar polymer to antibody ratio was approximately 110:1, equivalent to the maximum polymer dose tested in mice (250 mg/kg) and a clinically relevant antibody dose (15 mg/kg). Antibody-polymer conjugation was confirmed by non-reducing, non-denaturing protein gel electrophoresis. Conjugates (5 ug antibody, 83 ug polymer)

were run on a 4-20% precast Mini-PROTEAN TGX Precast Gel (Bio-Rad) in a Tris-Glycine buffer (Bio-Rad).

5.2.8 Synthesis of Z-DEVD-aminoluciferin ***(Scheme 5.2)***

5.2.8.1 Synthesis of Protected Z-DEVD Peptide

Using an automated PS3 peptide synthesizer (Protein Technologies) and standard FMOC chemistry, a protected Z-DEVD peptide fragment was synthesized on a selectively cleavable solid support resin (H-Asp(OtBu)HMPB NovaPEG, EMD Millipore) from Z-Asp(OtBu)-OH, FMOC-Glu(OtBu)-OH, and FMOC-Val-OH amino acids (EMD Millipore). To selectively cleave the protected peptide fragment from the resin, the resin was transferred to a fritted filter and washed at least five times with dichloromethane (DCM) (10-20 ml/g, contact time of at least 5 minutes). The resin was then treated with 1% trifluoroacetic acid (TFA) in DCM (10-15 mL/g) for 2-5 minutes, which was then sucked into a vessel containing 10% pyridine in methanol (2 ml/g). This treatment was

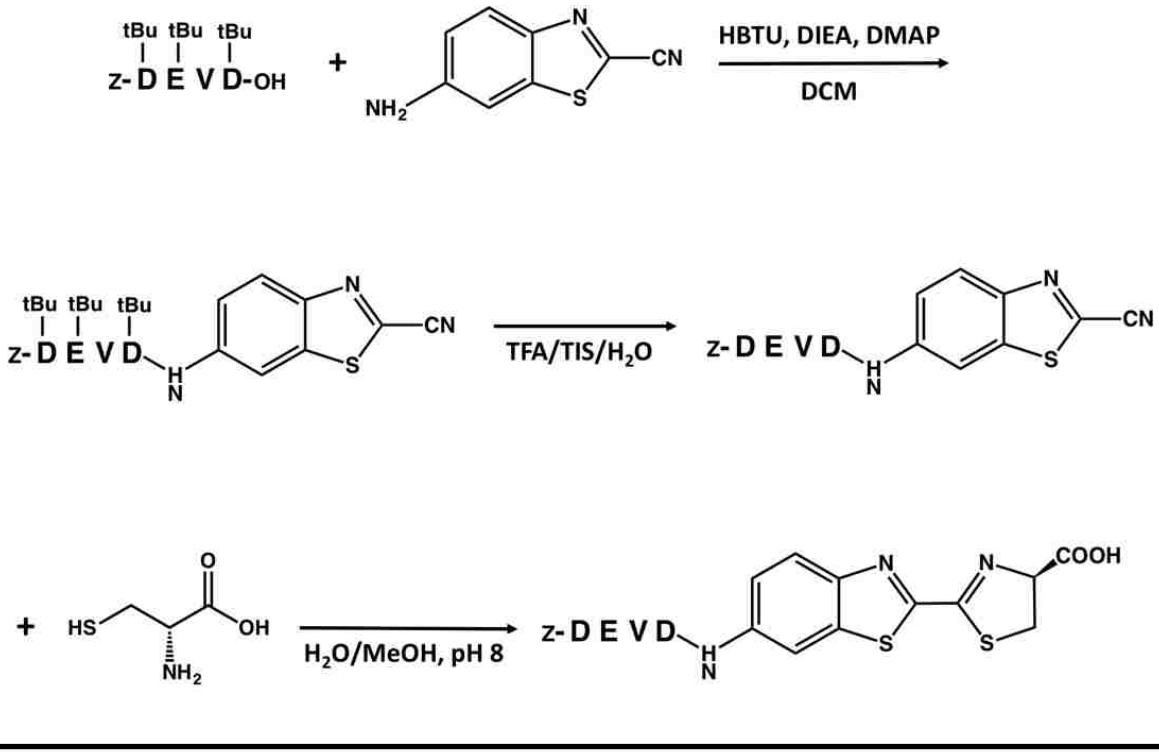

Scheme 5.2. Synthesis of the caspase 3/7 pro-luciferase substrate Z-DEVD-aminoluciferin.

repeated 6 times. Methanol/DCM was removed by rotoevaporation and the protected Z-DEVD peptide fragment was dried under high vacuum.

5.2.8.2 Synthesis of Z-DEVD-2-cyanobenzothiazole

Protected Z-DEVD peptide acid (1 equivalent) was dissolved in DCM and activated with 1.5 equivalents of HBTU and 3 equivalents of DIEA under stirring for 15 minutes. 6-amino-2-cyanobenzothiazole (Sigma Aldrich) (1 equiv) and DMAP (0.1 equiv) were added and allowed to react in the dark, under stirring, overnight. Excess HBTU was removed by filtration and DCM was removed by rotoevaporation. Amino acid protecting groups were removed by treatment with TFA/triisopropylsilane/H_2O (9.5:2.5:2.5, v/v/v)

for 4 hours, after which deprotected Z-DEVD-2-cyanbenzothiazole was precipitated in cold ether/hexane (6:4, v/v) and dried under a high vacuum pump.

5.2.8.3 Cyclization of Z-DEVD-2-cyanobenzothiazole

D-Cysteine hydrochloride monohydrate (5 equiv) was dissolved in water under nitrogen bubbling and the pH of the solution was adjusted to 8 with potassium carbonate (0.5 M). The Z-DEVD-2-cyanobenzothiazole compound (1 equiv) was dissolved in methanol with nitrogen bubbling and added to the cysteine solution. The reaction pH was once again adjusted to 8 with potassium carbonate (0.5 M), and then stirred at room temperature under nitrogen atmosphere in the dark for 3 hours. The methanol was removed by rotoevaporation and the Z-DEVD-aminoluciferin product was purified by semi-preparative HPLC. The identity of the purified product was confirmed by mass spectrometry (**Figure 5.1)**.

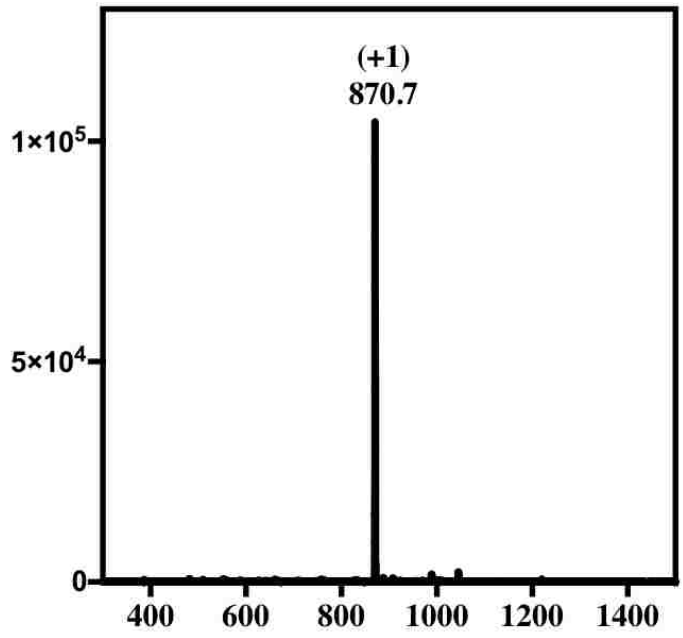

Figure 5.1. Mass spectrum of Z-DEVD-aminoluciferin.

5.2.9 Cell Lines and Culture

SKOV3 cells were obtained from the American Type Cell Culture Collection (ATCC) and SKOV3-luc-D3 cells were obtained from Caliper Life Sciences. The luciferase-expressing SKOV3 clone EA8 was made by transduction of SKOV3 cells with a retrovirus encoding the firefly luciferase-Thy1.1-Neo construct. Transduced cells were sorted for Thy1.1 signly by flow cytometry and selected under culture with G418. The SKOV3 EA8 clone was subquently obtained by limiting dilution cloning. SKOV3 and SKOV3 EA8 cells were culture in RPMI 16040 media supplemented with 10% fetal bovince serum (Gibco), 100 IU/ml penicillin, 100 mcg/ml streptomycine, and 2 mM l-glutamine. SKOV3 EA8 media was additional supplemented with 800 mcg/ml G418. All cells were maintained 37 °C and 5% CO_2.

5.2.10 Luciferase Activity of Cell Lines

To confirm luciferase expression prior to SKOV3 tumor engraftment in mice, non-luciferase expressing SKOV3s, SKOV3-luc-D3s, and SKOV3 EA8s were plated in a 96-well plate at increasing cell densities (1000-5000 cells per well). After 24 hours, luciferase activity was measured using a Firefly Luciferase Assay Kit (Biotium) as per the manufacturer's instructions.

5.2.11 Flow Cytometric Analysis of Thy1.1 Expression

SKOV3 and SKOV3 EA8 cell suspensions in media ($2x10^6$ cells/mL) were incubated with PE anti- CD90.1 antibody for 30 minutes at 4 °C. Cells were then washed with PBS, resuspended in flow buffer (2.5% FBS/PBS), and analyzed on a BD LSRII flow cytometer with untreated SKOV3 EA8 cells set as a background reference.

5.2.12 Polymer Toxicity in Healthy Mice

Healthy athymic nu/nu mice were injected intraperitoneally with 4 doses of PBS or PolCathBIM (250 mg/kg) at 3 day intervals. 72 hours after the final dose, blood was collected via retroorbital bleed for CBC analysis, mice were sacrificed, and the remaining blood was collected via cardiac puncture. For a blood toxicity metabolic panel, plasma was isolated by centrifugation. CBC and metabolic analyses were conducted by Phoenix Central Laboratory.

5.2.13 Tumor Xenografts Experiments

All in vivo experiments were conducted with the approval of the Fred Hutchinson Cancer Research Center Institutional Animal Case and Use Committee. 5-6 week old female athymic nu/nu mice weighing about 20 grams were purchased from Envigo and housed in specific pathogen-free housing. Mice were injected intraperitoneally with 10 million SKOV3 EA8 luciferase-expressing cells suspended in PBS (Gibco). To suppress neutrophils, mice were injected IP with anti-asialo GM-1 (rabbit) (WAKO Pure Chemical) -1 day before and +4 days after tumor cell injection, and then weekly thereafter. To verify tumor establishment and monitor tumor growth, bioluminescence was measured weekly using firefly D-luciferin (Biosynth International) injected IP (150 mg/kg) and a Xenogen Spectrum system. For all experiments, mice were divided into treatment groups of similar mean luminescent intensity in the days prior to treatment initiation. Mice were maintained on a biotin-free diet (Purina Feed) beginning 7 days prior to treatment.

5.2.14 Apoptotic Activity in Tumor Xenografts

33 days after tumor cell injection, 4 groups of xenograft mice (n=5) were injected IP with either (1) PBS, (2) carboplatin, (3) Herceptin-PolCathBIM + carboplatin or (4) Herceptin-PolCathScrBIM + carboplatin. Carboplatin, polymer and antibody doses were 35 mg/kg, 250 mg/kg, and 15 mg/kg, respectively. 24 hours after treatment, in vivo caspase 3/7 activity was measured using the modified firely luciferase substrate, Z-DEVD-aminolucifein. Z-DEVD-aminoluciferin was injected IP (~50 mg/kg) and luminescent intensity was measured using IVIS imaging. For each mouse, the caspase 3/7 signal was normalized to tumor luciferase activity measured 24 hours later using firefly D-luciferin. Results are reported as percent of the average

activity of the control (PBS) group. 48 hours after treatment, mice were euthanized via carbon dioxide inhalation and tumors were excised. For each mouse, a large and small tumor were recovered. Tumors were fixed in neutral buffered formalin for 72 hours and submitted to the Seattle Children's Histopathology core for immunohistochemical staining of cleaved caspase 3 (CC-3) and the proliferation marker Ki-67. Stained tumor sections will be imaged on a TissueFAXS microscope and analysis will be conducted using HistoQuest software. The percent of CC-3 positive cells and the density of Ki-67 positive will be reported for each tumor.

5.2.15 Survival /Tumor Regression Study

Two weeks after tumor cell injection, 6 groups of xenograft mice (n=9) will be treated with either (1) PBS, (2) carboplatin, (3) Herceptin-PolCathBIM, (4) Herceptin-PolCathScrBIM (6) Herceptin-PolCathBIM + carboplatin, or (6) Herceptin-PolCathScrBIM + carboplatin. Carboplatin, polymer and antibody doses will be 35 mg/kg, 250 mg/kg, and 15 mg/kg, respectively. Mice will be administered a total of 4 doses at three day intervals. Mice will be weighed twice per week and tumor response will be monitored once per week using IP injected D-luciferin (150 mg/kg) and a bioluminescent imaging system. Mice will be euthanized via carbon dioxide inhalation when excessive tumor burden or signs of distress are observed.

5.3 Results

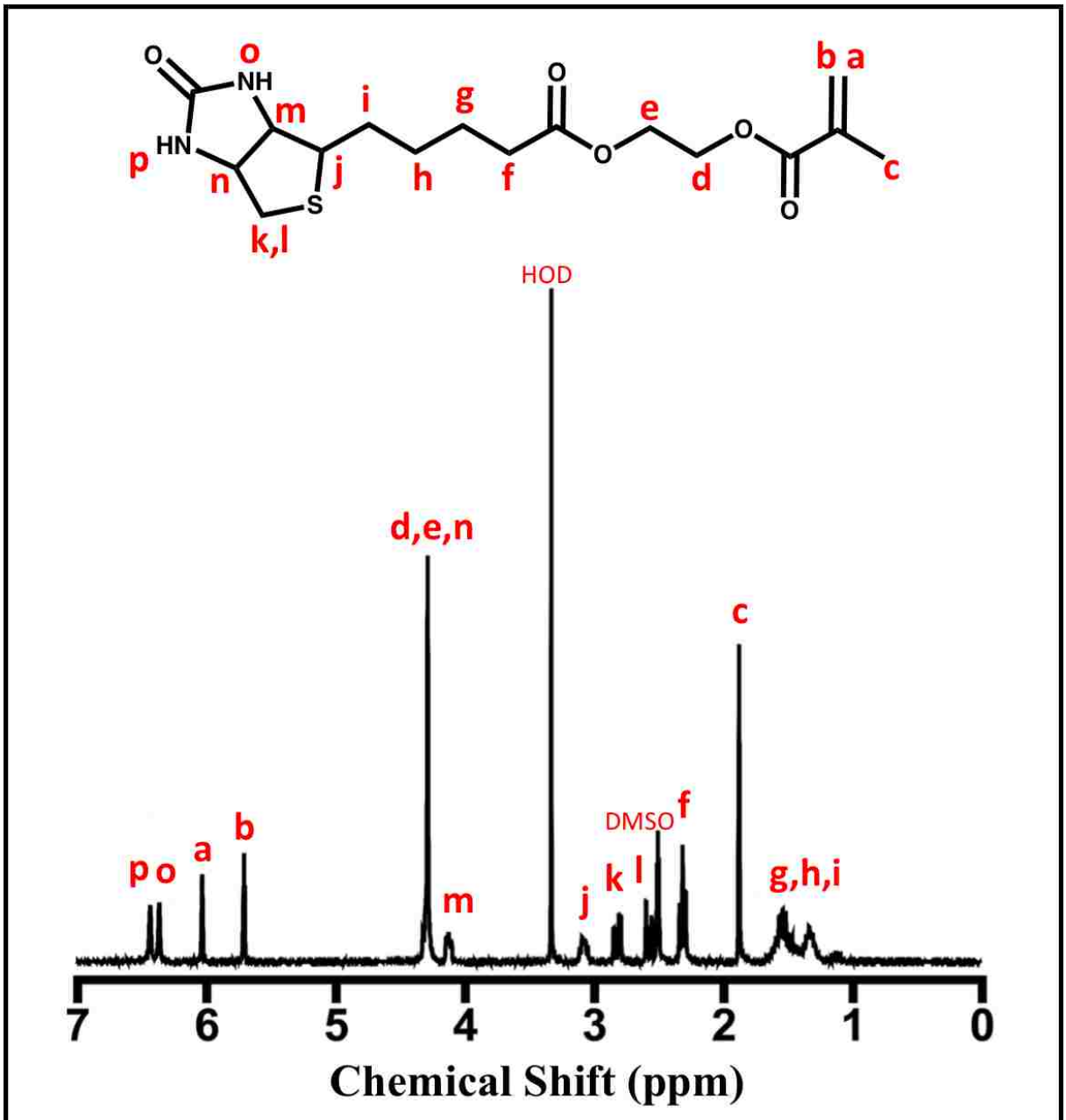

Figure 5.2. 1H-NMR of spectrum of biotin hydroxyethyl methacrylate (bioHEMA) monomer.

5.3.1 Polymer Synthesis and Characterization

As described in Chapter 4, a cathepsin B-cleavable BIM peptide macromonomer was synthesized containing BIM capped with the cathepsin B substrate FKFL flanked on either side by

a six-carbon spacer (Ahx) and functionalized its N-terminus with methacrylamide (MaAhxFKFLAhxBIM). A cathepsin B- cleavable peptide macromonomer containing a scrambled BIM sequence (MaAhxFKFLAhxScrBIM) was also synthesized as a control. Using RAFT polymerization, peptide macromonomers were directly integrated into pH-responsive diblock copolymers equivalent to those in Chapter 4, but with the addition of biotin hydroxyl ethyl methacrylate (bioHEMA) (**Figure 5.2**) for binding to tumor-specific antibody-streptavidin conjugates.

For the synthesis of diblock copolymers (**Scheme 5.1**), a poly[(DEAEMA)-co(BMA)] macroCTA was first synthesized composed of DEAEMA and BMA at a targeted molar ratio of 60:40. This formulation has been shown previously to possess optimal pH-responsive membrane destabilizing activity and trigger the endosomal release of biologic drugs. The poly[(DEAEMA)-co(BMA)] macroCTA was them employed for the block copolymerization of $PEGMA_{300}$ (92 mol%), peptide macromonomer (4 mol %) and bioHEMA (4 mol %). Two diblock copolymers containing either MaAhxFKFLAhxBIM or MaAhxFKFLAhxScrBIM were notated PolCathBIM and PolCathScrBIM, respectively.

Targeted and experimentally determined characteristics of PolCathBIM and PolCathScrBIM are summarized in **Table 5.1**. GPC and 1H-NMR polymer characterization data for the polymers are shown in **Figure 5.3.** The poly[(DEAEMA)-co(BMA)] macroCTA had a molecular weight of 16,800 g/mol, a narrow PDI (1.05) and a molar composition of 56%

Polymer	macroCTA					Diblock Copolymer						
	DP	% feed / comp		M_n	PDI	DP	% feed / comp			Peptide /Pol	M_n	PDI
		DEAEMA	BMA				bioHEMA	$PEGMA_{300}$	Peptide			
PolCathBIM	200	60 / 56	40 / 44	16,800	1.05	50	4	96	4	1.27	30,600	1.12
PolCathScrBIM	200	60 / 56	40 / 44	16,800	1.05	50	4	96	4	1.02	29,200	1.06

Table 5.1. Characterization of PolCathBIM and PolCathScrBIM. RAFT polymerization of DEAEMA and BMA at a feed ratio of 60:40 was employed for the synthesis of a poly[(DEAEMA)-co-(BMA)] macroCTA with endosomolytic activity. The macroCTA was subsequently employed for block copolymerization of $PEGMA_{300}$, bioHEMA, and peptide monomer (MaAhxFKFLAhxBIM or MaAhxFKFLAhxScrBIM) at a feed ratio of 92:4:4. Experimental M_n and PDI values were measured by gel permeation chromatography (GPC). Molar compositions were determined by ^{1}H-NMR and RP-HPLC analysis of reaction aliquots taken at T_o and T_x.

DEAEMA and 44% BMA. The molecular weights and PDIs of PolCathBIM and PolCathScrBIM were determined to be 30,600 Da and 29,200 Da, and 1.12 and 1.06, respectively. RP-HPLC analysis of reaction aliquots taken at T_o and T_x were used to determine the peptide content of the polymers. PolCathBIM and PolCathScrBIM contained 1.27 and 1.02 peptide units per polymer chain, respectively.

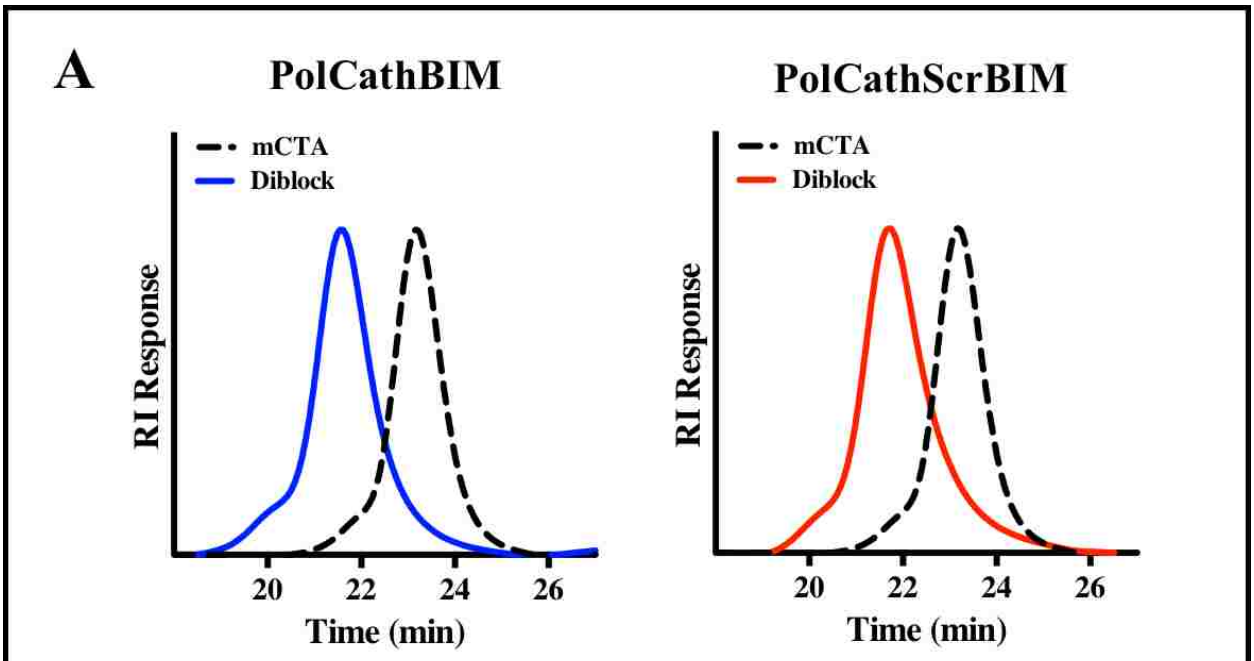

Figure 5.3. Continued on next page.

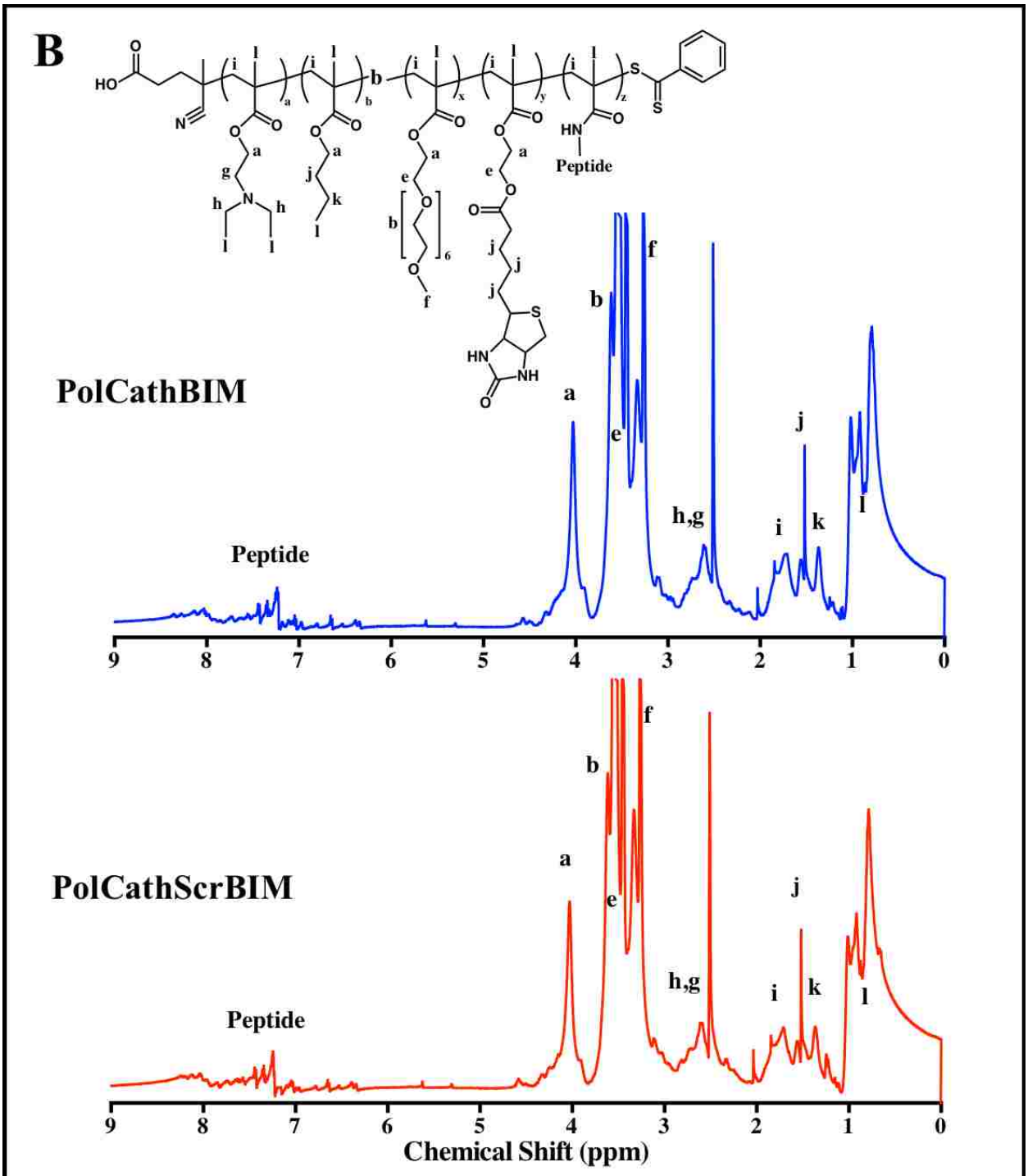

Figure 5.3. (A) GPC chromatograms and (B) ^{1}H-NMR spectra of biotin-containing PolCathBIM and PolCathScrBIM. The same poly[(DEAEMA)-co-(BMA)] macroCTA was employed for block copolymerization of both PolCathBIM and PolCathScrBIM. The resulting diblock copolymers had similar molecular weights (~30,000 kDa) and exhibited narrow polydispersities (<1.12).^{1}H-NMR scans were conducted in C_2D_6OS (20 mg/mL) at 499 Mhz. Chemical composition was confirmed by presence of resonances associated with the individual monomers.

5.3.2 Polymer-antibody Conjugation

PolCathBIM and PolCathScrBIM were specifically targeted to the ovarian cancer xenografts using Herceptin antibodies which bind to the HER2/neu surface receptor. To incorporate Herceptin antibodies into the delivery platform, Herceptin was conjugated to streptavidin as previously described[22-23] and biotin monomer was directly polymerized into the diblock copolymers. To formulate the polymers into micelles, they were dissolved in either ethanol or DMSO, diluted into sodium phosphate buffer (PBS), and solvent was removed by centrifugal filtration. Binding of streptavidin to the biotin-containing polymer micelles was quantified using a 4'-hydroxyazobenzene-2-carboxylic acid (HABA) displacement assay (**Figure 5.4A-B**). An equimolar mixture of PolCathBIM and PolCathScrBIM with streptavidin resulted in 1.5 and 1.6 binding events, respectively. Protein gel electrophoresis was employed to confirm antibody-polymer conjugation. Either CD19-SA (**Figure 5.4C)** or Herceptin-SA (**Figure 5.4D)** conjugates were incubated with PolCathBIM, PolCathScrBIM or an equivalent polymer synthesized without biotin (Pol (-) bioHEMA) at the injected antibody:polymer molar ratios (~1:110). For both antibody-SA conjugates, incubation with PolCathBIM or PolCathScrBIM resulted in a clear shift of the antibody band to higher molecular weights and disappearance of free antibody. By contrast, conjugation was not observed upon mixing with the biotin-negative polymer.

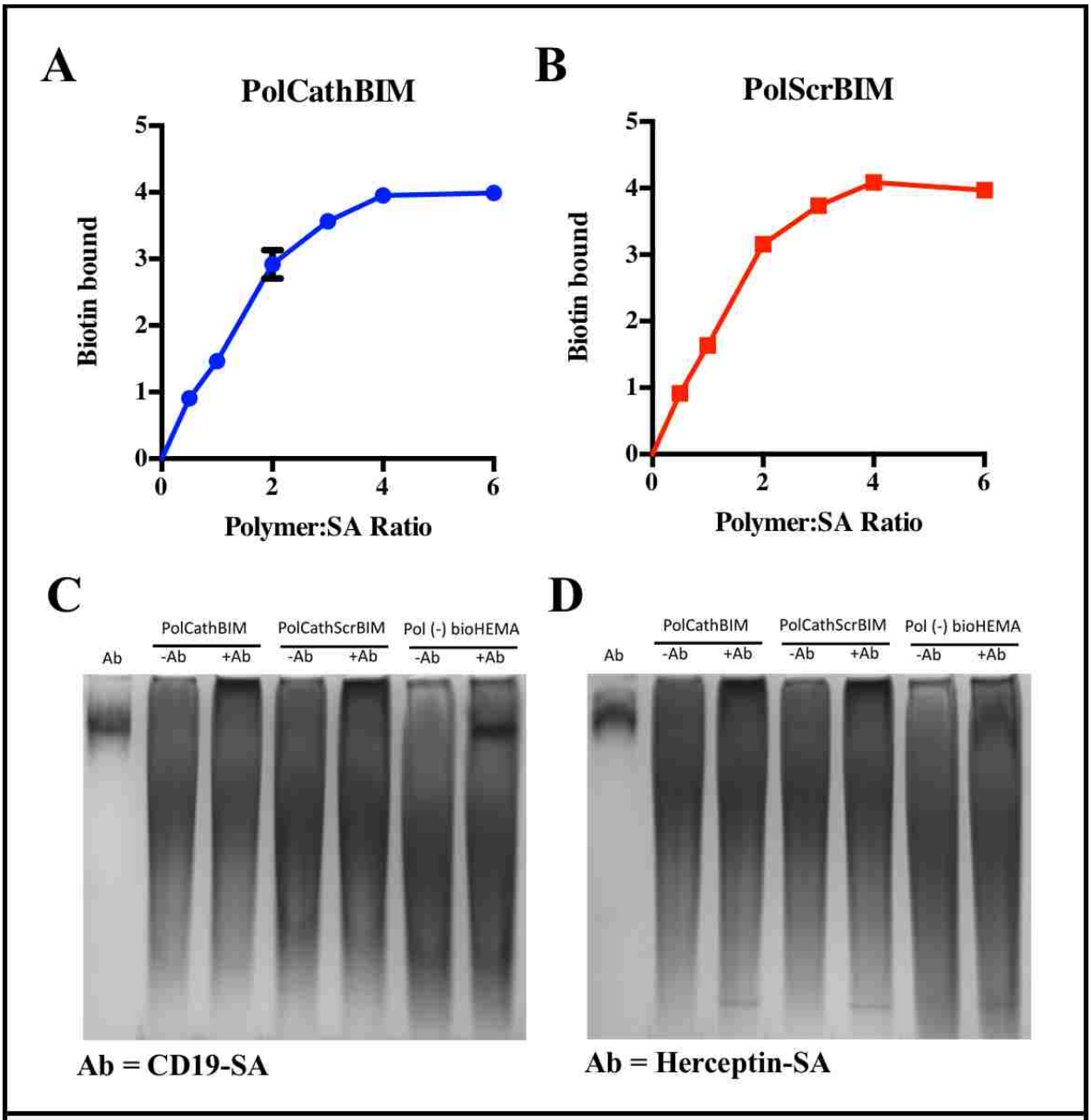

Figure 5.4. Characterization of antibody-polymer conjugation. **(A & B)** After formulating polymers in PBS, a HABA assay quantified binding of **(A)** PolCathBIM and **(B)** PolCathScrBIM to streptavidin (SA). SA was incubated with a 40-fold molar excess of HABA in the presence of increasing polymer concentrations for 1 hour. Displacement of HABA by biotinylated polymer was measured by UV spectroscopy (abs 500 nm) and compared to a biotin standard curve. **(C & D)** Conjugation was evaluated by non-reducing, non-denaturing protein gel electrophoresis. An approximately 100 molar excess of PolCathBIM, PolCathScrBIM, or an equivalent biotin-negative polymer (Pol (–) biotin) was incubated with either **(C)** CD19-SA or **(D)** Herceptin-SA conjugates for 2 hours. Antibodies were observed to conjugate to PolCathBIM and PolCathScrBIM, but not to the biotin-negative polymer. 5 ug of antibody and 83 ug of polymer were loaded per well.

5.3.3 Polymer Toxicity in Healthy Mice

A toxicity screen of multiple IP doses of polymer was conducted in healthy mice. Two groups of mice (n=3) were administered either increasing doses of PolCathBIM (150-250 mg/kg) or PBS on days 0, 3, 6, and 9. 72 hours following administration of the last dose, blood was harvested and submitted for CBC and metabolic analysis (**Figure 5.5**). All CBC values fell within the normal ranges and no distinct differences were observed between treatment groups. BUN, creatinine and ALP levels were also normal without significant differences between polymer and PBS groups. However, the liver enzymes aspartate aminotransferase (AST) and alanine aminotransferase (ALT) were elevated across groups, with significantly lower levels observed in the polymer-treated mice. One possible cause of elevated liver enzymes in laboratory mice is acute viral hepatitis. In any case, the ALT/AST levels were even higher in the PBS control group than the polymer-treated group, so it is unlikely they are due to polymer-related liver toxicity. In combination, these data suggest that multiple high does of PolCathBIM can be safely administered to mice via IP injection.

Figure 5.5. CBC and metabolic analysis demonstrates the safety of multiple doses of PolCathBIM. Healthy athymic nude mice were injected IP with four doses of PBS or PolCathBIM (150-250 mg/kg) every three days. Blood was harvested and analyzed 72 hours after the final dose. Dotted lines indicate average normal values for the gender and strain of mouse provided by the supplier (Envigo).

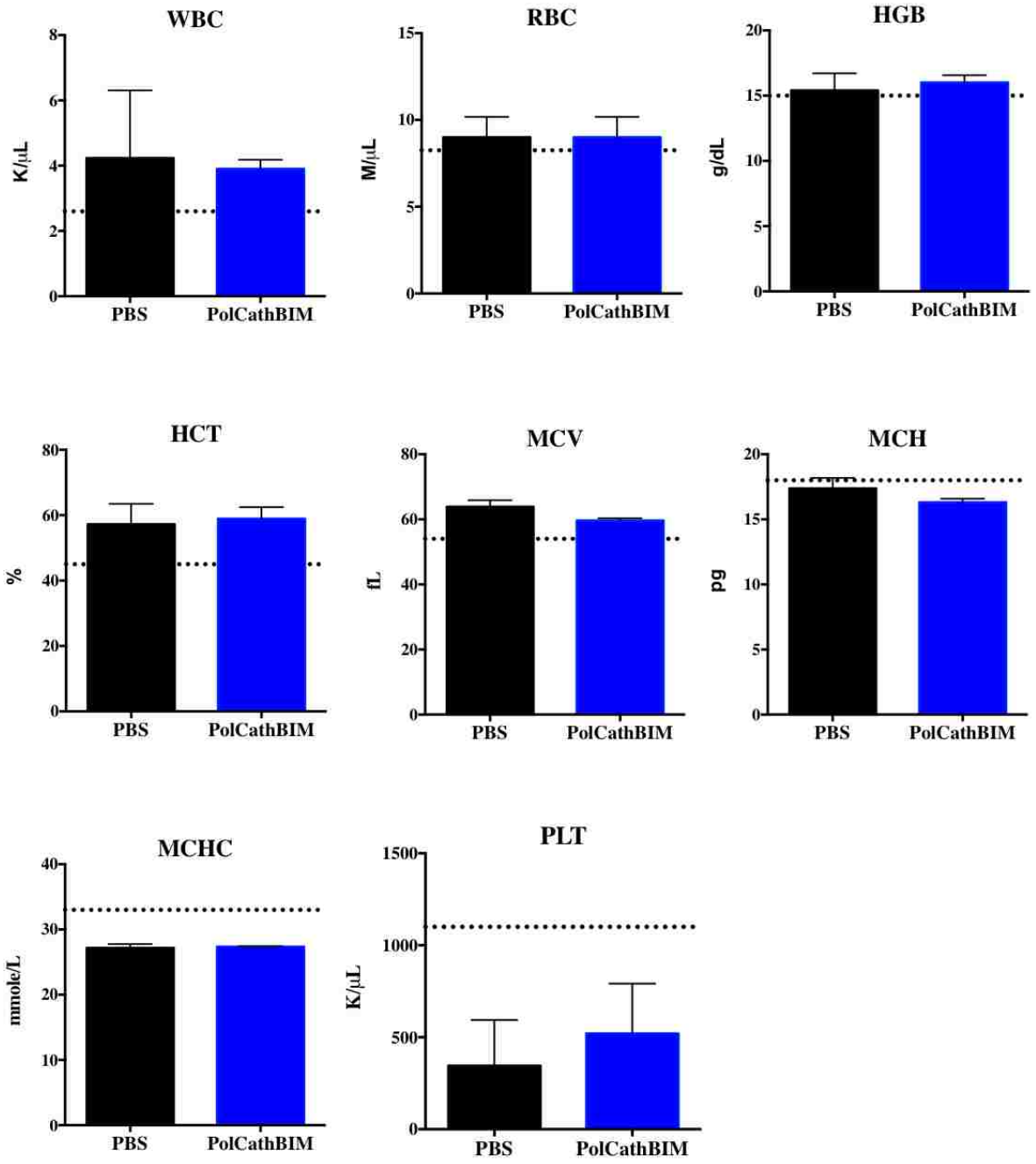

Figure 5.5 Continued.

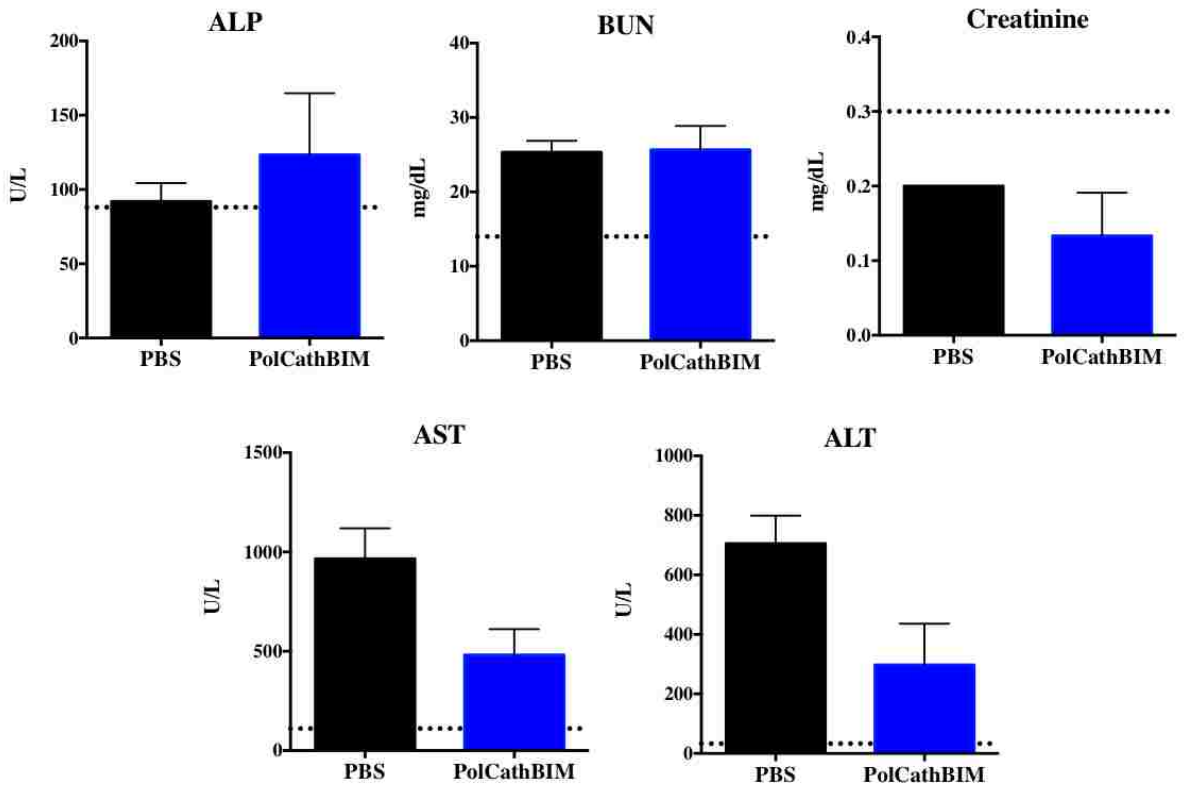

5.3.4 Intraperitoneal Luciferase-expressing SKOV3 Ovarian Cancer Xenografts

This work employed an intraperitoneal ovarian cancer xenograft model in order to recapitulate characteristic ovarian cancer spread within the peritoneal cavity and clinical presentation. To obtain quantitative tumor growth data, mice were implanted with ovarian SKOV3 tumor cells expressing the firefly luciferase reporter gene. Expression of luciferase permits real-time *in vivo* visualization of tumors using the substrate D-luciferin and bioluminescent imaging.

Prior to tumor injection, the expression of firefly luciferase in the implanted SKOV3 EA8 clone was validated *in vitro*. Three cells lines were tested: (1) untransfected luciferase-negative SKOV3 cells, (2) luciferase-expressing SKOV3-luc-D3 cells supplied by Caliper Life Sciences,

and (3) the SKOV3 clone EA8 made by transfection with a firefly luciferase-Thy1.1-Neo construct. Cells were plated in 96-well plates at cell densities ranging from 1-5,000 cells/well and assayed for luciferase activity (**Figure 5.6A**). As expected, SKOV-luc-D3 and SKOV3 EA8 cells exhibited high levels of activity, in comparison to the negligible activity exhibited by SKOV3s. The measured luminescence of the cell lines were 81.25 $\pm$ 10.48, 97.16 $\pm$ 8.81, and 0.01 $\pm$ 0.002 units/cell, respectively. SKOV EA8 cells were selected for implantation because they exhibited the highest level of luciferase activity and are know to grow at faster rates both *in vitro* and *in vivo*.

To evaluate the homogeneity of the SKOV3 EA8 cell population, cell suspensions were incubated with fluorescently (PE)-labeled anti-Thy1.1 and analyzed by flow cytometry (**Figure 5.6B**). Both anti-Thy1.1 treated SKOV3s and untreated SKOV3 EA8 cells were analyzed as negative controls. The implanted SKOV3 EA8 cells uniformly expressed high levels of Thy1.1, in contrast to untransfected SKOV3s.

Figure 5.6C represents tumor growth data obtained for 5 weeks following IP injection of athymic mice with $10x10^6$ SKOV3 EA8 cells. Average tumor luminescnce steadily increased over time. However, a great deal of variability was observed at 35 days for all mice and within individual treatment groups. Immediately following luminescent imaging on day 35, mice were euthanized and tumors were excised for histological analysis. While tumor metastasis was present with the peritoneal cavity, each mouse also had a single tumor that constituted the largest portion of the total tumor burden. The large tumor was excised from each mouse and weighed. It was observed that the quantitative luminescence measurements did not necessarily reflect the sizes of the large tumors. A plot of tumor luminescence versus large tumor mass clearly

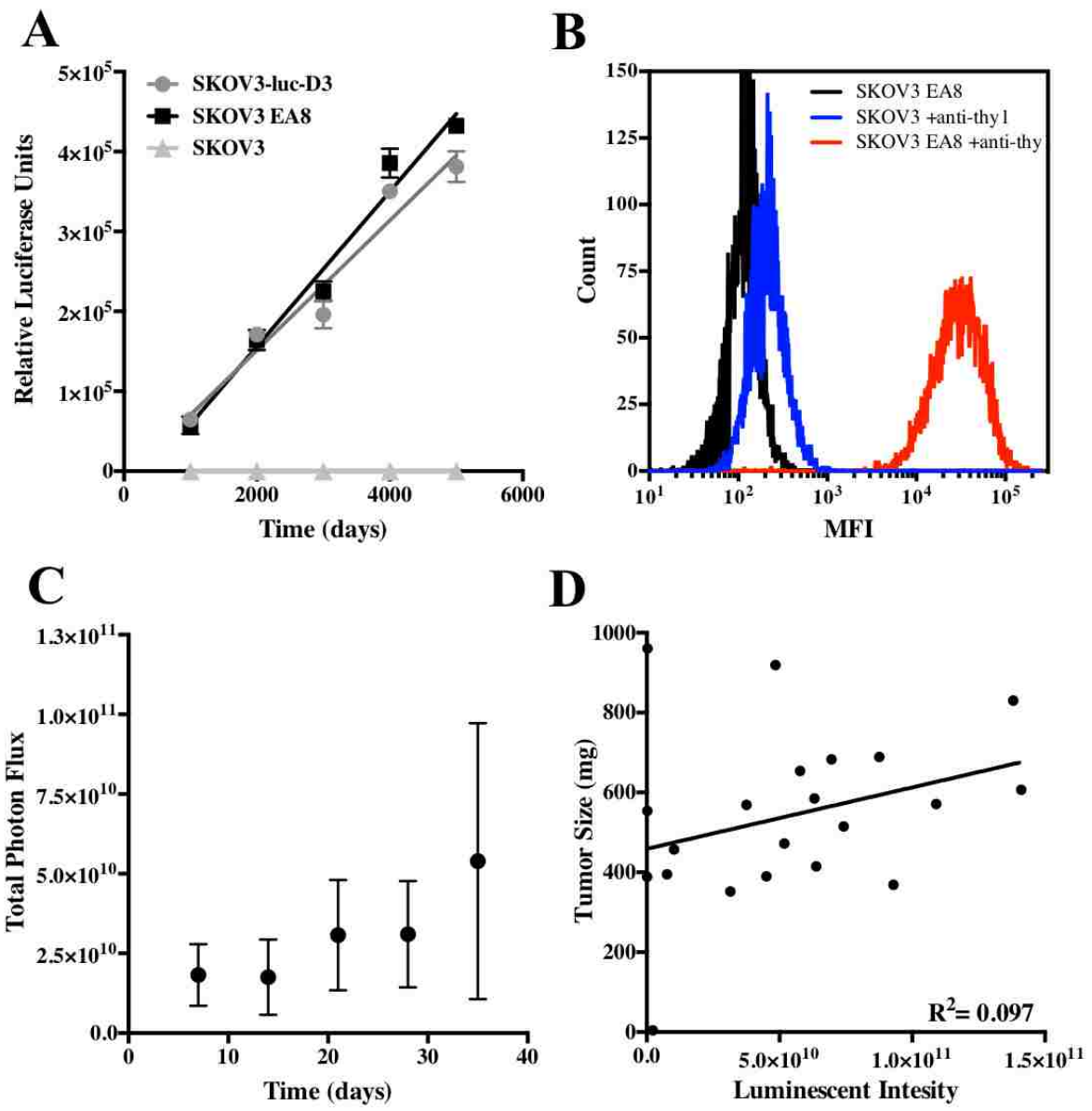

Figure 5.6. Intraperitoneal, luciferase-expressing SKOV3 EA8 xenografts. **(A)** SKOV3-D3-luc cells and SKOV3 EA8 cells exhibit luciferase activity, in contrast to non-transfected SKOV3 cells. Cells were plated in a 96-well plate at increasing cell densities and luciferase expression was measured using a Luciferase Reporter Assay Kit. **(B)** SKOV3 EA8 cells homogenously express high levels of Thy1.1. SKOV3 EA8 and SKOV3 cell suspensions were incubated with PE anti-mouse CD90.1 (Thy 1.1) and antibody binding was analyzed via flow cytometry. **(C)** Athymic nude mice were injected IP with $10x10^6$ SKOV3 EA8 cells, and tumor growth was monitored weekly using D-aminoluciferin (150 mg/kg) and IVIS imaging. **(D)** Measured tumor luminescence may not correlate with tumor size. After 35 days, tumor bioluminescence was measured, the mice were sacrificed, and a single large tumor was harvested from each mouse and weighed. A poor correlation was found between tumor luminescence and large tumor mass.

demonstrates a poor linear correlation (R^2 = 0.097) (**Figure 5.6D**). This brings into question the accuracy of IVIS imaging for tumor size measurements, particularly at later time points. However, it is conceded that the mass of the large tumors does not fully capture the tumor burden of each mouse.

5.3.5 Induction of Apoptosis by the Cathepsin B-cleavable BIM Polymer in an Ovarian Tumor Model

The ability of the BIM peptide to antagonize pro-survival Bcl-2 proteins and induce apoptotic signaling was evaluated by measuring caspase activation and cell proliferation (Ki-67) within IP SKOV3 ovarian cancer xenografts. Mice were injected IP with either PBS, low-dose carboplatin (35 mg/kg), or carboplatin in combination with either Herceptin-PolCathBIM or Herceptin-PolCathScrBIM.

At 24 hours after treatment, in vivo caspase 3/7 activity was measured using a modified firefly luciferase substrate, Z-DEVD-aminoluciferin[24]. Z-DEVD-aminoluciferin is cleaved by caspase-3/7 to liberate the luciferase substrate aminoluciferin. Animals were injected IP with 50 mg/kg Z-DEVD-aminoluciferin and bioluminescent images were acquired every 5-20 minutes for 1 h. Across treatment groups (n=4) a parallel set of animals were treated identically. The *in vivo* caspase 3/7 luciferase activity was quantified using region-of-interest (ROI) analysis of images acquired 20 minutes after substrate injection. For each animal, caspase 3/7 luminescence was normalized to total tumor luminescence measured using D-aminoluficerin. The percent caspase 3/7 activity for each animal was reported relative to the average of the PBS control group. Results were inconclusive (**Figure 5.6**). No significant difference was observed between treatment groups and a large amount of variability was observed. Since no caspase 3/7 activation

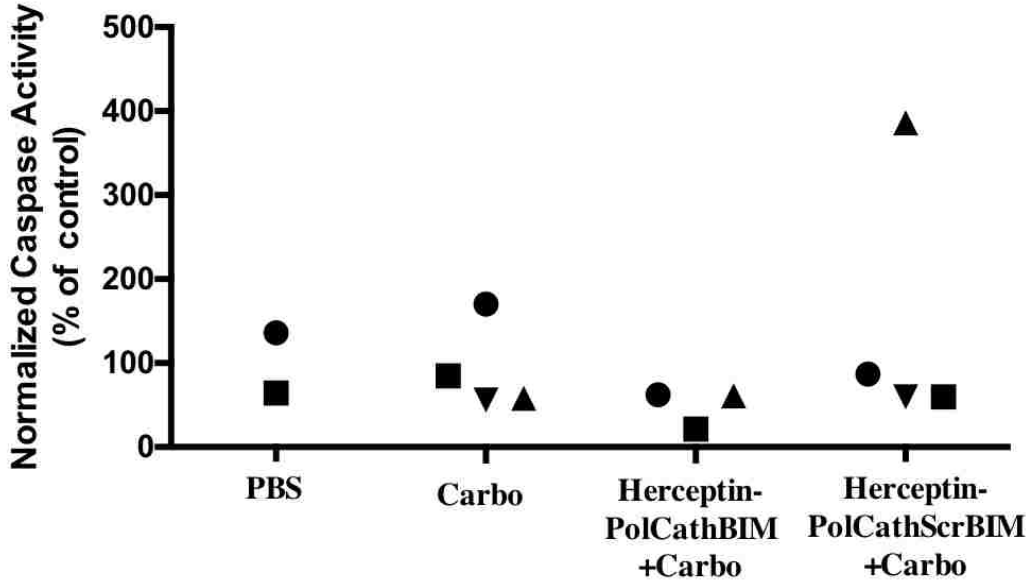

Figure 5.7. Bioluminescent imaging of caspase 3/7 activity in IP SKOV3 EA8 tumors using Z-DEVD-aminoluciferin. 24 hours after treatment, mice were injected IP with Z-DEVD-aminoluciferin (50 mg/kg) and bioluminescent images were acquired every 10-20 min for 1 hour. For each mouse, *in vivo* caspase activity was normalized to total tumor luminescence (measured 24 hours later) and reported as percent of PBS average. Represented data were acquired 20 minutes after Z-DEVD-aminoluciferin injection. Results are inconclusive.

was observed in response to treatment with either carboplatin or Herceptin, it is more likely these findings represent a failure in experimental methodology rather than a failure of treatment. Potential problems include an inadequate substrate dose, poor time point selection, or inaccuracy/imprecision of IVIS imaging for tumor monitoring. In the future, I would recommend protocol optimization prior to experiments or reliance on histological analysis.

At 48 hours after treatment, tumors were excised and fixed for evaluation of intratumoral markers of apoptosis. To examine the effect of tumor size on apoptotic induction, both a large tumor (300-700 mg) and small (5-15 mg) tumor were harvested from each mouse. Tumors are currently being IHC stained for cleaved caspase 3 and Ki-67. Results will be reported to Supervisory Committee members as they become available.

5.3.6 Tumor Growth Inhibition and Survival

The therapeutic efficacy of Herceptin-targeted PolCathBIM is currently being evaluated both alone and in combination with low dose carboplatin. Athymic nude mice were injected IP with luciferase-expressing EA8 cells and tumors were allowed to establish for two weeks. Tumors were sized using D-luciferin and IVIS imagaing, and mice were sorted into 6 treatment groups of 8-9 mice with similar mean luminescent intensity: (1) PBS, (2) carboplatin, (3) Herceptin-PolCathBIM, (4) Herceptin-PolCathScrBIM, (5) Herceptin-PolCathBIM + carboplatin, and (6) Herceptin-PolCathScrBIM + carboplatin. Mice were treated with four IP doses on days 15, 19, 23, and 27 following tumor establishment. Tumor growth is being monitored weekly via bioluminescent imaging, and mice are being euthanized with excess tumor burden or when signs of distress are observed. Tumor growth and animal survival data will be reported to Supervisory Committee members as they become available.

5.4 Discussion

Peptides that bind intracellular drug targets hold potential for the treatment of a wide array of diseases. However, the clinical development of peptides has been stymied by drug delivery barriers including poor circulation stability and an inability to cross cell membranes. This thesis developed an antibody-targeted, intracellular delivery system for the pro-apoptotic peptide BIM. The multifunctional carrier consists of a biocompatible corona composed primarily of PEG graft units to provide peptide shielding in the blood. This was combined with a pH-responsive endosomal-destabilizing core to provide the BIM peptide access to its cytosolic target. In addition, a critical and novel feature of the described carrier is a chemically stable

peptide linker that is also cleaved by the endo/lysosomal enzyme cathepsin B to release BIM inside target cells. In comparison to previously developed disulfide linkages, this linker promises to extend BIM circulation time and enhance tumor delivery while also maintaining drug activity. In Chapter 4 this polymeric BIM prodrug demonstrated promising apoptotic activity in SKOV3 ovarian cancer cell cultures. However, efficacious intracellular delivery to tumor cells *in vivo* presents a more critical hurdle in the development of peptide drugs such as BIM. This work evaluates the cathepsin B-cleavable BIM polymer (PolCathBIM) in a clinically relevant IP ovarian cancer model.

Initially the biocompatibility of the polymer was demonstrated in healthy mice. IP administration of four polymer doses (150-250 mg/kg) every three days did not result in any concerning CBC or metabolic changes. This favorable safety profile is important for permitting the administration of therapeutically efficacious peptide doses. The maximum tolerated dose was not determined, and, given the absence of animal distress or biomarker changes, it is possible much higher peptide/polymer doses may be safely achieved. In the future this should be investigated for enhanced therapeutic efficacy.

Ongoing studies are investigating the apoptotic activity and therapeutic efficacy of Herceptin-targeted PolCathBIM in IP luciferase-expressing SKOV3 xenografts. In the coming weeks, tumor-bearing mice will be administered four doses of Herceptin-PolCathBIM in combination with carboplatin and tracked for tumor growth and survival in comparison to controls. It is also important to verify induction of apoptosis as the mechanism of action. To this end, tumor bearing mice were administered a single dose of either PBS, carboplatin alone, or carboplatin in combination with Herceptin-PolCathBIM or Herceptin-PolScrBIM, and tumors were excised after 48 hours. Tumors are currently being IHC stained for the markers cleaved

caspase 3 and Ki-67. In addition, polymer penetration and apoptotic activity may be impacted by tumor size and the timing of treatment. Consequently, both a large and small tumor were excised from each mouse, and the effect of tumor size on apoptotic induction will be measured. If these pending studies are successful, they will demonstrate the potential utility of the enzyme-cleavable BIM delivery system as an ovarian cancer therapy. Furthermore, the design may be more broadly applied, as it could be easily modified to incorporate different peptide sequences and target different tumor types.

If the studies are unsuccessful, a number of improvements may be made to the initial design. First, the zwiterionic monomer carboxybetaine methacrylate (CBM) presents a promising alternative to PEGMA. A previous study comparing diblock copolymers made with $PEGMA_{300}$ (MW = 300 Da) and $PEGMA_{950}$ (MW = 950 Da) showed increased circulation half-life and tumor distribution with the longer-chain $PEGMA_{950}$ monomers[25]. Unfortunately, $PEGMA_{950}$ was found to sterically block cathepsin B access to the linker and could not be employed in this system. If the $PEGMA_{300}$ polymers exhibit sub-optimal tumor delivery, carboxybetaine (CB) offers to combine superior "stealth" properties with decreased steric hindrance. Due to its zwitterionic nature, carboxybetaine binds more strongly to water via electrostatic-induced hydration and demonstrates higher resistance to protein adsorption[26]. In addition, in contrast to PEG, CB does not induce a specific antibody response after repeated injections[26]. These properties have been shown to translate into substantially increased circulation times and decreased toxicity. In one study comparing CB and PEG-coated nanoparticles, the half-life of CP-nanoparticles was ~56 hours in comparison to ~9 hours for PEG[26]. Substitution of $PEGMA_{300}$ for CB promises to enhance the performance of the described system and should be investigated in future studies, regardless of the activity achieved in this chapter.

An alternative targeting modality may also prove critical. While it is difficult to match the targeting power of monoclonal antibodies, they face dosing limitations. At the doses administered in this work, the antibody to polymer ratio is only 1:110. Due to its nature as an equilibrium structure, polymeric micelle stability in both systemic circulation and the potentially low-pH tumor microenvironment is cause for concern. If micelles destabilize, only a small fraction of polymers are conjugated to internalizing Herceptin antibodies. Consequently, it may be beneficial to incorporate at least one targeting ligand per polymer chain. Multiple ligands per chain would provide the added advantage of multivalency. Such alternative targeting options include a peptide monomer that, for example, binds epidermal growth factor receptor[27-28]. In Chapter 6, one such peptide is developed for enhancing the delivery of a campothecin prodrug.

REFERENCES

[1] SEER Stat Fact Sheets: "Ovary Cancer." *NCI.* Retrieved November 5, 2015.

[2] Goff BA. Ovarian cancer: screening and early detection. *Obstet Gynecol Clin North Am*. 2012 Jun;39(2):183-94.

[3] Cannistra SA. Cancer of the ovary. *N Engl J Med*. 2004 Dec 9;351(24):2519-29.

[4] Helm CW. The role of hyperthermic intraperitoneal chemotherapy (HIPEC) in ovarian cancer. *Oncologist*. 2009 Jul;14(7):683-94.

[5] Markman M. Intraperitoneal chemotherapy in the management of malignant disease. *Expert Rev Anticancer Ther*. 2001 Jun;1(1):142-8.

[6] Wright AA, Cronin A, Milne DE, Bookman MA, Burger RA, Cohn DE, Cristea MC, Griggs JJ, Keating NL, Levenback CF, Mantia-Smaldone G, Matulonis UA, Meyer LA, Niland JC, Weeks JC, O'Malley DM. Use and Effectiveness of Intraperitoneal Chemotherapy for Treatment of Ovarian Cancer. *J Clin Oncol*. 2015 Sep 10;33(26):2841-7.

[7] Armstrong DK, Bundy B, Wenzel L, Huang HQ, Baergen R, Lele S, Copeland LJ,Walker JL, Burger RA; Gynecologic Oncology Group. Intraperitoneal cisplatin and paclitaxel in ovarian cancer. *N Engl J Med*. 2006 Jan 5;354(1):34-43.

[8] NCI Clinical Announcement on Intraperitoneal Chemotherapy for Ovarian Cancer. January 5, 2006.

[9] Reddy LH, Murthy RS. Pharmacokinetics and biodistribution studies of Doxorubicin loaded poly(butyl cyanoacrylate) nanoparticles synthesized by two different techniques. *Biomed Pap Med Fac* Univ Palacky Olomouc Czech Repub. 2004 Dec;148(2):161-6.

[10] Werner ME, Karve S, Sukumar R, Cummings ND, Copp JA, Chen RC, Zhang T, Wang AZ. Folate-targeted nanoparticle delivery of chemo- and radiotherapeutics for the treatment of ovarian cancer peritoneal metastasis. *Biomaterials*. 2011 Nov;32(33):8548-54.

[11] Goldberg MS, Xing D, Ren Y, Orsulic S, Bhatia SN, Sharp PA. Nanoparticle-mediated delivery of siRNA targeting Parp1 extends survival of mice bearing tumors derived from Brca1-deficient ovarian cancer cells. *Proc Natl Acad Sci USA*. 2011 Jan 11;108(2):745-50.

[12] Huang YH, Zugates GT, Peng W, Holtz D, Dunton C, Green JJ, Hossain N, Chernick MR, Padera RF Jr, Langer R, Anderson DG, Sawicki JA. Nanoparticle-delivered suicide gene therapy effectively reduces ovarian tumor burden in mice. *Cancer Res*. 2009 Aug 1;69(15):6184-91.

[13] Kamei T, Kitayama J, Yamaguchi H, Soma D, Emoto S, Konno T, Ishihara K, Ishigami H, Kaisaki S, Nagawa H. Spatial distribution of intraperitoneally administrated paclitaxel nanoparticles solubilized with poly (2 methacryloxyethyl phosphorylcholine-co n-butyl methacrylate) in peritoneal metastatic nodules. *Cancer Sci.* 2011 Jan;102(1):200-5.

[14] Hudis CA. Trastuzumab--mechanism of action and use in clinical practice. *N Engl J Med*. 2007 Jul 5;357(1):39-51.

[15] Park SI, Shenoi J, Frayo SM, Hamlin DK, Lin Y, Wilbur DS, Stayton PS, Orgun N, Hylarides M, Buchegger F, Kenoyer AL, Axtman A, Gopal AK, Green DJ, Pagel JM, Press OW. Pretargeted radioimmunotherapy using genetically engineered antibody-streptavidin fusion proteins for treatment of non-hodgkin lymphoma. *Clin Cancer Res*. 2011 Dec 1;17(23):7373-82.

[16] Cirstoiu-Hapca A, Buchegger F, Lange N, Bossy L, Gurny R, Delie F. Benefit of anti-HER2-coated paclitaxel loaded immuno-nanoparticles in the treatment of disseminated ovarian cancer: Therapeutic efficacy and biodistribution in mice. *J Control Release*. 2010 Jun 15;144(3):324-31.

[17] Kirpotin DB, Drummond DC, Shao Y, Shalaby MR, Hong K, Nielsen UB, Marks JD, Benz CC, Park JW. Antibody targeting of long-circulating lipidic nanoparticles does not increase tumor localization but does increase internalization in animal models. *Cancer Res*. 2006 Jul 1;66(13):6732-40.

[18] Palanca-Wessels MC, Booth GC, Convertine AJ, Lundy BB, Berguig GY, Press MF, Stayton PS, Press OW. Antibody targeting facilitates effective intratumoral siRNA nanoparticle delivery to HER2-overexpressing cancer cells. Oncotarget. 2016 Feb 23;7(8):9561-75Ma C, Yin G, You F, Wei Y, Huang Z, Chen X, Yan D. A specific cell-penetrating peptide induces apoptosis in SKOV3 cells by down-regulation of Bcl-2. *Biotechnol Lett*. 2013 Nov;35(11):1791-7.

[19] Zhu H, Zhang L, Dong F, Guo W, Wu S, Teraishi F, Davis JJ, Chiao PJ, Fang B. Bik/NBK accumulation correlates with apoptosis-induction by bortezomib (PS-341, Velcade) and other proteasome inhibitors. *Oncogene*. 2005 Jul 21;24(31):4993-9.

[20] Chen J, Jin S, Abraham V, Huang X, Liu B, Mitten MJ, Nimmer P, Lin X, Smith M, Shen Y, Shoemaker AR, Tahir SK, Zhang H, Ackler SL, Rosenberg SH, Maecker H, Sampath D, Leverson JD, Tse C, Elmore SW. The Bcl 2/Bcl-X(L)/Bcl-w inhibitor, navitoclax, enhances the activity of chemotherapeutic agents in vitro and in vivo. *Mol Cancer Ther*. 2011 Dec;10(12):2340-9.

[21] Hylarides MD, Mallett RW, Meyer DL. A robust method for the preparation and puri cation of antibody/streptavidin conjugates. Bioconjugate chemistry. 2001; 12:421–427.

[22] Pagel JM, Hedin N, Subbiah K, Meyer D, Mallet R, Axworthy D, Theodore LJ, Wilbur DS, Matthews DC, Press OW. Comparison of anti-CD20 and anti-CD45 antibodies for conventional and pretargeted radioimmunotherapy of B-cell lymphomas. Blood. 2003 Mar 15;101(6):2340-8.

[23] Scabini M, Stellari F, Cappella P, Rizzitano S, Texido G, Pesenti E. In vivo imaging of early stage apoptosis by measuring real-time caspase-3/7 activation. *Apoptosis*. 2011 Feb;16(2):198-207.

[24] Berguig GY, Convertine AJ, Frayo S, Kern HB, Procko E, Roy D, Srinivasan S, Margineantu DH, Booth G, Palanca Wessels MC, Baker D, Hockenbery D, Press OW,

Stayton PS. Intracellular delivery system for antibody-Peptide drug conjugates. *Mol Ther*. 2015 May;23(5):907-17.

[25] Keefe AJ, Zhang L, Ella-Menye JR, Li Y, Jiang S. Poly(carboxybetaine) nanomaterials enable long circulation and prevent polymer-specific antibody production. *Nano Today*. 2014 Feb;9(1):10-16.

[26] Li Z, Zhao R, Wu X, Sun Y, Yao M, Li J, Xu Y, Gu J. Identification and characterization of a novel peptide ligand of epidermal growth factor receptor for targeted delivery of therapeutics. FASEB J. 2005 Dec;19(14):1978-85.

[27] Song S, Liu D, Peng J, Sun Y, Li Z, Gu JR, Xu Y. Peptide ligand-mediated liposome distribution and targeting to EGFR expressing tumor in vivo. Int J Pharm. 2008 Nov 3;363(1-2):155-61.

CHAPTER 6. A Peptide-targeted Polymeric Camptothecin Prodrug

Abstract

Peptides as targeting agents are advantageous in their small size, low cost, low immunogenicity, synthetic scalability, and adaptability to different conjugation chemistries. Employing RAFT polymerization, a methacrylamide-peptide monomer consisting of an EGFR-targeting sequence, GE11, was directly incorporated into a hydrophilic polymeric drug delivery scaffold. Long-chain polyethylene glycol monomers of two different sizes (300 Da & 950 Da) and the zwitterionic monomer carboxybetaine methacrylate (CBM) were investigated as hydrophilic comonomers. Flow cytometric analysis of SKOV3 ovarian cancer cells treated with rhodamine-B labeled polymers showed that only the low steric carboxybetaine monomer permitted targeting by copolymerized GE11. A copolymer of GE11 and CBM was taken up at 18-fold higher levels than a control polymer synthesized with the unrelated peptide HW12. In the context of both small (300 Da) and large (950 Da) PEG grafts, no GE11-mediated uptake was observed. RAFT polymerization was also employed for the synthesis of polymeric campothecin prodrugs. Two prodrug monomers were synthesized by reacting the carboxylic acid of mono-2-(methacryloyloxy)ethyl succinate (SMA) with hydroxyl groups in the structure of the drug. Depending on the site of conjugation, prodrug monomers with either an aliphatic ester or aromatic ester linkage were synthesized and incorporated into carboxybetaine polymeric scaffolds. RP-HPLC analysis of drug release in human serum showed that the aromatic ester-linked prodrug hydrolyzed at a significantly faster rate than the aliphatic ester-linked drug. After 9 days, 57% of the aromatic-ester linked camptothecin was released, in comparison to 33% of the aliphatic ester-linked camptothecin. These release kinetics correlated with cytotoxic activity

in SKOV3 ovarian cancer cell cultures. At 72 hours, the IC50s of aromatic-ester and aliphatic-ester linked prodrugs were 56 nM and 4776 nM, respectively. Finally, the GE11 peptide monomer and aromatic-ester linked camptothecin prodrug were integrated into a single targeted polymeric prodrug system. In comparison to an HW12-control polymer, GE11 enhanced the targeting and activity of the polymeric prodrug in SKOV3 cell cultures. Following pulse treatment (15 min, 37 ºC), the 72 hour IC50 of GE11 targeted prodrug was 1597 nM, in contrast to 3399 nM for the non-targeted control. Targeted and non-targeted control polymers synthesized without drug exhibited negligible toxicity at all concentrations. In summary, peptide monomer technology was successfully implemented for tumor cell targeting and increased activity of a cancer therapeutic *in vitro*.

6.1 Introduction

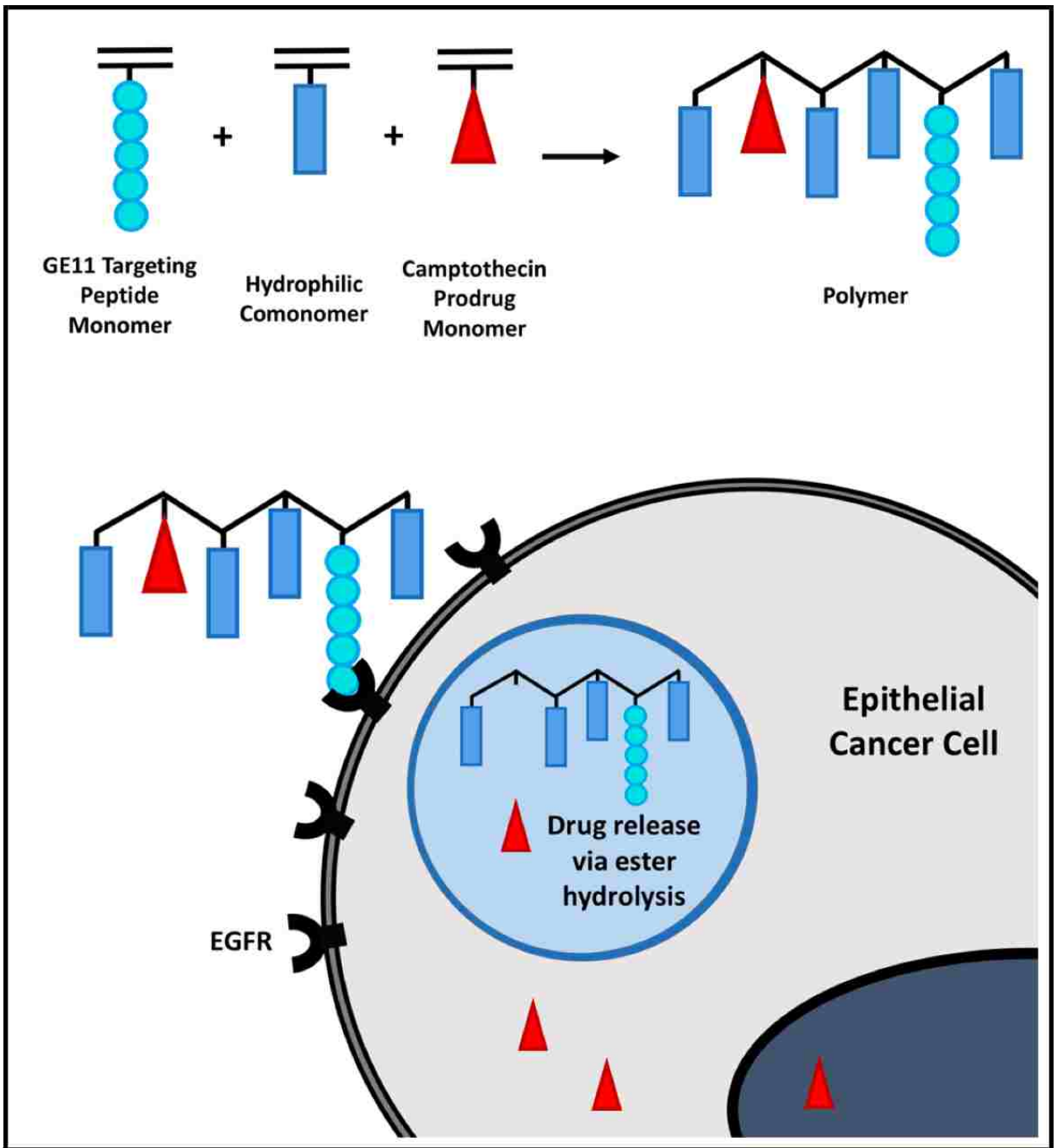

Figure 6.1. A GE11-targeted polymeric camptothecin produg.

Targeted drug delivery systems are designed to enhance the therapeutic index of cancer therapeutics by increasing drug localization in tumors while minimizing off-target interactions with healthy tissues. Active targeting is achieved through the incorporation of cancer-specific

ligands, which may be proteins, peptides, carbohydrates, vitamins, aptamers or antibodies[1]. Of particular promise are antibody-drug conjugates consisting of a highly potent cytotoxic drug coupled to a cancer-specific antibody. Currently, two ADCs have been market approved for the treatment of some relapsed and refractory lymphomas[2] and HER2-positive metastatic breast cancer[3]. More than 30 ADCs are currently under clinical investigation[4].

Peptides hold great potential as cancer-specific ligands and offer a number of advantages over antibodies. First, peptides are of low immunogenicity and their discovery is not dependent on the antigenicity of the target[5]. Rather, novel peptide ligands targeting a wide array of receptors or cell types can be readily developed using in vitro or in vivo phage display screening[6]. Another key advantage is that peptides are approximately two orders of magnitude smaller than antibodies. Consequently, they more readily penetrate into the high pressure interstitial tumor environment[7], and they are relatively easy to produce, modify, and incorporate into drug delivery technologies. In recent years, peptide manufacturing processes have dramatically improved in cost efficiency and been scaled up to multiton levels[8]. Furthermore, a number of synthetic chemistry techniques have been developed to overcome some of the shortcomings of peptides, including unnatural amino acids for increased peptide stability and PEG conjugation for increased circulation[9]. Lastly, in comparison to antibodies, peptide conjugation can be achieved with a greater degree of flexibility. Available chemistries include hydrazones, carboxylic acid esters, thioethers and amides[10]. Additional advances in conjugation techniques are expected to expand the utility of peptides even further.

To date, numerous peptide ligands targeting a variety of receptors have been identified and successfully incorporated into a wide array of drug delivery platforms[1, 11]. The most widely studied are the integrin-targeting RGD peptides[12]. Tumor-specific peptides may also be directly

conjugated to cytotoxic drugs or radionuclides. In peptide receptor radionuclide therapy (PRRT), a somatostatin analog coupled to a radionuclide is employed for the treatment of metastasized neuroendocrine tumors[13]. AEZS-108 is a peptide drug conjugate (PDC) currently under investigation for the treatment of prostate cancer, which consists of a peptide of LHRH conjugated to doxorubicin[14,15]. Similarly, GRN1005 is an anigiopeptin-2-paclitaxol PDC that targets the lipoprotein receptor protein-1 in the blood brain barrier and glioma cells [16]. Other PDCs are in the pipeline for the of treatment of leukemias, lymphomas, SCLC, pancreatic cancer and prostate cancer[5,17].

One target of great interest in cancer is the epidermal growth factor receptor (EGFR), a tyrosine kinase receptor that is known to promote cell proliferation, differentiation, and migration and inhibit apoptosis[18]. EGFR is overexpressed in a wide array of epithelial cancers making it a promising target for preferential tumor delivery[19]. Additionally, EGFR receptors have been shown to constitutively internalize via receptor-mediated endocytosis[20]. However, native EGF has strong mitogenic and neoangiogenic activity that would be counterproductive for an anticancer therapeutic[18].

Using *in vitro* phage display methods, Li et al. identified a novel peptide, GE11, that binds to EGFR with high affinity (Kd ~22nM) and internalizes into EGFR-overexpressing cancer cell lines[21]. Furthermore, in contrast to human EGF, GE11 demonstrated negligible mitogenic activity in cancer cell cultures[21]. Post-synthetic conjugation of GE11 to both poly(PEI) and liposomal drug carriers successfully enhanced delivery to EGFR-overexpressing tumor cells both *in vitro* and in tumor xenograft models[21,22]. In combination, these findings recommend GE11 as a cheap, safe, and specific targeting alternative for the delivery of cancer drugs to EGFR-overexpressing cancers.

In this chapter, the peptide monomer strategy developed in Chapters 4 & 5 was implemented for cancer-specific targeting. A methacrylamide-GE11 peptide monomer was synthesized and directly polymerized into a hydrophilic drug delivery scaffold in combination with an aromatic ester-linked camptothecin prodrug (**Figure 6.1**). GE11 was shown to significantly enhance targeting and polymeric prodrug activity in SKOV3 ovarian cancer cell cultures.

6.2 Materials and Methods

6.2.1 Monomer Synthesis

6.2.1.1 Synthesis of Rhodamine-labeled Peptides and Peptide Monomers

Using an automated PS3 peptide synthesizer (Protein Technologies), peptides were synthesized on a solid support (rink amide MBHA resin (100-200 mesh), EMD Millipore) from FMOC protected (L) amino acids (EMD Millipore) and an FMOC protected 6-aminohexanoic acid (Ahx) spacer (AnaSpec). For synthesis of peptide monomers, the amino termini of the peptides were coupled to N-succinimidyl methacrylate (TCI America) prior to cleavage from the resin. For synthesis of fluorescently-labeled peptides, the N-termini were instead coupled to rhodamine B (Rho). The peptides/monomers were deprotected and cleaved from the resin by treatment with trifluoroacetic acid/triisopropylsilane/H_2O (9.5:2.5:2.5, v/v/v) for 4 hours and precipitated in cold ether. Crude peptides/monomers were purified by reverse phase high performance liquid chromatography (RP-HPLC) on a Jupiter 5 μm C18 300Å column (Phenomenx) with an Agilent 1260 HPLC. Ion trap mass spectrometry with electrospray (Bruker Esquire) was used to confirm the molecular weights of the purified products. The following peptides/monomers were synthesized:

Methacrylamido(Ma)-AhxYHWYGYTPQNVI (MaAhxGE11)

MaAhxHYPYAHPTHPSW (MaAhxHW12)

MaAhxSGSGSGSGYHWYGYTPQNVI ((MaAhx$(SG)_4$GE11)

RhoB-AhxYHWYGYTPQNVI (RhoGE11)

RhoB-AhxARPLEHGSDKAT (RhoAT12)

The targeting peptide GE11 was synthesized with either Ahx or an $Ahx(SG)_4$ spacer between the targeting sequence and monomer. The unrelated peptides HW12 and AT12 were employed as negative controls.

6.2.1.2 Synthesis of Rhodamine-hydroxy ethyl methacrylate (RhoHEMA)

To rhodamine B 5.26 g (11 mmol), N,N'-dicyclohexylcarbodimide 2.88 g (14 mmol) and 4-dimethylaminopyridine 134 mg (1.1 mmol) in CH_2Cl_2 (75 mL), was added 2-hydroxyethyl methacrylate 1.82 g (14 mmol) at 0 °C. After 30 min, the ice bath was removed and the reaction mixture was stirred at room temperature for 16 h. After filtering off the byproduct dicyclohexylurea, the solvent was evaporated under reduced pressure. The residue was redissolved in 30 mL acetonitrile and the insoluble materials were filtered off. The crude product obtained after evaporating acetonitrile was purified by flash column chromatography using 6 % methanol in chloroform. Purified monomer was characterized by 1H-NMR (**Figure 6.2A**). Yield: 5.89 g (91%).

6.2.1.3 Synthesis of Camptothecin-SAM (CAM-SMA)

To a solution of mono-2-(methacryloyloxy)ethyl succinate (SMA) 460 mg (2 mmol), *N*-(3-dimethylaminopropyl)-*N′*-ethylcarbodimide hydrochloride (EDCI.HCl) 767 mg (4 mmol) and N,N-dimethylpyridin-4-amine (DMAP) 122 mg (1 mmol) in 60 mL CH_2Cl_2 was added camptothecin 348 mg (1 mmol) as solid. After stirring at RT for 6 h, the reaction mixture was washed with water (2 X 30mL) and the organic phase was dried over anhydrous sodium sulfate. After evaporation of the solvent under reduced pressure, the resulting crude product was purified by silica gel column chromatography using 7 %

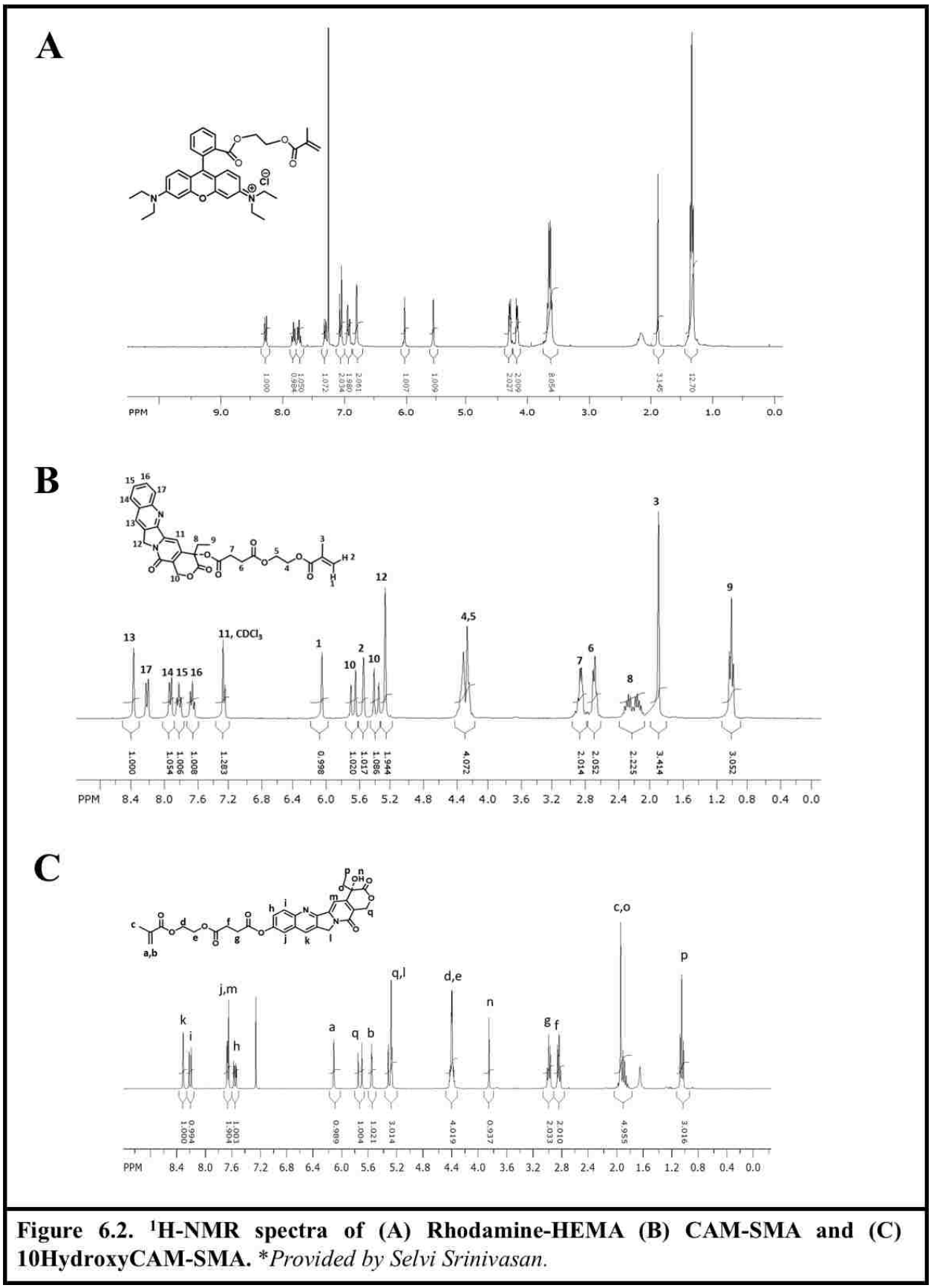

Figure 6.2. ^{1}H-NMR spectra of (A) Rhodamine-HEMA (B) CAM-SMA and (C) 10HydroxyCAM-SMA. **Provided by Selvi Srinivasan.*

methanol in chloroform. Purified monomer was characterized by 1H-NMR (**Figure 6.2B**). Yield = 544 mg (97.0 %).

6.2.1.4 Synthesis of 10-HyroxyCAM-SMA (10CAM-SMA)

First, 2-Methacryloyloxyethylsuccinoyl chloride was synthesized following the reported procedure[23]: Briefly, mono-2-(methacryloyloxy)ethyl succinate (SMA) 11.5g (50 mmol) was added to neat thionyl chloride 23 mL (320 mmol). The reaction mixture was stirred at room temperature for 30 min and at 50 ^{o}C for 1h. After evaporation of the excess thionyl chloride and other volatiles, the resulting 2-methacryloyloxyethylsuccinoyl chloride was used for the next step without further purification. 2-Methacryloyloxyethylsuccinoyl chloride 1.84 g (7.42 mmol) was added slowly to a solution of 10-hydroxylcamptothecin 900 mg (2.47 mmol) and trimethylamine 6.98 mL (50mmol) in 250 mL tetrahydrofuran at 4 ^{o}C. The reaction mixture was stirred at 4 ^{o}C for 15 min and at room temperature for 1h. Triethylammonium chloride formed was filtered off and the filtrate was concentrated under reduced pressure. The crude ester was purified by column chromatography with 30% tetrahydrofuran in chloroform. Column purified product was redissolved in 10 mL tetrahydrofuran and precipitated in 90 mL of 80 % ether/hexane. Purified monomer was characterized by 1H-NMR (**Figure 6.2C**). Yield = 976 mg (68.7%).

6.2.2 Polymer Synthesis

6.2.2.1 Synthesis of Poly(ethylene glycol) Methyl Ether Methacrylate (PEGMA)-peptide Copolymers

The GE11-targeting peptide monomer (MaGE11) and control monomer (MaHW12) were copolymerized with PEGMA monomer of either molecular weight 950 Da ($PEGMA_{950}$) or 300 Da ($PEGMA_{300}$). Polymerizations were conducted under nitrogen in DMSO (20 wt% monomer) for 24 hours at 70 °C using azobis(4-cyanopentanoic acid) (ABCVA) as the radial initiator and 4-cyanopentanoic acid dithiobenzoate (CTP) as the chain transfer agent (CTA). The molar composition of the reaction feed was 4% peptide monomer and 96% PEGMA. In addition, polymers were synthesized with trace amounts (~0.1 %) of the fluorescent monomer RhoHEMA. Initial monomer ([M]o) to CTA ([CTA]o) to initiator ([I]o) ratios for $PEGMA_{950}$ and $PEGMA_{300}$ copolymers were 25:1:0.1 and 50:1:0.1, respectively. The resulting polymers were precipitated in diethyl ether and the unreacted peptide monomer was subsequently precipitated in acetone. This two-step precipitation scheme was repeated six times and the isolated polymers were dried by lyophilization.

6.2.2.2 Synthesis of Carboxybetaine Methacrylate (CBM)-peptide Copolymers

For synthesis of the peptide-CBM copolymers, CTP (8.4 mg, 30 μmol), ABCVA (1.12 mg, 3 μmol), peptide monomer (60 μmol), tQuat (0.432 g, 1.44 mmol), RhoHEMA (4 mg, 6.75 μmol) and DMSO (2.2 mL) ($[M]_o$:$[CTA]_o$:$[I]_o$ = 50:1:0.1) were added to a 5 mL round bottom flask. The polymerization solutions were then transferred to a septa-

sealed vial and purged with nitrogen for 30 minutes. After this time the polymerizations were transferred into a preheated oil bath at 70 ^{o}C and allowed to polymerize for 16 hours. The polymers were then isolated via precipitation into diethyl ether followed by dialysis against deionized water at 5 ^{o}C and subsequent lyophilisation. The dry polymers were then dissolved in neat trifluoroacetic acid (TFA) at a concentration of 20 mg/mL and allowed to react at room temperature for 8 hours. After this time the polymers were precipitated into cold diethyl ether and isolated via centrifugation. The polymers were then neutralized with 50 mL of ice cold phosphate buffer (0.2 M, pH 7.4) and dialyzed at 5 ^{o}C against deionized water. The final deprotected copolymers were isolated via lyophilisation.

6.2.2.3 Synthesis of Carboxybetaine Camptothecin Prodrug Polymers

For synthesis of the prodrug-CBM copolymers, CTP (37 mg, 132 μmol), ABCVA (3.7 mg, 13.2 μmol), 10CAM-SMA (0.312 g, 0.541 mmol) or CAM-SMA (0.303 g, 0.541 mmol), tQuat (0.936 g, 2.77 mmol), RhoHEMA (7.82 mg, 13.2 μmol) and DMSO (5.0 mL) ($[M]_o$:$[CTA]_o$:$[I]_o$ = 25:1:0.1) were added to a 10 mL round bottom flask. For synthesis of a non-drug CBM control polymer, CTP (66 mg, 237 μmol), ABCVA (6.6 mg, 23.7 μmol), tQuat (4.00 g, 11.8 mmol), RHoEMA (14.0 mg, 23.7 μmol) and DMSO (16 mL) ($[M]_o$:$[CTA]_o$:$[I]_o$ = 50:1:0.1) were added to a 10 mL round bottom flask. The polymerization solutions were then transferred to a septa-sealed vial and purged with nitrogen for 30 minutes. After this time the polymerizations were transferred into a preheated oil bath at 70 ^{o}C and allowed to polymerize for 16 hours. The polymers were then isolated via precipitation into diethyl ether followed by dialysis against deionized water at 5 ^{o}C and subsequent lyophilisation. The dry polymers were then dissolved in neat

TFA at a concentration of 20 mg/mL and allowed to react at room temperature for 8 hours. After this time the polymers were precipitated into cold diethyl ether and isolated via centrifugation. The polymers were then neutralized with 50 mL of ice cold phosphate buffer (0.2 M, pH 7.4) and dialyzed at 5 ^{o}C against deionized water. The final deprotected copolymers were isolated via lyophilisation.

6.2.2.4 Synthesis of Peptide Camptothecin-prodrug Polymers

For the synthesis of peptide-containing diblock copolymers, non-deprotected p(10CAM-co-CBM) and p(CBM) from part 6.2.2.3 were employed as macroCTAs. To a macroCTA solution (21 μmol) in DMSO (1.77 mL) were added tQuat (0.344 g, 1.02 mmol), MaAhxGE11 or MaAhxHW12 (42.44 μmol), and ABCVA (0.59 mg, 2.12 μmol) ($[M]_o$:$[CTA]_o$:$[I]_o$ = 50:1:0.1). The polymerization solutions were then transferred to a septa-sealed vial and purged with nitrogen for 30 minutes. After this time the polymerization vial was transferred into a preheated oil bath at 70 ^{o}C and allowed to polymerize for 16 hours. The polymers were then isolated via precipitation into diethyl ether followed by dialysis against deionized water at 5 ^{o}C and subsequent lyophilisation. The dry polymers were then dissolved in neat TFA at a concentration of 20 mg/mL and allowed to react at room temperature for 8 hours. After this time the polymers were precipitated into a 25 times excess of cold diethyl ether and isolated via centrifugation. The polymer was then neutralized with 50 mL of ice cold phosphate buffer (0.2 M pH, 7.4) and then dialyzed at 5 ^{o}C against deionized water. The final deprotected copolymer was then isolated via lyophilization.

6.2.3 Polymer Characterization

The number average molecular weights (Mn) and polydispersities (PDIs) of the polymers were or will be determined by gel permeation chromatography (GPC). Analysis of $PEGMA_{co}$peptide polymers was conducted in a mobile phase of 0.1 wt% lithium bromide in N,N-dimethylformamide using Tosoh SEC TSK GEL α-3000 and α-4000 columns (Tosoh Bioscience), a 1200 Series liquid chromatography system (Agilent), and a miniDAWN TREOS three-angle light scattering instrument with an Optilab TrEX refractive index detector (Wyatt Technology). Polymer compositions will be confirmed by ^{1}H-NMR spectroscopy. For quantification of peptide content, reaction aliquots were collected at T_o and T_x and analyzed by RP-HPLC (abs 280 nm). Percent monomer conversion was calculated by the equation (Peak[T_o]-Peak[T_x])/(Peak[T_o]) and used to estimate the number of peptides per polymer chain.

6.2.4 Flow Cytometry

For measuring polymer binding and uptake, polymers were synthesized containing trace quantities of the fluorescent monomer RhoHEMA. SKOV3 cells were plated in 6-well plates at a density of 100,000 cells per well, allowed to adhere overnight, and treated with 1 μm polymer in media for 15 min at 37 °C. Cells were then trypsinized, washed with PBS, and analyzed on a BD LSRII flow cytometer. For measuring the binding of rhodamine B-labeled peptides, SKOV3 cells were treated with either 0.1 or 1 μm peptide for 30 minutes at 4 °C.

6.2.5 Drug Release Kinetics

To evaluate release of camptothecin from the prodrugs, the CBM-prodrug copolymers (6 mg/mL) were incubated in 100% human serum at 37 °C. At various time points, reaction aliquots

were taken and diluted 1:1 with methanol/water (75/25, v/v) and 1:1 with acetonitrile to precipate serum proteins. Samples were centrifuged (15 min, 12,000 g) and supernatants were collected, filtered (0.45 μm low protein binding), and analyzed by RP-HPLC (abs 370 nm). RP-HPLC analysis was conducted at ambient temperature using a Zorbax RX-C_{18} (4.6 x 150 mm; 5 μm) analytical column (Agilent Technologies, CA) on an Agilent 1260 system. The amount of released drug was quantified in comparison to free drug standards. The total drug content of the polymers was determined by polymer dissolution in 10% aq. H_2SO_4 (72 h, 25 °C), and percent drug release was calculated according to the following equation: % drug released = [Peak(t_x)-Peak(t_o)]/[Peak(H_2SO_4)], where t_x and t_o are the peaks at time x and zero, and Peak(H_2SO_4) is for total drug.

6.2.6 Cell Culture

SKOV3 human ovarian cancer cells (ATCC) were maintained in RPMI 1640 Medium (+L-glutamine, + HEPES) supplemented with 10% FBS (GIBCO) and 1% penicillin/streptomycin (GIBCO). Cells were maintained in log-phase growth at 37 °C and 5% CO_2.

6.2.7 Cell Viability Assay

For peptide targeting studies, SKOV3 cells were plated in 96-well plates at a density of 3,000 cells per well and pulsed with polymer solutions in culture medium (0-10,000 nM) for 15 min. Cells were then washed twice with media and cell viability was measured after 72 hours using an MTS Cell Proliferation Colorimetric Assay (Biovision). For studying the camptothecin

prodrug monomers, SKOV3 cells were plated in 96-well plates at 5,000 cells per well and treated continuously with polymer or free drug for 72 hours, after which cell viability was measured.

6.3 Results

6.3.1 Validation of the GE11 Peptide for Targeting SKOV3 Ovarian Cancer Cells

The GE11 peptide, identified via phage display, has been shown to bind strongly and specifically to the epidermal growth factor receptor overexpressed in a wide array of epithelial malignancies. Prior to employing GE11 for targeting a polymeric drug delivery system, we wanted to validate its ability to bind to EGFR overexpressed in SKOV3 ovarian cancer cell cultures. In particular, we were interested in the binding activity of a GE11 peptide modified on its N-terminus, which would be the site of polymer conjugation. Consequently, GE11 was synthesized with a six carbon spacer (aminohexanoic acid (Ahx)) and N-terminal rhodamine B fluorescent label (RhoAhxGE11). As a control, the unrelated peptide AT12 was also synthesized with Ahx and rhodamine B (RhoAhxAT12). Next the ability the rhodamine-peptides to bind to SKOV3 cells was examined. Cells were treated with RhoAhxGE11 or RhoAhxAT12 at concentrations of 0.1 or 1 μM, and binding was determined by flow cytometric analysis (**Figure 6.3**). At both concentrations, RhoAhxGE11 bound much more strongly than RhoAhxAT12. At 0.1 μM, RhoAhxGE11 bound to cells at a 158-fold higher level than RhoAhxAT12, whose binding was nearly undetectable. At 10 μM, RhoAhxGE11 binding was 70-fold higher than RhoAhxAT12. These findings confirm the power of GE11 for targeting EGFR-overexpressing tumors and its potential as a targeting agent in polymeric drug delivery systems.

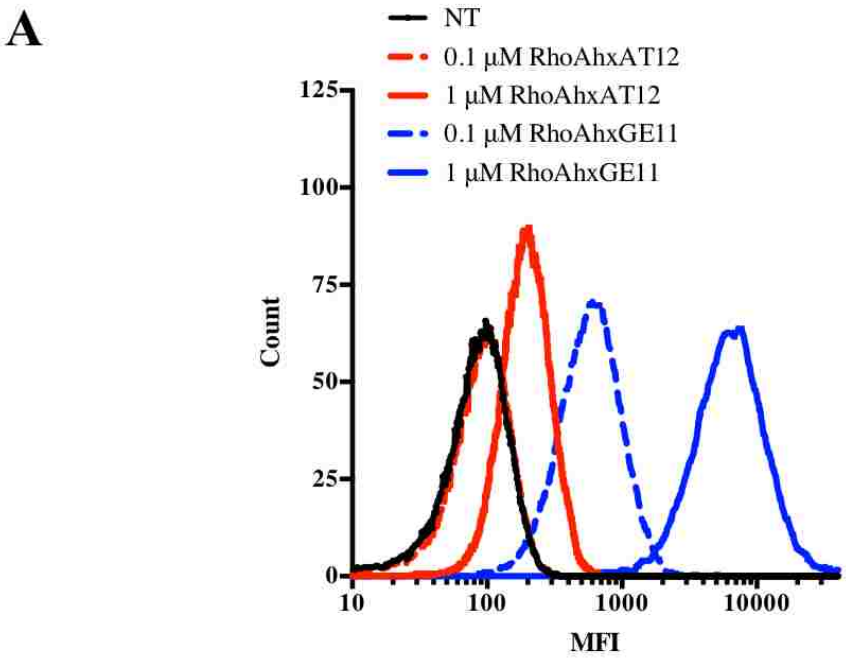

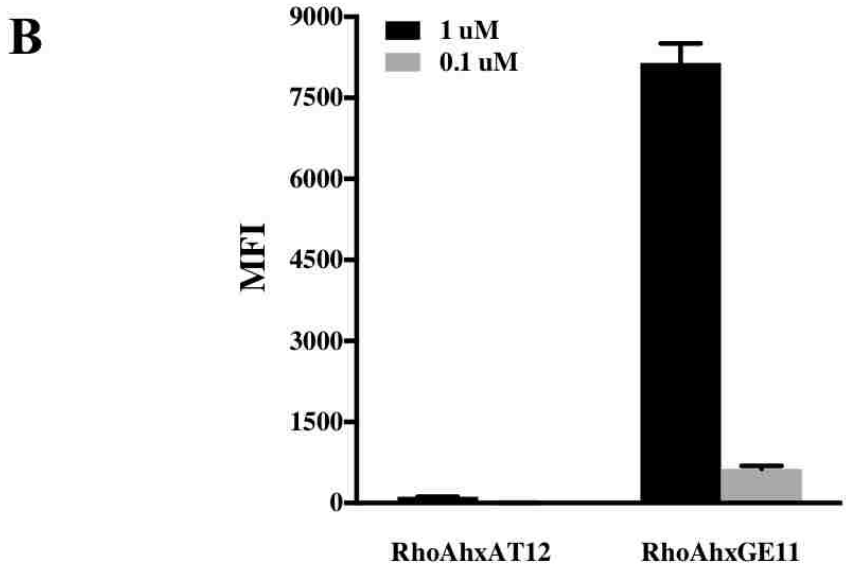

Figure 6.3. The GE11 peptide targets SKOV3 ovarian cancer cells. SKOV3 cells were incubated with Rhodamaine B-labeled GE11 (RhoAhxGE11) or AT12 (RhoAhxAT12) at concentrations of 0.1 µM and 1 µM for 30 minutes at 4 °C. Cells were then washed, trypsinized, and analyzed by flow cytometry for peptide binding. At both concentrations, RhoAhxGE11 bound to cells at significantly higher levels than RhoAhxAT12, validating the ability of GE11 to target SKOV3 cells.

6.3.2 Carboxybetaine Methacrylate Permits Targeting by Copolymerized GE11 Peptide Monomer

6.3.2.1 Synthesis of a GE11 Peptide Monomer

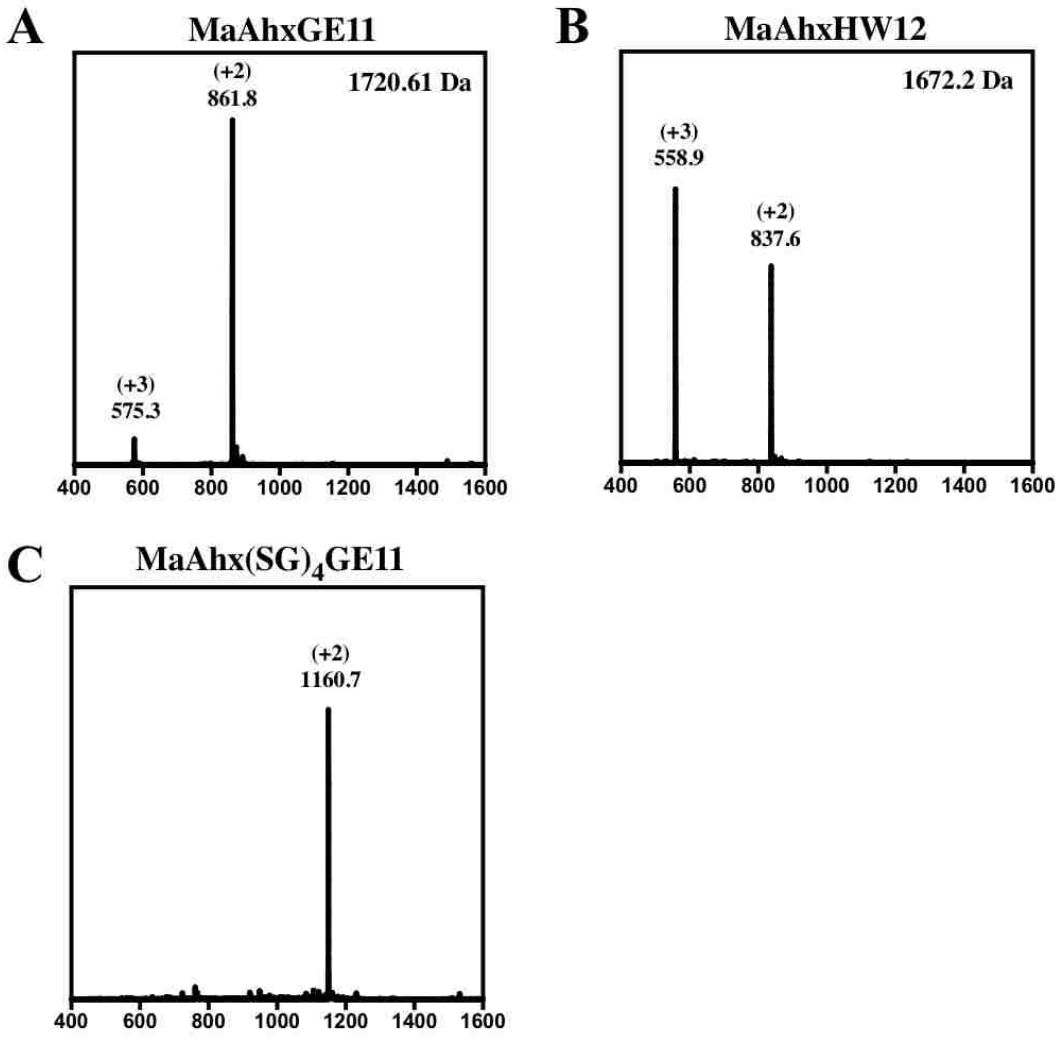

Figure 6.4. Mass spectrum of (A) MaAhxGE11, (B) MaAhxHW12 and (C) MaAhx(SG)$_4$GE11. Peptides were synthesized by FMOC solid phase synthesis and functionalized on their N-termini with methacrylamide using NHS chemistry. Deprotected peptide monomers were purified by RP-HPLC and molecular weights were confirmed by mass spectrometry.

A GE11 peptide monomer was synthesized for direct incorporation into polymeric carriers. The monomer consisted of GE11 modified on its N-terminus with Ahx and methacrylamide (MaAhxGE11) (**Figure 6.4A**). An Ahx spacer was inserted between the binding peptide and monomer to facilitate receptor-binding and polymerization. A non-targeting control monomer was synthesized substituting GE11 for HW12 (MaAhxHW12) (**Figure 6.4B**). In addition, to investigate whether a longer and more hydrophilic spacer would improve targeting, a GE11 monomer was synthesized with four serine-glycine repeats inserted between Ahx and the GE11 motif (MaAhx$(SG)_4$GE11) (**Figure 6.4C**).

6.3.2.2 Copolymerization of GE11 with Carboxybetaine Methacrylate and Poly(ethylene glycol) Methacrylate

The GE11 monomer was next incorporated into unimeric hydrophilic polymers in order to test the ability of polymerized peptide to target SKOV3 cells (**Figure 6.5**). Three different hydrophilic comonomers were investigated with different charge and steric properties. Two were neutral long chain PEGMA monomers either 300 Da or 950 Da in size, corresponding to 6 or 19 ethylene oxide repeats, respectively. The third was the neutral but zwitterionic monomer carboxybetaine methacrylate, which has demonstrated advantages over PEGMA including increased hydration and decreased steric hindrance.

Employing RAFT polymerization, both the GE11 peptide monomer and HW12 control monomer were copolymerized with either $PEGMA_{300}$, $PEGMA_{950}$ or CBM. The MaAhx(SG)4GE11 monomer was copolymerized with only CBM. For all polymers, the

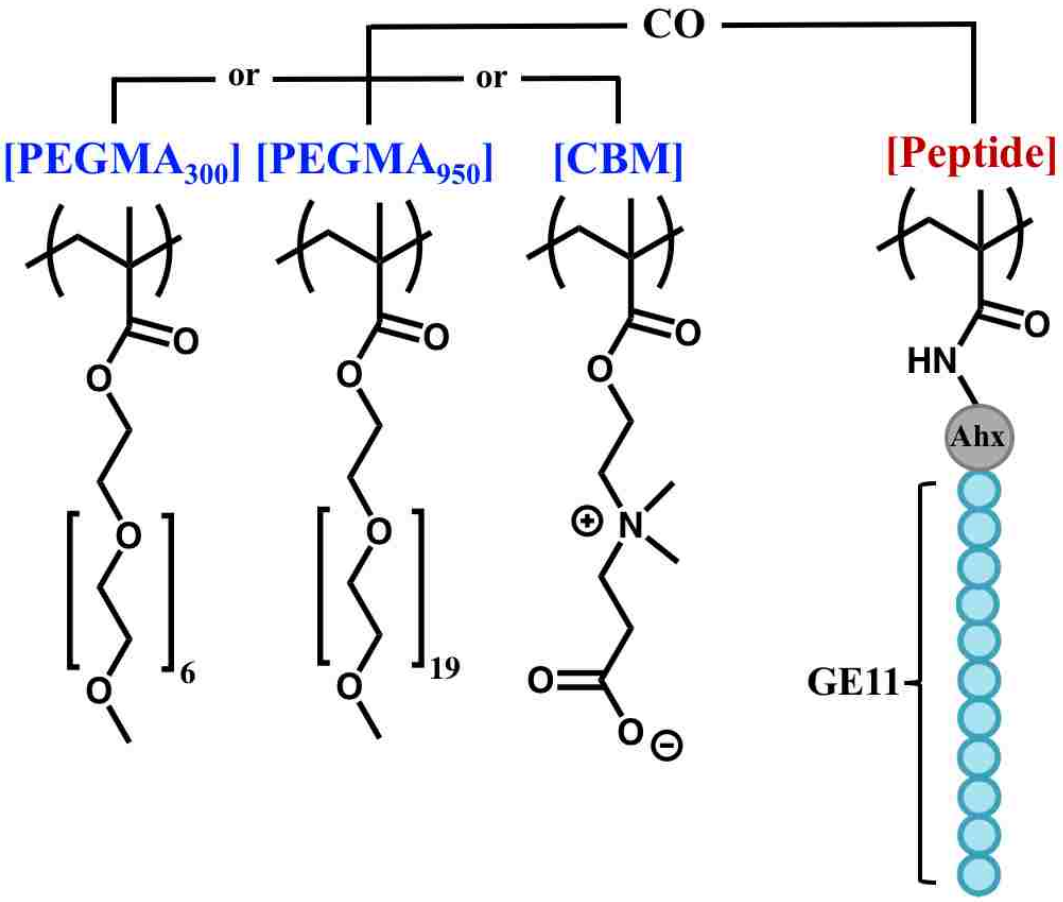

Figure 6.5. The GE11 targeting peptide monomer (MaAhxGE11) was incorporated into unimeric, hydrophilic polymer scaffolds via RAFT copolymerization. Three different methacrylate-based hydrophilic comonomers were investigated with different charge and steric properties. Two were neutral long chain polyethylene glycol monomers either 300 Da ($PEGMA_{300}$) or 950 Da ($PEGMA_{950}$) in size, with 6 or 19 ethylene oxide repeats, respectively. The third was the neutral, low steric, zwitterionic monomer carboxybetaine methacrylate (CBM).

molar composition of the reaction feed was 4% peptide and 96% comonomer. In addition, to fluorescently label the polymers for cell targeting studies, a trace amount (< 0.1 mol %) of rhodamine B monomer was added to each reaction. **Table 1** provides of summary of polymer synthesis and characterization details. Size-exclusion gel-permeation chromatography (**Figure 6.6**) measured the molecular weights and molar

mass dispersities of the polymers, and compositions will be confirmed by ^{1}H-NMR. In addition, peptide monomer conversion for each polymer was or will be quantified by RP-HPLC analysis of reaction aliquots taken at T_o and T_x.

Polymer	DP	% feed/comp		M_n	PDI	Peptide/ polymer
		PEGMA/CBM	Peptide			
p(PEGMA$_{950}$-co-MaAhxGE11)	25	96 /	4 /			
p(PEGMA$_{950}$-co-MaAhxHW12)	25	96 /	4 /			
p(PEGMA$_{300}$-co-MaAhxGE11)	50	96 / 97.7	4 / 2.3	14,300	1.14	0.74
p(PEGMA$_{300}$-co-MaAhxHW12)	50	96 / 98.4	4 / 1.6	15,400	1.16	0.98
p(CBM-co-MaAhxGE11)	50	96 /	4 /			0.97
p(CBM-co-MaAhxHW12)	50	96 /	4 /			1.24
p(CBM-co-MaAhx(SG)$_4$GE11)	50	96 /	4 /			0.75

Table 6.1. Synthesis and characterization of hydrophilic peptide copolymers. Using RAFT polymerization, the GE11-targeting peptide monomer (MaAhxGE11) or HW12-control monomer (MaAhxHW12) were copolymerized with either PEGMA$_{950}$, PEGMA$_{300}$, or CBM. In addition, CBM was copolymerized with a GE11-peptide monomer containing a longer hydrophilic spacer between methacrylamide and the GE11 targeting motif (MaAhx(SG)$_4$GE11). The degree of polymerization was 25 for PEGMA$_{950}$ copolymers and 50 for PEGMA$_{300}$ and CBM copolymers. For all polymers, the targeted peptide:comonomer molar ratio was 4:96. Polymer molecular weights and polydispersities were or will be measured by gel permeation chromatography (GPC), and polymer compositions will be determined by ^{1}H-NMR. Peptide monomer conversions were or will be quantified by RP-HPLC analysis of reaction aliquots taken at T_o and T_x.

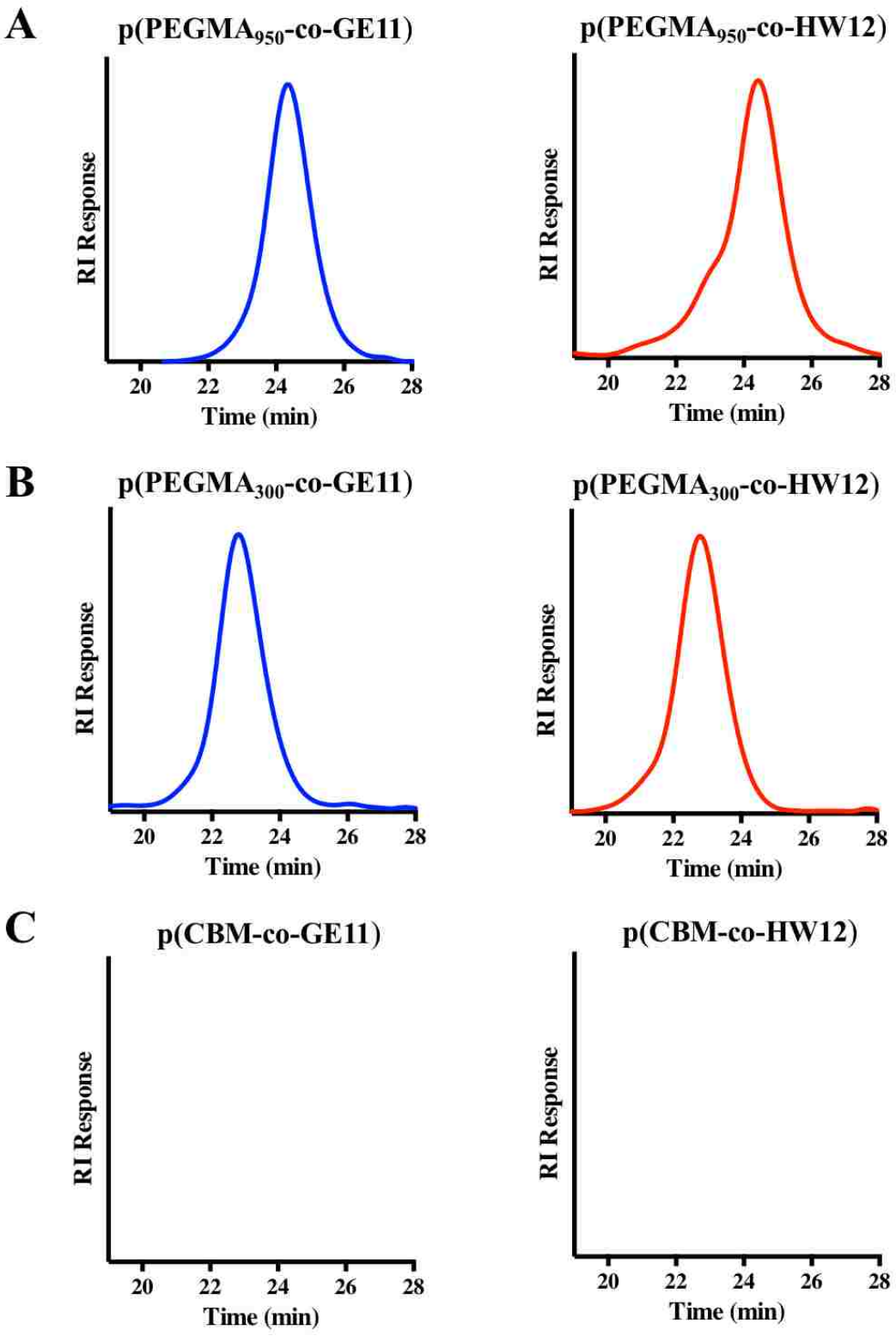

Figure 6.6. SEC-GPC chromatographs of the GE11 (blue) and HW12 (red) peptide monomers copolymerized with either (A) $PEGMA_{950}$, (B) $PEGMA_{300}$ or (C) CBM.

6.3.2.3 GE11-targeting of Copolymers in SKOV3 Ovarian Cancer Cells

The ability of GE11 to enhance polymer targeting in SKOV3s was assessed for each hydrophilic comonomer. SKOV3 cells were pulsed with 1 μM polymer for 15 min at 37 °C, after which the binding/uptake of the rhodamine-B labeled polymers was assessed by flow cytometry. GE11 did not enhance uptake over the corresponding control polymer when copolymerized with either $PEGMA_{950}$ or $PEGMA_{300}$ (**Figure 6.7A-B**). The $PEGMA_{950}$ copolymers were taken up similarly, and for $PEGMA_{300}$ the control polymer was even taken up slightly better than the GE11-targeted polymer. This is possibly a result of the positive charge on the HW12 peptide. In contrast, GE11 lead to a significant 18-fold increase in polymer binding and uptake when copolymerized with CBM (**Figure 6.7C)**. It is likely that the PEGMA monomers, but not CBM, sterically interfere with GE11-receptor binding. This lack of steric hindrance by CBM is corroborated by the finding that a longer hydrophilic spacer placed between GE11 and the polymer backbone did not further increase uptake. For cells treated with p(CBM-co-$MaAhx(SG)_4GE11$), the average mean fluorescent intensity (MFI) was 1334 ± 82, in contrast to 1777 ± 36 for p(CBM-co-MaAhxGE11)), 219 ± 7 for p(CBM-co-MaAhxHW12) and 127 ± 6 for untreated cells. In combination, these findings confirm GE11's utility as a targeting agent and recommend CBM as a comonomer for drug delivery.

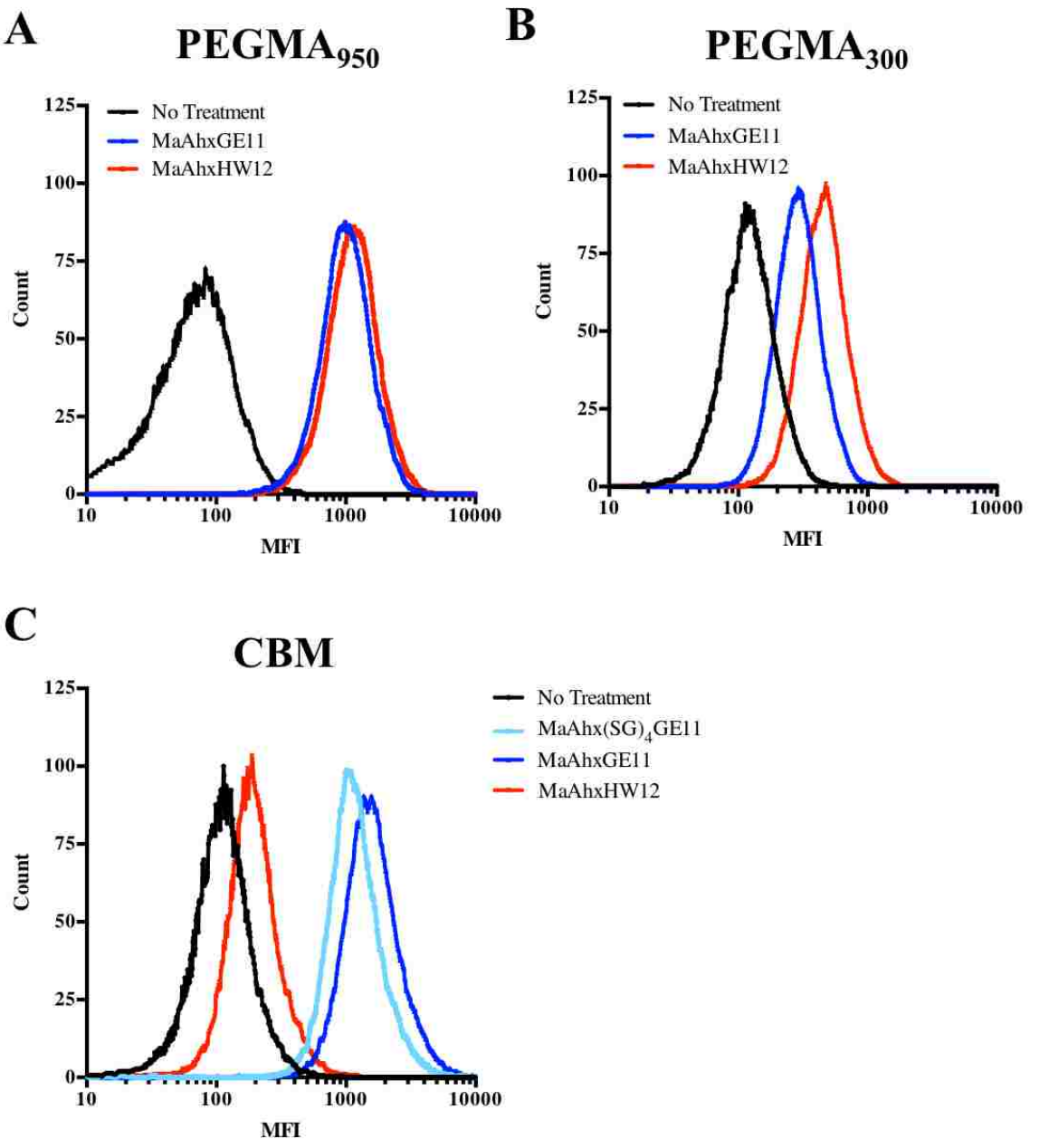

Figure 6.7. Carboxybetaine permits GE11-mediated targeting of polymers to SKOV3 ovarian cancer cells, while both small (300 Da) and large (950 Da) PEGMA monomers block targeting. SKOV3 cells were incubated with fluorescently labeled copolymers (1 uM) for 15 minutes at 37 and polymer binding was analayzed by flow cytometry. GE11-peptide monomer copolymerized with **(A)** $PEGMA_{950}$ or **(B)** $PEGMA_{300}$ did not enhance polymer uptake in comparison to corresponding HW12 control polymers. In contrast, GE11 copolymerized with **(C)** carboxybetaine methacrylate enhanced polymer uptake 18-fold. Inserting a longer hydrophilic spacer (–$(SG)_4$-) between the methacrylamide monomer and peptide sequence did not impact GE11's targeting activity.

6.3.3 Polymeric Camptothecin Prodrugs

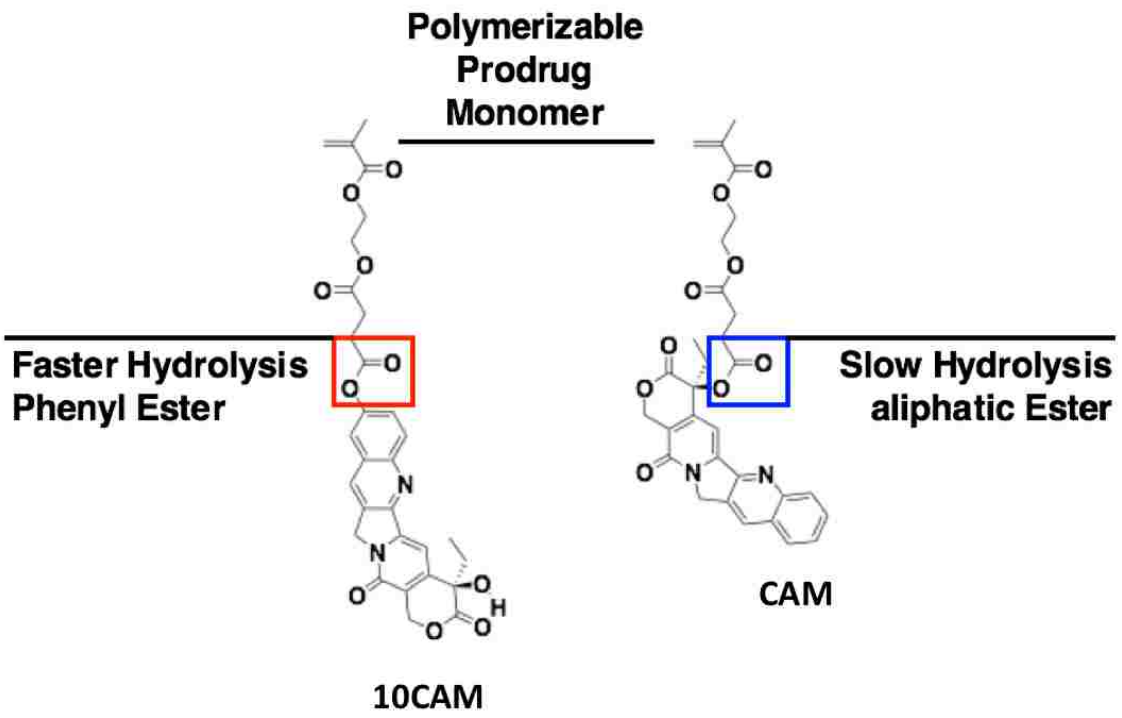

Figure 6.8. Ester-linked camptothecin prodrug monomers. Camptothecin prodrug monomers were synthesized by conjugating the carboxylic acid of mono-2-(methacryloyloxy)ethyl succinate (SMA) to hydroxyl groups present in the drug. SMA was conjugated to camptothecin at two distinct sites to create either aliphatic (CAM) or aromatic (10CAM) ester linkages.

6.3.3.1 Synthesis and Characterization of Polymeric Camptothecin Prodrugs

Polymerizable prodrugs may be incorporated into polymeric platforms in order to increase drug solubility, target delivery to tumors, and decrease off-target toxicity. **Figure 6.8** shows the chemical structures of two methacrylate-based camptothecin prodrug monomers. Camptothecin is a potently toxic topisomerase I inhibitor use for the treatment of cancer. Both camptothecin prodrug monomers were synthesized by

conjugating the carboxylic acid of mono-2-(methacryloyloxy)ethyl succinate (SMA) to hydroxyl groups present in the drug. SMA was conjugated at two distinct sites to create either aliphatic (CAM) or aromatic ester (10CAM) linkages. In contrast to the smaller monomer methacrylic acid, SMA creates a spacer between the drug and polymer backbone, which may improve copolymerization and/or aid ester hydrolysis.

CBM was employed as a biocompatible comonomer for the prodrugs. Both CAM and 10CAM were copolymerized with CBM in DMSO at 70 °C with CTP and ABCVA employed as the RAFT chain transfer agent and radical initiator, respectively. For both reactions, the molar composition of the feed was 16% drug and 86% CBM.

6.3.3.2 Drug Release in Human Serum

The drug release kinetics of the two polymeric prodrugs were evaluated and compared. The polymers were incubated in 100% human serum at 37 °C, and over time drug release was quantified by RP-HPLC in comparison to free drug standards. Camptothecin was found to release from p(10CAM -co-CBM) at a significantly faster rate than from p(CAM -co-CBM) (**Figure 6.9A).** 57% of the aromatic ester linked drug was released after 9 days, in comparison to 33% for the aliphalic ester-linked drug. These results confirm the release of active drug from the polymers and demonstrate that the physiochemical properties of the linkage significantly influence the rate of release.

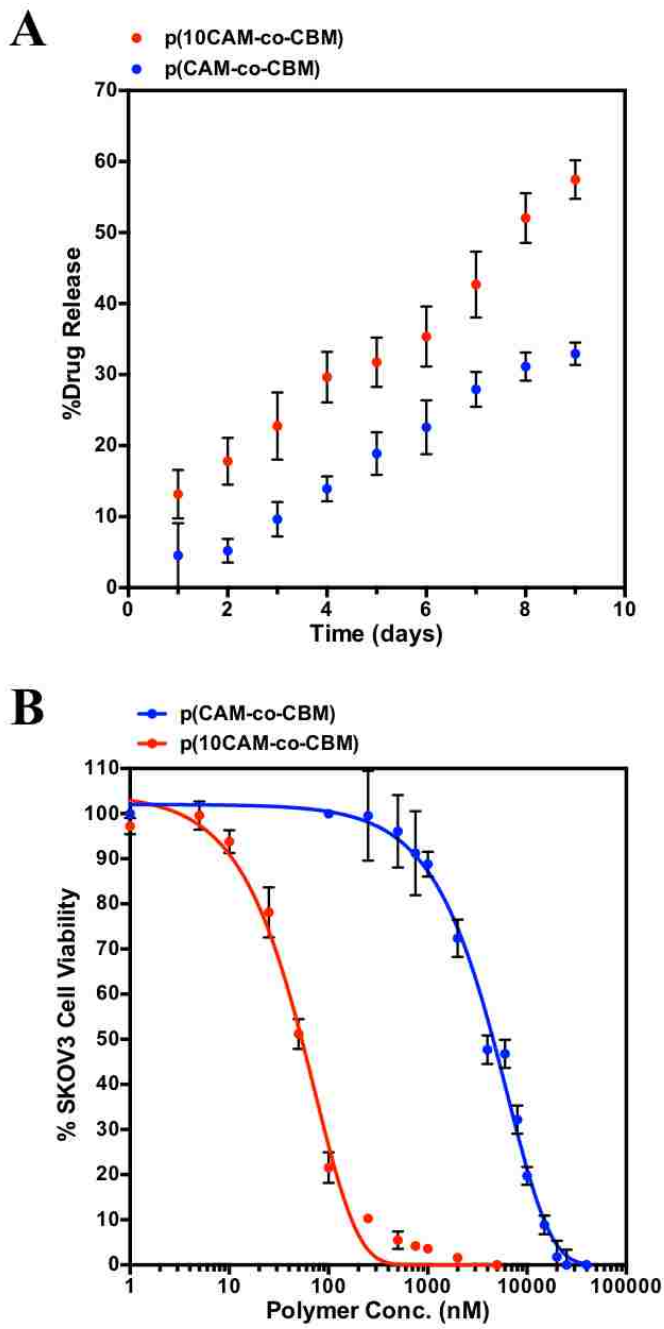

Figure 6.9. The aromatic ester-linked polymeric prodrug releases active camptothecin at a faster rate and is more cytotoxic than the alphatic ester-linked prodrug. Both the aromatic (10CAM) and aliphatic (CAM) ester-linked drug monomers were copolymerized with CBM to synthesize soluble polymeric prodrugs. **(A)** Release of camptothecin from the copolymers in human serum (37 °C) was evaluated over 9 days using RP-HPLC analysis. **(B)** The cytotoxic activity of the polymeric prodrugs was evaluated in SKOV3 cell cultures after 72 hours of treatment using an MTS cell viability assay.

6.3.3.3 In Vitro Cytotoxicity of p(CAM -co-CBM) and p(CAM10-co-CBM) in SKOV3 Ovarian Cancer Cells

The toxicities of free camptothecin and the polymeric prodrugs were tested in SKOV3 ovarian cancer cell cultures. The cells were treated with free drug or polymer for 72 hours, after which cell viability was measured. As can be seen in **Figure 6.9B** the phenyl ester-linked prodrug was significantly more active than the aliphatic ester-linked drug. The IC50s for p(10CAM-co-CBM) and p(CAM -co-CBM) were 56 nM and 4776 nM respectively. This toxicity trend correlates with the drug release kinetics measured in section 6.3.3.2. These measurements demonstrate the ability of the polymer prodrug system to release the linked drug in an active form in a controlled manner. In addition, the two polymeric produgs demonstrated markedly different activity levels, both of which may be useful depending on the clinical context and drug delivery needs.

6.3.4 A GE11-targeted Polymeric Camptothecin Prodrug System

6.3.4.1 Polymer Synthesis and Characterization

Next the targeting capabilities of GE11 were employed to enhance the delivery and cytotoxic activity of the phenyl-ester linked camptothecin prodrug. Using RAFT polymerization, both the GE11 peptide monomer and 10CAM prodrug monomer were incorporated into a single carboxybetaine polymeric scaffold **(Figure 6.10).** First, a copolymer of carboxybetaine and 10CAM was synthesized as in 6.3.3.1. Additionally, a small amount of Rhodamine B monomer was doped into this reaction for targeting experiments. The resulting polymer, p(10CAM-co-CBM), was then employed as a

macroCTA for the block copolymerization of CBM and either MaAhxGE11 or the non-targeting monomer MaAhxHW12. The molar feed ratio of peptide to CBM in the second

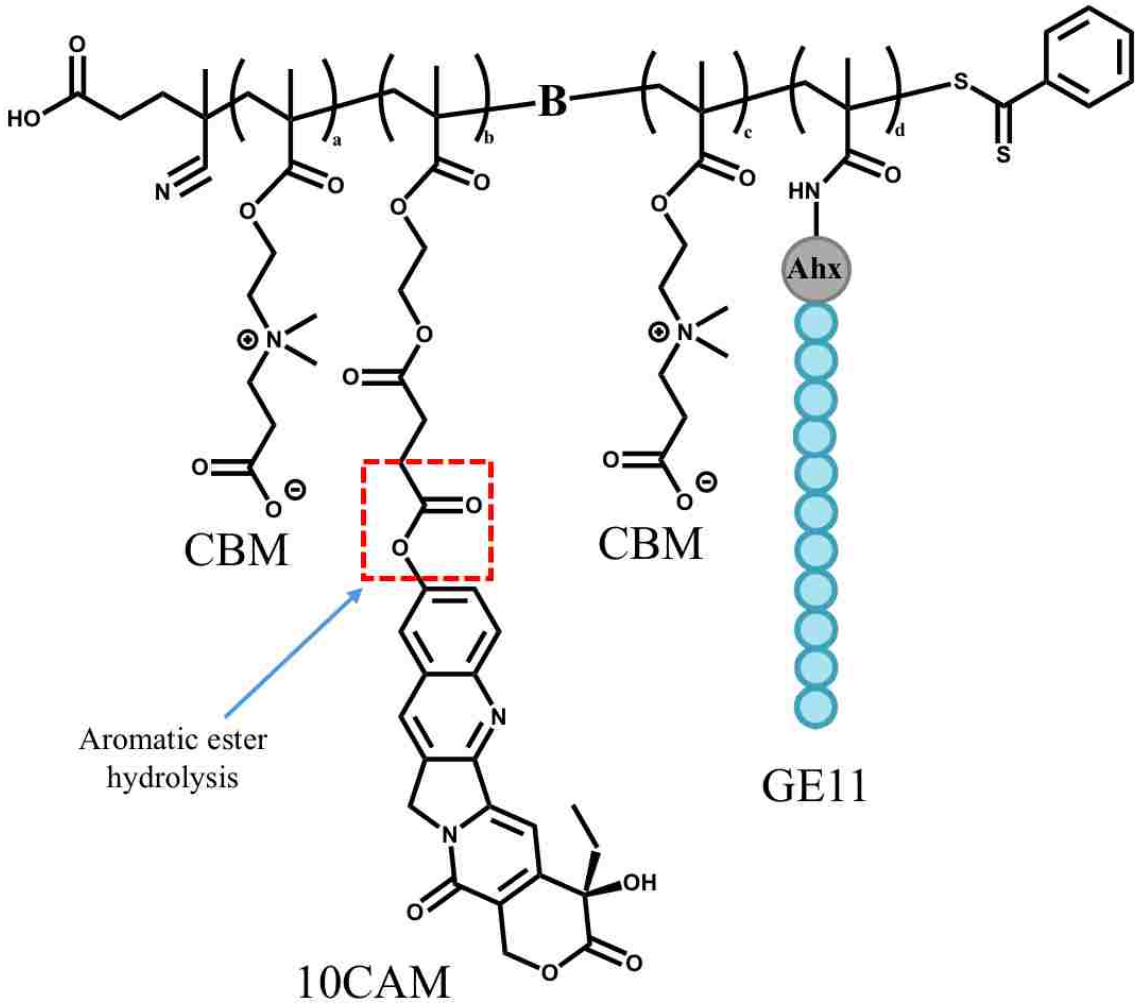

Figure 6.10. A GE11-targeted Polymeric Camptothecin Prodrug. Using RAFT polymerization, a diblock copolymer was synthesized incorporating both the GE11 peptide monomer (MaAhxGE11) and aromatic-ester linked camptothecin prodrug (10CAM) into a single polymeric carboxybetaine polymeric scaffold. The first polymer block contained CBM and the prodrug, while the second polymer block consisted of CBM and the peptide targeting functionality.

block was 4:96. Two corresponding non-drug control polymers were also synthesized without 10CAM. Polymer synthesis and characterization details are summarized in **Table 6.2**. Polymer molecular weights and polydispersities will be determined by GPC, and

polymer compositions will be confirmed by ^{1}H-NMR. The peptide content of the polymers was determined by RP-HPLC analysis of reaction aliquots taken at reaction start and end times.

Polymer	macroCTA					Diblock Copolymer					
	DP	% feed / comp		M_n	PDI	DP	% feed / comp		M_n	PDI	Peptide/ Polymer
		CBM	10CAM				CBM	Peptide			
GE11 Prodrug	50	84	16			50	96 /	4 /			1.03
HW12 Prodrug	50	84	16			50	96 /	4 /			1.26
GE11 Control	50	100	0			50	96 /	4 /			1.79
HW12 Control	50	100	0			50	96 /	4 /			1.82

Table 2. Synthesis and Characterization of Peptide Prodrug Diblock Copolymers. Employing RAFT polymerization, a prodrug macroCTA was first synthesized consisting of 16 mol% 10CAM and 84 mol% CBM. As a non-drug control, a second macroCTA was synthesized consisting of 100% CBM. The macroCTAs were then employed for the block copolymerization of CBM (84 mol%) and either the GE11-targeting peptide monomer or HW12 control monomer (16 mol%). Experimental molecular weights and polydispersities will be measured by aqueous gel permeation chromatography (GPC) and polymer compositions will be determined by ^{1}H-NMR. Peptide monomer conversions were quantified by RP-HPLC analysis of reaction aliquots taken at T_o and T_x.

6.3.4.2 The GE11 Peptide Enhances Polymer Targeting to SKOV3 Ovarian Cancer Cells

To confirm the targeting effect of GE11 within the context of the diblock polymeric prodrug system, SKOV3 cells were incubated with the fluorescently labeled GE11-targeted prodrug polymer or the HW12 control and binding was measured by flow cytometry. The GE11-targeted polymer was taken up at approximately 2-fold higher levels than the HW12 polymer (**Figure 6.11A)**. This effect is less pronounced than that observed for the peptide-CBM copolymers in part 6.3.2.3, possibly as a result of the larger size and/or lower peptide content of the polymers. These polymers have a drug block that is void of peptide. However, a promising targeting effect was still observed.

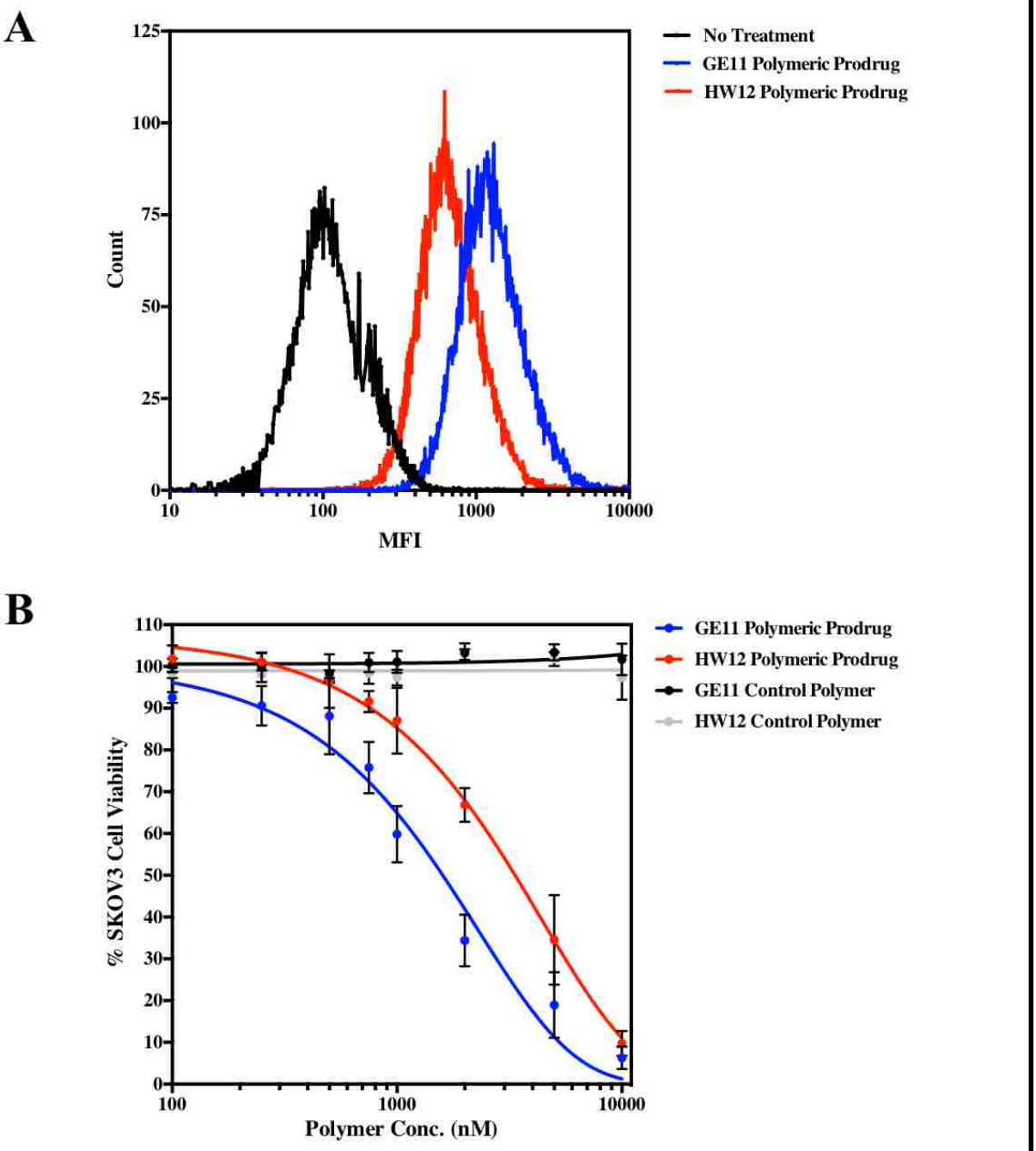

Figure 6.11. GE11-targeting Enhances the Cytotoxic Activity of the Polymeric Camptothecin Prodrug. (A) GE11-targeting of the polymeric prodrug system was confirmed by flow cytometric analysis of SKOV3 cells treated with 1 μM polymer for 15 min at 37 °C. The GE11 peptide lead to an approximately 2-fold increase in diblock copolymer uptake relative to the HW12 non-targeting control. **(B)** SKOV3 cells were pulse-treated with polymer for 15 min at 37 °C and cell viability was measured after 72 hours by MTS assay. GE11 enhanced the cytotoxic activity of the polymer prodrug. Non-drug control polymers exhibited negligible cytoxicity.

6.3.4.3 GE11-targeting Enhances the Activity of the Camptothecin Prodrug System

The impact of peptide targeting on polymeric prodrug activity was tested in SKOV3 cells. To more closely mimic *in vivo* exposure, cells were pulsed with polymer (100-10,000 nM) for 15 minutes at 37 ºC. Cells were then washed and given fresh media, and viability was measured after 72 hours (**Figure 6.11B**). Neither of the non-drug control polymers exhibited cytotoxicity at doses up to 10 μM. As expected, both of the polymers containing 10CAM killed SKOV3 cells in a dose dependent manner. However, the GE11-peptide significantly enhanced the cytotoxic activity of the polymer prodrug. Under the pulse treatment conditions tested, the IC50 of p[(10CAM-co-CBM)-b-(GE11-co-CBM)] was 1597 nM, in constrast to 3399 nM for p[(10CAM-co-CBM)-b-(HW12-co-CBM)]. This is consistent with the 2-fold increased in polymer binding observed in part 6.3.4.2. In the future, increasing the peptide load and incorporating peptide throughout the polymer may improve both targeting and activity.

6.4 Discussion

It was the objective of this chapter to implement peptide monomer technology for the tumor-specific targeting of a therapeutic agent. To this end, GE11 was selected as a model peptide. GE11, identified via phage display, binds with high affinity to the epidermal growth factor receptor (EGFR) overexpressed in a wide variety of malignancies. For polymerization of GE11, its N-terminus was modified with a six carbon spacer (Ahx) and coupled to methacrylamide.

When incorporating the GE11 peptide monomer into a polymer, the choice of comonomer proved to be important for maintaining GE11's targeting activity. This work tested a number of hydrophilic comononers, as would be required for solubilizing hydrophobic peptides/drugs and for compatibility in biological systems. Two of the monomers tested were long chains of polyethylene glycol. $PEGMA_{950}$ consists of 19 ethylene oxide repeats, while $PEGMA_{300}$ consists of only six. In comparison to $PEGMA_{950}$, disadvantages of $PEGMA_{300}$ include decreased hydrophilicity, decreased circulation, and the need for higher degrees of polymerization. However, $PEGMA_{300}$ offers the advantage of decreased steric hindrance, which proved to be critical for permitting the enzyme cathepsin B to access a copolymerized peptide linker (Chapter 4). The zwitterionic monomer CBM offers both hydrophilic and steric advantages, and consequently was also tested. Unexpectedly, $PEGMA_{300}$, as well as $PEGMA_{950}$, did not permit GE11-targeting. While $PEGMA_{300}$ permitted cathepsin B access, it is possible it sterically blocks the much larger EGF-receptor and/or interferes with a prolonged ligand-receptor interaction. This hypothesis is supported by the finding that $PEGMA_{300}$ significantly slows the kinetics of cathepsin B cleavage (**Figure 4.11)**, indicating some degree of steric hindrance. In contrast to the PEGMA monomers, CBM allowed for a strong targeting effect. The

GE11-CBM copolymer was taken up at an 18-fold higher level than the corresponding HW12 copolymer. A GE11 peptide monomer with a longer hydrophilic –$(SG)_4$- spacer was also tested in combination with CBM, but did not lead to any increase in uptake. This suggests minimal steric interference by CBM. In the future, it would be interesting to test the alternative spacer in the context of $PEGMA_{300}$ grafts, especially if some degree of steric protection would be important for a copolymerized drug, such as the BIM peptide. In this chapter, as a consequence of these combined findings, CBM was selected as a polymeric scaffold.

As proof-of-concept, the GE11 peptide monomer was employed for delivering a prodrug monomer of a highly potent chemotherapeutic agent. Camptothecin is a topoisomerase I inhibitor whose therapeutic efficacy is often limited by its off-target toxic side effects. Two ester linked camptothecin prodrugs were prepared by conjugating the carboxylic-acid of the monomer SMA to hydroxyl functionalities within the structure of the drug. It was hypothesized that the physiochemical nature of the ester linkage would influence the extent and rate of ester hydrolysis and drug activity. Consequently, SMA was linked to camptothecin to create either a phenyl-ester or aliphatic-ester linkage. The corresponding prodrug monomers were copolymerized with CBM and drug release kinetics in human serum were measured by RP-HPLC. As expected, the the phenyl-ester linkage hydrolyzed at a significantly higher rate than the aliphatic linkage (**Figure 6.9A)**. At later time points, approximately twice as much free drug was released. The observed drug release kinetics corresponded with the cytotoxic activity of the prodrugs in SKOV3 ovarian cancer cell cultures (**Figure 6.9B)**. The measured IC50 of the phenyl-ester linked 10CAM prodrug (56 nM) was much lower than for the aliphatic-ester linkage (4776 nM). The difference in activity between the two prodrugs was much larger than suggested by the release kinetics. This may very well be due to enzymatic and/or chemical differences between the cell culture

environment and human serum. However, to confirm this finding, the experiment will be repeated with a newly synthesized p(CAM-co-CBM) polymer.

When the phenyl-ester linked prodrug and GE11-targeting peptide were combined into a single polymeric system, GE11 successfully enhanced polymer binding and cytotoxic activity in SKOV3 cell cultures (**Figure 6.11)**. The approximately two-fold increase observed correlated with a two-fold increase in cellular targeting for this system. It was determined that none of the observed cytotoxicity was due to polymeric components other than the drug, as control polymers synthesized without drug demonstrated negligible toxicity at all doses.

There are a number of directions in which to build on these initial findings. First, multivalency should be investigated for enhancing GE11-mediated polymer targeting. The polymers synthesized herein contained approximately one peptide per polymer chain. While, the binding of rhodamine labeled GE11 peptide to SKOV3s was at least 70-fold higher than for HW12 (**Figure 6.3)**, this effect was reduced to an 18-fold increase for the peptide-CBM copolymers (**Figure 6.7)**. For the camptothecin prodrug polymers, which contain a similar number of peptide residues but are much larger in size, only a 2-fold increase was observed (**Figure 6.11)**. Studies be Luo et al. demonstrated a 600-fold increase in peptide-mediated cell targeting for multivalent versus monovalent conjugates. In combination, this suggests that GE11-targeting of the prodrug polymer can be greatly improved by incorporating multiple peptides per polymer chain. Consequently, peptide valency is a parameter that should be optimized.

The targeting potential of GE11 will next require *in vivo* validation in a preclinical tumor model. *In vivo* testing will also be required to fully understand the safety and activity profiles of the camptothecin prodrugs. Additionally, the GE11-targeting peptide might be considered in combination with the cathepsin B-cleavable BIM polymeric carrier studied in Chapters 4 & 5. It

was not practical to develop a GE11-targeted BIM prodrug system in an *in vitro* environment, as high enough peptide doses could not have been achieved with the pulse treatment regimen required to observe targeting. However, peptide targeting will more likely have an observable effect in an *in vivo* environment. Potential advantages of the GE11 peptide over Herceptin antibodies are reduced cost, reduced immunogenicity, increased stability, and higher achievable peptide:polymer ratios.

In conclusion, this chapter employed methacrylate-based monomers to directly integrate targeting and therapeutic functionalities into a single polymeric platform. This design is advantageous in its tumor-specificity, stability, synthetic simplicity, and versatility. While this work specifically developed the GE11 peptide and a campthotehcin prodrug, the described system can easily be adapted for other targeting sequences and drug classes, with application across a wide range of diseases.

REFERENCES

[1] Zhang XX, Eden HS, Chen X. Peptides in cancer nanomedicine: drug carriers,targeting ligands and proteasesubstrates. J Control Release. 2012 Apr 10;159(1):2-13.

[2] National Cancer Institute. FDA Approval for Brentuximab Vedotin. http://www.cancer.gov/about-cancer/treatment/drugs/fda-brentuximabvedotin

[3] National Cancer Institute. FDA Approval for Ado-Trastuzumab Emtansine. http://www.cancer.gov/about-cancer/treatment/drugs/fda-ado-trastuzumab-emtansine

[4] Jerjian TV, Glode AE, Thompson LA, O'Bryant CL. Antibody-Drug Conjugates: A Clinical Pharmacy Perspective on an Emerging Cancer Therapy. Pharmacotherapy.2016 Jan;36(1):99-116. (or ADC website)

[5] Firer MA, Gellerman G. Targeted drug delivery for cancer therapy: the otherside of antibodies. J Hematol Oncol. 2012 Nov 9;5:70.

[6] Molek P, Strukelj B, Bratkovic T. Peptide phage display as a tool for drug discovery: targeting membrane receptors. Molecules. 2011 Jan 21;16(1):857-87.

[7] Heine M, Freund B, Nielsen P, Jung C, Reimer R, Hohenberg H,Zangemeister-Wittke U, Wester HJ, Lüers GH, Schumacher U. High interstitial fluid pressure is associated with low tumour penetration of diagnostic monoclonal antibodies applied for molecular imaging purposes. PLoS One. 2012;7(5):e36258.

[8] Bruckdorfer T, Marder O, Albericio F. From production of peptides in milligram amounts for research to multi-tons quantities for drugs of the future. Curr Pharm Biotechnol. 2004 Feb;5(1):29-43.

[9] Vlieghe P, Lisowski V, Martinez J, Khrestchatisky M. Synthetic therapeutic peptides: science and market. Drug Discov Today. 2010 Jan;15(1-2):40-56.

[10] Majumdar S, Siahaan TJ. Peptide-mediated targeted drug delivery. Med Res Rev. 2012 May;32(3):637-58.

[11] Laakkonen P, Vuorinen K. Homing peptides as targeted delivery vehicles. Integr Biol (Camb). 2010 Aug;2(7-8):326-37.

[12] Garanger E, Boturyn D, Dumy P. Tumor targeting with RGD peptide ligands-design of new molecular conjugates for imaging and therapy of cancers. Anticancer Agents Med Chem. 2007 Sep;7(5):552-8.

[13] De Jong M, Valkema R, Jamar F, Kvols LK, Kwekkeboom DJ, Breeman WA, Bakker WH,Smith C, Pauwels S, Krenning EP. Somatostatin receptor-targeted radionuclide therapy of tumors: preclinical and clinical findings. Semin Nucl Med. 2002 Apr;32(2):133-40.

[14] Liu SV, Tsao-Wei DD, Xiong S, Groshen S, Dorff TB, Quinn DI, Tai YC, Engel J, Hawes D, Schally AV, Pinski JK. Phase I, dose-escalation study of the targeted cytotoxic LHRH analog AEZS-108 in patients with castration- and taxane-resistant prostate cancer. Clin Cancer Res. 2014 Dec 15;20(24):6277-83.

[15] Emons G, Gorchev G, Harter P, Wimberger P, Stähle A, Hanker L, Hilpert F,Beckmann MW, Dall P, Gründker C, Sindermann H, Sehouli J. Efficacy and safety of AEZS-108 (LHRH agonist linked to doxorubicin) in women with advanced or recurrent endometrial cancer expressing LHRH receptors: a multicenter phase 2 trial(AGO-GYN5). Int J Gynecol Cancer. 2014 Feb;24(2):260-5.

[16] Drappatz J, Brenner A, Wong ET, Eichler A, Schiff D, Groves MD, Mikkelsen T,Rosenfeld S, Sarantopoulos J, Meyers CA, Fielding RM, Elian K, Wang X, Lawrence B, Shing M, Kelsey S, Castaigne JP, Wen PY. Phase I study of GRN1005 in recurrent malignant glioma. Clin Cancer Res. 2013 Mar 15;19(6):1567-76.

[17] Thundimadathil J. Cancer treatment using peptides: current therapies and future prospects. J Amino Acids. 2012;2012:967347.

[18] Normanno N, De Luca A, Bianco C, Strizzi L, Mancino M, Maiello MR, Carotenuto A, De Feo G, Caponigro F, Salomon DS. Epidermal growth factor receptor (EGFR)signaling in cancer. Gene. 2006 Jan 17;366(1):2-16.

[19] Salomon DS, Brandt R, Ciardiello F, Normanno N. Epidermal growth factor-related peptides and their receptors in human malignancies. Crit Rev Oncol Hematol. 1995 Jul;19(3):183-232.

[20] Henriksen L, Grandal MV, Knudsen SL, van Deurs B, Grøvdal LM. Internalization mechanisms of the epidermal growth factor receptor after activation with different ligands. PLoS One. 2013;8(3):e58148.

[21] Li Z, Zhao R, Wu X, Sun Y, Yao M, Li J, Xu Y, Gu J. Identification and characterization of a novel peptide ligand of epidermal growth factor receptor for targeted delivery of therapeutics. FASEB J. 2005 Dec;19(14):1978-85.

[22] Song S, Liu D, Peng J, Sun Y, Li Z, Gu JR, Xu Y. Peptide ligand-mediated liposome distribution and targeting to EGFR expressing tumor in vivo. Int J Pharm. 2008 Nov 3;363(1-2):155-61.

[23] Kristensen TE, Vestli K, Fredriksen KA, Hansen FK, Hansen T. Synthesis of acrylic polymer beads for solid-supported proline-derived organocatalysts. OrgLett. 2009 Jul 16;11(14):2968-71.